Title

Poly(dehydroalanine) Based Polypeptides for Stimuli Responsive Biomaterials

ISBN

9798293869978

Author

Morrison, Casey

Publication Date

2025-09-22

Peer reviewed|Thesis/dissertation

UNIVERSITY OF CALIFORNIA

Los Angeles

Poly(dehydroalanine) Based Polypeptides for Stimuli Responsive Biomaterials

A dissertation submitted in partial satisfaction of the

Requirements for the degree Doctor of Philosophy

In Chemistry

by

Casey Austin Morrison

2025

ABSTRACT OF THE DISSERTATION

Poly(dehydroalanine) Based Polypeptides for Stimuli Responsive Biomaterials

by

Casey Austin Morrison

Doctor of Philosophy in Chemistry

University of California, Los Angeles, 2025

Professor Timothy J Deming, Chair

Functionalized polypeptides provide access to unique biomaterials that can be varied by the identity of the amino acid side chain; however, access to highly functionalized polypeptides is limited by the routes for sidechain modification. Modification of the polypeptide side chain requires careful post polymerization modification to ensure quantitative functionalization or the synthesis and stringent purification of functionalized monomers. The Deming group recently developed methods for the synthesis of high molecular weight poly(dehydroalanine) ($\mathbf{A^{DH}}$), which possesses reactive electrophilic groups that allows its efficient modification to functionalized polypeptides after reactions with thiol and amine nucleophiles. In this dissertation, I will detail the synthesis and characterization of various biomaterials derived from functionalized $\mathbf{A^{DH}}$ polypeptides.

Chapter 2 describes the synthesis and characterization of amino acid-functionalized poly(S-alkyl-*rac*-cysteines) polypeptides. These polypeptides possessed

the ability to form coacervates with a variety of anions and ssRNA under physiological conditions. Furthermore, these coacervates could be tuned to respond to environmental stimuli, such as temperature, pH, and redox conditions to trigger coacervation formation and dissolution.

Chapter 3 describes the synthesis and characterization of amphiphilic poly(L-methionine sulfoxide)$_x$-b-poly(dehydroalanine)$_y$, diblock copoly-peptides, $\mathbf{M^O_xA^{DH}_y}$, and their self-assembly into submicrometer-diameter unilamellar vesicles in aqueous media. The formation of vesicles was observed over an unprecedented range of copolypeptide compositions due to the unique properties and chain conformations of the $\mathbf{A^{DH}}$ hydrophobic segments. These copolypeptides incorporate two distinct thiol reactive components where each segment can respond differently to a single thiol stimulus, allowing for *in situ* inversion of the vesicle assemblies and vesicle disruption via glutathione under intra-cellular mimetic conditions.

Chapter 4 details the assembly and characterization of $\mathbf{M^O_xA^{DH}_y}$ copolypeptides to form membranes that provide plasticity and selective permeability in aqueous mixtures, which allows predictable control of vesicle shape by variation of dialysis conditions. These findings expand upon vesicle shape transformation methods for biodegradable and thiol responsive polypeptide vesicles, which are amenable to development for applications in therapeutic delivery.

Chapter 5 describes the synthesis and characterization of racemic mucin analogues bearing native glycans from the functionalization of $\mathbf{A^{DH}}$ with un-protected thiol modified monosaccharides. Functionalization of $\mathbf{A^{DH}}$ resulted in the formation of

glycosylated poly(*rac*-cysteine) polypeptides, with no unnatural sidechain modification and high saccharide conjugation.

The dissertation of Casey Austin Morrison is approved.

Andrea Kasko

Irene Chen

William Gelbart

Timothy J Deming, Committee Chair

University of California, Los Angeles

2025

Table of Contents

List of Figures

List of Tables

List of Schemes

List of Abbreviations

Ac_2O	acetic anhydride
A^{DH}_x	poly(dehydroalanine)$_x$
αGalNAcSH	2-acetamido-2-deoxy-1-thio-α-D-galactopyranose
αGalNAc-*rac*-C_{150}	poly(S-(2-acetamido-2-deoxy-1-thio-α-D-galactopyranosyl)-*rac*-cysteine)$_{150}$
αGalNAcSer$_{300}$	poly(O-(2-acetamido-2-deoxy-1-thio-α-D-galactopyranosyl) L-serine)$_{300}$
AFM	atomic force microscopy
Ala	L-alanine
βGlcSH	β-D-glucopyranoside sodium salt
βGlc-*rac*-C_{150}	poly(S-(β-D-glucopyranosyl)-*rac*-cysteine)$_{150}$
BOC	tert-butyloxycarbonyl
bpy	2,2'-bipyridine
bpyNiCOD	2,2′-bipyridyl-Ni(1,5-cyclooctadiene)
C^{BCM}_x	poly(S-(*tert*-butylcarboxymethyl)-L-cysteine)$_x$
C^{CM}_x	poly(S-carboxymethyl-L-cysteine)$_x$, sodium salt
CD	circular dichroism
COD	1,5-cyclooctadiene
CO	carbon monoxide
CO_2	carbon dioxide
CSA	camphor sulfonic acid
C^{rR}	poly(S-alkyl-*rac*-cysteine)

CuAAC	copper catalyzed azide-alkyne cycloaddition
Cys	L-cysteine
Đ	dispersity
Da	Dalton
DCM	dichloromethane
DMAP	4-Dimethylaminopyridine
DMF	dimethylformamide
DMSO	dimethyl sulfoxide
DIC	differential interference contrast
DI H_2O	deionized water
$DIOC_{18}$	3,3'-Dioctadecyloxacarbocyanine perchlorate
DIPEA	diisopropylethylamine
DLS	dynamic light scattering
DMSO	dimethyl sulfoxide
d.nm	average hydrodynamic diameter in nanometers
$E_{88}A^{DH}_{85}$	poly(L-glutamate Na^+ salt)$_{88}$-*block*-poly(dehydroalanine)$_{85}$
eq	equivalent
FTIR	Fourier transform infrared spectroscopy
g	gram
GPC	gel permeation chromatography
H	hour
HATU	hexafluorophosphate azabenzotriazole tetramethyl uronium

HCl	hydrochloric acid
HFIP	1,1,1,3,3,3-hexafluoroisopropanol
HOBT	hydroxybenzotriazole
H_2S	hydrogen sulfide
K_{60}	poly(l-lysine·HCl)$_{60}$
KTFA	potassium trifluoroacetate
L	liter
LCST	lower critical solution temperature
Leu	L-leucine
Leu-C^{H}_{60}	(poly(*S*-(3-(2-L-leucine amido)ethoxy)-2-hydroxypropyl)-L-homocysteine hydrochloride)$_{60}$
L/F	poly(L-leucine-*stat*-L-phenylalanine)
LSCM	laser scanning confocal microscopy
mPEG-NCO	α-methoxy-ω-isocyanoethyl-poly(ethylene glycol)
M	molar
M_x	poly(L-methionine)$_x$
$M_{35}C^{rGT}_{30}$	poly(Lmethionine)$_{35}$-*b*-poly(S-(glutathione)-*rac*-cysteine, Na+ salt)$_{30}$

$M_{35}C^{rMC}_{30}$	poly(L-methionine)$_{35}$-*b*-poly(S-(carboxymethyl)-*rac*-cysteine, Na^+ salt)$_{30}$
MeI	methyl iodide
Met	L-methionine
mg	milligram
min	minute
mL	milliliter
mM	millimolar
$M^M_xA^{DH}_y$	poly(S-methyl-L-methionine sulfonium chloride)$_x$-*b*-poly(dehydroalanine)$_y$
mMol	milimolar
MeOH	methanol
M_n	number average molar mass
M^O	poly(L-methionine sulfoxide)
$M^O_xA^{DH}_y$	poly(L-methionine sulfoxide)$_x$-*b*-poly(dehydroalanine)$_y$
$M^O_xC^{CMO}_y$	poly(L-methionine sulfoxide)-*b*-poly(S-(carboxymethyl)-L-cysteine sulfoxide)
M_w	weight average molar mass
MW	molecular weight

MWCO	molecular weight cutoff
$M_xC^{BCM}_y$	poly(L-methionine)$_x$-*b*-poly(S-(*tert*-butylcarboxymethyl)-L-cysteine)$_y$
$M_xC^{CM}_y$	poly(L-methionine)$_x$-*b*-poly(S-(*tert*-butylcarboxymethyl)-L-cysteine)$_y$
$NaBH_4$	sodium borohydride
NaCl	sodium chloride
$NaHCO_3$	sodium bicarbonate
NaOH	sodium hydroxide
NaTFA	sodium trifluoroacetate
NCA	N-carboxyanhydride
NCL	native chemical ligation
NH_4OH	ammonium hydroxide
nm	nanometer
nM	nanomolar
NMR	nuclear magnetic resonance
NNCA	N-substituted glycine *N*-carboxyanhydrides
NO	nitrous oxide

OEG	oligoethylene glycol
PEG	polyethylene glycol
PBS	phosphate buffered saline
PDI	polydispersity index
PIC	polyion complexes
pK_a	acid dissociation constant
PMe_3	trimethylphosphine
PMMA	poly(methyl methacrylate)
polyA	poly(adenylic acid)
PPM	post-polymerization modification
Pro	L-proline
rac	racemic
rac-C^{HE}_{150}	poly(S-(2-hydroxyethyl)-*rac*-cysteine)$_{150}$
E^{P2}	poly(ɣ-[2-(2-methoxyethoxy)ethyl]-glutamate)
ROP	ring opening polymerization
RPM	revolutions per minute
s	second
Ser	L-serine

SPPS	solid phase peptide synthesis
ssRNA	single strand RNA
TBHP	*tert*-butyl hydrogen peroxide
tBuCM-Cys	S-(*tert*-butylcarboxymethyl)-L-cysteine
T_{cp}	cloud point temperature
TFA	trifluoroacetic acid
TFE	trifluoroethanol
TGA	thioglycolic acid
THF	tetrahydrofuran
Thr	L-threonine
TLC	thin layer chromatography
TPP	tripholyphosphate
TR	Texas Red
Val	L-valine
Xaa	generic amino acid
Xaa-C^H	poly(S-alkyl-L-homocysteines)
Xaa-*rac*-C	poly(S-alkyl-*rac*-cysteines)
µL	microliter

μm	micrometer

Acknowledgements

Obtaining my Ph.D. in chemistry would never have been possible without the overwhelming support of many individuals. I would like to begin by thanking Professor Tim Deming for the opportunity to conduct research in his laboratory at UCLA and for pushing me to perform excellent research. Although my time in this program was extremely divisive, from starting my first year during the COVID-19 pandemic and concluding it with severe funding restrictions from the current government administration, I'm glad we were able to make the most of uncertain times. I would also like to thank my committee members, Professors Andrea Kasko, Irene Chen, and Bill Gelbart. Their support during my candidacy exam and towards the end of my PhD has helped guide me through the program and establish collaborations and connections with graduate students across many disciplines.

Throughout the past few years, I have heard the saying, "A PhD is a marathon, not a sprint" many times. However, as someone who has completed 8 marathons, I can say that a marathon is significantly easier than earning a PhD. This accomplishment would not have been possible without the help of many close friends, lab mates, and mentors who supported me during the lows, and celebrated my victories. Emily Mobley, Shelby Vexler, Kirstie Fetah, and Vivian Dao, thank you for always having my back, allowing me instrument access, always providing troubleshooting support, and for giving me opportunities to explore personal research interests I never could have on my own. I would also like to thank my friends who supported me outside of lab and reminding me there is more to grad school than just research and classes: Dharbi Jens, Joy Kim and Jasmine Keane. In addition, I have been very lucky to have the support of Caitlin Halligan,

you have helped me grow so much as a scientist and person since we met at Pomona College so many years ago. I also extend my gratitude to my former undergraduate mentees, Ethan Chan and Thatcher Lee, who synthesized and purified countless compounds for my experiments. I'm so proud of everything we were able to accomplish together and forever thankful for your contributions to my publications. To my undergraduate mentors, Professors Dan O'Leary, Jane Liu, and Fred Grieman, thank you for inspiring my passion in chemistry and for laying the foundation that made me the scientist I am today. I have always appreciated the relationship the Pomona Chemistry Department allowed us to develop. Finally, I would like to thank my family for supporting me throughout this endeavor. Without you all, I would never have had this opportunity.

Funding to support this doctoral work was provided by the National Sciences Foundation and the California NanoSystems Institute.

Vita

Education

2021

Pomona College

B.A. Chemistry

2023

University of California, Los Angeles

M.S. Chemistry

Teaching Experience

2018 – 2019

General Chemistry Teaching Assistant

2019 – 2021

Organic Chemistry Teaching Assistant

Department of Chemistry

Pomona College

2021 – 2025

Graduate Student Teaching Assistant

Department of Chemistry & Biochemistry; Department of Bioengineering; Department of Molecular, Cell, and Developmental Biology

University of California, Los Angeles

Research Experience

2019 – 2021

Undergraduate Researcher

Pomona College

Dr. Daniel O'Leary

2022 – 2025

Graduate Student Researcher

University of California, Los Angeles

Dr. Timothy J Deming

Publications

Morrison, C. A.; Chan, E. P.; Lee, T.; Deming, T. J. Switchable Coacervate Formation via Amino Acid Functionalization of Poly(Dehydroalanine). *Biomacromolecules* **2024,** *25* (4), 2554-2562.

Morrison, C. A.; Chan, E. P.; Deming, T. J. Triggered Inversion of Dual Responsive Diblock Copolypeptide Vesicles. *J. Am. Chem. Soc.* **2025**, *147* (9), 7617–7623.

Morrison, C. A. and Deming, T. J. Shape Transformation of poly(L-methionine sulfoxide)-*b*-poly(dehydroalanine) Vesicles. *ACS Macro Lett*. In press.

Morrison, C. A.; Deming, T. J. Facile Preparation of Mucin Mimetic Glycosylated Poly(cysteines) from Poly(dehydroalanine). *Manuscript in Progress*.

Vexler, S.; **Morrison, C. A**.; Jain, S.; Yang, Y.; Annabi, N.; Deming, T. J.; Chen, I. A. Antimicrobial polylysine-phage conjugates for improved biocompatibility. *Manuscript in Progress*.

Dao, V. P.; Kaneshiro, M. J.; **Morrison, C. A**.; Chakraborty, S.; Deming, T. J. Mechanistic Studies on N-Alkyl Amino Acid *N*-Carboxanhydride Polymerization Using Metallacycle Initiators. *Manuscript in Progress.*

Dao, V. P.; **Morrison, C. A**.; Kaneshiro, M. J; Chakraborty, S.; Deming, T. J. Metallacycle Initiated N-Alkyl Amino Acid N-Carboxyanhydride Polymerization. *Manuscript in Progress.*

Chapter 1: Synthesis and Applications of Polypeptide Based Biomaterials

1.1 Introduction to Polypeptides and Proteins

Polypeptides and proteins cover a wide range of structures and serve a diverse field of functions within biological systems. Cell signaling, biomolecule transport and recognition, structural support and catalyzing reactions are among their possible functions.[1] At their simplest level, proteins are synthesized from amino acids linked together through peptide bonds.[2] Additionally, proteins have the extraordinary ability to form unique tertiary and quaternary structures defined from their sequence.[2] The synthesis of proteins begins with the transcription or synthesis of their primary sequence or a chain of amino acids.[2] Through hydrogen bonding interactions, these polypeptides form their secondary structure motifs, mainly α-helices and β-sheets.[2] Non-covalent interactions between side chains, such as hydrophobic interactions, electrostatic interactions, or hydrogen bonding, organize these α-helices and β-sheets into the protein's tertiary structure.[2] Multiple tertiary structures can then come together through similar interactions to form quaternary structures. The tertiary and quaternary structures of proteins have evolved to serve the highly specialized roles proteins provide among cell interactions.[3]

Due to the various chemical functionalities and near limitless sequence possibilities of the 20 canonical amino acids, multiple synthetic approaches have been developed to produce polypeptides and proteins. Synthetic approaches mostly rely on four techniques: recombinant protein expression, solid phase peptide synthesis (SPPS), solution phase peptide synthesis, and ring opening polymerization of α-amino acid N-carboxyanhydrides (NCA). Recombinant expression is typically used for larger proteins, while the synthesis of specific shorter peptide sequences utilizes solution phase peptide

synthesis or SPPS.[4,5] The polymerization of NCAs differs by having the capability of synthesizing low or high molecular weight polypeptides, creating defined sequences based on monomer addition.[6] However, NCA polymerization comes at the cost of losing precise sequence control.[6]

1.2 Current Approaches for Protein and Polypeptide Synthesis

1.2.1 Recombinant Protein Expression

Since its development in 1976, recombinant protein expression has been exploited to produce naturally occurring proteins for almost 50 years.[4] Recombinant protein expression is most effective for producing large proteins in mass quantities.[4] Target proteins are produced by identifying and cloning specific DNA sequences, transforming the plasmid into prokaryotic or eukaryotic cells, and isolating the target protein (**Figure 1.1**).[7] Once the DNA sequences are transformed into the cells, mass quantities of the protein can be expressed. Typically, the proteins can be expressed with affinity tags, such as the common hexahistidine tag, for facile purification.[8] Several therapeutic proteins have been produced from recombinant protein expression, including insulin and human growth hormone.[9,10] Mass production of these hormones has drastically improved the quality of life for individuals suffering from diabetes and growth hormone deficiency.

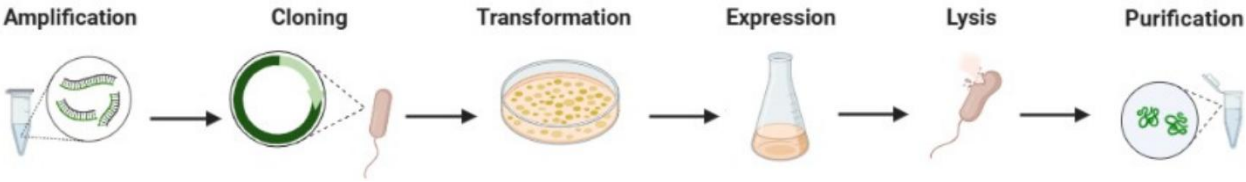

Figure 1.1. Schematic representation of the recombinant protein expression process. Image generated with Biorender.

However, there are some drawbacks to recombinant protein expression. While prokaryotic cells provide cheap and efficient means for mass protein production, these cells lack the many of the enzymes found in eukaryotic cells.[11] This can lead to non-functioning proteins as post translational modification and proper protein folding will not occur.[11] Furthermore, the introduction of non-canonical amino acids into proteins produced through recombinant expression is not straight forward.[12] Attempts to incorporate non-canonical amino acids can lead to cell apoptosis, misfolded proteins, and low production quantities.[12] While some techniques exist to simplify the introduction of non-canonical amino acids into proteins, such as the methods developed by the Tirrell and Schultz laboratories, these protocols require additional substrates, enzymes, or tRNAs to be added to the cell cultures.[13,14]

1.2.2 Stepwise Peptide Synthesis

Prior to 1963, stepwise peptide synthesis was solely performed via solution-phase chemistry. Solution-phase peptide synthesis brought forward the production of short peptide sequences that were difficult to express in bacteria, such as the incorporation of unnatural amino acids, D-amino acids, and peptide backbone modification.[15] However, solution-phase peptide synthesis consisted of laborious and repetitive steps. Amino acids required an N-terminus protecting group which would need to be removed after C-terminus activation and coupling with an unprotected amine or amino acid.[15] The intermediates would also need to be isolated and purified after each coupling reaction.[5] Furthermore, solubility issues arose as peptide lengths increased, leading to poor yields and reactivity.[5] Luckily, these issues were soon to be remedied upon the publication of Robert Merrifield's seminal report on solid-phase peptide synthesis in 1963.[16]

Merrifield's contribution to peptide synthesis allowed for efficient peptide synthesis and simplified purification. The improvements SPPS brought forth relied on the use of resins as an insoluble solid phase support.[16] SPPS begins with cross-linked polystyrene resin beads that are swelled in an organic solvent such as dimethylformamide or dichloromethane.[17] This process allows for peptide synthesis to take place inside of the swollen pores of the beads.[17] The first amino acid is then attached to the resin via a covalent bond at the C-terminus.[17] Each subsequent amino acid is then coupled one at a time until the desired sequence is synthesized.[17] Since the resin is insoluble in the solvents used throughout the coupling process, it can easily be washed after each coupling, deprotection, and neutralization.[17] The final peptide is obtained by cleavage from the resin (**Figure 1.2**).[17]

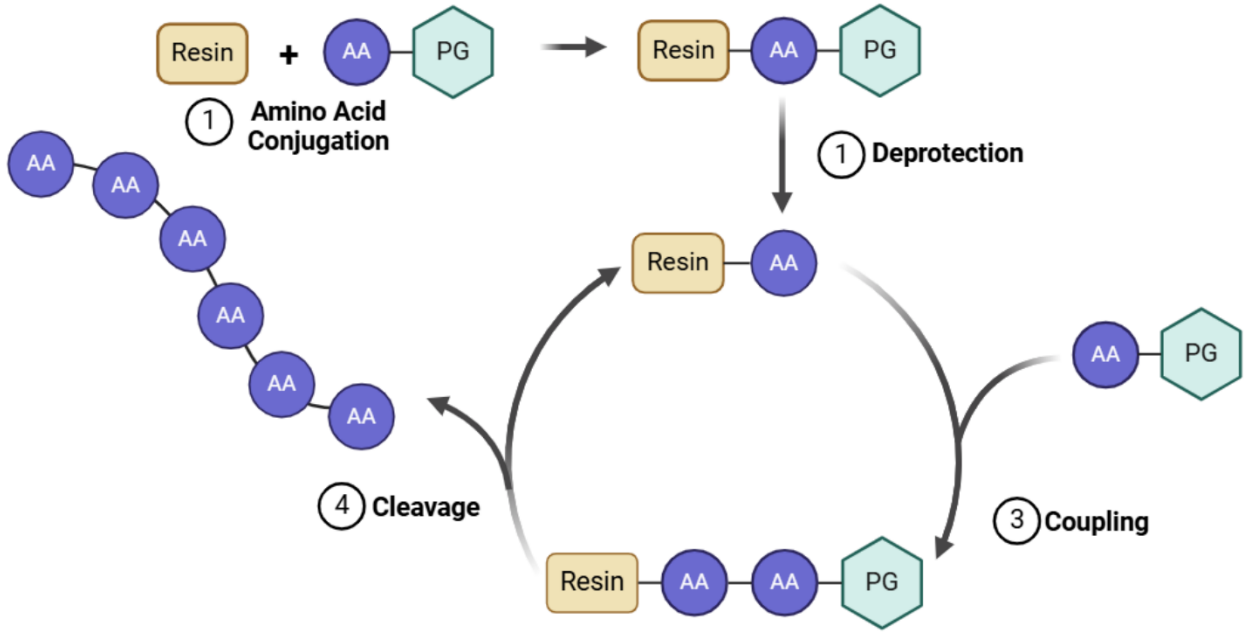

Figure 1.2. Schematic of solid-phase peptide synthesis process. Image generated in Biorender.

Since its development, SPPS has become the primary method for synthesizing polypeptides up to 50 residues long. The use of different amino acid protecting groups, solvents, and coupling agents have also been optimized over the years, providing many methods for orthogonal protection and deprotection strategies.[18,19] However, a few major drawbacks of SPPS are the production of undesirable side products, incomplete coupling, and reduced yield when synthesizing long polypeptide sequences (>50 residues).[17] Improvements to the synthesis of longer, high molecular weight polypeptides have been introduced though native chemical ligation (NCL) and copper catalyzed azide-alkyne cycloaddition (CuAAC).[20,21]

Native chemical ligation was first reported in 1992 by Stephen Kent and Martina Schnölze.[20] NCL utilizes a *trans*-thioesterification reaction between a thioester on the C-terminus of one peptide and the thiol sidechain of a cysteine residue on the N-terminus of another peptide.[22] The thiol group performs a nucleophilic attack on the thioester, forming a new thioester linkage between the two peptides.[22] The new thioester undergoes an S-N acyl shift to create a new amide bond.[22] NCL improves upon the solubility and coupling efficiency issues introduced by SPPS by allowing the coupling of unprotected peptides in aqueous media under physiological conditions.[22,23] As NCL techniques have improved, its use in combination with SPPS has allowed for peptides with over 350 residues to be synthesized.[22]

Copper catalyzed azide-alkyne cycloaddition is another technique that utilizes biorthogonal chemistry under physiological conditions to create a triazole linkage between two peptide sequences.[24] CuAAC utilizes a regioselective Cu(I) catalytic reaction between a terminal azide and alkyne group.[25] CuAAC is effective for the ligation of peptide

segments as this reaction is efficient, selective, insensitive to the changes in pH and temperature, and can be done under aqueous conditions with deprotected peptides.[21] For peptide conjugation, an azide and alkyne group are covalently bonded to the C and N-terminus of two separate peptides. Conjugation of the azide and alkyne group typically occurs through amine or carboxylate coupling reactions with either terminus. The two individual sequences are mixed with Cu^{+} salts under aqueous conditions where triazole formation occurs to produce the ligated peptide sequence.[24]

1.2.3 Ring Opening Polymerization of *N*-Carboxyanhydrides

While recombinant protein expression and SPPS are effective tools for synthesizing sequence specific proteins and peptides, neither are as efficient as ring opening polymerization (ROP) of NCAs for preparing high molecular weight polypeptides that do not require sequence specificity.[6,26,27] Although sequence specificity is required for proper protein folding and the generation of tertiary structures, secondary structure motifs, such as α-helices and β-sheets, as well as disordered segments, can be formed from repeats of the same amino acid.[6,28,29] In this case, the specific amino acid dictates which secondary structure will from. For example, poly(L-methionine) and poly(L-leucine) assemble into α-helices, poly(L-cysteine) and poly(L-serine) form β-sheets, and poly(L-glutamate) and poly(L-lysine) have disordered confirmations when charged in aqueous environments.[30–34] These structural motifs can be harnessed to prepare multi-block copolypeptides of different secondary structures to create supramolecular assemblies such as hydrogels, vesicles and micelles.[33,35,36]

1.2.4 Preparation of polypeptides from NCAs

NCAs are commonly prepared through the cyclization of amino acids using phosgene or triphosgene to form the cyclic anhydrides (**Figure 1.3**).[37] The resulting monomers can then be purified through a combination of extraction, recrystallization, and anhydrous column chromatography to remove unwanted impurities, such as HCl, unreacted amino acids, residual triphosgene, and unwanted side products.[32,38] Similarly to SPPS, amino acids with reactive side-chains, i.e. amines, thiols, carboxylates, or alcohols, must also be protected prior to cyclization to prevent the formation of side products. However, recent developments in NCA synthesis by Lu and coworkers have provided pathways to synthesize NCAs with unprotected carboxylate and thiol side-chains through the addition of propylene oxide or epichlorohydrin during NCA synthesis.[38] Since a wide variety of canonical or unnatural amino acids can be converted into NCAs, this provides a near limitless variety of polypeptides that can be synthesized.[39–42] For acid sensitive NCAs, acid scavengers such as α-pinene or triethylamine with trimethylsilyl chloride are commonly employed to neutralize the HCl produced during the cyclization.[32,43] Recently, the introduction of propylene oxide or epichlorohydrin has been used as an efficient means for the removal HCl. This method also eliminates the need for NCAs to be cyclized under anhydrous conditions.[38]

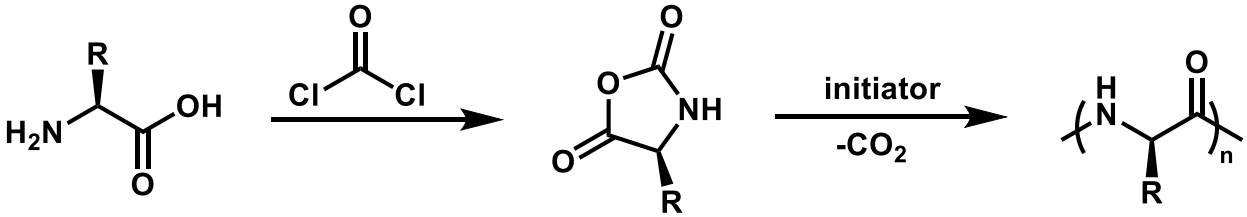

Figure 1.3. NCA preparation and polypeptide synthesis via ring-opening polymerization

The polymerization of NCAs requires an initiator to begin the propagation reaction. Initiation begins through the nucleophilic ring-opening or base activation of NCAs.[44–47]

Typically, amines are used as the initiating species for NCA polymerization, but this can lead to poor control over the preparation of block copolypeptides and hybrid block copolymers.[6,45] This difficulty is caused by amines functioning as either a nucleophile or a base during polymerization (**Figure 1.4**).[44,45]

When functioning as a nucleophile, the amine will react with a NCA to open the ring, form an amide bond, release CO_2, and generate a new N-terminal amine to continue the chain propagation.[6] When functioning as a base, the amine will deprotonate a NCA and activate the monomer for chain growth.[45] Since the polymerization mechanism can oscillate between the two propagation mechanisms, these subsequent polypeptides can have compositions and structures that differ from those predicted by the monomer feed ratio.

The initiation and propagation conditions for NCAs have been empirically optimized to reduce side reactions and generate polypeptides with low dispersity. These optimizations include using low temperatures, reduced pressure, and careful solvent selection.[48–50] Another optimization method has been to utilize alternative initiators for improved polymerization control. Alternative initiator species used for the living ROP of NCAs include rare earth metal complexes, silazane derivatives, and amine hydrochlorides.[51–54] These strategies have led to alternative methods of generating well-defined polypeptides with low dispersity.

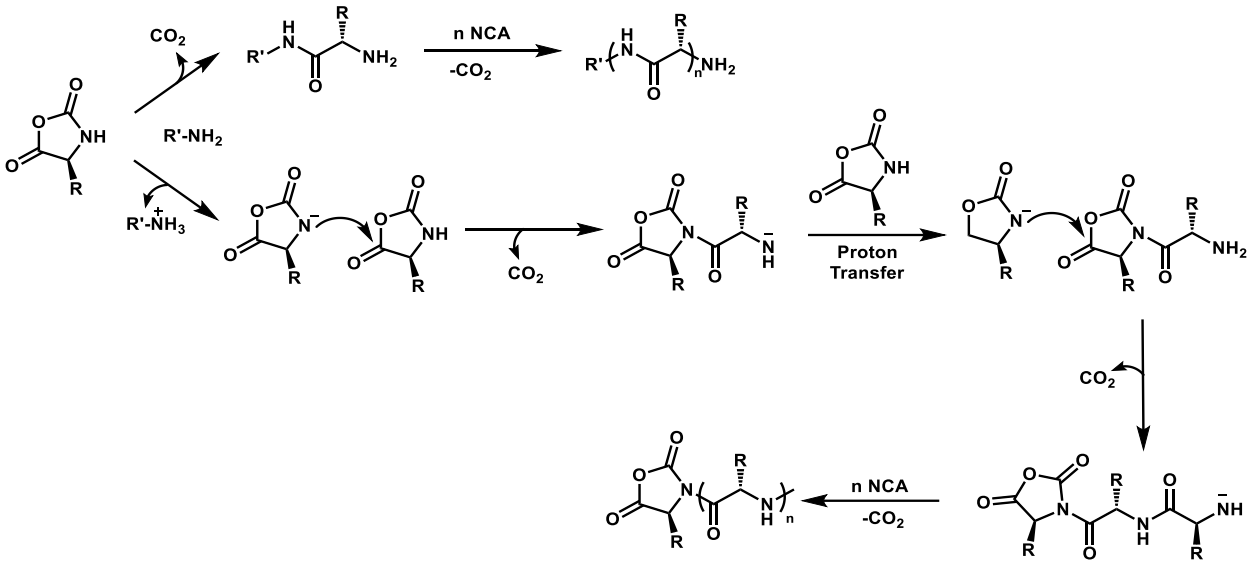

Figure 1.4. Amine-initiated polymerization of NCAs

1.2.5 Transition Metal Initiator Mediated Polymerization of NCAs

Many of the initiation and propagation issues observed with amine initiators were remedied by the development of transition metal initiators for ring opening polymerization of NCAs. Transition metal initiators drastically improved control over the addition of NCA monomers to active chain ends during propagation reactions. This led to decreased side products and improved yields as well as improved access to high molecular weight polypeptides with narrow dispersity.[26]

The first transition metal initiator studied in detail was bpyNi(COD), a zero valent Ni-based complex, where bpy = 2,2'-bipyridine and COD = 1,5-cyclooctadiene.[26] This initiator was capable of synthesizing high molecular weight block copolypeptides in high yields with low dispersity.[26] After the successful demonstration of living polymerization of NCAs using bpyNi(COD), further studies were performed using nickel amido-amidate metallacycle initiators.[51] These initiators were found to be the true active species in NCA polymerizations that were initiated using bpyNi(COD).[52] The amido-amidate functionality

also allowed for the conjugation of a variety of C-terminal end group functionalities, such as azides or other biomolecules like cholesterol.[27,52–54] Furthermore, direct preparation of these active divalent Ni complexes gave much higher initiation efficiency compared to zerovalent Ni precursors.[27,52]

Further research by the Deming group focused on a zerovalent cobalt initiator, $Co(PMe_3)_4$, where PMe_3 = trimethylphosphine.[55] Similarly to bpyNi(COD), $Co(PMe_3)_4$ could be used to synthesize high molecular weight polypeptides with narrow dispersity and in high yields.[55] $Co(PMe_3)_4$ also initiated NCA polymerizations at a faster rate than bpyNi(COD) and had similar broad NCA compatibility as Ni initiators.[27] Following their discovery, the mechanism of initiation and propagation of the cobalt and nickel initiators were studied (**Figure 1.5**).

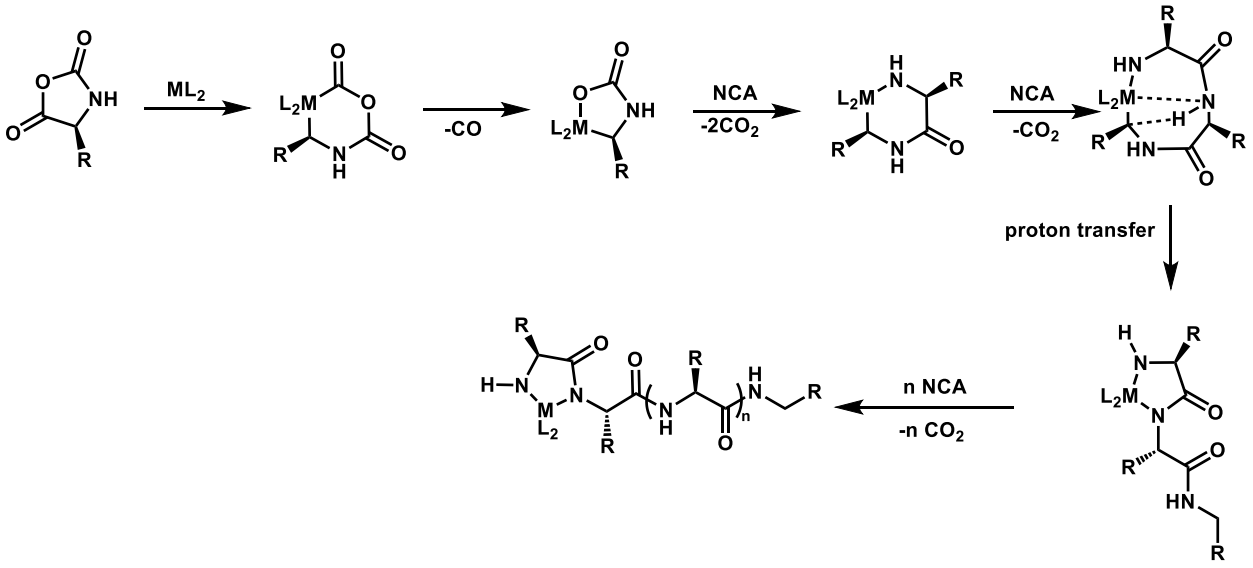

Figure 1.5. NCA polymerization mechanism using zerovalent Ni and Co initiators.

First, oxidative addition occurs at the O-C_5 anhydride bond, resulting in the loss of CO_2 at the C_5 position and creating a five-membered ring.[55] Another NCA monomer then reacts with the complex to form a 6 membered ring after the loss of CO_2. This reaction is

followed by a proton transfer from the amide proton to the metal bound carbon, leading to a rearrangement into a five-membered amido-amidate metallacycle.[55] This complex has now become an active propagating species, where the C-terminal amide is the chainend group. Further NCA addition will lengthen the polypeptide chain by following the same CO_2 loss and proton transfer processes.[55] It was found that zerovalent Ni and Co initiators follow the same polymerization mechanism.[27,55]

1.2.6 Transition Metal Initiator Mediated Polymerization of *N*-substituted amino acid *N*-carboxyanhydrides

Recently, there has been increased interest in the development of N-substituted glycine *N*-carboxyanhydrides (NNCAs) for polypeptoid synthesis. Polypeptoids, or poly(N-alkyl glycine)s, such as poly(sarcosine) and poly(proline) are of interest for biomedical applications due to their similarities to polyethylene glycol and temperature induced phase separation properties, respectively. NNCAs had been previously polymerized from living poly(γ-benzyl-L-glutamate) chains that possessed nickel amido-amidate propagating species, however, in 2021, the Kramer group began investigating transition metal-mediated polymerization of L-proline (Pro) and sarcosine (Sar) NNCAs using divalent Ni-based initiators.[26,27,56] As described earlier, these Ni complexes already have the amido-amidate propagating species formed before NNCA addition.[27,53,54] Addition of Pro NNCA to the Ni complex polymerized poly(Pro) in high yields with a narrow dispersity.[54]

These results confirmed that the nickel amido-amidate propagating species can initiate the living polymerization of Pro NNCA and other N-substituted NCAs, which provides a means for controlled preparation of polypeptoids. Although the mechanism of

initiation and propagation of NNCAs is still under investigation, transition metal amido-amidate metallacycles have now been proven to provide controlled polymerization of polypeptide and polypeptoid containing multiblock polymers.[54]

1.3 Addition of Non-canonical Amino Acids into Polypeptide-based Materials

The wide variety of amino acid side chain functionality enables the synthesis of diverse biomaterials. Although the 20 naturally occurring amino acids offer a range of side chain functional groups, their functionality is limited to hydrophobicity, ionic charge, hydrogen bonding, and consist of only four reactive functional groups. The incorporation of non-canonical amino acids into synthetic polypeptides enables more opportunities for further control over polypeptide functionalities. Non-canonical amino acid incorporation allows for the design of new biomaterials with specific properties, structures, and stimulus responsive behaviors. These types of biomaterials consist of hydrogels, vesicles, micelles, or coacervates and can be designed to respond to physiologically relevant stimuli, such as redox switches, pH triggers, counterion concentration, or temperature.[33,35,36,57,58]

Incorporating non-canonical amino acids into polypeptides synthesized via ROP relies on two methods, the synthesis and polymerization of functional monomers or post-polymerization modification (PPM) of polypeptides with reactive side-chains. The polymerization of functional monomers guarantees full incorporation of the target functional monomer at the desired composition and segment location within the polypeptide sequence. This method is particularly effective for synthesizing statistical and block copolypeptides that utilize multiple different functional monomers as all the functional monomers can be incorporated directly. However, two major potential

limitations of using functional NCA monomers are their synthesis and polymerization. The design of new monomers is often limited by their successful synthesis and rigorous purification.[40,59] Often, these monomers must be recrystallized or undergo anhydrous chromatography more thoroughly than canonical amino acid monomers.[32] Even after the successful preparation and purification of the new monomers, their polymerization may not proceed well due to poor solubility of the monomer or active polypeptide chain, slow polymerization kinetics, or side-reactions leading to high dispersity.

Post polymerization modification provides an alternative route to non-canonical side-chain functionality by modifying polypeptides prepared from NCA monomers with reactive side-chains. Although PPM can suffer from incomplete functionalization or cause polypeptide chain degradation, optimization of the coupling reactions can lead to near-quantitative modification without degrading the polypeptide. Click chemistry, Michael addition, and alkylation have all proved useful for PPMs such as the azide-alkyne cycloaddition, thiol-ene addition, amine or thiol addition, and pegylation.[41,42,60,61] These methods all provide high efficiency functionalization under mild conditions. In particular, work by Deming and coworkers has resulted in many methods for functional biomaterial production via modification of thioethers and α, β unsaturated sidechain groups.[58,60]

Thioether groups are naturally found in L-methionine and provide a facile method for polypeptide modification. Thioethers can undergo modification via oxidation or alkylation reactions to add new functional groups, introduce ionic charge, increase solubility, or trigger conformational changes.[58,61] In either homopolymers or copolymers, poly(L-methionine) can be modified to introduce any of these functionalities. Poly(L-methionine) is most often alkylated using alkyl halides, alkyl triflates, and epoxides to

introduce new functional groups.[61] Alkylation of the poly(L-methionine) results in the formation of cationic sulfonium salts and conversion of the α-helix favoring, hydrophobic thioether side-chains to charged sulfonium ion containing side-chains that results in improved water solubility and a disordered secondary structre.[58,61,62] Regardless of the functional group attached, this transformation induces a change within the secondary structure of poly(L-methionine) from an α-helix to a disordered confirmation.[62] The methyl group of the sulfonium can be selectively removed by dealkylation to remove the ionic charge and potentially alter the secondary structure.[63] Common functional groups attached via alkylation of poly(L-methionine) include sugars, ethylene glycol units, alkynes, or azides.[58,61]

Thioethers can also be reversibly oxidized to increase polypeptide water solubility and induce the same α-helix to a disordered confirmation change.[64] Oxidation of hydrophobic, α-helical poly(L-methionine) produces a water soluble, disordered poly(L-methionine sulfoxide). Further oxidation converts the sulfoxide into a sulfone, producing a water-insoluble, and α-helical poly(L-methionine sulfone).[64,65]

Research into poly(L-methionine) modifications has provided efficient and effective methods for synthetic polypeptide PPM. Many of these modifications have been useful for biomaterial development such as enzyme responsive vesicles, stem cell compatible non-fouling hydrogels, cell recognition via sugar conjugation, and synthetic coacervate mimetics.[35,62,65,66]

Additionally, Deming and coworkers have recently focused on the development of poly(dehydroalanine) based biomaterials. Poly(dehydroalanine) possesses α, β unsaturated alkene sidechains that allow for facile incorporation of nucleophiles via

Michael addition.[60,67] Poly(dehydroalanine) side-chains can be modified with amines or thiols to introduce desired chemical moieties allowing for a diverse array of new biomaterials to be fabricated, such as dual responsive copolypeptide vesicles and synthetic coacervates.[57,60,68]

1.4 Stimuli-Responsive Behavior of Polypeptides and Polypeptide-based Biomaterials

To mimic the signaling, structural support, and enzymatic catalysis functions that proteins provide in cells, chemists have prepared synthetic polypeptides that can respond to environmental stimuli.. By utilizing the functionality of amino acid side-chains and chain confirmations, responsive biomaterials can be created. Due to the variety of functional groups available, polypeptides can be specifically synthesized to respond to changes in temperature, redox reactions, pH, enzymes, and counterions. The ability to respond to these stimuli enable polypeptides to function as “smart” materials and allow them to undergo rapid changes in structure, solubility, and charge under physiologically relevant conditions.

1.4.1 Temperature Responsive Polypeptides

Temperature responsive behavior or thermo-responsiveness is a common goal for stimulus-responsive polypeptides. Due to the difference between ambient and physiological temperature, many chemists have utilized this aspect to generate biomaterials that respond to increases in temperature.[69,70] Polypeptide solutions can be designed to be liquid at ambient temperature and gel at physiological temperature or be miscible with aqueous media at ambient temperature, but phase separate at elevated temperatures.[66,71] These materials, gels or coacervates, rely on the use of lower critical

solution temperature (LCST) phenomena to transition from soluble to insoluble polymers as temperature increases. An example of a well-studied thermo-responsive hydrogel is the polypeptide poly(γ-[2-(2-methoxyethoxy)ethyl]-*rac*-glutamate-*b*-(γ-[2-(2-methoxyethoxy)ethyl]-L-glutamate)-*co*-L-leucine), **(*rac*-E^{P2})$_{180}$(E^{P2}/L)$_{30}$** designed by the Deming group. Once solubilized in aqueous media, ***rac*-E^{P2}$_{180}$(E^{P2}/L)$_{30}$** rapidly transitions between flowing as a liquid at ambient temperatures and forming a rigid hydrogel at 40 °C.[71] The ***rac*-E^{P2}** segment of ***rac*-E^{P2}$_{180}$(E^{P2}/L)$_{30}$** imparts water solubility to the copolymer and the resulting hydrogel, while the **E^{P2}/L** segment drives the solution to gel transition at physiological temperatures.[72] Although the **E^{P2}/L** block, is water soluble at ambient temperatures, it becomes hydrophobic at elevated temperatures due to LCST induced phase separation.[72] Unlike ***rac*-E^{P2}** which is water soluble at ambient and elevated temperatures due to its disordered and racemic confirmation, enantiomerically pure **E^{P2}** becomes hydrophobic at temperatures above 37 °C.[72] This leads to aggregation of the **E^{P2}/L** segments and hydrogel formation.[72]

Further work by the Deming group has helped to elucidate the relationship between ethylene glycol side-chains and their influence on LCST and thermo-responsive properties. In one study, poly(L-methionine) was alkylated with various oligoethylene glycol (OEG) groups and then demethylated to afford a series of poly(S-alkyl-L-homocysteine) polypeptides.[73] The OEG pendant groups possessed differing terminal groups and ethylene glycol repeat units, both of which were found to have predictable and scalable effects on LCST properties.[73] This discovery provided a modular approach towards controlling the transition temperature of thermo-responsive polypeptides.

1.4.2 Redox Responsive Polypeptides

Within the 20 naturally occurring amino acids, cysteine and methionine both contain sulfur in the sidechain. Cysteine and methionine are both highly sensitive to redox conditions.[74] Polypeptides containing cysteine or methionine residues can be formulated to respond to reducing or oxidizing reagents, such as the reducing intracellular space or the oxidative environments of cancerous cells.[58,75,76] Under oxidative conditions, cysteine residues and poly(L-cysteine) from disulfide bridges, while the thioethers in methionine residues and poly(L-methionine) are converted to sulfoxides.[74] The disulfide bridges formed during the oxidization of poly(L-cysteine) to poly(L-cystine) provide reversible chemical cross-links. These cross-links have been utilized for facile formation of nanostructures that can be disassembled in reducing environments. Previous work has utilized copolymers containing poly(L-cystine) for gene and drug encapsulation and *in vivo* delivery.[77] Poly(L-cysteine) has also been utilized for oxidation induced self-assembly into nanoparticles and gels.[78,79]

Oxidation of poly(L-methionine) has also been utilized for the design of redox responsive biomaterials. Upon oxidation, hydrophobic poly(L-methionine) is converted to water-soluble poly(L-methionine sulfoxide).[80] This change in solubility provides a valuable stimulus response to redox conditions. Previous work by the Deming group has produced poly(L-methionine sulfoxide) based vesicles that could be reduced by methionine reductase, triggering vesicle rupture and cargo release.[35] Furthermore, recent work by the Deming group has produced synthetic coacervates based on amino acid functionalized alkyl poly(L-homocysteine) and alkyl *rac*-poly(L-cysteine) polypeptides that could undergo reversible coacervate formation when oxidized and reduced.[57,66]

1.4.3 pH Responsive Polypeptides

pH responsive behavior is invaluable for the design of biomaterials to respond to differences between the physiological pH and the pH of endosomes, lysosomes, carcinogenic tissues, and the intra/extracellular space.[81,82] Polypeptides can be designed to respond to changes in pH to trigger assembly and disassembly of various biomaterials such as polyion complexes (PIC), hydrogels, and coacervates.[66,83,84] pH sensitive residues, such as poly(L-histidine) or poly(L-lysine) have previously been used for gene transfection and drug delivery.[83,85] Due to its pK_a being near physiological pH, poly(L-histidine) has been thoroughly studied for its pH responsive properties.[83,86] The Langer group has reported nanoparticles based on poly(L-histidine)–*b*-polyethylene glycol (PEG) copolymers for gene delivery.[85] In this work, the copolymers assembled into nanoparticles when complexed with DNA. These assemblies possessed a hydrophobic core due to the stoichiometric charge balance between the positively charged histidine residues and the negatively charged phosphate backbone of DNA.[85] Surrounding this core was a hydrated shell of water-soluble PEG chains. Once internalized, the nanoparticles are brought into endosomes where the acidic environment further protonates the poly(L-histidine) residues and triggers endosomal escape through the proton sponge effect.[83,87] The highly protonated poly(L-histidine) and genetic material are released into the intracellular space.[87] Similar strategies have also been utilized to design pH responsive nanoparticles for drug release and other forms of PIC mediated transfection via membrane penetration.[88]

Recent work on the development of synthetic coacervates has also utilized pH responsive behaviors to transition between miscible and bulk phases. These synthetic

coacervates relied on the pH sensitivity of primary amine groups within the polypeptide sidechains.[57,66] Since the pK_a of an N-terminal amino acid primary amine is close to physiological pH, the solubility of the polymers was greatly affected by the solution pH.[89] Under physiological conditions with chloride or phosphate counterions, these polypeptides were miscible with the aqueous solvent, but at slightly elevated pH, liquid-liquid phase separation would occur, leading to coacervate formation.[57,66] Lowering the pH would resolubilize the turbid solutions as the charged amines would increase the water solubility of the polypeptide.[57,66]

1.5 Conclusions Future Perspectives

The stimuli-responsive properties, facile polymerization, and vast range of functionality make polypeptides an invaluable material for biomedical applications. The chemical and structural diversity among amino acids provides polypeptides with near limitless functions along with superior biocompatibility. Furthermore, polypeptide chains can be readily degraded via enzymes. Advances in polypeptide chemistry have introduced non-canonical amino acids with a diverse range of functional groups into synthetic polypeptides, leading to novel and unique biomaterials with potential for therapeutic delivery. As research continues, the improved understanding of polypeptide self-assembly and composition will undoubtedly lead to the design of more stimuli-responsive materials.

As the field of polypeptide biomaterials expands, improvements in reducing the cost of synthesizing polypeptides and increasing production scale will be necessary. Currently, most synthetic polypeptides are produced on the gram scale and require extensive monomer purification and specific storage conditions. These barriers have

been reduced as new synthetic procedures for monomers are developed, but the cost and availability will need to be further reduced before synthetic polypeptides have widespread therapeutic applications.

1.6 References

1) Morris, R.; Black, K. A.; Stollar, E. J. Uncovering Protein Function: From Classification to Complexes. *Essays Biochem.* **2022**, *66* (3), 255–285.

2) Anfinsen, C. B. The Formation and Stabilization of Protein Structure. *Biochem. J.* **1972**, *128* (4), 737–749.

3) Sanvictores, T.; Farci, F. Biochemistry, Primary Protein Structure. In *StatPearls*; StatPearls Publishing: Treasure Island (FL), 2025.

4) Rosano, G. L.; Ceccarelli, E. A. Recombinant Protein Expression in Escherichia Coli: Advances and Challenges. *Front. Microbiol.* **2014**, *5*.

5) Jaradat, D. M. M. Thirteen Decades of Peptide Synthesis: Key Developments in Solid Phase Peptide Synthesis and Amide Bond Formation Utilized in Peptide Ligation. *Amino Acids* **2018**, *50* (1), 39–68.

6) Wu, Y.; Chen, K.; Wang, J.; Chen, M.; Dai, W.; Liu, R. Recent Advances and Future Developments in the Preparation of Polypeptides via N-Carboxyanhydride (NCA) Ring-Opening Polymerization. *J. Am. Chem. Soc.* **2024**, *146* (35), 24189–24208.

7) Brondyk, W. H. Selecting an Appropriate Method for Expressing a Recombinant Protein. *Methods Enzymol.* **2009**, *463*, 131–147.

8) Mishra, V. Affinity Tags for Protein Purification. *Curr. Protein Pept. Sci.* **2020**, *21* (8), 821–830.

9) Hayes, V. Y.; Urban, R. J.; Jiang, J.; Marcell, T. J.; Helgeson, K.; Mauras, N. Recombinant Human Growth Hormone and Recombinant Human Insulin-Like Growth Factor I Diminish the Catabolic Effects of Hypogonadism in Man: Metabolic and Molecular Effects1. *J. Clin. Endocrinol. Metab.* **2001**, *86* (5), 2211–2219.

10) Ashikaga, H.; Ben-Yehuda, O.; Chien, K. R. Chapter 1 - Biotechnology and Cardiovascular Medicine: Recombinant Protein Therapy. In *Molecular Basis of Cardiovascular Disease (Second Edition)*; Chien, K. R., Ed.; W.B. Saunders: Philadelphia, 2004; pp 1–15.

11) Beygmoradi, A.; Homaei, A.; Hemmati, R.; Fernandes, P. Recombinant Protein Expression: Challenges in Production and Folding Related Matters. *Int. J. Biol. Macromol.* **2023**, *233*, 123407.

12) Hou, Z.; Tuo, J.; Ma, X.; Huo, Y.-X. Recent Advances in Biosynthesis of Non-Canonical Amino Acids and Their Potentials in Strain Engineering. *Results Eng.* **2025**, *25*, 103641.

13) Chen, P. R.; Groff, D.; Guo, J.; Ou, W.; Cellitti, S.; Geierstanger, B. H.; Schultz, P. G. A Facile System for Encoding Unnatural Amino Acids in Mammalian Cells. *Angew. Chem. Int. Ed Engl.* **2009**, *48* (22), 4052–4055.

14) Fang, K. Y.; Lieblich, S. A.; Tirrell, D. A. Incorporation of Non-Canonical Amino Acids into Proteins by Global Reassignment of Sense Codons. *Methods Mol. Biol. Clifton NJ* **2018**, *1798*, 173–186.

15) Tymecka, D.; Misicka, A. Solution Phase Peptide Synthesis: The Case of Biphalin. *Methods Mol. Biol. Clifton NJ* **2020**, *2103*, 1–11.

16) Palomo, J. M. Solid-Phase Peptide Synthesis: An Overview Focused on the Preparation of Biologically Relevant Peptides. *RSC Adv.* **2014**, *4* (62), 32658–32672.

17) Coin, I.; Beyermann, M.; Bienert, M. Solid-Phase Peptide Synthesis: From Standard Procedures to the Synthesis of Difficult Sequences. *Nat. Protoc.* **2007**, *2* (12), 3247–3256.

18) Adhikary, R.; Dawson, P. E. In Situ Neutralization Protocols for Boc-SPPS. *Methods Mol. Biol. Clifton NJ* **2020**, *2103*, 29–40.

19) Behrendt, R.; White, P.; Offer, J. Advances in Fmoc Solid-phase Peptide Synthesis. *J. Pept. Sci.* **2016**, *22* (1), 4–27.

20) Dawson, P. E.; Muir, T. W.; Clark-Lewis, I.; Kent, S. B. H. Synthesis of Proteins by Native Chemical Ligation. *Science* **1994**, *266* (5186), 776–779.

21) Gong, H.; Holcomb, I.; Ooi, A.; Wang, X.; Majonis, D.; Unger, M. A.; Ramakrishnan, R. Simple Method To Prepare Oligonucleotide-Conjugated Antibodies and Its Application in Multiplex Protein Detection in Single Cells. *Bioconjugate Chem.* **2016**, *27* (1), 217–225.

22) Giesler, R. J.; Erickson, P. W.; Kay, M. S. Enhancing Native Chemical Ligation for Challenging Chemical Protein Syntheses. *Curr. Opin. Chem. Biol.* **2020**, *58*, 37–44.

23) Agouridas, V.; El Mahdi, O.; Diemer, V.; Cargoët, M.; Monbaliu, J.-C. M.; Melnyk, O. Native Chemical Ligation and Extended Methods: Mechanisms, Catalysis, Scope, and Limitations. *Chem. Rev.* **2019**, *119* (12), 7328–7443.

24) Presolski, S. I.; Hong, V. P.; Finn, M. G. Copper-Catalyzed Azide-Alkyne Click Chemistry for Bioconjugation. *Curr. Protoc. Chem. Biol.* **2011**, *3* (4), 153–162.

25) Meldal, M.; Tornøe, C. W. Cu-Catalyzed Azide−Alkyne Cycloaddition. *Chem. Rev.* **2008**, *108* (8), 2952–3015..

26) Deming, T. J. Facile Synthesis of Block Copolypeptides of Defined Architecture. *Nature* **1997**, *390* (6658), 386–389.

27) Deming, T. J.; Curtin, S. A. Chain Initiation Efficiency in Cobalt- and Nickel-Mediated Polypeptide Synthesis. *J. Am. Chem. Soc.* **2000**, *122* (24), 5710–5717.

28) Deming, T. J. Polypeptide Materials: New Synthetic Methods and Applications. *Adv. Mater.* **1997**, *9* (4), 299–311.

29) Deming, T. J. Synthesis and Self-Assembly of Well-Defined Block Copolypeptides via Controlled NCA Polymerization. In *Hierarchical Macromolecular Structures: 60 Years after the Staudinger Nobel Prize II*; Percec, V., Ed.; Springer International Publishing: Cham, 2013; pp 1–37.

30) Wu, X.; Yang, S.; Njus, J. M.; Nagarajan, R.; Cholli, A. L.; Samuelson, L. A.; Kumar, J. Solvent Specified Conformation in Poly(α-l-Glutamic Acid) Thin Films. *Biomacromolecules* **2004**, *5* (4), 1214–1218

31) Dong, L.; Chen, H.; Liu, T.; Zhu, J.; Yu, M.; Yuan, Q. Poly(l-Cysteine) Peptide Amphiphile Derivatives Containing Disulfide Bonds: Synthesis, Self-Assembly-Induced β-Sheet Nanostructures, pH/Reduction Dual Response, and Drug Release. *Biomacromolecules* **2021**, *22* (12), 5374–5381.

32) Kramer, J. R.; Deming, T. J. General Method for Purification of α-Amino Acid-N-Carboxyanhydrides Using Flash Chromatography. *Biomacromolecules* **2010**, *11* (12), 3668–3672.

33) Nowak, A. P.; Breedveld, V.; Pakstis, L.; Ozbas, B.; Pine, D. J.; Pochan, D.; Deming, T. J. Rapidly Recovering Hydrogel Scaffolds from Self-Assembling Diblock Copolypeptide Amphiphiles. *Nature* **2002**, *417* (6887), 424–428.

34) Benavides, I.; Deming, T. J. Controlled Synthesis and Properties of Poly(l-Homoserine). *ACS Macro Lett.* **2023**, *12* (4), 518–522.

35) Rodriguez, A. R.; Kramer, J. R.; Deming, T. J. Enzyme-Triggered Cargo Release from Methionine Sulfoxide Containing Copolypeptide Vesicles. *Biomacromolecules* **2013**, *14* (10), 3610–3614.

36 Gaucher, G.; Dufresne, M.-H.; Sant, V. P.; Kang, N.; Maysinger, D.; Leroux, J.-C. Block Copolymer Micelles: Preparation, Characterization and Application in Drug Delivery. *J. Controlled Release* **2005**, *109* (1), 169–188.

37) Leuchs, H. Ueber Die Glycin-Carbonsäure. *Berichte Dtsch. Chem. Ges.* **1906**, *39* (1), 857–861.

38) Tian, Z.-Y.; Zhang, Z.; Wang, S.; Lu, H. A Moisture-Tolerant Route to Unprotected α/β-Amino Acid N-Carboxyanhydrides and Facile Synthesis of Hyperbranched Polypeptides. *Nat. Commun.* **2021**, *12* (1), 5810.

39) Yakovlev, I.; Deming, T. J. Controlled Synthesis of Phosphorylcholine Derivatives of Poly(Serine) and Poly(Homoserine). *J. Am. Chem. Soc.* **2015**, *137* (12), 4078–4081.

40) Kramer, J. R.; Deming, T. J. Glycopolypeptides via Living Polymerization of Glycosylated-l-Lysine N-Carboxyanhydrides. *J. Am. Chem. Soc.* **2010**, *132* (42), 15068–15071.

41) Rhodes, A. J.; Deming, T. J. Soluble, Clickable Polypeptides from Azide-Containing N-Carboxyanhydride Monomers. *ACS Macro Lett.* **2013**, *2* (5), 351–354.

42) Perlin, P.; Gharakhanian, E. G.; Deming, T. J. Homoallylglycine Residues Are Superior Precursors to Orthogonally Modified Thioether Containing Polypeptides. *Chem. Commun.* **2018**, *54* (48), 6196–6199.

43) Smeets, N. M. B.; van der Weide, P. L. J.; Meuldijk, J.; Vekemans, J. A. J. M.; Hulshof, L. A. A Scalable Synthesis of L-Leucine-N-Carboxyanhydride. *Org. Process Res. Dev.* **2005**, *9* (6), 757–763.

44) Naamneh, M. S.; Lazarovici, P.; Katzhendler, J. Ring-Opening Polymerization (ROP) of Phenylalanine Derived O-Carboxyanhydride (OCA) Using Different Mono- and

Bimolecular Conjugated Catalysts and Amino or Alcohol Initiators. *ACS Appl. Polym. Mater.* **2022**, *4* (10), 7699–7709.

45 Kricheldorf, H. R.; and Mülhaupt, R. Mechanism of NCA Polymerization. VIII. The Base-Initiated Polymerization of β-Amino Acid NCAs. *J. Macromol. Sci. Part - Chem.* **1980**, *14* (3), 349–377.

46) Gradišar, Š.; Žagar, E.; Pahovnik, D. Ring-Opening Polymerization of N-Carboxyanhydrides Initiated by a Hydroxyl Group. *ACS Macro Lett.* **2017**, *6* (6), 637–640.

47) Kricheldorf, H. R.; Von Lossow, C.; Schwarz, G. Tertiary Amine Catalyzed Polymerizations of α-Amino Acid N-Carboxyanhydrides: The Role of Cyclization. *J. Polym. Sci. Part Polym. Chem.* **2006**, *44* (15), 4680–4695.

48) Vayaboury, W.; Giani, O.; Cottet, H.; Deratani, A.; Schué, F. Living Polymerization of α-Amino Acid N-Carboxyanhydrides (NCA) upon Decreasing the Reaction Temperature. *Macromol. Rapid Commun.* **2004**, *25* (13), 1221–1224.

49) Pickel, D. L.; Politakos, N.; Avgeropoulos, A.; Messman, J. M. A Mechanistic Study of α-(Amino Acid)-N-Carboxyanhydride Polymerization: Comparing Initiation and Termination Events in High-Vacuum and Traditional Polymerization Techniques. *Macromolecules* **2009**, *42* (20), 7781–7788.

50) Zou, J.; Fan, J.; He, X.; Zhang, S.; Wang, H.; Wooley, K. L. A Facile Glovebox-Free Strategy to Significantly Accelerate the Syntheses of Well-Defined Polypeptides by

N-Carboxyanhydride (NCA) Ring Opening Polymerizations. *Macromolecules* **2013**, *46* (10), 4223–4226.

51) Deming, T. J. Amino Acid Derived Nickelacycles: Intermediates in Nickel-Mediated Polypeptide Synthesis. *J. Am. Chem. Soc.* **1998**, *120* (17), 4240–4241.

52) Curtin, S. A.; Deming, T. J. Initiators for End-Group Functionalized Polypeptides via Tandem Addition Reactions. *J. Am. Chem. Soc.* **1999**, *121* (32), 7427–7428.

53) Detwiler, R. E.; Schlirf, A. E.; Kramer, J. R. Rethinking Transition Metal Catalyzed N-Carboxyanhydride Polymerization: Polymerization of Pro and AcOPro N-Carboxyanhydrides. *J. Am. Chem. Soc.* **2021**, *143* (30), 11482–11489.

54) Clauss, Z. S.; Kramer, J. R. Polypeptoids and Peptoid–Peptide Hybrids by Transition Metal Catalysis. *ACS Appl. Mater. Interfaces* **2022**, *14* (20), 22781–22789.

55) Deming, T. J. Cobalt and Iron Initiators for the Controlled Polymerization of α-Amino Acid-N-Carboxyanhydrides. *Macromolecules* **1999**, *32* (13), 4500–4502.

56) Deming, T. J.; Yu, M.; Curtin, S. A.; Hwang, J.; Wyrsta, M. D. Methods and Compositions for Controlled Polypeptide Synthesis. WO2000068252A1, November 16, 2000.

57) Morrison, C. A.; Chan, E. P.; Lee, T.; Deming, T. J. Switchable Coacervate Formation via Amino Acid Functionalization of Poly(Dehydroalanine). *Biomacromolecules* **2024**.

58) Deming, T. J. Sulfur Switches for Responsive Peptide Materials. *Acc. Chem. Res.* **2024**, *57* (5), 661–669.

59) Zhou, M. N.; Delaveris, C. S.; Kramer, J. R.; Kenkel, J. A.; Engleman, E. G.; Bertozzi, C. R. N-Carboxyanhydride Polymerization of Glycopolypeptides That Activate Antigen-Presenting Cells through Dectin-1 and Dectin-2. *Angew. Chem. Int. Ed.* **2018**, *57* (12), 3137–3142.

60) Benavides, I.; Raftery, E. D.; Bell, A. G.; Evans, D.; Scott, W. A.; Houk, K. N.; Deming, T. J. Poly(Dehydroalanine): Synthesis, Properties, and Functional Diversification of a Fluorescent Polypeptide. *J. Am. Chem. Soc.* **2022**, *144* (9), 4214–4223.

61) Kramer, J. R.; Deming, T. J. Preparation of Multifunctional and Multireactive Polypeptides via Methionine Alkylation. *Biomacromolecules* **2012**, *13* (6), 1719–1723.

62) Kramer, J. R.; Deming, T. J. Reversible Chemoselective Tagging and Functionalization of Methionine Containing Peptides. *Chem. Commun.* **2013**, *49* (45), 5144–5146.

63) Gharakhanian, E. G.; Deming, T. J. Chemoselective Synthesis of Functional Homocysteine Residues in Polypeptides and Peptides. *Chem. Commun.* **2016**, *52* (30), 5336–5339.

64) Deming, T. J. Functional Modification of Thioether Groups in Peptides, Polypeptides, and Proteins. *Bioconjug. Chem.* **2017**, *28* (3), 691–700..

65) Wollenberg, A. L.; O'Shea, T. M.; Kim, J. H.; Czechanski, A.; Reinholdt, L. G.; Sofroniew, M. V.; Deming, T. J. Injectable Polypeptide Hydrogels via Methionine Modification for Neural Stem Cell Delivery. *Biomaterials* **2018**, *178*, 527–545.

66) Scott, W. A.; Gharakhanian, E. G.; Bell, A. G.; Evans, D.; Barun, E.; Houk, K. N.; Deming, T. J. Active Controlled and Tunable Coacervation Using Side-Chain Functional α-Helical Homopolypeptides. *J. Am. Chem. Soc.* **2021**, *143* (43), 18196–18203.

67) Bernardes, G. J. L.; Chalker, J. M.; Errey, J. C.; Davis, B. G. Facile Conversion of Cysteine and Alkyl Cysteines to Dehydroalanine on Protein Surfaces: Versatile and Switchable Access to Functionalized Proteins. *J. Am. Chem. Soc.* **2008**, *130* (15), 5052–5053.

68) Morrison, C. A.; Chan, E. P.; Deming, T. J. Triggered Inversion of Dual Responsive Diblock Copolypeptide Vesicles. *J. Am. Chem. Soc.* **2025**, *147* (9), 7617–7623.

69) Stuart, M. A. C.; Huck, W. T. S.; Genzer, J.; Müller, M.; Ober, C.; Stamm, M.; Sukhorukov, G. B.; Szleifer, I.; Tsukruk, V. V.; Urban, M.; Winnik, F.; Zauscher, S.; Luzinov, I.; Minko, S. Emerging Applications of Stimuli-Responsive Polymer Materials. *Nat. Mater.* **2010**, *9* (2), 101–113.

70) Wei, M.; Gao, Y.; Li, X.; Serpe, M. J. Stimuli-Responsive Polymers and Their Applications. *Polym. Chem.* **2016**, *8* (1), 127–143.

71) Zhang, S.; Alvarez, D. J.; Sofroniew, M. V.; Deming, T. J. Design and Synthesis of Non-Ionic Copolypeptide Hydrogels with Reversible Thermoresponsive and Tunable Physical Properties. *Biomacromolecules* **2015**, *16* (4), 1331–1340.

72) Zhang, S.; Alvarez, D. J.; Sofroniew, M. V.; Deming, T. J. Design and Synthesis of Non-Ionic Copolypeptide Hydrogels with Reversible Thermoresponsive and Tunable Physical Properties. *Biomacromolecules* **2015**, *16* (4), 1331–1340.

73) Gharakhanian, E. G.; Deming, T. J. Role of Side-Chain Molecular Features in Tuning Lower Critical Solution Temperatures (LCSTs) of Oligoethylene Glycol Modified Polypeptides. *J. Phys. Chem. B* **2016**, *120* (26), 6096–6101.

74) Bin, P.; Huang, R.; Zhou, X. Oxidation Resistance of the Sulfur Amino Acids: Methionine and Cysteine. *BioMed Res. Int.* **2017**, *2017*, 9584932.

75) Banerjee, R. Redox Outside the Box: Linking Extracellular Redox Remodeling with Intracellular Redox Metabolism. *J. Biol. Chem.* **2012**, *287* (7), 4397–4402.

76) Vučetić, M.; Cormerais, Y.; Parks, S. K.; Pouysségur, J. The Central Role of Amino Acids in Cancer Redox Homeostasis: Vulnerability Points of the Cancer Redox Code. *Front. Oncol.* **2017**, *7*.

77) Zhang, X.; Kang, Y.; Liu, G.; Li, D.; Zhang, J.; Gu, Z.; Wu, J. Poly(Cystine–PCL) Based pH/Redox Dual-Responsive Nanocarriers for Enhanced Tumor Therapy. *Biomater. Sci.* **2019**, *7* (5), 1962–1972.

78) Stavroulaki, D.; Kyroglou, I.; Skourtis, D.; Athanasiou, V.; Thimi, P.; Sofianopoulou, S.; Kazaryan, D.; Fragouli, P. G.; Labrianidou, A.; Dimas, K.; Patias, G.; Haddleton, D. M.; Iatrou, H. Influence of the Topology of Poly(L-Cysteine) on the Self-Assembly, Encapsulation and Release Profile of Doxorubicin on Dual-Responsive Hybrid Polypeptides. *Pharmaceutics* **2023**, *15* (3), 790.

79) Dong, H.; Wang, M.; Fan, S.; Wu, C.; Zhang, C.; Wu, X.; Xue, B.; Cao, Y.; Deng, J.; Yuan, D.; Shi, J. Redox-Regulated Conformational Change of Disulfide-Rich Assembling Peptides. *Angew. Chem. Int. Ed.* **2022**, *61* (44), e202212829.

80) Gharakhanian, E. G.; Bahrun, E.; Deming, T. J. Influence of Sulfoxide Group Placement on Polypeptide Conformational Stability. *J. Am. Chem. Soc.* **2019**, *141* (37), 14530–14533.

81) Hu, Y.-B.; Dammer, E. B.; Ren, R.-J.; Wang, G. The Endosomal-Lysosomal System: From Acidification and Cargo Sorting to Neurodegeneration. *Transl. Neurodegener.* **2015**, *4*, 18.

82) Del Pozo, M. L.; Aguanell, A.; García-Junceda, E.; Revuelta, J. Lysozyme-Responsive Hydrogels of Chitosan-Streptomycin Conjugates for the On-Demand Release of Biofilm-Dispersing Enzymes for the Efficient Eradication of Oral Biofilms. *Chem. Mater.* **2024**, *36* (19), 9860–9873.

83) Hwang, H. S.; Hu, J.; Na, K.; Bae, Y. H. Role of Polymeric Endosomolytic Agents in Gene Transfection: A Comparative Study of Poly(l-Lysine) Grafted with Monomeric l-Histidine Analogue and Poly(l-Histidine). *Biomacromolecules* **2014**, *15* (10), 3577–3586.

84) Rizwan, M.; Yahya, R.; Hassan, A.; Yar, M.; Azzahari, A. D.; Selvanathan, V.; Sonsudin, F.; Abouloula, C. N. pH Sensitive Hydrogels in Drug Delivery: Brief History, Properties, Swelling, and Release Mechanism, Material Selection and Applications. *Polymers* **2017**, *9* (4), 137.

85) Putnam, D.; Zelikin, A. N.; Izumrudov, V. A.; Langer, R. Polyhistidine–PEG:DNA Nanocomposites for Gene Delivery. *Biomaterials* **2003**, *24* (24), 4425–4433.

86) Leng, Q.; He, J.; Anand, A.; Mixson, A. J. Delivery of mRNA with Histidine-Lysine Peptides. *Methods Mol. Biol. Clifton NJ* **2024**, *2822*, 367–386.

87) Degors, I. M. S.; Wang, C.; Rehman, Z. U.; Zuhorn, I. S. Carriers Break Barriers in Drug Delivery: Endocytosis and Endosomal Escape of Gene Delivery Vectors. *Acc. Chem. Res.* **2019**, *52* (7), 1750–1760.

88) Li, W.; Liu, Y.; Du, J.; Ren, K.; Wang, Y. Cell Penetrating Peptide-Based Polyplexes Shelled with Polysaccharide to Improve Stability and Gene Transfection. *Nanoscale* **2015**, *7* (18), 8476–8484.

89) Chambers, R. W.; Carpenter, F. H. On the Preparation and Properties of Some Amino Acid Amides. *J. Am. Chem. Soc.* **1955**, *77* (6), 1522–1526.

Chapter 2: Switchable Coacervate Formation via Amino Acid Functionalization of Poly(dehydroalanine)

Adapted from: Morrison, C. A.; Chan, E. P.; Lee, T.; Deming, T. J. *Biomacromolecules* **2024** *25* (4), 2554-2562.

2.1 Abstract

Our group recently developed a family of side-chain amino acid-functionalized poly(S-alkyl-L-homocysteines), **Xaa-C^{H}** (Xaa = generic amino acid), which possess the ability to form environmentally responsive coacervates in water. In an effort to further study how the molecular structure affects polypeptide coacervate formation, we prepared side-chain amino acid-functionalized poly(S-alkyl-*rac*-cysteines), **Xaa-*rac*-C**, via post-polymerization modification of poly(dehydroalanine), **A^{DH}**. The use of the **A^{DH}** platform allowed straightforward synthesis of a diverse range of side-chain amino acid-functionalized polypeptides via direct reaction of unprotected L-amino acid 2-mercaptoethylamides with **A^{DH}**. Despite their differences in the main-chain structure, we found that **Xaa-*rac*-C** can form coacervates with properties similar to those seen with **Xaa-C^{H}**. These results suggest that the incorporation of side-chain amino acids onto polypeptides may be a way to generally favor coacervation. The incorporation of L-methionine in **Met-*rac*-C** allowed the preparation of coacervates with improved stability against high ionic strength media. Further, the presence of additional thioether groups in **Met-*rac*-C** resulted in an increased solubility change upon oxidation allowing facile reversible redox switching of coacervate formation in aqueous media.

2.2 Introduction

Biomimetic coacervates are of interest as model systems to enable a better understanding of natural condensates as well as for the delivery of therapeutics and for

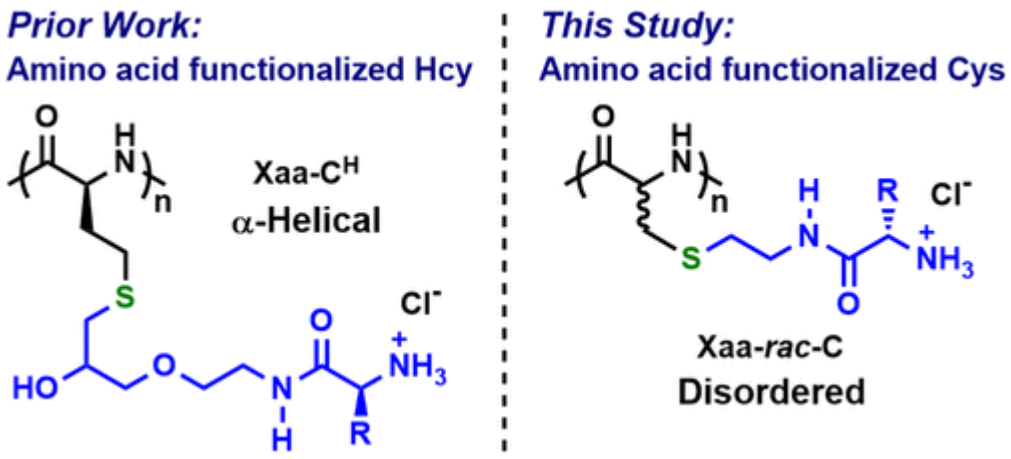

Scheme 2.1. Comparison of α-Helical polymers of amino acid-functionalized homocysteines (Hcy), **Xaa-C^{H}**, to disordered polymers of amino acid-functionalized cysteines (Cys), **Xaa-*rac*-C** Xaa = generic amino acid

the development of environmental stimuli-responsive biomaterials.[1–4] For these uses, it is desirable that coacervate formation and properties can be adjusted at the molecular level, and that coacervation can also be readily switched on or off under physiologically relevant conditions.[5-9] Many coacervate systems are either based on complex biopolymers (e.g., proteins or statistical copolymers) where structure–property relationships are not well understood leading to challenges in predictable tuning of properties or based on simple polymers (e.g., poly(L-lysine)) that lack the ability to respond to physiologically relevant stimuli.[10-15] Our group recently developed a class of α-helical, side-chain amino acid-functionalized poly(S-alkyl-L-homocysteines), **Xaa-C^{H}**, that possess the ability to form environmentally responsive coacervates in water (**Scheme 2.1**).[16]

Since they are compositionally uniform, **Xaa-C^{H}** homopolypeptides allow for a more detailed molecular understanding of structure–property relationships when polymer

side-chain groups are altered, as compared to side-chain variation in statistical copolymers or protein sequences.[16] We had previously found that hydrophobicity of side-chain amino acid groups could be varied to control coacervate versus precipitate formation and to adjust how temperature, pH, and counterion valency affect coacervate formation.[16] Further, oxidation of thioether linkages in **Leu-C^{H}** was found to result in the formation of disordered conformations and increased polypeptide hydrophilicity, which acted as a mild, biomimetic switch to turn off coacervate formation via active control.[16]

Here, we sought to test if the incorporation of side-chain amino acid groups onto a different polypeptide backbone could also enable coacervate formation. These experiments were expected to aid understanding of how polypeptide chain conformation and flexibility influence coacervate formation and properties. Poly(dehydroalanine), **A^{DH}**, was chosen as it can be prepared with controlled length, and it is readily post-polymerization functionalized under mild conditions in high yield by reaction with thiol nucleophiles.[17] The products of such functionalization are poly(S-alkyl-*rac*-cysteines), which are expected to adopt disordered conformations in solution due to backbone heterochirality.[17] Reactions of **A^{DH}** with unprotected L-amino acid 2-mercaptoethylamides were thus envisioned to give side-chain amino acid-functionalized poly(S-alkyl-*rac*-cysteines), **Xaa-*rac*-C**, which would possess side chains structurally similar to those in **Xaa-C^{H}** but with backbones that would be expected to adopt disordered instead of α-helical conformations (**Scheme 2.1**). In addition to the goal of creating new coacervate-forming polypeptides with tunable properties, we also sought to develop **Xaa-*rac*-C** polypeptide synthetic methodology since it has the potential for more straightforward

preparation of a diverse range of polypeptides with highly functional side-chain groups as compared to our method for the synthesis of **Xaa-C^{H}**.[16-17]

2.3 Results and Discussion

To obtain samples for comparison to previously reported **Xaa-C^{H}**, a series of amino acid-functionalized poly(S-alkyl-*rac*-cysteines), **Xaa-*rac*-C$_n$**, were prepared (**Scheme 2.2**). These samples all contain nonpolar amino acids and terminal primary α-amine groups in the side chains, which allow the formation of cationic polypeptides similar to **Xaa-C^{H}**. A modular approach was used to prepare samples of **Xaa-*rac*-C$_{65}$** by using readily prepared L-amino acid 2-mercaptoethylamides **1a**–**1e**, (**Table 2.1**), where the amino acids L-alanine (Ala), L-valine (Val), L-leucine (Leu), methionine (Met), and L-proline (Pro) were selected to provide a range of hydrophobicity.

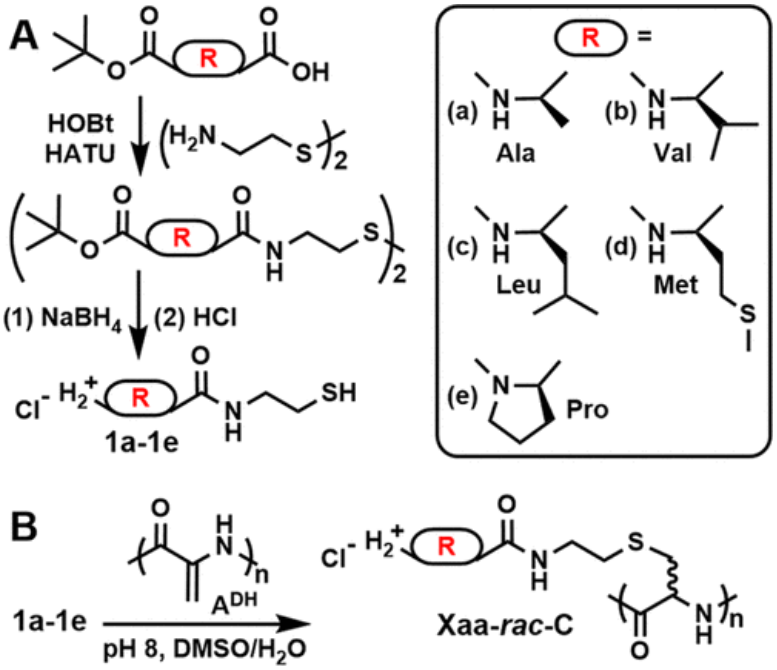

Scheme 2.2. Synthesis of L-Amino Acid 2-Mercaptoethylamides **1a**–**1e** and Corresponding Polypeptides **Xaa-*rac*-C$_n$**.

Table 2.1. Isolated yields of L-amino acid 2-mercaptoethylamides (**1a-1e**) and isolated yields and molecular weight properties of poly(*S*-(*tert*-butoxycarbonylmethyl)-L-cysteine)$_{65}$ (**C$^{BCM}_{65}$)** and **Xaa-*rac*-C$_{65}$** polypeptides. All polypeptides had average degrees of polymerization ranging from 62 to 68 by ^{1}H NMR end-group analysis. a = Yields are total isolated yield from starting amino acid (3 steps). b = M_n and M_w for **Xaa-*rac*-C$_{65}$** polypeptides were calculated relative to PMMA standards in NaTFA/TFE; M_n and M_w for **C$^{BCM}_{65}$** was calculated relative to polyethylene glycol (PEG) standards in KTFA/HFIP. C = ***Đ* =** M_w/M_n. N/A = not applicable.

Sample	Yield 1a-1e (%)[a]	Yield Polymer (%)	M_n[b]	M_w[b]	*Đ*[c]
C$^{BCM}_{65}$	N/A	92	5,000	6,940	1.38
Ala-*rac*-C$_{65}$	65	71	11,040	14,600	1.32
Val-*rac*-C$_{65}$	83	70	10,330	13,240	1.28
Leu-*rac*-C$_{65}$	73	81	9,320	14,020	1.50
Met-*rac*-C$_{65}$	68	93	10,230	12,960	1.27
Pro-*rac*-C$_{65}$	74	61	10,280	14,310	1.39

Using our recently developed methodology for preparation and modification of **A^{DH}**, the free thiol groups in **1a**–**1e** were individually reacted with a common **A$^{DH}_{65}$** precursor to give each **Xaa-*rac*-C$_{65}$** sample (overall isolated yields for complete polypeptide modification *ca*. 70–93%, **Scheme 2.2** and **Table 2.1**).[17] The chain length used was selected to enable comparison to previously published **Xaa-C^{H}** samples of similar length.[16] **Xaa-*rac*-C$_{65}$** was purified by dialysis against aqueous HCl (3 mM) followed by deionized water to give polypeptides as white powders after lyophilization. All

of the isolated protonated polypeptides **Xaa-*rac*-C$_{65}$** as Cl^- salts were soluble in deionized water at 20 °C.

A^{DH} residues were fully converted into the corresponding functionalized residues for each **Xaa-*rac*-C$_{65}$** as determined by ^{1}H and ^{13}C NMR analyses, and we also found no evidence for chain degradation during modification similar to other previously reported reactions on **A^{DH}** (**Figure 2.1**).[17] Circular dichroism analysis of **Leu-*rac*-C$_{65}$** in water gave no signal as expected for a racemic polypeptide (**Figure 2.2**).[17] This result suggests that there is no chiral ordering of the homochiral side-chain groups, which also supports the adoption of disordered conformations. GPC analysis of **Xaa-*rac*-C$_{65}$** samples was accomplished using trifluoroethanol (TFE) containing sodium trifluoroacetate mobile phase.

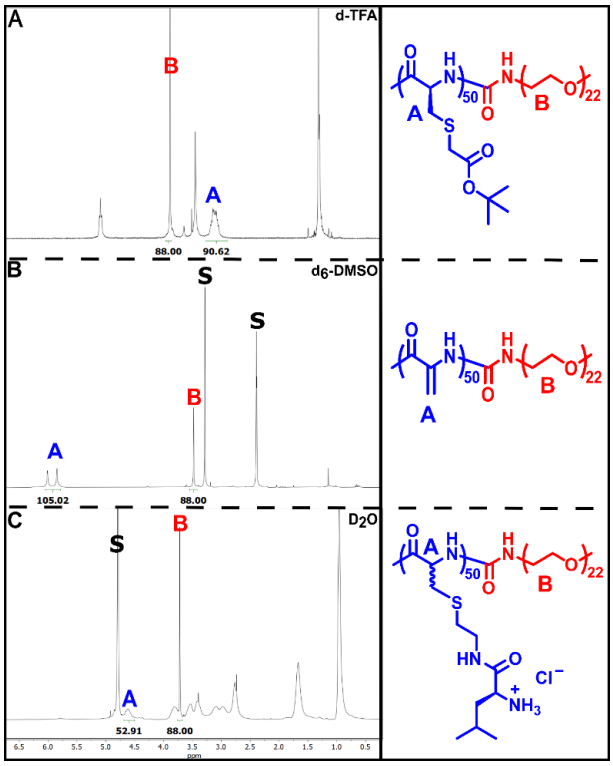

Figure 2.1. ^{1}H NMR spectra of pegylated polypeptide intermediates in the synthesis of **Leu-*rac*-C$_{50}$** showing negligible polypeptide chain cleavage during modifications. ^{1}H NMR spectra and structures of A) **PEG$_{22}$-*b*-C$^{BCM}_{50}$**, B) **PEG$_{22}$-*b*-A$^{DH}_{50}$**, and C) **PEG$_{22}$-*b*-(Leu-*rac*-C)$_{50}$**, where PEG = polyethylene glycol. Solvents are noted in upper right of each spectrum. S = solvent resonances. Degree of polymerization of the polypeptide segments was designated as an average value of 50.

Under these conditions, all **Xaa-*rac*-C$_{65}$** samples gave monomodal distributions with some apparent high molecular weight tailing likely due to polypeptide aggregation (**Figure 2.3**). Chain lengths were also determined using end-group analysis (**Table 2.1**). Attempts to perform GPC in other solvents (DMF, hexafluoroisopropanol) or at higher concentrations in TFE showed increased levels of polypeptide aggregation. Molecular weights and dispersity values were found to be similar for all **Xaa-*rac*-C$_{65}$** samples analyzed in trifluoroethanol (**Table 2.1**), consistent with the expected structures.

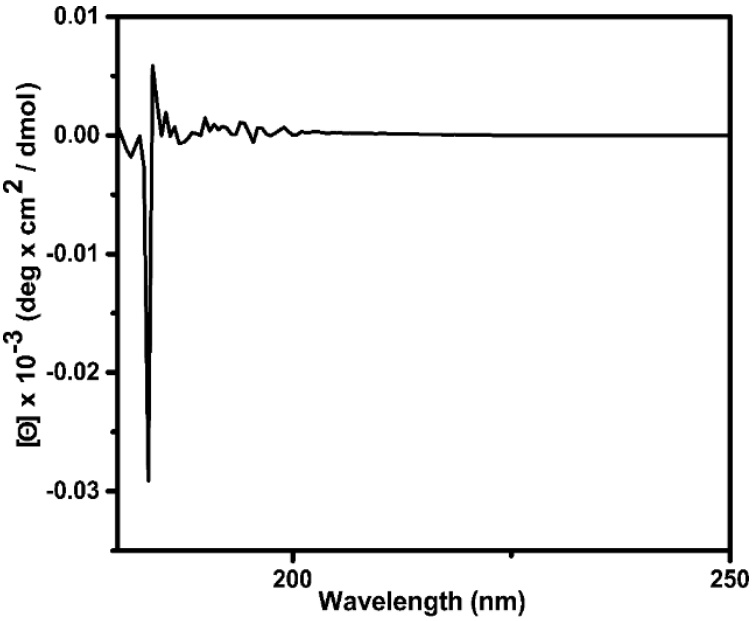

Figure 2.2. Circular dichroism spectrum of **Leu-*rac*-C$_{65}$** (0.5 mg/mL) in DI water adjusted to pH 7.0 with 0.1 M NaOH.

Overall, **Xaa-*rac*-C$_{65}$** were successfully prepared in good yields and high purity. A potential advantage of this process for preparation of **Xaa-*rac*-C** versus that for **Xaa-C^{H}** is the ability to directly conjugate a more diverse range of amino acids (e.g., Met) to the polypeptide backbone. In addition, the enhanced reactivity of **A^{DH}** with thiols versus amines eliminates the need to protect amine groups during conjugation.

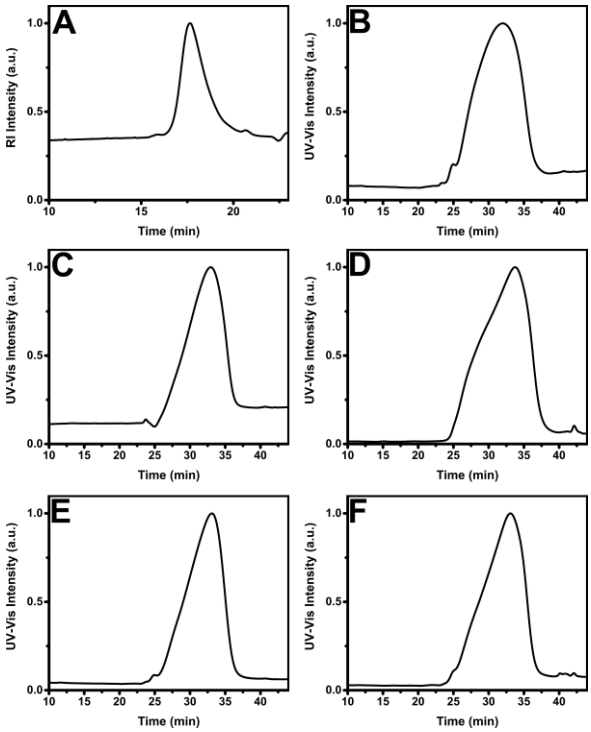

Figure 2.3. GPC analysis of polypeptides. A) $\mathbf{C^{BCM}_{65}}$ (20 mg/mL) in HFIP with 0.5% (w/v) KTFA at 40 °C. B) **Ala-*rac*-C$_{65}$** (0.5 mg/mL) in TFE with 20 mM NaTFA. C) **Val-*rac*-C$_{65}$** (0.5 mg/mL) in TFE with 20 mM NaTFA. D) **Leu-*rac*-C$_{65}$** (1.0 mg/mL) in TFE with 20 mM NaTFA. E) **Met-*rac*-C$_{65}$** (0.5 mg/mL) in TFE with 20 mM NaTFA. F) **Pro-*rac*-C$_{65}$** (0.5 mg/mL) in TFE with 20 mM NaTFA. All GPC analyses in TFE were at 25 °C.

To compare the solution properties of **Xaa-*rac*-C$_{65}$** with those of $\mathbf{Xaa\text{-}C^{H}}$, we examined the degree of **Xaa-*rac*-C$_{65}$** protonation in 20 mM aqueous NaCl as a function of pH. Similar to results obtained with $\mathbf{Xaa\text{-}C^{H}}$, ζ-potentials for solutions of **Xaa-*rac*-C$_{65}$** measured at different pH revealed transitions from positive to moderately negative values between pH 7 and 10, which indicate a change in the α-amine groups from protonated to nonprotonated states over this pH range (**Figure 2.4**).[16, 24] This transition correlates with the expected pK_a range of α-amino amide groups (*ca*. 8) and was corroborated by analysis of other control samples that included $\mathbf{Leu\text{-}C^{H}_{60}}$ and poly(l-

lysine·HCl)$_{60}$, **K$_{60}$**, where the latter undergoes a charged to noncharged transition at a much higher pH (pK_a *ca.* 10) (**Figure 2.4**).[24-26]

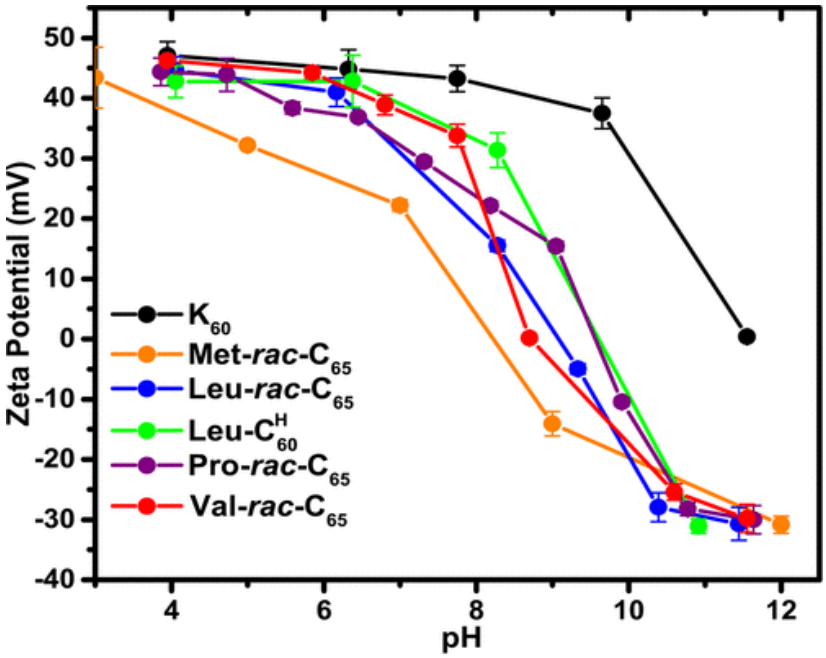

Figure 2.4. ζ-Potential measurements of polypeptide samples as a function of solution pH. Measurements of **Xaa-*rac*-C$_{65}$** and reference polypeptides were performed at 5.0 mg/mL in 20 mM NaCl at 20 °C. **Met-*rac*-C$_{65}$** = orange; **Leu-*rac*-C$_{65}$** = blue; **Pro-*rac*-C$_{65}$** = magenta; **Val-*rac*-C$_{65}$** = red; poly(L-lysine·HCl)$_{60}$ (**K$_{60}$**) = black; **Leu-C$^{H}_{60}$** = green. Error bars represent standard deviations of triplicate measurements.

It is noteworthy that the **Met-*rac*-C$_{65}$** sample was found to be partially protonated at lower pH compared to the other **Xaa-*rac*-C$_{65}$** samples, where the observed broader transition may reflect a wider range of pK_a values for this polypeptide. Overall, it was found that **Xaa-*rac*-C$_{65}$** can undergo protonation and deprotonation in water within a physiologically relevant range that is advantageous for adjustment of physical properties.

We evaluated physical properties by studying the phase behavior of **Xaa-*rac*-C$_{65}$** as functions of varying pH, temperature, and counterions in water. Initially, dilute

aqueous solutions of **Xaa-*rac*-C$_{65}$** (3.0 mg/mL) were prepared in 150 mM phosphate buffer saline (PBS) buffer at pH values ranging from 6.8 to 8.0, which were chosen to include varying degrees of polypeptide protonation. These solutions were heated at a controlled rate up to 90 °C, and optical transmittance at 500 nm was measured as a function of temperature. The samples **Ala-*rac*-C$_{65}$** and **Pro-*rac*-C$_{65}$** were the least hydrophobic and were found to both remain soluble up to 90 °C (**Table 2.2**). The **Leu-*rac*-C$_{65}$** and **Met-*rac*-C$_{65}$** samples are more hydrophobic and were found to phase separate by variation of both pH and temperature (**Figures 2.5** and **Table 2.2**).

Reversible cloud points were observed for the Leu and Met samples upon increase in temperature, indicative of lower critical solution temperature (LCST) induced phase separation, with cloud point temperatures (T_{cp}) that decreased with increasing hydrophobicity of side-chain amino acids in the approximate order Val < Leu ~ Met (**Table 2.2**).[27-28] Cloud point temperatures for these samples also decreased as pH was increased, which is consistent with the properties previously observed with **Xaa-C^{H}**.[16] These results confirm that **Leu-*rac*-C$_{65}$**, and **Met-*rac*-C$_{65}$** in 150 mM PBS buffer are able to phase separate by variation of temperature, ionic strength, and solution pH within a physiologically relevant range. It was also possible to tune T_{cp} in a predictable manner by variation of polypeptide side-chain amino acid hydrophobicity.

Table 2.2. Coacervate transition temperatures for aqueous solutions of **Xaa-*rac*-C$_{65}$** containing different counterions[a]

		T_{cp} (°C) for Xaa-*rac*-C$_{65}$				
counterion	**ion valency at pH 7.0**	**Ala**	**Val**	**Leu**	**Met**	**Pro**
chloride	–1.0	sol	sol	sol	sol	sol
phosphate	–1.4	sol	71	45	41	sol
pyrophosphate	–2.7	×	×	–	–	×
tripolyphosphate	–4.0	ppt	–	–	–	ppt

[a]Cloud point temperatures (T_{cp}) were measured for 3.0 mg/mL solutions of **Xaa-*rac*-C$_{65}$** in the presence of different counterions (12 mM) in 150 mM NaCl at pH 7.0. sol = polypeptide was soluble up to 90 °C; – = polypeptide formed a coacervate at 20 °C; × = not performed; ppt = polypeptide formed a solid precipitate, not a coacervate, at 20 °C.

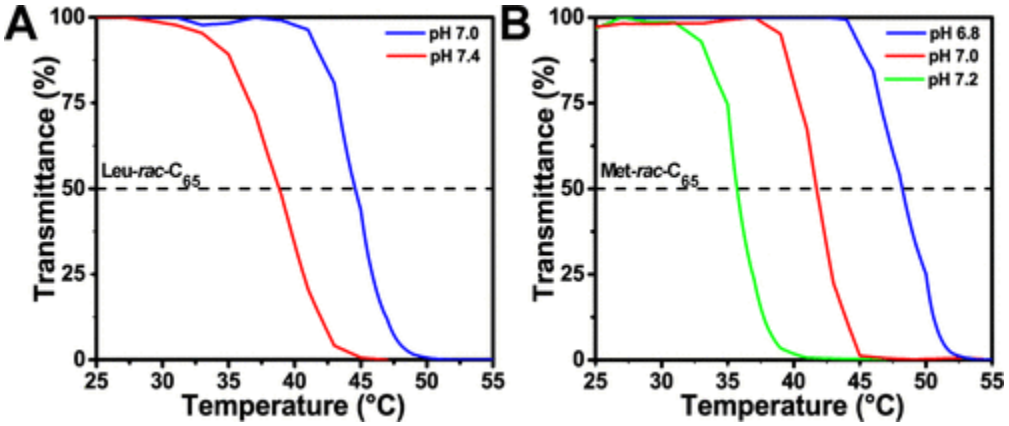

Figure 2.5. Temperature-dependent coacervate formation in solutions of (A) **Leu-*rac*-C$_{65}$** and (B) **Met-*rac*-C$_{65}$** as a function of pH. Panels show optical transmittance at 500 nm for 3.0 mg/mL solutions of polypeptides in 150 mM PBS buffer measured over a range of temperatures at different pH.

Since we observed that the substitution of phosphate for chloride decreased the solubility of **Xaa-*rac*-C$_{65}$** in water, the effects of counterion valency on aqueous phase

separation were further investigated. Aqueous samples of **Xaa-*rac*-C$_{65}$** (3.0 mg/mL) were prepared in 150 mM NaCl at pH 7.0 and then mixed with sodium salts of anionic counterions with different valencies (12 mM final concentration, **Table 2.2**). Similar to results observed with **Xaa-C^{H}**, as anion valency was increased, all samples became less soluble in water.[16] This result is explained by increased stability of ion complexes between the cationic polypeptides and anions with higher valency. Even the more hydrophilic **Ala-*rac*-C$_{65}$** and **Pro-*rac*-C$_{65}$** samples were found to undergo phase separation in the presence of tripolyphosphate anions at 20 °C.

As they both contain the same side-chain amino acid functionality, comparison of the **Leu-*rac*-C$_{65}$** and **Leu-C$^{H}_{60}$** samples can provide some insight into how the different polypeptide backbones affect phase separation properties. In the presence of counterions of different valencies, **Leu-*rac*-C$_{65}$** possesses a lower T_{cp} compared **Leu-C$^{H}_{60}$** under otherwise identical conditions (e.g., T_{cp} =< 20 °C versus 57 °C with pyrophosphate, respectively).[16] This trend suggests that disordered ***rac*-C** chains provide a more hydrophobic local environment compared to the α-helical **C^{H}** chains, which may also be partially explained by the presence of polar hydroxyl groups in the side-chains of **Xaa-C$^{H}_{60}$** polypeptides.

To investigate the nature of phase separation described above for **Xaa-*rac*-C_{65}** samples, the suspensions formed in the presence of tripolyphosphate anions at pH 7.0 were allowed to settle onto glass slides and were examined using optical microscopy. Images of the complexes formed with least hydrophobic **Ala-*rac*-C_{65}** and **Pro-*rac*-C_{65}** samples showed irregular edges and clusters consistent with the formation of solid precipitates (**Figure 2.6**).

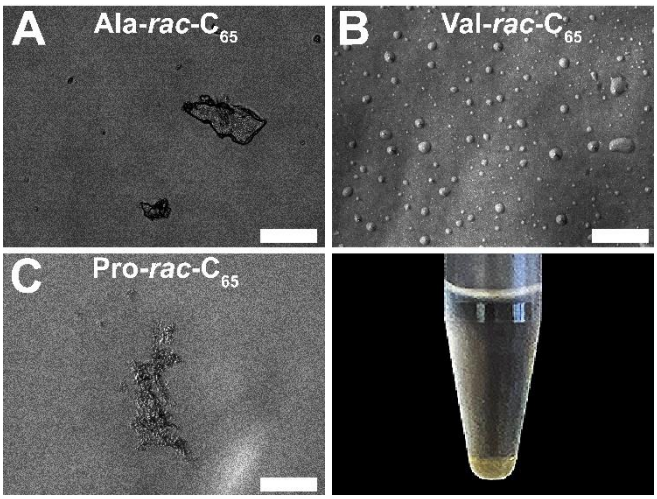

Figure 2.6. Optical micrographs of **Xaa-*rac*-C_{65}** polypeptides mixed with sodium tripolyphosphate (TPP). Solutions of **Xaa-*rac*-C_{65}** at 3.0 mg/mL in 150 mM NaCl at 20 °C and pH 7.0 were mixed with TPP (12 mM final concentration) and the resulting turbid suspensions were allowed to settle onto glass slides before imaging. A) **Ala-*rac*-C_{65}** + TPP; B) **Val-*rac*-C_{65}** + TPP; C) **Pro-*rac*-C_{65}** + TPP. Scale bars = 20 μm. D) Image of **Met-*rac*-C_{65}** + TPP coacervate (3.0 mg/mL in 150 mM NaCl at 20 °C and pH 7.0) after centrifugation. Condensed coacervate bulk phase can be seen at the bottom of the tube.

However, images of tripolyphosphate complexes with **Val-*rac*-C_{65}**, **Leu-*rac*-C_{65}**, and **Met-*rac*-C_{65}** all showed smooth outlines and coalescing droplets consistent with the formation of liquid coacervate phases **(Figure 2.7a,b and Figure 2.6b**).[5, 6]

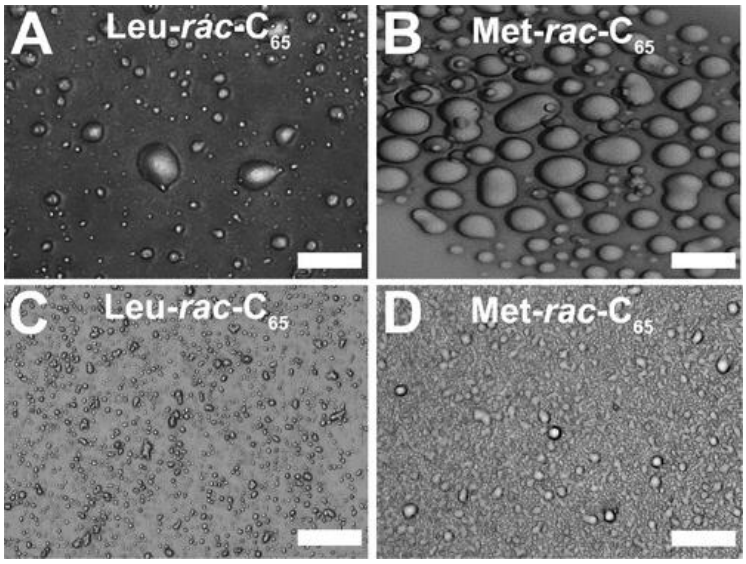

Figure 2.7. Optical micrographs of **Leu-*rac*-C$_{65}$** and **Met-*rac*-C$_{65}$** mixed with sodium tripolyphosphate (TPP) or polyadenylic acid (polyA). Solutions of either **Leu-*rac*-C$_{65}$** or **Met-*rac*-C$_{65}$** at 3.0 mg/mL in 150 mM NaCl at 20 °C and pH 7.0 were mixed with TPP (12 mM final concentration) or at 5.0 mg/mL in 150 mM NaCl at 20 °C and pH 7.0 with polyA (0.015 mM final concentration). The resulting turbid suspensions were allowed to settle onto glass slides before imaging. (A) **Leu-*rac*-C$_{65}$** + TPP; (B) **Met-*rac*-C$_{65}$** + TPP; (C) **Leu-*rac*-C$_{65}$** + polyA; (D) **Met-*rac*-C$_{65}$** + polyA. Scale bars = 20 μm.

For additional confirmation of coacervate formation, centrifugation of **Met-*rac*-C$_{65}$** with tripolyphosphate suspension resulted in the formation of two separate liquid layers (**Figure 2.8**). A thin film of the coacervate of **Met-*rac*-C$_{65}$** with tripolyphosphate was also spread as a thin film on a glass slide. A defect made in the film was observed to heal

by the flow of coacervate within *ca.* 30 min, which confirmed that the sample possessed viscous liquid properties (**Figure 2.8**).

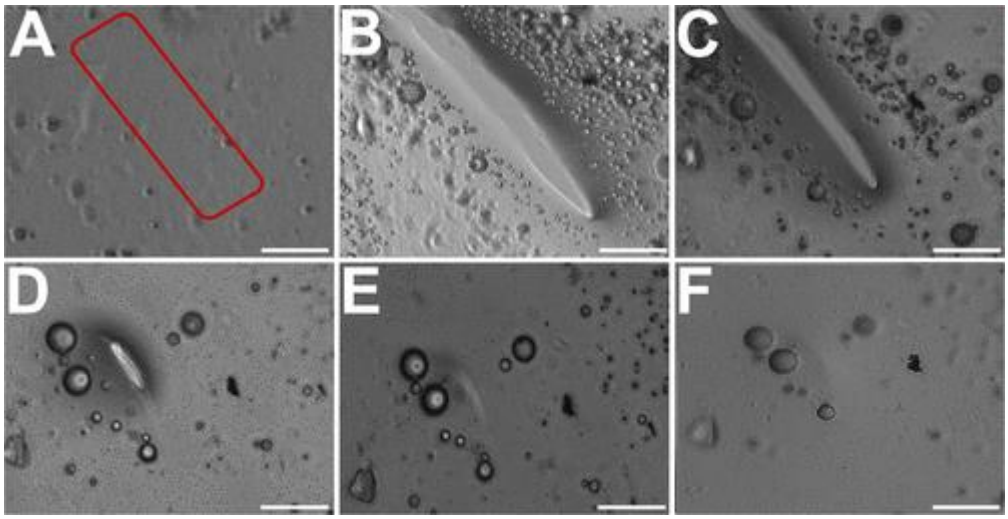

Figure 2.8. Viscous liquid properties observed over time in optical micrographs of a coacervate film prepared by mixing **Met-*rac*-C_{65}** at 3.0 mg/mL with TPP in 150 mM NaCl at 20 °C and pH 7.0. (A) The coacervate was collected by centrifugation and then spread as a film on a glass slide. PBS buffer (150 mM, pH 7.0) was placed on top of the film to prevent evaporation, and a defect was made by scraping the film with a needle (red box area). (B) Image of the film 5 min after defect was made. (C) Image of the film after 10 min; note decrease in defect size due to flow of coacervate. (D) Image of the film after 20 min. (E) Image of the film after 25 min. (F) Image of the film after 30 min; note defect has completely healed. Scale bars = 20 μm.

In addition to coacervation with tripolyphosphate, **Leu-*rac*-C_{65}** and **Met-*rac*-C_{65}** were also able to form complex coacervates with a model RNA sequence, polyadenylic acid, at 20 °C (**Figure 2.7 c,d**). These results are comparable to those found with **Xaa-C^H** samples and suggest that the combination of hydrophobic and charged

amino acid groups in side chains is a robust means to obtain coacervate-forming polypeptides.

Coacervate formation with **Leu-*rac*-C$_{65}$** and **Met-*rac*-C$_{65}$** was found to be reversible with no irreversible formation of polypeptide aggregates. Multiple heating and cooling cycles were applied to samples of **Leu-*rac*-C$_{65}$** and **Met-*rac*-C$_{65}$** in PBS buffer at pH 7.2 and monitored by optical transmittance, where coacervation and complete dissolution were observed with each thermal cycle **(Figure 2.9a,b**). Finally, to assess salt stability, complexes of **Leu-*rac*-C$_{65}$** and **Met-*rac*-C$_{65}$** with tripolyphosphate were prepared in aqueous solutions containing 0.1 to 2 M NaCl. The fraction of each polypeptide that partitioned into the coacervate phase decreased with increasing ionic strength, and phase separation did not occur at higher salt concentrations (**Figure 2.9c,d**). The **Leu-*rac*-C$_{65}$** and **Met-*rac*-C$_{65}$** coacervates were found to be significantly more stable at higher ionic strength (stable to 1 and 2 M NaCl, respectively) compared to the previously reported **Leu-C$^{H}_{60}$** sample (stable to 250 mM NaCl) under otherwise identical conditions.[16] The increased stability of the **Xaa-*rac*-C$_{65}$** samples is likely due to their increased hydrophobicity compared to **Xaa-C^{H}** samples, as noted above. The

increased salt stability of **Met-*rac*-C$_{65}$** coacervates may be beneficial for downstream applications.

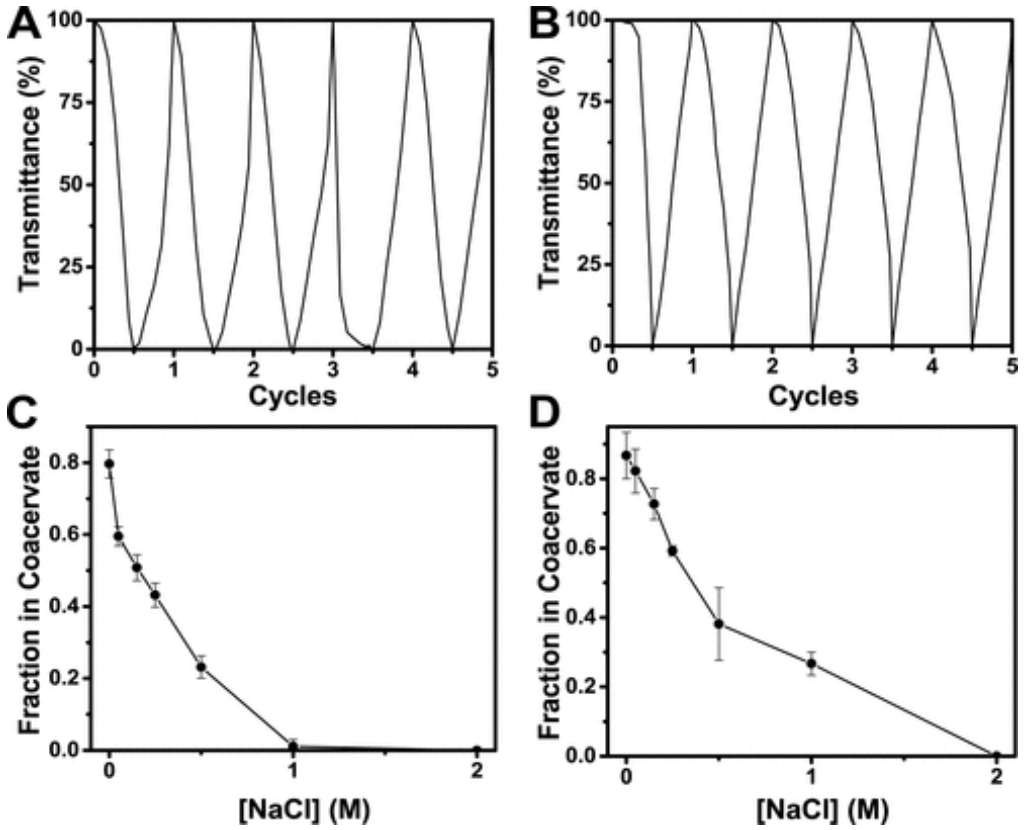

Figure 2.9. Reversibility of temperature-dependent coacervate formation for (A) **Leu-*rac*-C$_{65}$** and (B) **Met-*rac*-C$_{65}$** in PBS buffer as determined by optical transmittance at 500 nm. Samples were prepared at 3.0 mg/mL in 150 mM PBS buffer at pH 7.2 and subjected to repeated thermal cycling between 25 and 40 °C. Samples were heated and cooled at the rate of 3 °C/min. Coacervate formation of (C) **Leu-*rac*-C$_{65}$** and (D) **Met-*rac*-C$_{65}$** both mixed with TPP as a function of sodium chloride concentration. Fraction in Coacervate = (mass of polypeptide in coacervate phase)/(total mass of polypeptide). Samples were prepared by mixing each polypeptide (3.0 mg/mL) in media with TPP (12 mM) and different concentrations of NaCl at 20 °C and pH 7.0. Error bars represent standard deviations of triplicate measurements.

We had previously shown that the thioether linkages in **Leu-C^{H}_{60}** could be oxidized under mild conditions, which resulted in the disruption of its α-helical conformation as well as dissolution of its coacervate with tripolyphosphate due to increased hydrophilicity of the resulting sulfoxide groups.[16] Since thioether oxidation provides a mild means to actively control coacervation under physiologically relevant conditions, we sought to evaluate its effect on coacervates of **Leu-*rac*-C_{65}** and **Met-*rac*-C_{65}**. Samples of **Leu-*rac*-C_{65}** and **Met-*rac*-C_{65}** were oxidized to give the corresponding sulfoxide derivatives **Leu-*rac*-C^{O}_{65}** and **Met^{O}-*rac*-C^{O}_{65}** using *tert*-butyl hydroperoxide in water (**Scheme 2.3**).[24] The increased hydrophilicity of **Leu-*rac*-C^{O}_{65}** and **Met^{O}-*rac*-C^{O}_{65}** relative to the unoxidized precursors had a striking effect on their ability to form coacervates. Mixtures of aqueous solutions of **Leu-*rac*-C^{O}_{65}** and **Met^{O}-*rac*-C^{O}_{65}** with tripolyphosphate anions at pH 7.0 and 20 °C did not form coacervates and appeared to remain as transparent solutions.

However, heating of the **Leu-*rac*-C^{O}_{65}** sample containing tripolyphosphate was able to induce coacervate formation at *ca*. 33 °C. Alternatively, raising the pH of this mixture to 8.5 at 20 °C also resulted in coacervate formation (**Figure 2.10**). Mixture of an aqueous solution of **Leu-*rac*-C^{O}_{65}** with polyadenylic acid at pH 7.0 and 20 °C also resulted in coacervate formation (**Figure 2.11**). These results show that **Leu-*rac*-C^{O}_{65}** is more hydrophilic than its unoxidized precursor **Leu-*rac*-C_{65}** but can still form coacervates under certain conditions.

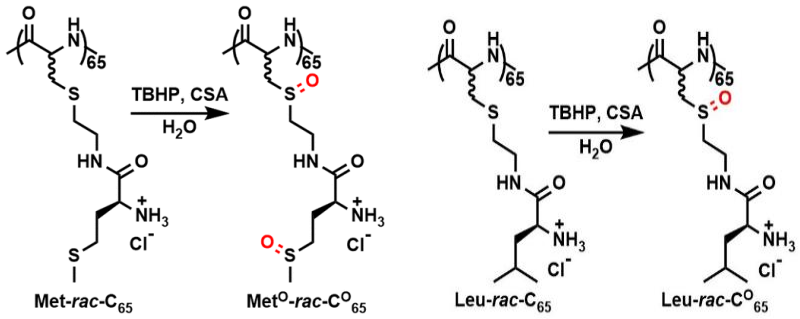

Scheme 2.3. Synthesis of sulfoxide derivative **Met^{O}-*rac*-C$^{O}_{65}$** from **Met-*rac*-C$_{65}$** and **Leu-*rac*-C$^{O}_{65}$** from **Leu- *rac*-C^{65}.** TBHP = tert-butyl hydroperoxide. CSA = camphorsulfonic acid.

On the contrary, the sample of **Met^{O}-*rac*-C$^{O}_{65}$** containing tripolyphosphate at pH 7.0 did not phase separate even up to 90 °C. The mixture of an aqueous solution of **Met^{O}-*rac*-C$^{O}_{65}$** with polyadenylic acid at pH 7.0 and 20 °C also resulted in no visible phase separation. To study these samples in more detail, the mixtures of **Met^{O}-*rac*-C$^{O}_{65}$** with tripolyphosphate and polyadenylic acid were analyzed using dynamic light scattering, which revealed the presence of coacervate nanodroplets **(Figure 2.12**). Solutions of the individual components showed negligible aggregation on their own, which supports the formation of polyion complexes in the mixtures (**Figure 2.13).**

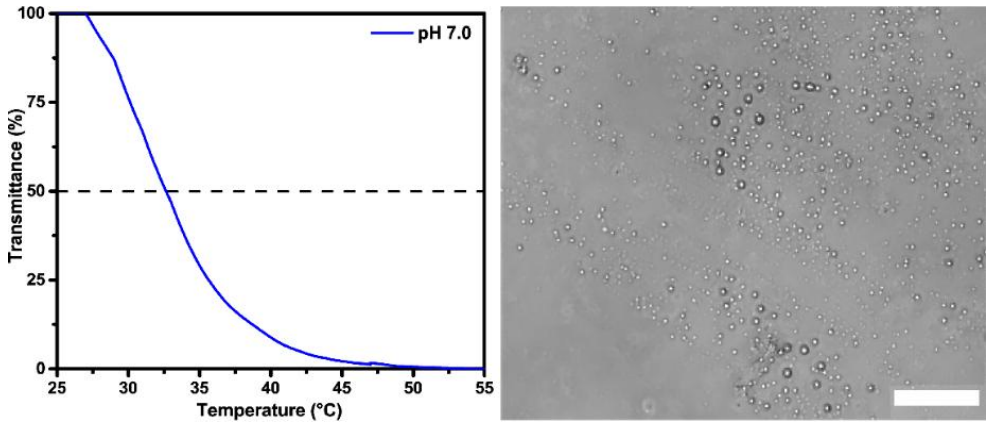

Figure 2.10. A) Temperature dependent coacervate formation in a 3.0 mg/mL solution of **Leu-*rac*-C$^{O}_{65}$** at pH 7.0. Plot shows optical transmittance at 500 nm for a 3.0 mg/mL solution of **Leu-*rac*-C$^{O}_{65}$** in 150 mM PBS buffer measured over a range of temperature at pH 7.0. B) Optical micrograph of **Leu-*rac*-C$^{O}_{65}$** mixed with sodium tripolyphosphate (TPP). A solution of **Leu-*rac*-C$^{O}_{65}$** at 3.0 mg/mL in 150 mM NaCl at 20 °C and pH 8.5 was mixed with TPP (12 mM final concentration) and the resulting turbid suspension was allowed to settle onto a glass slide before imaging. Scale bar = 20 μm.

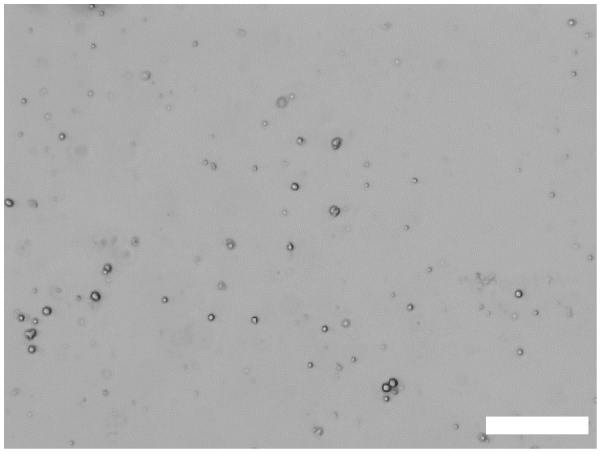

Figure 2.11. Optical micrograph of **Leu-*rac*-C$^{O}_{65}$** mixed with polyadenylic acid. A solution of **Leu-*rac*-C$^{O}_{65}$** at 5.0 mg/mL in 150 mM NaCl at 20 °C and pH 7.0 was mixed with polyadenylic acid (0.015 mM final concentration) and the resulting turbid suspension was allowed to settle onto a glass slide before imaging. Scale bar = 20 μm.

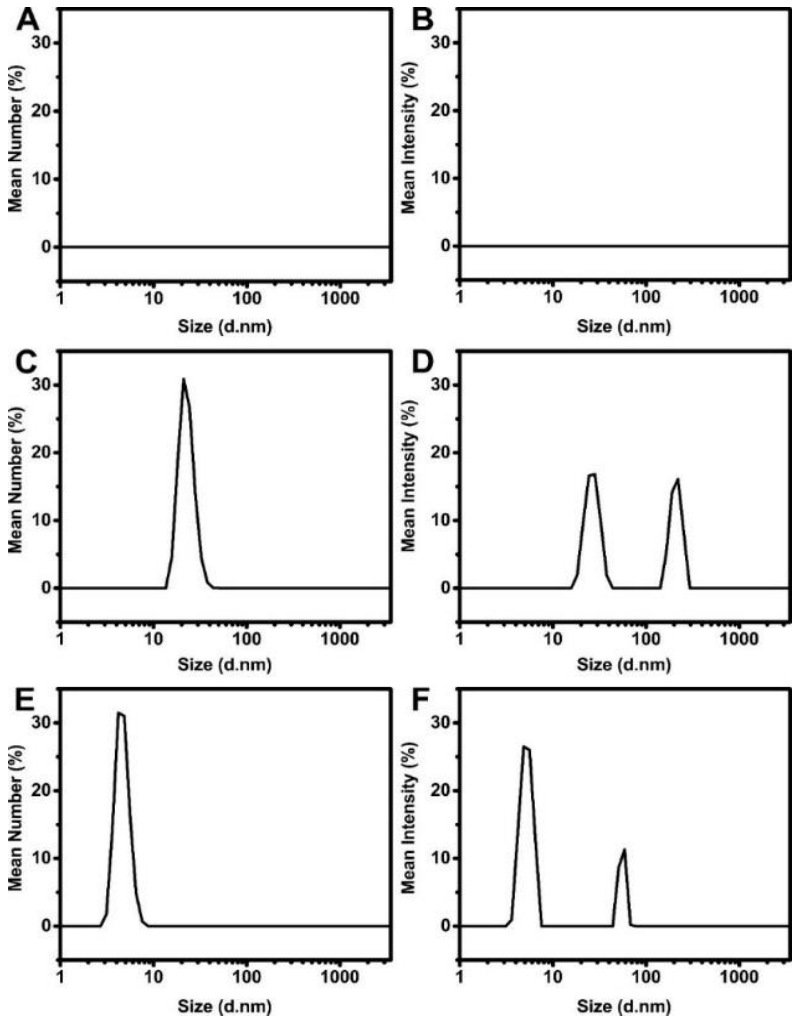

Figure 2.12. Size distributions from dynamic light scattering analysis of TPP, polyA, and **Met^{O}-*rac*-C$^{O}_{65}$** solutions. (A) Number and (B) intensity size distributions of a solution of 12 mM TPP in 150 mM NaCl at pH 7.0. (C) Number and (D) intensity size distributions of a solution of 5.0 mg/mL polyA in 150 mM NaCl at pH 7.0. (E) Number and (F) intensity size distributions of a solution of 3.0 mg/mL **Met^{O}-*rac*-C$^{O}_{65}$** in 150 mM NaCl at pH 7.0. d.nm = average hydrodynamic diameter in nanometers.

Measurement of ζ-potential on the nanodroplets formed with **Met^{O}-*rac*-C$^{O}_{65}$** containing tripolyphosphate at pH 7.0 gave a value of −4.4 ± 0.8 mV, which may explain the colloidal stability of the droplets being due to incorporation of excess

tripolyphosphate anions. Greater hydrophilicity of **Met^{O}-*rac*-C$^{O}_{65}$** compared to **Leu-*rac*-C$^{O}_{65}$** may also explain the decreased ability of **Met^{O}-*rac*-C$^{O}_{65}$** to form macroscopic coacervates. We hypothesize that the oxidation of two thioether groups per residue in **Met-*rac*-C$_{65}$** allows for a greater range of polarity switching compared to **Leu-*rac*-C$_{65}$** that has only a single thioether group per residue. The extra thioether groups in **Met-*rac*-C$_{65}$** allow for switching between highly hydrophobic and highly hydrophilic states via oxidation.

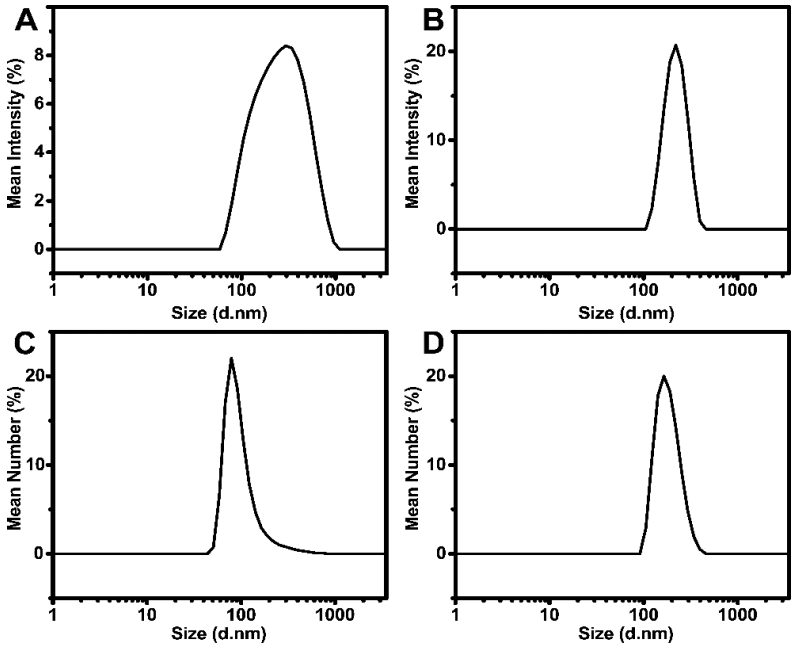

Figure 2.13. Size distributions from dynamic light scattering analysis of polypeptide suspensions over time. Intensity size distributions of suspensions of (A) 3.0 mg/mL **Met^{O}-*rac*-C$^{O}_{65}$** prepared in 150 mM NaCl at pH 7.0 with 12 mM tripolyphosphate, and (B) 5.0 mg/mL **Met^{O}-*rac*-C$^{O}_{65}$** prepared in 150 mM NaCl at pH 7.0 with 0.015 mM polyadenylic acid. Number size distributions of suspensions of (C) 3.0 mg/mL **Met^{O}-*rac*-C$^{O}_{65}$** prepared in 150 mM NaCl at pH 7.0 with 12 mM tripolyphosphate, and (D) 5.0 mg/mL **Met^{O}-*rac*-C$^{O}_{65}$** prepared in 150 mM NaCl at pH 7.0 with 0.015 mM polyadenylic acid. d.nm = average hydrodynamic diameter in nanometers.

To further examine the redox-mediated coacervate switching properties of **Met-*rac*-C_{65}**, we sought to demonstrate *in situ* oxidation and reduction of a coacervate of **Met-*rac*-C_{65}** and tripolyphosphate. Slightly more than 1 eq of $NaIO_4$ oxidant was added to a coacervate suspension of **Met-*rac*-C_{65}** with tripolyphosphate in NaCl (150 mM) at 0 °C and pH 7.0 (**Figure 2.14**). Within 5 min, the coacervate droplets had completely dissolved as **Met-*rac*-C_{65}** was oxidized to **Met^{O}-*rac*-C^{O}_{65}**. After 2 h, excess $NaIO_4$ was removed by brief dialysis against water containing tripolyphosphate and NaCl. The sample was then adjusted to pH 5 to 6 by addition of NaOH and excess thioglycolic acid, which resulted in complete reduction back to **Met-*rac*-C_{65}** and consequent reformation of the coacervate suspension after pH was increased to 7.0 (**Figure 2.14**). ^{1}H NMR spectroscopy of aliquots of oxidized and reduced samples gave spectra identical to those of purified **Met^{O}-*rac*-C^{O}_{65}** and **Met-*rac*-C_{65}** (see Spectral Data Section), indicating that both reactions went to completion.

While we had reported similar coacervate switching of **Leu-C_{60}^{H}** and tripolyphosphate, it was difficult to achieve a complete reduction in that system due to phase separation during the reaction.[16] The wider pK_a range of **Met-*rac*-C_{65}** and greater aqueous solubility of **Met^{O}-*rac*-C^{O}_{65}** compared to the **Leu-C^{H}_{60}** system appear to provide an advantage in facilitating the redox reactions under mild conditions. These properties result in robust actively controlled polypeptide coacervation with **Met-*rac*-C_{65}** that utilizes nondestructive, physiologically compatible oxidation and reduction conditions. For example, the intracellular oxidation of methionine residues in proteins is well-known, and intracellular thiols and ubiquitous reductase enzymes can readily reduce methionine sulfoxide residues in proteins.[29-32]

Figure 2.14. Reversible oxidation and reduction of a **Met-*rac*-C$_{65}$** and TPP coacervate. Coacervate suspension (left) was formed by mixing **Met-*rac*-C$_{65}$** at 5.0 mg/mL with TPP (13 mM) in 150 mM NaCl at 20 °C and pH 7.0. The coacervate was cooled to 0 °C and then oxidized by addition of 1.1 equivalents of $NaIO_4$ to give a transparent mixture of **Met^{O}-*rac*-C$^{O}_{65}$** and TPP after 2 hours (middle). Excess $NaIO_4$ was then removed from the sample by dialysis against TPP (13 mM) in 150 mM NaCl at 20 °C and pH 7.0. Adjustment of this **Met^{O}-*rac*-C$^{O}_{65}$** sample pH to 8.5 with 0.1M NaOH followed by addition of excess thioglycolic acid over 5 days, giving a pH of 5 to 6, resulted in complete reduction to **Met-*rac*-C$_{65}$**. Reformation of the coacervate suspension (right) occurred when pH was increased to 7.0 using 12M NaOH after reduction was complete.

2.4 Conclusions

Building off of prior results on **Xaa-C^{H}** polypeptides that form coacervates in water, we prepared a new class of side-chain amino acid-functionalized **Xaa-*rac*-C** via post-polymerization modification of **A^{DH}**.[16,17] The **A^{DH}** platform allowed straightforward incorporation of a wider range of side-chain amino acid functional groups in **Xaa-*rac*-C** compared to the **Xaa-C^{H}** platform and also allowed use of fewer protecting groups. We

found that **Xaa-*rac*-C** can also form coacervates with properties similar to those seen with **Xaa-C^{H}**, where side-chain amino acid hydrophobicity can be used to alter coacervation properties, specifically the ability to respond to physiologically relevant environmental changes in pH, temperature, and counterions. These results suggest that incorporation of side-chain amino acids onto polypeptides may be a general way to obtain coacervation. Coacervates formed using **Met-*rac*-C** were found to possess improved stability against high ionic strength media. Further, the presence of an additional thioether group in each **Met-*rac*-C** side chain resulted in an increased solubility change upon oxidation allowing facile reversible redox switching of coacervate formation in aqueous media. These **Xaa-*rac*-C** polypeptides may be amenable for use as mimics of coacervate-forming proteins and in applications such as therapeutic delivery and protein separation.

2.5 Materials and Instrumentation

The following chemicals were used as received from vendors: L-cysteine hydrochloride monohydrate (Fisher), HOBT hydrate (Oakwood), *tert*-butyl bromoacetate (Fisher), triphosgene (Oakwood), iodomethane (Oakwood), HATU (Oakwood), N-BOC-L-amino acids (Oakwood), diisopropylethylamine (DIPEA) (Fisher), dichloromethane (DCM) (Fisher), ethyl acetate (Fisher), trifluoroacetic acid (TFA) (Fisher), 2,2′-bipyridine (bpy) (Sigma), and $Ni(COD)_2$ (Strem). Tetrahydrofuran (THF) and hexanes were each degassed with dinitrogen and passed through an alumina column before use. All other reagents and solvents were used as received. In-house deionized water (DI H_2O) was used for all aqueous chemistry and dialysis unless otherwise specified. bpyNiCOD, poly(l-lysine·HCl)$_{60}$ (**K$_{60}$**), (poly(*S*-(3-(2-L-leucine amido)ethoxy)-2-hydroxypropyl)-L-

homocysteine hydrochloride)$_{60}$ (**Leu-C$^{H}_{60}$**), and α-methoxy-ω-isocyanoethyl-poly(ethylene glycol), mPEG-NCO (M_n = 1 kDa) were prepared according to literature procedures.[16,18-20] NCA purifications and polymerizations were performed in an N_2-filled glovebox. Reactions at elevated temperatures were controlled using a Corning PC 420D thermostat-controlled hot plate equipped with a thermocouple probe. Room-temperature reactions were performed at *ca*. 20 °C ambient temperature. Small molecule chemistry was performed in heat-dried glassware under ambient atmosphere, unless otherwise specified. Unless otherwise specified, all post-polymerization modification chemistry was performed in glass vials under an ambient atmosphere. Thin-layer chromatography was performed with EMD gel 60 F254 plates (0.25 mm thickness), and spots were visualized using $KMnO_4$ stain. Silicycle Siliaflash G60 silica (60–200 μm) was used for all column chromatography. Silica used for chromatographic purification of NCA monomers was dried under vacuum at 250 °C for 48 h and then stored in a dinitrogen-filled glovebox. Compositions of mobile phases used for chromatography are given in volume percentages. Dialysis was performed with regenerated cellulose tubing obtained from Spectrum laboratories with 1000 Da molecular weight cutoff (MWCO). NMR spectra of solution samples were recorded on Bruker AV400 and Bruker AV300 instruments with chemical shifts reported relative to deuterated solvent resonances. For the **C^{BCM}** precursor, gel permeation chromatography was performed at 40 °C with 1,1,1,3,3,3-hexafluoroisopropanol (HFIP) containing 0.5% (w/w) potassium trifluoroacetate (KTFA) eluent at a 1.0 mL/min flow rate using an LC-20AD Prominence HPLC Pump (Shimadzu) equipped with 100 and 1000 Å PSS-PFG 7 μm columns (PSS Agilent). Samples were prepared at 20 mg/mL and were detected using an RID-20A

Refractive Index detector (Shimadzu). A calibration curve was prepared using monodisperse polyethylene glycol standards ranging from 1 to 40 kDa that were purchased from Scientific Polymer Products, Inc. For **Xaa-*rac*-C** samples, gel permeation chromatography was performed at 25 °C with trifluoroethanol (TFE) containing 20 mM sodium trifluoroacetate (NaTFA) eluent at a 0.5 mL/min flow rate using a JASCO PU-4180 LC pump system equipped with two 300 mm PFG analytical linear S 5 μm columns (PSS Agilent). Samples were prepared at 0.5 or 1.0 mg/mL and were detected using a JASCO UV-4075 detector. A calibration curve was prepared using monodisperse poly(methyl methacrylate) (PMMA) standards ranging from 1 to 60 kDa that were purchased from PSS Agilent. Samples for circular dichroism (CD) spectroscopy were prepared using DI H_2O. CD spectra were collected using solutions of polypeptide (0.5 mg/mL) on a Chirascan VX spectrophotometer using a 0.1 cm path length quartz cuvette. Cloud point temperature measurements were recorded at a wavelength of 500 nm on an HP 8453 spectrophotometer equipped with an Agilent 8909A temperature control. ζ-potential data were collected using a Malvern Zetasizer NanoZS. Brightfield images were taken using a Zeiss Axio Observer Z1 optical microscope. FTIR spectroscopy was performed on a PerkinElmer Spectrum RX spectrometer.

S-(*tert*-butylcarboxymethyl)-L-cysteine L-cysteine hydrochloride monohydrate (3.0 g, 28 mmol, 1.0 eq) and NaOH (1.35 g, 57 mmol, 2.0 eq) were dissolved in DI H_2O (15 mL) with stirring. The reaction mixture was cooled to 0 °C in an ice-water bath before the dropwise addition of *tert*-butyl bromoacetate (2.8 mL, 31 mmol, 1.1 eq) over 30 min. The ice bath was then removed and 10 mL of THF was added. The reaction mixture was stirred at room temperature overnight resulting in formation of a white solid precipitate.

The while solid was collected via filtration and washed with a 3:7 mixture of 95% EtOH and diethyl ether. The solids were placed in a 50 mL centrifuge tube and washed 3 times with a 95:5 mixture of diethyl ether and methanol to remove residual impurities. The sticky white solid was then dried under vacuum to give the product. (4.1 g, 61%). Spectra data were in agreement with previously reported values.[19]

S-(*tert*-butylcarboxymethyl)-L-cysteine N-carboxyanhydride (tBuCM-Cys NCA)[5,6] S-(*tert*-butylcarboxymethyl)-L-cysteine (2.0 g, 8.5 mmol, 1.0 eq) was suspended in analytical grade THF (40 mL) in a heavy walled glass container. Epichlorohydrin (6.7 mL, 85 mmol 10 eq) was then added**.** In a well-ventilated fume hood, triphosgene (1.3 g, 4.6 mmol, 0.55 eq) was added, and the vessel was sealed and allowed to react for 2 h at room temperature. ***WARNING: Triphosgene is an extremely dangerous chemical and proper precautions must be taken to avoid exposure.*** The resulting turbid mixture was then cooled to 4 ^{o}C and 10 mL of cold DI H_2O was added. The reaction mixture was stirred for 1 minute before extraction with ethyl acetate, which was then washed with brine and dried with anhydrous sodium sulfate. The resulting solution was transferred to an oven dried Schlenk flask and the solvent was removed under vacuum. The crude product was transferred to a N_2 filled glove box, resuspended in minimal THF, and layered under 5x hexanes (v/v) to give white or slightly off-white crystals. (1.1 g, 50%). Spectral data were in agreement with previously reported values.[19]

Procedure for synthesis of poly(S-(*tert*-butylcarboxymethyl)-L-cysteine) (C^{BCM}_{65}) Samples of $\mathbf{C^{BCM}_{65}}$ were prepared at *ca*. 500 mg scale in a N_2 filled glove box. bpyNiCOD initiator solution (3.1 mL, 20 mg/mL in THF) was quickly added to a solution of tBuCM-Cys NCA (10 mL, 50 mg/mL in THF). After *ca*. 90 min, complete consumption of NCA was

confirmed by FTIR spectroscopy. In order to determine polypeptide chain lengths a small aliquot of the reaction mixture (*ca*. 200 μL) was removed for end-group analysis where active chain-ends were reacted with mPEG-NCO (*vide infra*). The remaining polypeptide solution was then end capped with excess acetic anhydride, precipitated by addition to DI H_2O (50 mL), and isolated by centrifugation. The solid was then washed two additional times with DI H_2O and dried under reduced pressure to yield $\mathbf{C^{BCM}_{65}}$ as a lightly purple colored powder. (460 mg, 92%) Spectral data were in agreement with previously reported values.[19]

General procedure for determination of polypeptide chain length using end-group analysis after reaction with mPEG-NCO[19] The procedure for synthesis of $\mathbf{C^{BCM}_{65}}$ was followed. Once the polymerization reaction was determined to be complete by FTIR, a solution of mPEG-NCO (M_n = 1000 Da, 50 mg/mL in THF, 4 eq per bpyNiCOD) was added in a N_2 filled glove box to a *ca*. 200 μL aliquot of active polymerization reaction mixture. The sample was let stand overnight, and then removed from the glove box and the polypeptide was precipitated by addition to DI H_2O. The sample was centrifuged at 3000 rpm and the supernatant was discarded. The pellet was washed 3 times with DI H_2O and centrifuged to remove unconjugated mPEG-NCO, and the resulting pellet was then lyophilized to yield the PEG-polypeptide conjugate as a white solid (typical yields = 90 to 95%). To determine the molecular weight (M_n) of the polypeptide, a ^{1}H NMR spectrum was obtained in deuterated trifluoroacetic acid (TFA-d). The ratio of the integral of the methylene unit closest to the polypeptide backbone to the integral of the PEG methylene resonance was used to calculate polypeptide length.

General procedure for synthesis of poly(S-carboxymethyl-L-cysteine), sodium salt ($\mathbf{C^{CM}_{65}}$)[5] A sample of $\mathbf{C^{BCM}_{65}}$ (450 mg) was dissolved in TFA (20 mg/mL) and allowed to stand for 5 h. The reaction mixture was diluted to 10 mg/mL by slowly adding 50 mM $NaHCO_3$ and then transferred to a 1000 Da MWCO dialysis bag and dialyzed against aqueous 50 mM $NaHCO_3$ (24 h, 3 dialyzate changes) followed by DI H_2O (24 h, 4 dialyzate changes). The retentate was then lyophilized to give the product as a white fluffy solid. (340 mg, 89%). Spectral data were in agreement with previously reported values.[19]

General procedure for synthesis of poly(dehydroalanine) ($\mathbf{A^{DH}_{65}}$) A sample of $\mathbf{C^{CM}_{65}}$ (340 mg) was dissolved in 150 mM sodium phosphate buffer (pH 8) at a concentration of 20 mg/mL. Iodomethane (25 eq per S-(carboxymethyl)-L-cysteine residue) was added, and the reaction flask was sealed and placed in a heating block at 37 °C, covered in foil and allowed to react for 3 days. The resulting suspension was mixed with a solution of BHT in dinitrogen sparged DMSO (0.2 mg/mL) to give a final 0.01 mol% ratio of BHT to dehydroalanine residues and then transferred to a 2000 Da MWCO dialysis bag and dialyzed against dinitrogen sparged DI H_2O (48 h, 4 dialyzate changes, dialysis jar covered in foil). The retentate was then lyophilized to give the product as a white solid (130 mg, 100%). Spectral data were in agreement with previously reported values.[19]

General Procedure for Synthesis of L-Amino Acid 2-Mercaptoethylamides[21,22]

N-Boc protected amino acids (2.0 g, 1.0 eq) were dissolved in DCM (30 mL) followed by the sequential addition of solid HOBT (1.1 eq) and HATU (1.0 eq). The resulting solutions were stirred at room temperature for 20 min and then cooled to 0 °C. To the reaction mixtures, a suspension of cystamine dihydrochloride (0.50 eq) in DCM (50 mL) followed

by DIPEA (3.0 eq) was added dropwise. The reactions were allowed to warm to room temperature and were stirred overnight. The resulting solutions were washed with saturated $NaHCO_3$, 10% citric acid (aq), saturated $NaHCO_3$, and then brine. The solutions were then dried with anhydrous sodium sulfate and concentrated under vacuum. The crude products were purified via flash column chromatography with hexanes/ethyl acetate (1:1) for Ala, Val, Leu, and Met or with DCM/MeOH (95:5) for Pro. Sample fractions were combined and concentrated under reduced pressure to give white solids. These samples were then dissolved into MeOH (50 mL) and placed in an ice bath and cooled to 0 °C. Under constant stirring, $NaBH_4$ (4.0 eq) was added to each sample. The reactions were allowed to continue for 30 min in the ice bath and then for 30 additional min at room temperature. The reactions were then concentrated under reduced pressure and diluted with ethyl acetate. The solutions were adjusted to pH 3 by the addition of 1 M HCl and left to stir for 15 min. The organic phases were washed 2× with brine, dried with sodium sulfate, and concentrated under reduced pressure to yield white solids. Finally, the Boc groups were removed by dissolving the solids into ethyl acetate followed by the addition of 12 M HCl until the concentration of HCl in ethyl acetate was 3 M. The products were left to stir at room temperature for 2 h and then concentrated under reduced pressure. The products were used without further purification.

General Procedure for Modification of A^{DH}_{65} with L-Amino Acid 2-Mercaptoethylamides

A sample of $\mathbf{A^{DH}_{65}}$ was dissolved in DMSO at 20 mg/mL. The desired L-amino acid 2-mercaptoethylamide (5 eq per dehydroalanine residue) was dissolved in minimal DI H_2O (~300 mg/mL), and the pH was adjusted to pH 7.0 with 5 M NaOH. The L-amino acid 2-

mercaptoethylamide solution was then added to the **A^{DH}_{65}** solution followed by the addition of 2 M NaOH (1.5 eq per dehydroalanine residue). DMSO was then added to give a final **A^{DH}_{65}** concentration of 10 mg/mL. The reaction mixture was allowed to stir at room temperature for 18 h. The resulting solution was transferred to a 1000 Da MWCO dialysis bag and dialyzed against pH 4 DI H_2O for 1 day with 2 dialyzate changes and then pH 7 DI H_2O for 1 day with 2 dialyzate changes. The solution was lyophilized to give the product as a white fluffy solid.

General Procedure for Oxidation of Thioether Groups in Xaa-*rac*-C_{65} Polypeptides

This procedure was adapted from a literature method.[23] Into a scintillation vial containing **Xaa-*rac*-C_{65}** (25 mg) was added 70 wt % aqueous *tert*-butyl hydroperoxide (TBHP) (16 eq per thioether group), a catalytic amount of camphorsulfonic acid (CSA) solution in DI water (0.2 eq per thioether group, 20 mg/mL), and additional DI water to bring the final concentration of **Xaa-*rac*-C_{65}** to 20 mg/mL. The reaction mixture was stirred vigorously for 24 h at room temperature, and the solution was then transferred to a 2000 Da MWCO dialysis bag and dialyzed against DI H_2O (3.5 L) containing sodium thiosulfate (1.2 g, 2.2 mM) to neutralize residual peroxide (48 h, 4 dialyzate changes), followed by 3 mM HCl (24 h, 3 dialyzate changes) and H_2O (8 h, 3 dialyzate changes). The retentate was lyophilized to provide the sulfoxide product, **Xaa-*rac*-C^{O}_{65}**.

***In Situ* Oxidation and Reduction of Met-*rac*-C_{65}[16]**

A sample of **Met-*rac*-C_{65}** was dissolved in DI H_2O (10 mg/mL) and was mixed with an equal volume of aqueous 26 mM TPP and 300 mM NaCl at pH 7.0. The resulting turbid coacervate suspension was then treated with 0.5 M sodium periodate solution (1.05 eq

per thioether group over 2 additions) while stirring at 0 °C. Complete dissolution of the coacervate was observed after 5 min. After 2 h, the solution was dialyzed against aqueous 150 mM NaCl and 13 mM TPP (24 h, 1 dialyzate change) to remove residual sodium periodate. The sample (ca. 5 mg/mL) was then transferred to a glass vial, and thioglycolic acid (150 eq per sulfoxide group) and 100 µL of 0.1 M NaOH were added. After 24 h, additional thioglycolic acid (150 eq per sulfoxide group) and 100 µL of 0.1 M NaOH were added. The reaction mixture (pH ca. 5–6) was allowed to stir at room temperature. After 4 days, the pH was increased to 7.0 by the addition of 12 M NaOH whereupon coacervate formation occurred. Spectral data for the *in situ* oxidized and reduced products matched those for **Met^{O}-*rac*-C$^{O}_{65}$** and **Met-*rac*-C$_{65}$**, respectively.

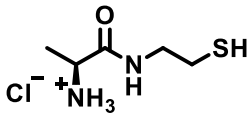

L-Alanine 2-mercaptoethylamide hydrochloride, 1a Prepared from N-Boc-L-alanine using general procedure for the synthesis of L-amino acid 2-mercaptoethylamides. Yield given in Table 2.1. ^{1}H NMR (400 MHz, D_2O, 25 °C) δ 4.11 (s, 1H), 3.7-3.4 (m, 2H), 3.0-2.6 (d, 2H), 1.6-1.5 (d, 3H)

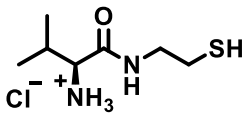

L-Valine 2-mercaptoethylamide hydrochloride, 1b Prepared from N-Boc-L-valine using general procedure for the synthesis of L-amino acid 2-mercaptoethylamides. Yield given in Table 2.1. ^{1}H NMR (400 MHz, D_2O, 25 °C) δ 3.8 (s, 1H), 3.78 (m, 1H), 3.55 (m, 1H), 3.0-2.7 (m, 1H), 2.2 (m, 1H), 1.05 (d, 6H)

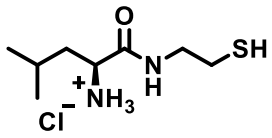

L-Leucine 2-mercaptoethylamide hydrochloride, 1c Prepared from N-Boc-L-leucine using general procedure for the synthesis of L-amino acid 2-mercaptoethylamides. Yield given in Table 2.1. ^{1}H NMR (400 MHz, D_2O, 25 °C) δ 4.05 (s, 1H), 3.78-3.35 (m, 2H), 3.0 -2.65 (m, 2H), 1.7 (m, 2H), 1.68 (m, 1H), 0.95 (s, 6H)

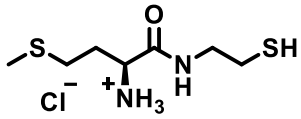

L-Methionine 2-mercaptoethylamide hydrochloride, 1d Prepared from N-Boc-L-methionine using general procedure for the synthesis of L-amino acid 2-mercaptoethylamides. Yield given in Table 2.1. ^{1}H NMR (400 MHz, D_2O, 25 °C) δ 4.2 (s, 1H), 3.8-3.3 (m, 2H), 2.9 (m, 1H), 2.75 (m, 1H), 2.7 (m, 1H), 2.22 (q, 2H) 2.18 (s, 3H)

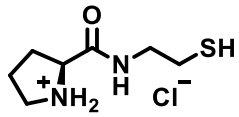

L-Proline 2-mercaptoethylamide hydrochloride, 1e Prepared from N-Boc-L-proline using general procedure for the synthesis of L-amino acid 2-mercaptoethylamides. Yield given in Table 2.1. ^{1}H NMR (400 MHz, D_2O, 25 °C) δ 4.25 (s, 1H), 3.55–3.45 (m, 2H), 3.3 (s, 2H) 2.8–2.5 (m, 2H), 2.35 (s, 1H), 1.90 (s, 1H), 1.85 (s, 2H)

General procedure for modification of A^{DH}_{65} with L-amino acid 2-mercaptoethylamides A sample of **A^{DH}_{65}** was dissolved in DMSO at 20 mg/mL. The desired L-amino acid 2-mercaptoethylamide (5 eq per dehydroalanine residue) was

dissolved in minimal DI H_2O (~300 mg/mL) and the pH was adjusted to pH 7.0 with 5 M NaOH. The L-amino acid 2-mercaptoethylamide solution was then added to the $\mathbf{A^{DH}_{65}}$ solution followed by addition of 2 M NaOH (1.5 eq per dehydroalanine residue). DMSO was then added to give a final $\mathbf{A^{DH}_{65}}$ concentration of 10 mg/mL. The reaction was let stir at room temperature for 18 hours. The resulting solution was transferred to a 1000 Da dialysis bag and dialyzed against pH 4 DI H_2O for 1 day with 2 dialyzate changes and then pH 7 DI H_2O for 1 day with 2 dialyzate changes. The solution was lyophilized to give the product as a white fluffy solid.

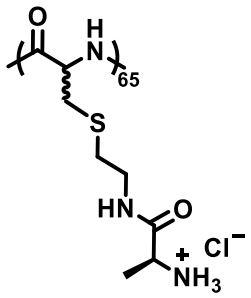

Ala-*rac*-$\mathbf{C_{65}}$ Prepared from **1a** and $\mathbf{A^{DH}_{65}}$ using the General procedure for modification of $\mathbf{A^{DH}_{65}}$ with L-amino acid 2-mercaptoethylamides. Yield given in Table 2.1. ^{1}H NMR (400 MHz, D_2O, 25 °C): δ 4.7-4.3 (br s, 1H), 4.0 (br s, 1H), 3.45 (br s, 2H), 3.0 (br d, 2H), 2.7 (br s, 2H), 1.55-1.15 (br d, 3H)

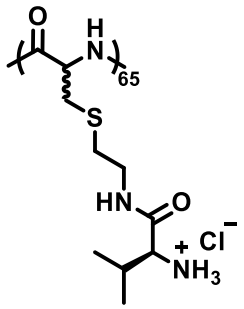

Val-*rac*-C$_{65}$ Prepared from **1b** and **A$^{DH}_{65}$** using the General procedure for modification of **A$^{DH}_{65}$** with L-amino acid 2-mercaptoethylamides. Yield given in Table 2.1. ^{1}H NMR (400 MHz, D_2O, 25 °C): δ 4.45 (br s, 1H), 3.5 (br s, 1H), 3.4-3.2 (br d, 2H), 2.85 (br d, 2H), 2.55 (br s, 2H), 2.0 (br s, 1H), 0.85 (s, 6H)

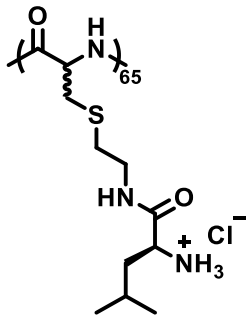

Leu-*rac*-C$_{65}$ Prepared from **1c** and **A$^{DH}_{65}$** using the General procedure for modification of **A$^{DH}_{65}$** with L-amino acid 2-mercaptoethylamides. Yield given in Table 2.1. ^{1}H NMR (400 MHz, D_2O, 25 °C): δ 4.55 (br s, 1H), 3.95 (br s, 1H), 3.45 (br d, 2H), 2.95 (br d, 2H), 2.7 (br s, 2H), 1.65 (br s, 3H), 0.90 (s, 6H)

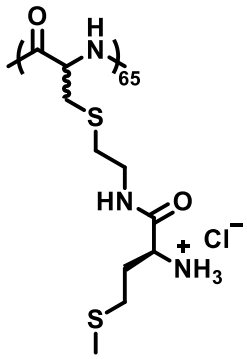

Met-*rac*-C_{65} Prepared from **1d** and **A^{DH}_{65}** using the General procedure for modification of **A^{DH}_{65}** with L-amino acid 2-mercaptoethylamides. Yield given in Table 2.1. ^{1}H NMR (400 MHz, D_2O, 25 °C): δ 4.65 (br s, 1H), 3.90 (br s, 1H), 3.5 (br d, 2H), 3.1 (br d, 2H), 2.78 (br s, 2H), 2.62 (br s, 2H), 2.1 (br s, 5H)

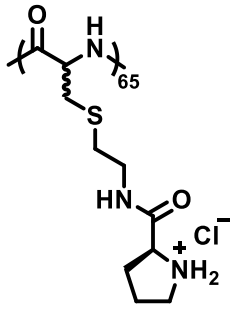

Pro-*rac*-C_{65} Prepared from **1e** and **A^{DH}_{65}** using the General procedure for modification of **A^{DH}_{65}** with L-amino acid 2-mercaptoethylamides. Yield given in Table 2.1. ^{1}H NMR (400 MHz, D_2O, 25 °C): δ 4.5 (br s, 1H), 4.35 (s, 1H), 3.5 (br, 2H), 3.25-2.65 (br m, 4H), 2.65 – 2.4 (br d, 3H), 2.2 – 2.0 (br d, 2H), 1.75 (br s, 1H)

Oxidation of thioether groups in Xaa-*rac*-C_{65} polypeptides This procedure was adapted from a literature method.[23] Into a scintillation vial containing **Xaa-*rac*-C_{65}** (25 mg) was added 70 wt % aqueous *tert*-butyl hydroperoxide (TBHP) (16 eq per thioether group), a catalytic amount of camphorsulfonic acid (CSA) solution in DI water (0.2 eq per thioether

group, 20 mg/mL), and additional DI water to bring the final concentration of **Xaa-*rac*-C$_{65}$** to 20 mg/mL. The reaction was stirred vigorously for 24 hours at room temperature and the solution was then transferred to a 2000 Da MWCO dialysis bag and dialyzed against DI H_2O (3.5 L) containing sodium thiosulfate (1.2 g, 2.2 mM) to neutralize residual peroxide (48h, 4 dialyzate changes), followed by 3mM HCl (24h, 3 dialyzate changes) and H_2O (8h, 3 dialyzate changes). The retentate was lyophilized to provide the sulfoxide product, **Xaa-*rac*-C$^{O}_{65}$**.

Leu-*rac*-C$^{O}_{65}$ (24 mg, 91.6%). ^{1}H NMR (400 MHz, D_2O, 25 °C): δ 4.6-4.2 (br s, 1H), 3.8 (br s, 1H), 3.7-2.7 (br m, 6H),1.55 (br s, 3H), 0.88 (s, 6H)

Met^{O}-*rac*-C$^{O}_{65}$ (25 mg, 91.5%). ^{1}H NMR (400 MHz, D_2O, 25 °C): δ 4.55 (br s, 1H), 3.78 (br s, 1H), 3.7-3.4 (br d, 2H), 3.1-2.95 (br d, 2H), 3.1 (br d, 2H), 2.9 (br s, 2H), 2.7 (br s, 3H), 2.1 (br s, 2H)

Analysis of chain length after modification of C$^{BCM}_{50}$ to A$^{DH}_{50}$ to Leu-*rac*-C$_{50}$ The procedure for synthesis of **C^{BCM}** was adapted to prepare **PEG$_{22}$-*b*-C$^{BCM}_{50}$**. After a small aliquot of the reaction mixture (*ca*. 200 µL) was removed for end-group analysis, a solution of mPEG$_{22}$-NCO (M_n = 1000 Da, 50 mg/mL in THF, 4 eq per bpyNiCOD) was added to the remaining polymerization reaction mixture in a N_2 filled glovebox. The general procedure for synthesis of poly(S-carboxymethyl-L-cysteine), sodium salt and the general procedure for synthesis of poly(dehydroalanine) were used to convert the product to **PEG$_{22}$-*b*-A$^{DH}_{50}$**. The procedure for modification of **A^{DH}** with L-amino acid 2-mercaptoethylamides was then followed using L-leucine 2-mercaptoethylamideto give **PEG$_{22}$-*b*-(Leu-*rac*-C)$_{50}$**. To compare average degrees of polymerization (DP) of the

polypeptide segments, ^{1}H NMR spectra were obtained for **PEG$_{22}$-*b*-C$^{BCM}_{50}$** in d-TFA, **PEG$_{22}$-*b*-A$^{DH}_{50}$** in d$_6$-DMSO, and **PEG$_{22}$-*b*-(Leu-*rac*-C)$_{50}$** in D_2O. The ratio of the integral of the CH_2 group closest to the polypeptide backbone to the integral of the PEG CH_2 was used to calculate polypeptide length for **Peg$_{22}$-*b*-C$^{BCM}_{50}$**, the ratio of the integral of the alkene CH_2 to the integral of the PEG CH_2 was used to calculate the length for **PEG$_{22}$-*b*-A$^{DH}_{50}$**, and the ratio of the integral of the polypeptide backbone alpha-CH to the integral of the PEG CH_2 was used to calculate the length for **PEG$_{22}$-*b*-(Leu-*rac*-C)$_{50}$** (see **Figure 2.1**). Negligible changes in DP were observed after each modification step.

General Procedure for Preparation of Polypeptide Coacervates[16]

Stock solutions of **Xaa-*rac*-C$_{65}$**, **Met^O-*rac*-C$^O_{65}$**, and **Leu-*rac*-C$^O_{65}$** (all with chloride counterions) were prepared at 6.0 mg/mL in DI H_2O. Separate stock solutions of **Met^O-*rac*-C$^O_{65}$** and **Leu-*rac*-C$^O_{65}$** were prepared at 10 mg/mL in DI H_2O containing NaCl (300 mM) for mixing with polyadenylic acid (polyA). Stock solutions (24 mM) of sodium salts of different counterions (phosphate, pyrophosphate, or tripolyphosphate) were prepared in DI H_2O containing NaCl (300 mM). A stock solution of 2× PBS buffer (300 mM) was also prepared, as well as a solution of 10 mg/mL polyA in DI H_2O. A single stock solution (sodium salts, 2× PBS, or polyA) was then mixed with a polypeptide stock solution in a 1:1 (v/v) ratio to test for coacervate formation.

Brightfield Microscopy[16]

Microscope slides were prepared by affixing a 1.5 mm Fisherbrand coverslip to a Fisherbrand Superfrost slide using a double-stick tape at all four sides with a small channel left open to allow the sample to be drawn under the coverslip by capillary action.

Each freshly prepared polypeptide coacervate sample was allowed to stand for 20 min to allow liquid coacervate droplets to condense or for precipitate to settle onto the slide surface. Samples were then imaged using a Zeiss Axio Observer Z1 optical Microscope. Microscope slides for imaging bulk coacervates isolated via centrifugation were prepared by spreading the sample on a Fisherbrand Superfrost slide and pipetting 50 μL of 150 mM PBS buffer on top to prevent evaporation.

Circular Dichroism Spectroscopy[16]

A sample of **Leu-*rac*-C_{65}** was analyzed at a concentration of 0.5 mg/mL in DI H_2O adjusted to pH 7.0 with 0.1 M NaOH. The data were reported in units of molar ellipticity [θ] (deg·cm^2·dmol^{-1}), which was calculated using [θ] = (θ × 100 × MW)/(*c* × *l*), where θ is the measured ellipticity (millidegrees), MW is the average residue molecular mass (g/mol), *c* is the polypeptide concentration (mg/mL), and *l* is the cuvette path length (cm).

ζ-Potential Measurements[16]

Samples of **Xaa-*rac*-C_{65}**, **Leu-C^H_{60}**, and **K_{60}** were each dissolved at 5 mg/mL in filtered (0.45 μm) DI H_2O containing 20 mM NaCl. A coacervate suspension of **Met^O-*rac*-C^O_{65}** was prepared at 5 mg/mL in filtered (0.45 μm) DI H_2O containing 150 mM NaCl and 12 mM TPP at pH 7.0. For polypeptides, samples were adjusted to pH 2.0 using filtered (0.45 μm) aqueous 1.0 M HCl. The samples were titrated to pH 12 with filtered (0.45 μm) aqueous 1.0 M NaOH. Aliquots (1 mL) were removed from the solutions over a range of pH values, and ζ-potential measurements of samples were acquired using a Zetasizer NanoZS instrument (Malvern Instruments Ltd., UK). The electrophoretic mobility was calculated in monomodal mode where only the fast field reversal (FFR) technique was

applied to avoid degradation of the cuvette electrodes. Malvern Zetasizer Software was used to calculate electrophoretic mobility using the Henry equation. For the coacervate suspension of **Met^{O}-*rac*-C$^{O}_{65}$** prepared with 150 mM NaCl and 12 mM TPP at pH 7.0, the ζ-potential was found to be −4.4 ± 0.8 mV.

Cloud Point Temperature Measurements[16]

Samples of **Xaa-*rac*-C$_{65}$** or **Leu-*rac*-C$^{O}_{65}$** were prepared at 3.0 mg/mL in DI H_2O containing a sodium salt of different counterions (12 mM) and NaCl (150 mM) or 1× PBS buffer (150 mM). Individual stock solutions of polypeptides (6.0 mg/mL) in DI H_2O and stock solutions of sodium salts (120 mM), NaCl (2 M), and 10× PBS (1500 mM) at pH 5.0, 7.0, and 9.0 were used in sample preparation. Samples were prepared by mixing a polypeptide sample solution, a pH 7.0 stock solution of a sodium salt (phosphate, pyrophosphate, or tripolyphosphate), and NaCl solution in a 1:0.2:0.15 (v/v/v) ratio and then diluting with DI H_2O to achieve a final polypeptide concentration of 3.0 mg/mL. The samples in PBS buffer were prepared by mixing a polypeptide sample solution and 2× pH 7.0 PBS buffer in a 1:1 (v/v) ratio to obtain a final polypeptide concentration of 3.0 mg/mL. The final pH of these samples was adjusted as desired by the addition of small volumes of the same polypeptide sample prepared using either pH 5.0 or 9.0 stock solutions. Transmittance of each sample at 500 nm was measured on a HP 8453 spectrophotometer equipped with an Agilent 8909A temperature controller. In initial runs, temperature was increased at a rate of 10 °C/min from 20 to 80 °C, followed by additional experiments within a selected temperature range at a heating rate of 2 °C/min. Absorbance data were converted to transmission and then normalized to span 0–100%. Cloud point temperatures (T_{cp}) were determined as the temperature at 50% transmission.

Reversibility of Thermal Coacervation[16]

Studies of the reversibility of thermal coacervation were performed using samples **Leu-*rac*-C_{65}** and **Met-*rac*-C_{65}** at concentrations of 3.0 mg/mL in 1× PBS (150 mM) prepared as described above. The transmittance of each sample at 500 nm was measured on an HP 8453 spectrophotometer equipped with an Agilent 8909A temperature controller as described above. For each sample, the temperature was cycled at a rate of 3 °C/min from 20 to 50 °C, and this cycle was repeated 5 times ending at 20 °C.

Coacervate Formation as a Function of NaCl Concentration[16]

A stock solution of **Leu-*rac*-C_{65}** or **Met-*rac*-C_{65}** at 6.0 mg/mL in DI H_2O was prepared and mixed in a 1:1 (v/v) ratio with separate stock solutions of TPP containing different concentrations of NaCl to give a series of samples with 3.0 mg/mL polypeptide and 12 mM TPP, with NaCl concentrations of 0, 0.05, 0.15, 0.25, 0.50, 1.0, and 2.0 M. Samples that formed coacervates were allowed to stand in 1.5 mL Eppendorf tubes for 24 h, followed by removal of the water-rich supernatant, which was then transferred into 2000 Da MWCO dialysis tubing. The samples were dialyzed against 1 M NaCl and 3 mM HCl (1×), 3 mM HCl (2×), and DI H_2O (3×), with a minimum of 4 h between dialysate changes, before being lyophilized and weighed. This procedure converted all counterions to chloride for accurate quantification of the polypeptide. The fraction of **Leu-*rac*-C_{65}** or **Met-*rac*-C_{65}** in the coacervate phase for each sample was calculated by subtracting the mass of polypeptide recovered in the supernatant from the total mass of polypeptide initially added to the sample, which is divided by the total mass of polypeptide initially added to the sample. Mass fraction measurements were performed in triplicate.

2.6 Spectral Data

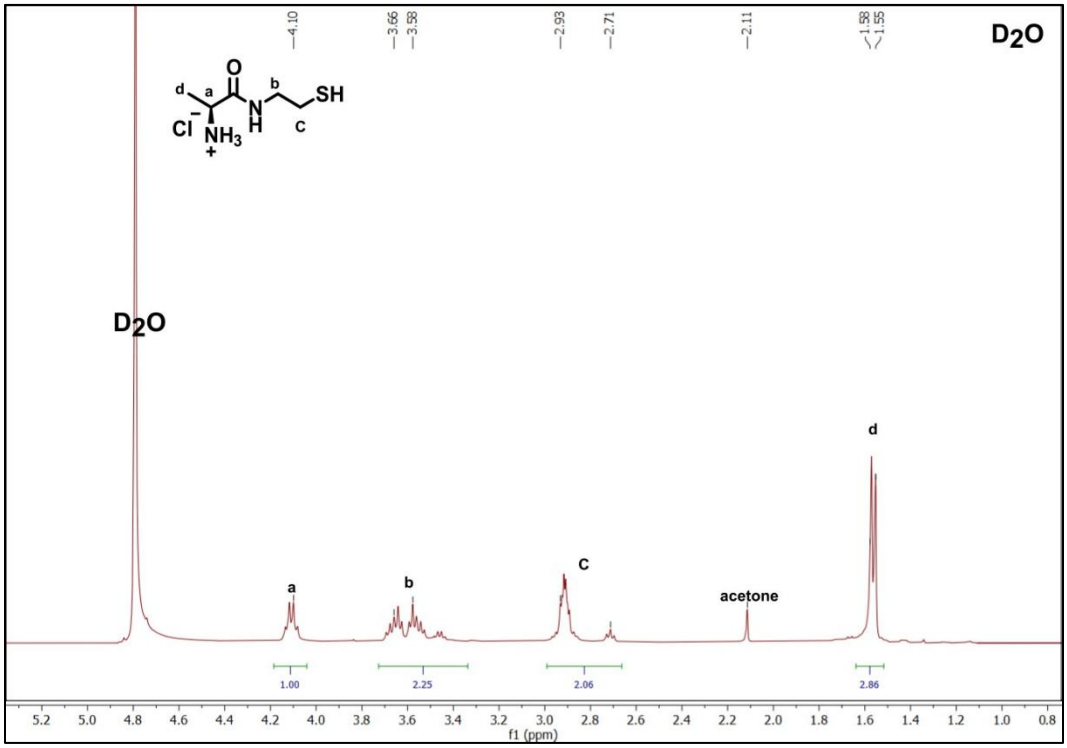

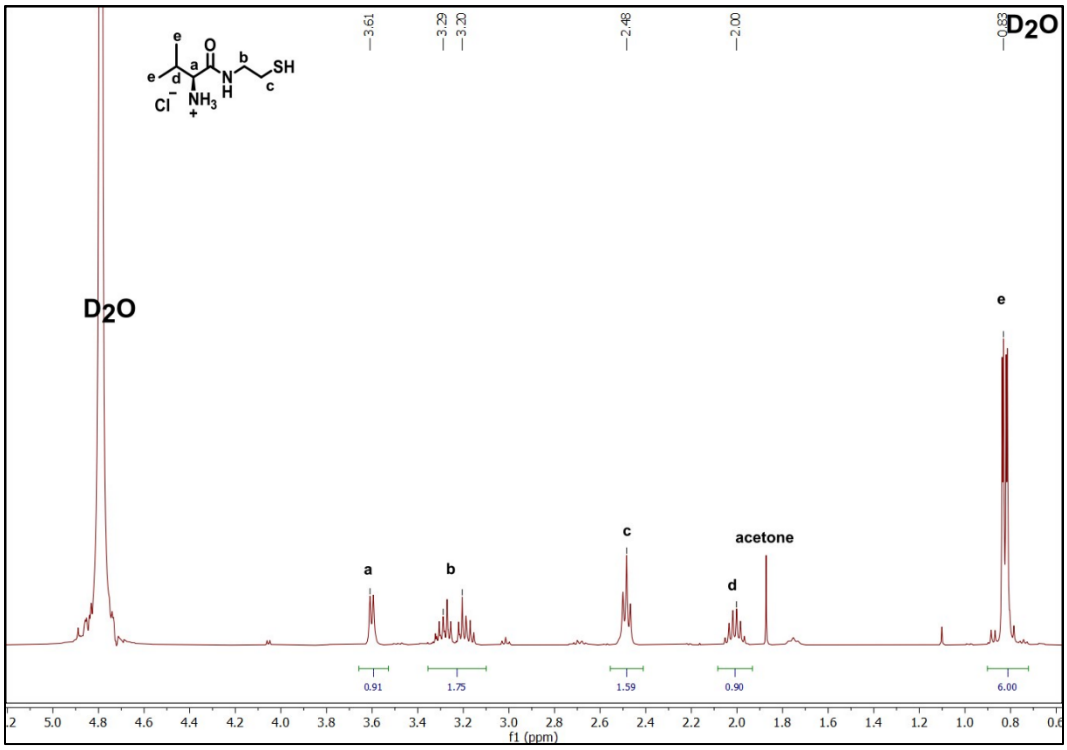

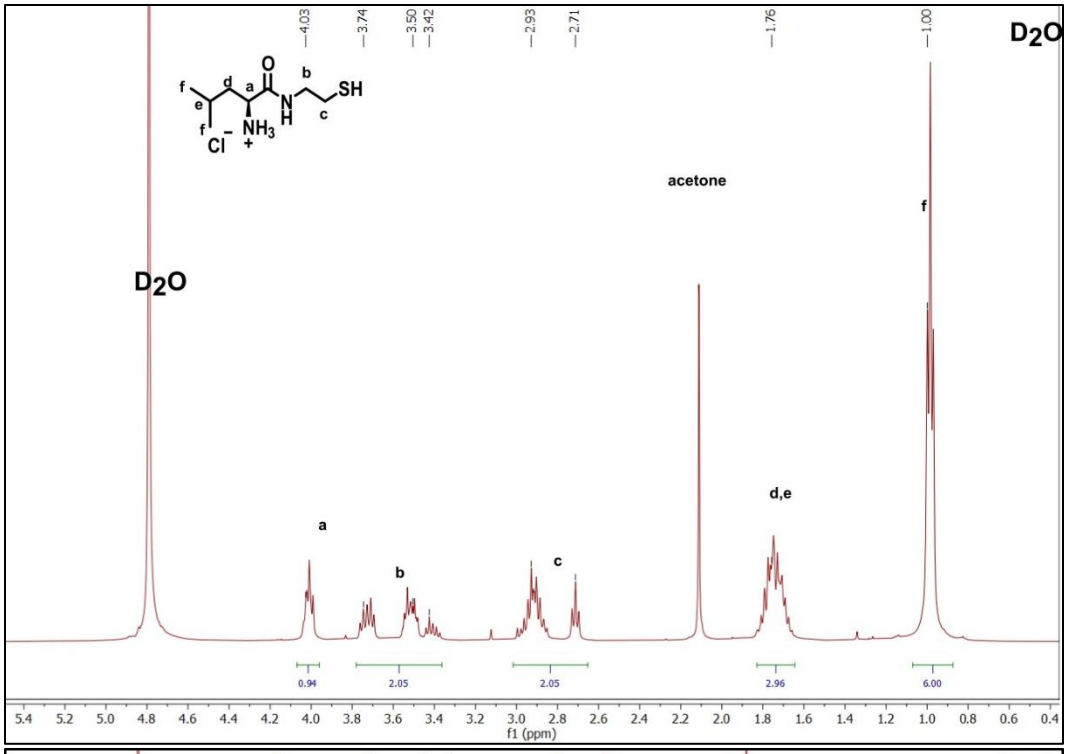
4.03
3.74
3.50
3.42
2.93
2.71
1.76
1.00
D2O
acetone
f
D2O
d,e
a
b
c
0.94
2.05
2.05
2.96
6.00
f1 (ppm)

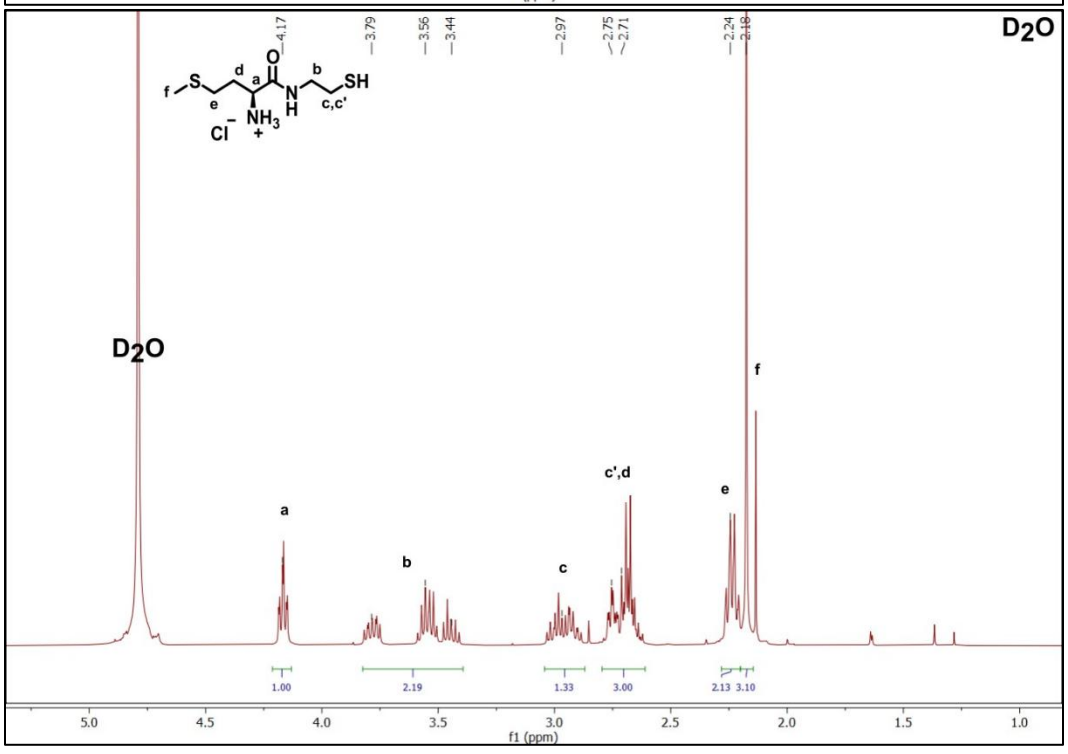
4.17
3.79
3.55
3.44
2.97
2.75
2.71
2.24
2.18
D2O
f
c',d
e
a
b
c
1.00
2.19
1.33
3.00
2.13
3.10
f1 (ppm)

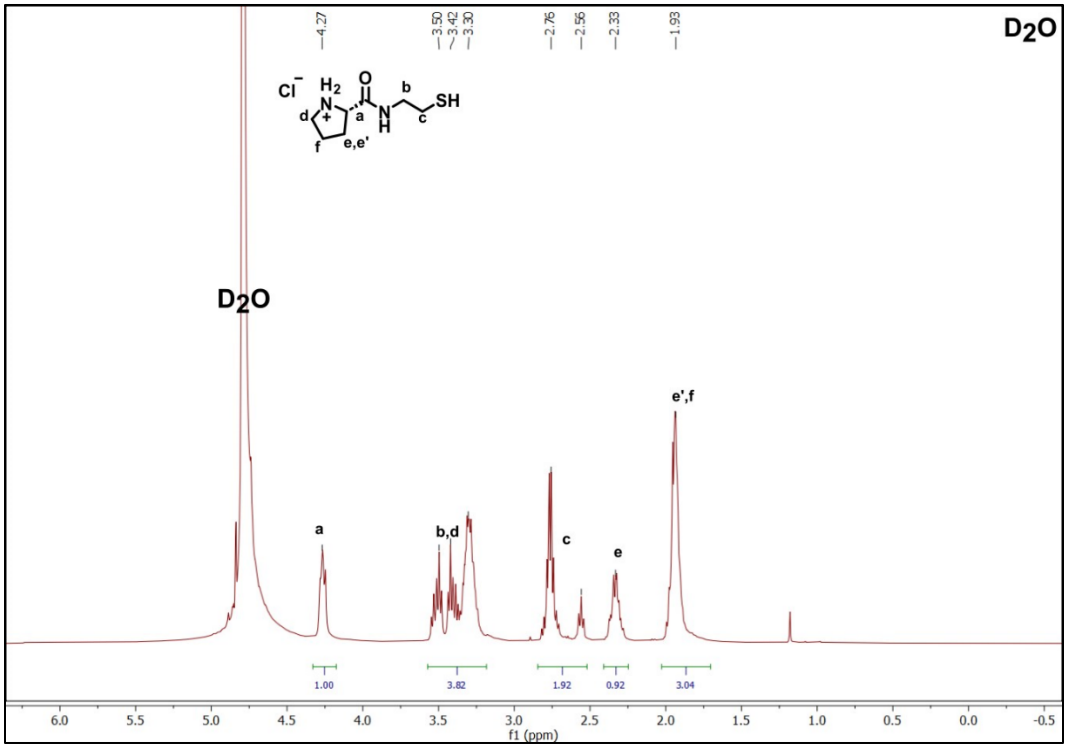
D2O
4.27
3.50
3.42
3.30
2.76
2.56
2.33
1.93
Cl⁻
H2
N
O
N
H
SH
a
b
c
d
e,e'
f
D2O
a
b,d
c
e
e',f
1.00
3.82
1.92
0.92
3.04
f1 (ppm)

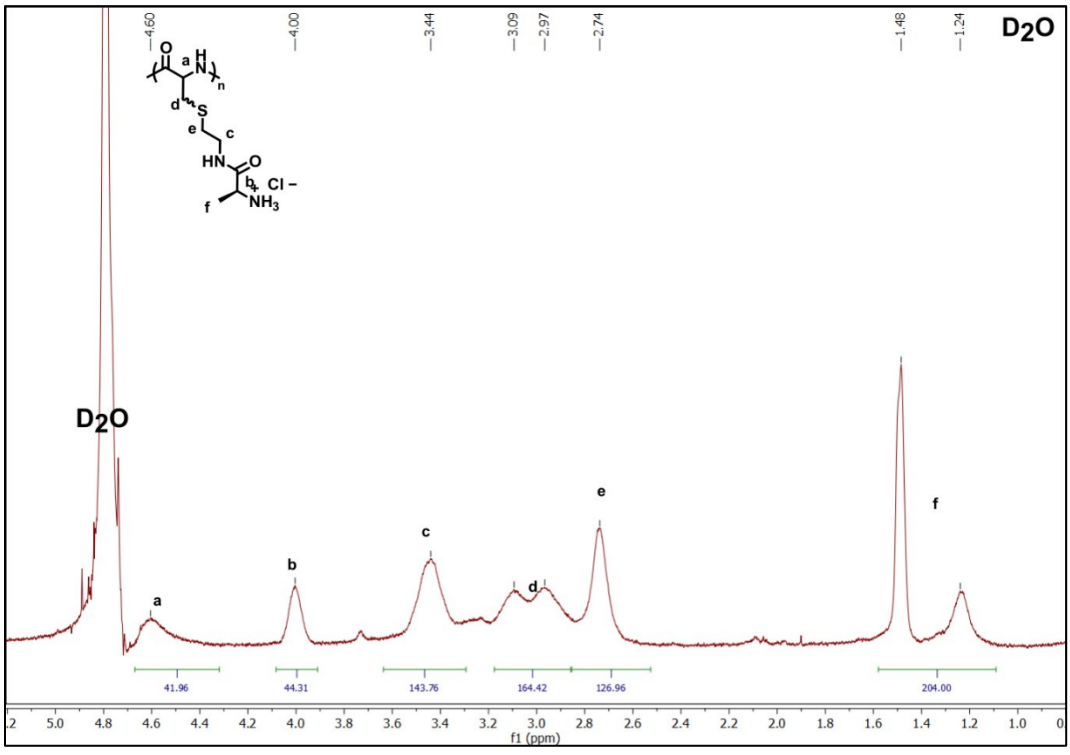
D2O
4.60
4.00
3.44
3.09
2.97
2.74
1.48
1.24
a
n
d
S
e
c
HN
O
b
Cl −
NH3
f
D2O
a
b
c
d
e
f
41.96
44.31
143.76
164.42
126.96
204.00
f1 (ppm)

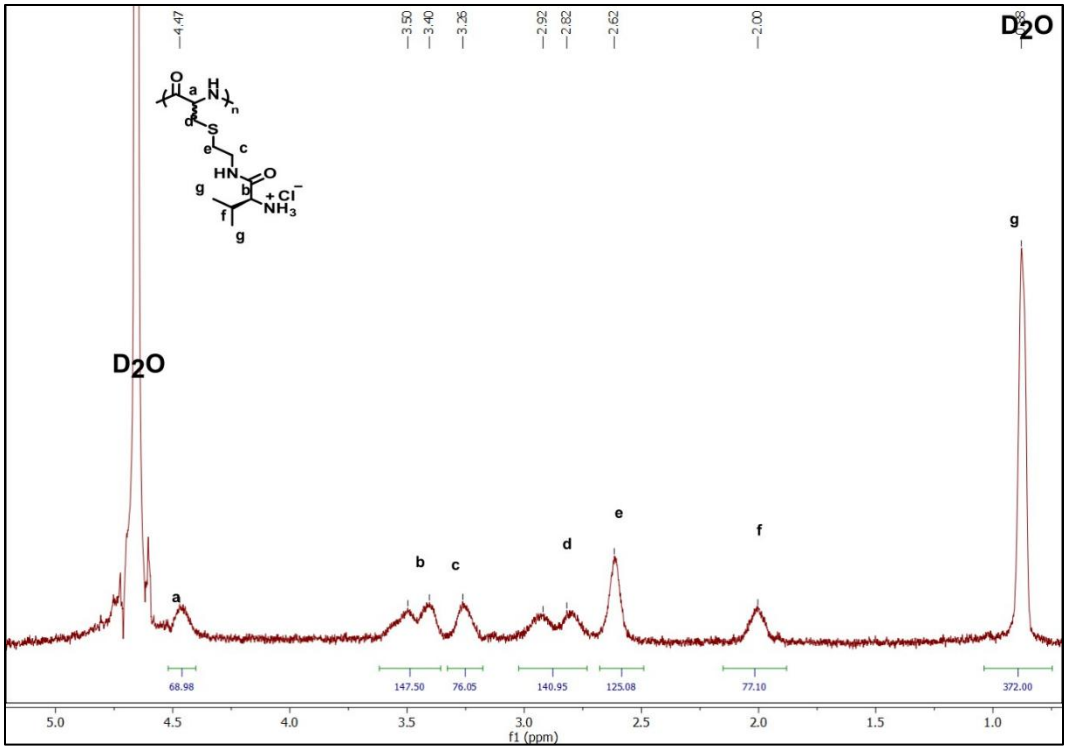
D2O
D2O
a
b
c
d
e
f
g
68.98
147.50
76.05
140.95
125.08
77.10
372.00
f1 (ppm)

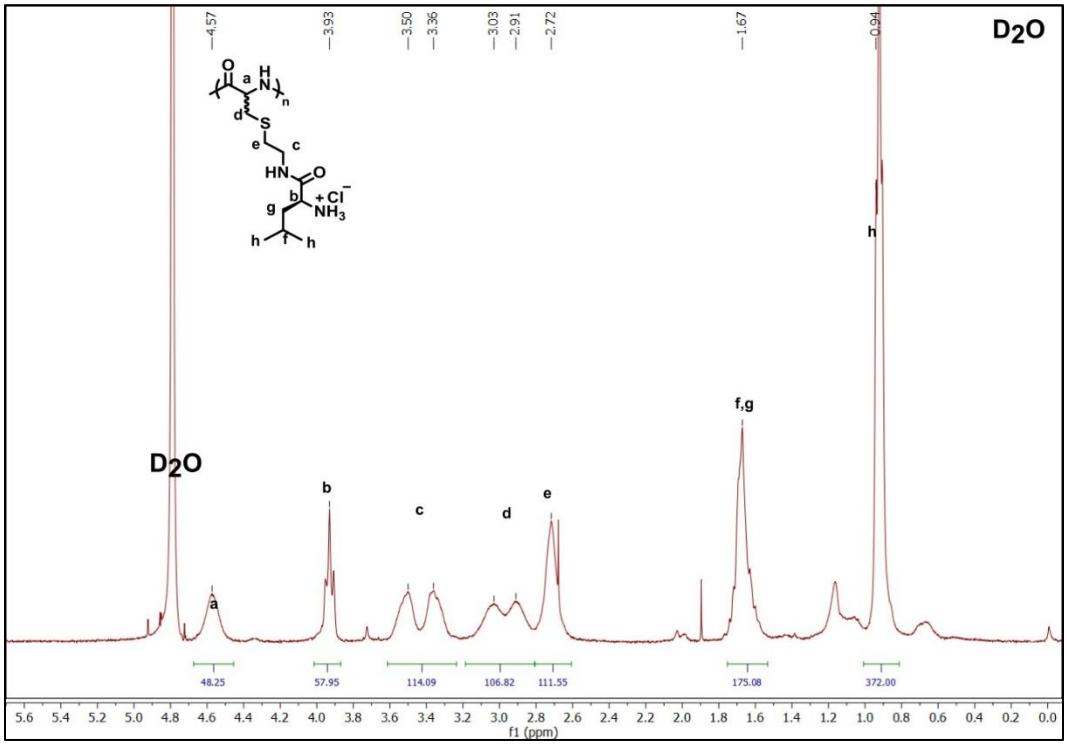
D2O
D2O
a
b
c
d
e
f,g
h
48.25
57.95
114.09
106.82
111.55
175.08
372.00
f1 (ppm)

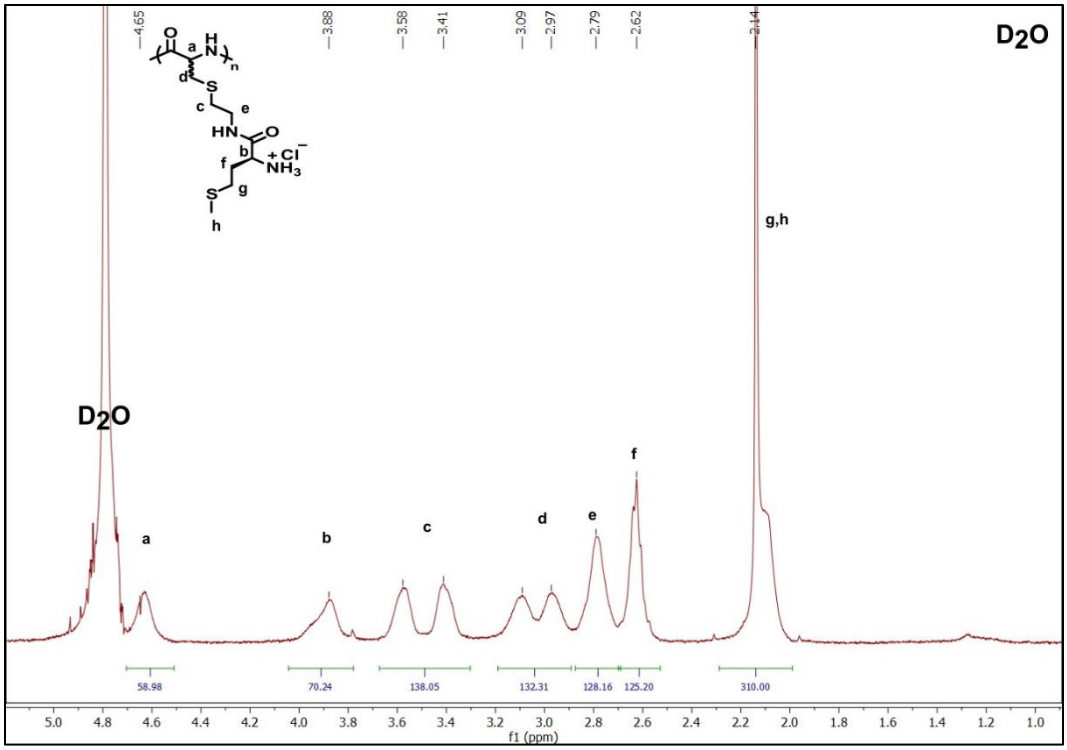
D2O
D2O
a
b
c
d
e
f
g,h
58.98
70.24
138.05
132.31
128.16
125.20
310.00
f1 (ppm)

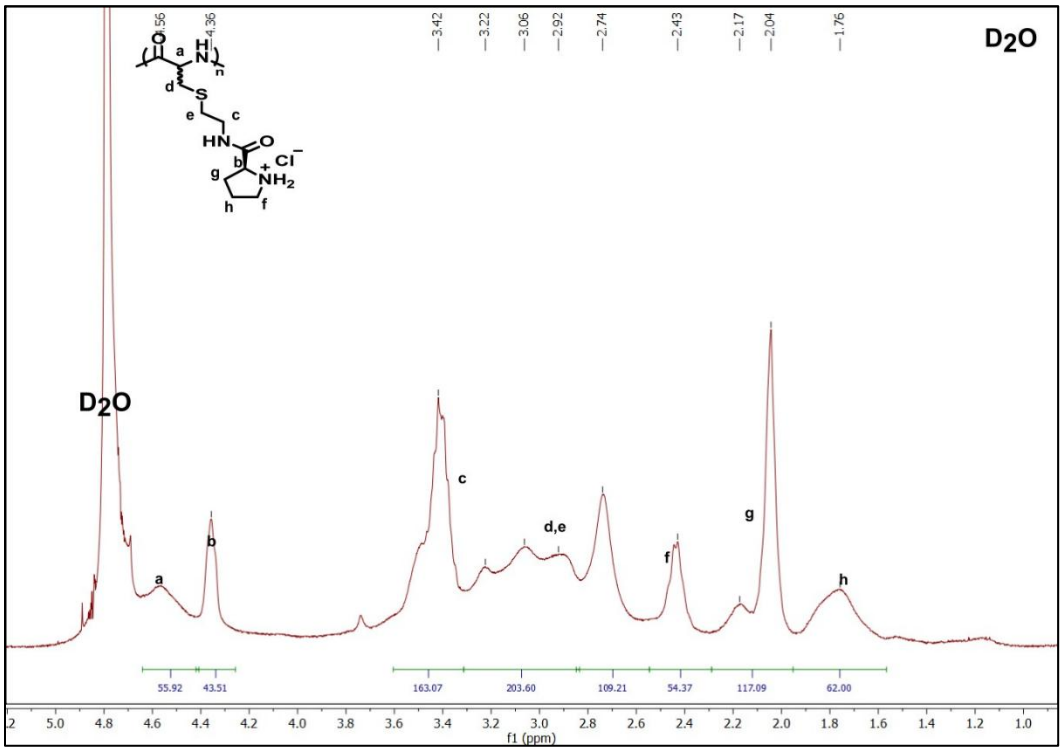
D2O
D2O
a
b
c
d,e
f
g
h
55.92
43.51
163.07
203.60
109.21
54.37
117.09
62.00
f1 (ppm)

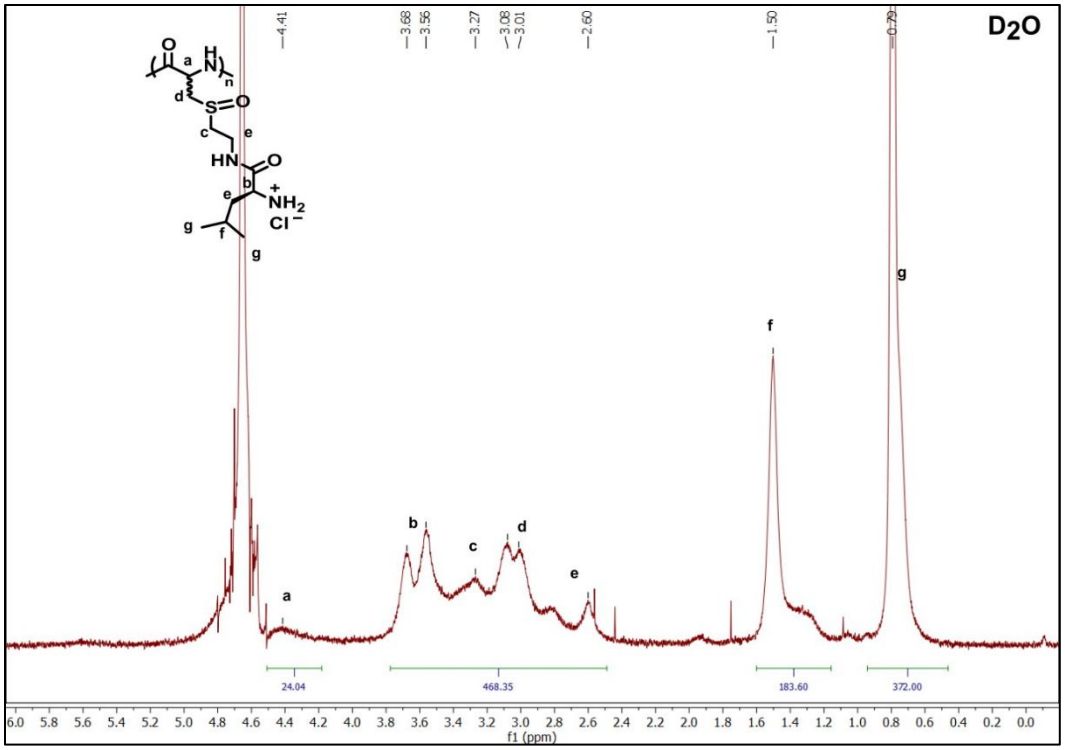
D2O
4.41
3.68
3.55
3.27
3.08
3.01
2.60
1.50
0.79
a
b
c
d
e
f
g
24.04
468.35
183.60
372.00
f1 (ppm)

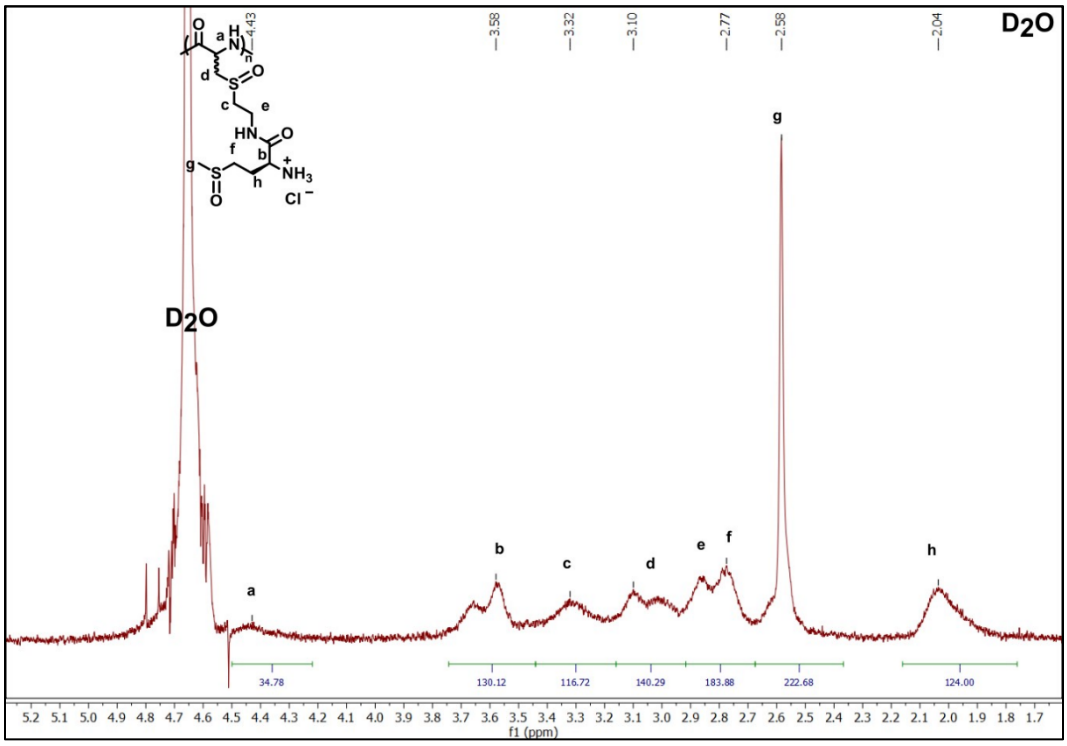
D2O
4.43
3.58
3.32
3.10
2.77
2.58
2.04
a
b
c
d
e
f
g
h
34.78
130.12
116.72
140.29
183.88
222.68
124.00
f1 (ppm)

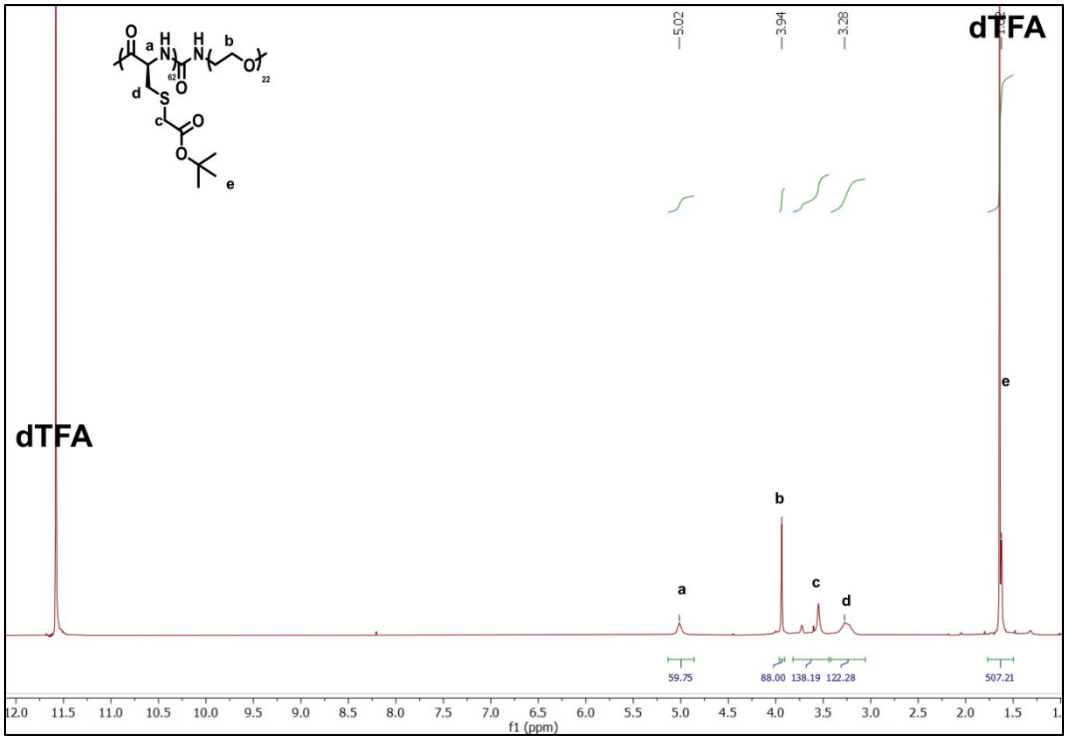
dTFA
dTFA
5.02
3.94
3.28
a
b
c
d
e
59.75
88.00
138.19
122.28
507.21
f1 (ppm)

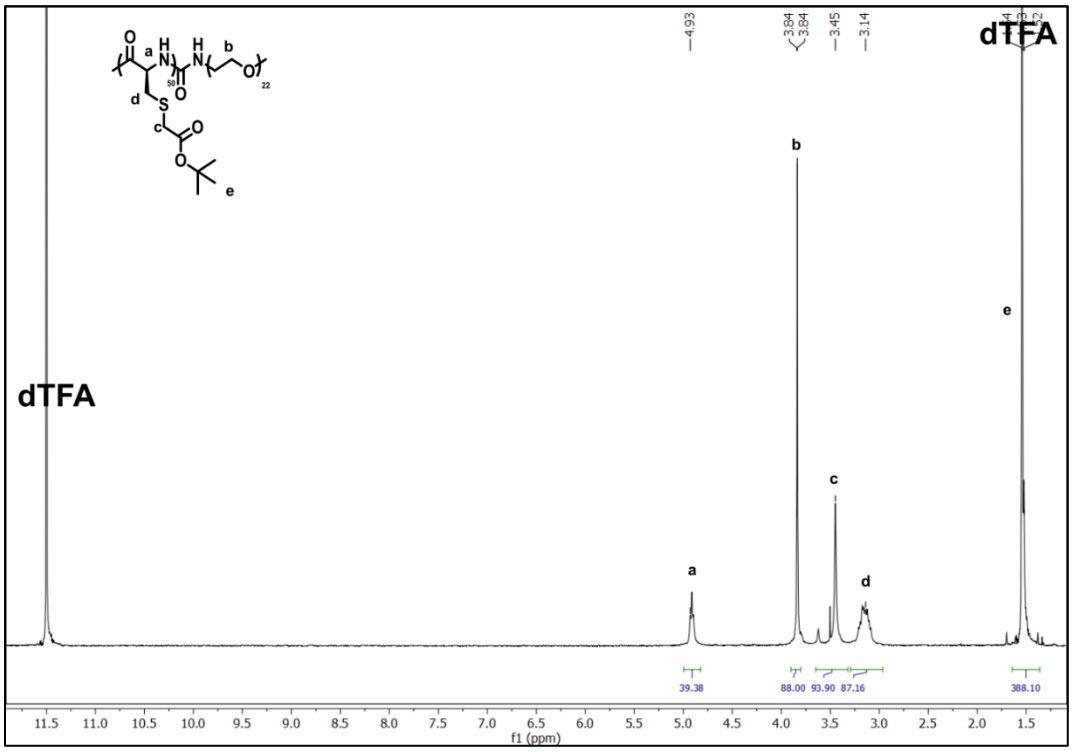
dTFA
dTFA
4.93
3.84
3.84
3.45
3.14
a
b
c
d
e
39.38
88.00
93.90
87.16
388.10
f1 (ppm)

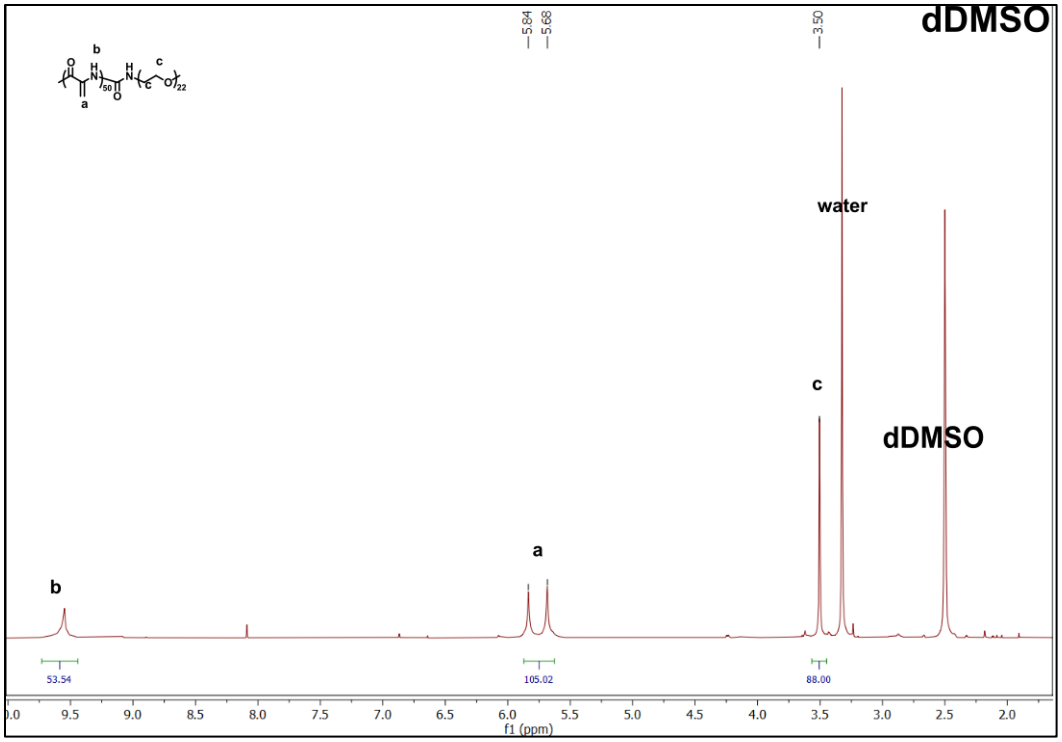
dDMSO
5.84
5.68
3.50
water
c
dDMSO
a
b
53.54
105.02
88.00
f1 (ppm)

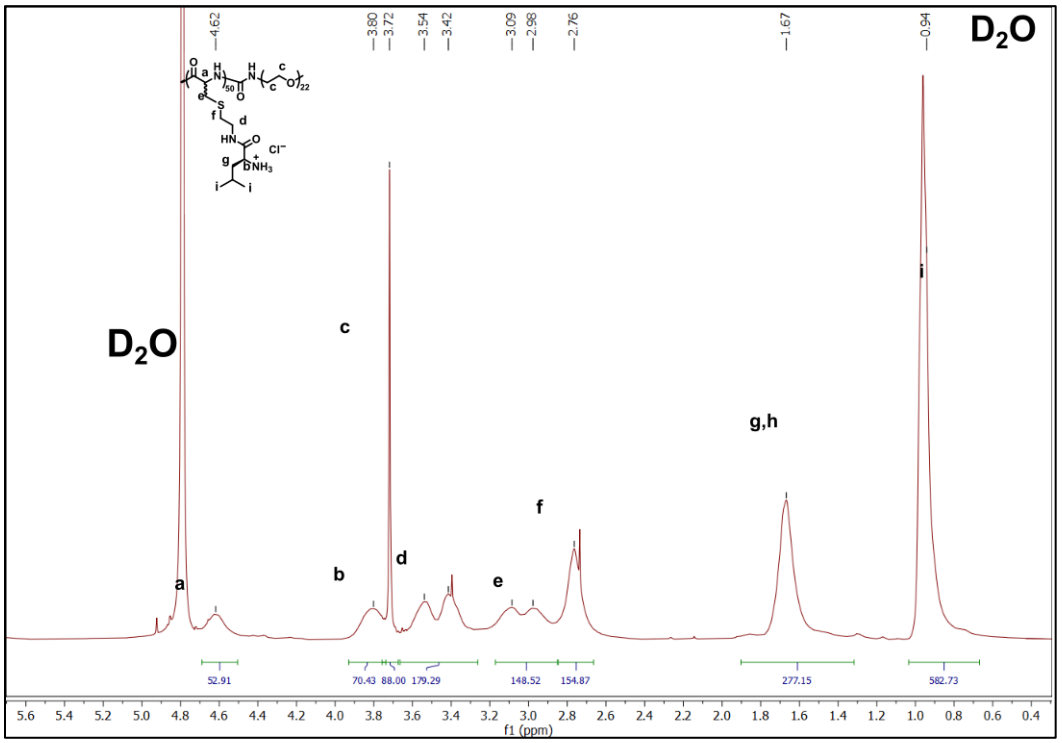
D2O
4.62
3.80
3.72
3.54
3.42
3.09
2.98
2.76
1.67
0.94
D2O
c
g,h
f
d
b
e
a
i
52.91
70.43
88.00
179.29
148.52
154.87
277.15
582.73
f1 (ppm)

2.7 References

1) Dzuricky, M.; Roberts, S.; Chilkoti, A. Convergence of artificial protein polymers and intrinsically disordered proteins. *Biochemistry* **2018**, *57*, 2405-2414.

2) Yewdall, N. A.; André, A. A. M.; Lu, T.; Spruijt, E. Coacervates as models of membraneless organelles. *Curr. Opin. Coll. Int. Sci*. **2021**, *52*, 101416.

3) Schuster, B. S.; Reed, E. H.; Parthasarathy, R.; Jahnke, C. N.; Caldwell, R. M.; Bermudez, J. G.; Ramage, H.; Good, M. C.; Hammer, D. A. Controllable protein phase separation and modular recruitment to form responsive membraneless organelles. *Nat. Commun.* **2018**, *9*, 2985.

4) Chang, L. W.; Lytle, T. K.; Radhakrishna, M.; Madinya, J. J.; Vélez, J.; Sing, C. E.; Perry, S. L. Sequence and entropy-based control of complex coacervates. *Nat. Commun.* **2017**, *8*, 1273.

5) Roberts, S.; Dzuricky, M.; Chilkoti, A. Elastin-like polypeptides as models of intrinsically disordered proteins. *FEBS Lett.* **2015**, *589*, 2477-2486.

6) Abbas, M.; Lipiński, W. P.; Wang, J.; Spruijt, E. Peptide-based coacervates as biomimetic protocells. *Chem. Soc. Rev.* **2021**, 50, 3690-3705.

7) Aumiller, W. M.; Keating, C. D. Phosphorylation-mediated RNA/peptide complex coacervation as a model for intracellular liquid organelles. *Nat. Chem.* **2016**, *8*, 129–137.

8) Nakashima, K. K.; Baaij, J. F.; Spruijt, E. Reversible generation of coacervate droplets in an enzymatic network. *Soft Matter* **2018**, *14*, 361-367.

9) Lu, T.; Nakashima, K. K.; Spruijt, E. Temperature-responsive peptide-nucleotide coacervates. *J. Phys. Chem. B* **2021**, *125*, 3080-3091.

10) Brangwynne, C. P. Soft active aggregates: mechanics, dynamics and self-assembly of liquid-like intracellular protein bodies. *Soft Matter* **2011**, *7*, 3052-3059.

11) Waite, J. H. Mussel adhesion – essential footwork. *J. Exp. Biol.* **2017**, *220*, 517-530.

12) Banani, S. F.; Lee, H. O.; Hyman, A. A.; Rosen, M. K. Biomolecular condensates: organizers of cellular biochemistry. *Nat. Rev. Mol. Cell. Biol*. **2017**, *18*, 285–298.

13) Perry, S. L.; Leon, L.; Hoffmann, K. Q.; Kade, M. L.; Priftis, D.; Black, K. A.; Wong, D.; Klein, R. A.; Piercel II, C. F.; Margossian, K. O.; Whitmer, J. K.; Qin, J.; de Pablo, J. J.; Tirrell, M. Chirality-selected phase behaviour in ionic polypeptide complexes. *Nat. Commun.* **2015**.

14) Koga, S.; Williams, D. S.; Perriman, A. W.; Mann, S. Peptide-nucleotide microdroplets as a step towards a membrane-free protocell model. *Nat. Chem.* **2011**, *3*, 720–724.

15) Rumyantsev, A. M.; Jackson, N. E.; Yu, B.; Ting, J. M.; Chen, W.; Tirrell, M. V.; de Pablo, J. J. Controlling complex coacervation via random polyelectrolyte sequences. *ACS Macro Lett.* **2019**, *8*, 1296-1302.

16) Scott, W. A.; Gharakhanian, E. G.; Bell, A. G.; Evans, D.; Bahrun, E.; Houk, K. N.; Deming, T. J. Active controlled and tunable coacervation using side-chain functional α-helical homopolypeptides. *J. Amer. Chem. Soc.* **2021**, *143*, 18196-1820.

17) Benavides, I.; Raftery, E. D.; Bell, A. G.; Evans, D.; Scott, W. A.; Houk, K. N.; Deming, T. J. Poly(dehydroalanine): synthesis, properties and functional diversification of a fluorescent polypeptide. *J. Amer. Chem. Soc.* **2022**, *144*, 4214-4223.

18) Deming, T. J.; Curtin, S. A. Chain initiation efficiency in cobalt- and nickel-mediated polypeptide synthesis. *J. Amer. Chem. Soc.* **2000**, *122*, 5710–5717.

19) Kramer, J. R.; Deming, T. J. Preparation of multifunctional and multireactive polypeptides via methionine alkylation. *Biomacromolecules* **2012**, *13*, 1719–1723.

20) Kramer, J. R.; Deming, T. J. General method for purification of α-amino acid-N-carboxyanhydrides using flash chromatography. *Biomacromolecules* **2010**, *11*, 3668–3672.

21) Chowdhury, S.; Schatte, G.; Kraatz, H.-B. Synthesis, structure and electrochemistry of ferrocene–peptide macrocycles. *Dalton Trans.* **2004**, No. 11, 1726–1730.

22) Budt, K.-H.; Stowasser, B.; Peyman, A.; Knolle, J.; Winkler, I.; Berscheid, H. G. Prodrug derivatives of enzyme inhibitors having hydroxyl groups, a process for preparing them, and their use. US5804559A, September 8, 1998. https://patents.google.com/patent/US5804559/en (accessed 2022-12-23).

23) Wollenberg, A. L.; O'Shea, T. M.; Kim, J. H.; Czechanski, A.; Reinholdt, L. G.; Sofroniew, M. V.; Deming, T. J. Injectable polypeptide hydrogels via methionine modification for neural stem cell delivery. *Biomaterials* **2018**, *178*, 527–545.

24) Wollenberg, A. L.; Perlin, P.; Deming, T. J. Versatile N-methylaminooxy functionalized polypeptides for preparation of neoglycoconjugates. *Biomacromolecules*, **2019**, *20*, 1756-1764.

25) Chambers, R. W.; Carpenter, F. H. On the preparation and properties of some amino acid amides. *J. Amer. Chem. Soc.* **1955**, *77*, 1522-1526.

26) Appel, P.; Yang, J. T. Helix-coil transition of poly-L-glutamic acid and poly-L-lysine in D_2O. *Biochemistry,* **1965**, *4*, 1244-1249.

27) Jochum, F. D.; Theato, P. Temperature- and light-responsive smart polymer materials. *Chem. Soc. Rev.* **2013**, *42*, 7468-7483.

28) Wimley, W. C.; Creamer, T. P.; White, S. H. Solvation energies of amino acid side chains and backbone in a family of host-guest pentapeptides. *Biochemistry* **1996**, *35*, 5109-5124.

29) Brot, N.; Weissbach, L.; Werth, J.; Weissbach, H. Enzymatic reduction of protein-bound methionine sulfoxide. *Proc. Natl. Acad. Sci. USA* **1981**, *78*, 2155-2158.

30) Levine, R. L.; Mosoni, L.; Berlett, B. S.; Stadtman, E. R. Methionine residues as endogenous antioxidants in proteins. *Proc. Natl. Acad. Sci. USA* **1996**, *93*, 15036-15040.

31) Levine, R. L.; Moskovitz, J.; Stadtman, E. R. Oxidation of methionine in proteins: roles in antioxidant defense and cellular regulation. *Life* **2000**, *50*, 301-307.

32) Moskovitz, J.; Bar-Noy, S.; Williams, W. M.; Requena, J.; Berlett, B. S.; Stadtman, E. R. Methionine sulfoxide reductase (MsrA) is a regulator of antioxidant defense and lifespan in mammals. *Proc. Natl. Acad. Sci. USA* **2001**, *98*, 12920-12925.

Chapter 3: Triggered Inversion of Dual Responsive Diblock Copolypeptide Vesicles

Adapted from Morrison, C. A.; Chan, E. P.; Deming, T. J. *J. Am. Chem. Soc.* **2025**, *147* (9), 7617–7623.

3.1 Abstract

We report the synthesis of amphiphilic poly(L-methionine sulfoxide)$_x$-*b*-poly(dehydroalanine)$_y$, diblock copolypeptides, $\mathbf{M^O_xA^{DH}_y}$, and their self-assembly into submicrometer-diameter unilamellar vesicles in aqueous media. The formation of vesicles was observed over an unprecedented range of copolypeptide compositions due to the unique properties and chain conformations of $\mathbf{A^{DH}}$ hydrophobic segments. These copolypeptides incorporate two distinct thiol reactive components where each segment can respond differently to a single thiol stimulus. The incubation of $\mathbf{M^O_{35}A^{DH}_{30}}$ vesicles with glutathione under intra-cellular mimetic conditions resulted in vesicle disruption and release of cargo. Further, incubation of $\mathbf{M^O_{35}A^{DH}_{30}}$ vesicles with thiolglycolic acid resulted in a reversal of amphipilicity and successful *in situ* inversion of the vesicle assemblies. This conversion of biomimetic polymer vesicles into stable inverted vesicles using a biologically relevant stimulus at physiological pH and temperature is unprecedented. These results provide insights toward the development of advanced functional synthetic assemblies with potential uses in biology and medicine.

3.2 Introduction

There is considerable interest in polymer assemblies that can undergo changes in structure and properties in response to biologically relevant stimuli.[1−3] Appropriate stimuli can include redox reagents, enzymes, and sugars as well as molecules such as NO, CO_2, and H_2S.[1−3] Such responsive assemblies have primarily been developed for use as

therapeutic delivery vehicles that can release their cargo in the presence of an appropriate stimulus.[4−6] Consequently, many of these assemblies have been designed to simply degrade or disassemble upon reaction with the stimulus. However, block copolymer assemblies have also been developed that are able to undergo changes in shape and morphology upon exposure to stimuli.[7−9] In addition, “invertible” assemblies have been developed where both block copolymer segments respond to stimuli, resulting in a reversal of amphiphilicity and consequent inversion of micellar or vesicular structures.[10−17] Invertible assemblies are intriguing since they can release cargos but can also allow for the encapsulation of surrounding media during inversion. While a variety of shape-changing transformations have been reported for assemblies under conditions that are not compatible with living systems, there are noteworthy exceptions.

Vesicle−micelle transformations have been achieved using redox and hydrolysis reactions as well as enzymes, and micelle−micelle inversions have been accomplished using light and/or heat.[1,2,11,13,15] However, to our knowledge, block copolymer vesicle-to-vesicle inversion has not been achieved under biologically relevant conditions, which would be valuable for the development of advanced functional synthetic assemblies as well as for potential uses in biology and medicine. Addressing this need, we describe the development of amphiphilic diblock copolypeptide vesicles in which each polypeptide segment responds differently to a single biomimetic stimulus, resulting in vesicle inversion under biologically relevant conditions. Pioneering examples of block copolymer vesicle inversion were reported by Eisenberg and Lecommandoux.[12,14] Both approaches utilized a combination of acidic and basic segments in block copolymers, where at low pH acidic segments are neutral and basic segments are charged and at high pH acidic segments

are charged and basic segments are neutral. Reversal of amphiphilicity upon switching the pH between 4 and 10 or 1 and 14 resulted in an inversion of vesicle assemblies. At pH 7, both acidic and basic segments in these systems were charged, and vesicles did not form. While these studies were the first to demonstrate the inversion of polymeric vesicles, their potential applications were limited by the extremes in pH required for vesicle interconversion and stability.

Consequently, we sought to develop self-assembled block copolymer vesicles that would be stable and capable of triggered inversion under biologically relevant conditions (e.g., pH 7.4, 150 mM NaCl, 37 °C). These conditions preclude the use of a large variation of temperature or solution pH to trigger inversion but do allow the use of reactive molecules that are found in biological systems.[1−3] We focused our vesicle design on block copolypeptides since both their chain conformations and sidechain functionality can be predictably manipulated.[18,19] If used for therapeutic applications, the peptide backbone also allows for enzymatic degradation *in vivo*.[20,21] Ordered chain conformations in polypeptides can guide structure formation during assembly, a feature which cannot be readily replicated in most other synthetic polymers.[18,19] Many studies, by our laboratory and others, have led to a detailed understanding of how polypeptide chain conformations and block compositions influence structure formation and properties in aqueous-based assemblies.[18,19] This work has resulted in robust designs for the creation of block copolypeptide micelles, vesicles, and fibril-based hydrogels utilizing readily obtained α-helical, β-sheet, and disordered chain conformations.[22−29] Block copolypeptide assemblies have also been developed that can respond to various biologically relevant stimuli.

In particular, there has been considerable interest in redox-responsive copolypeptide assemblies that can release cargo intracellularly by the reduction of one segment using thiols or enzymes present within cell cytosol.[1–3,26] However, to obtain invertible assemblies, both segments in block copolypeptides need to be stimuli responsive to achieve switching of the water solubility in both domains. To accomplish this, we envisioned the incorporation of two distinct thiol reactive polypeptide segments in block copolymers, where each segment would respond differently to a single stimulus. Upon reaction with thiols, each segment would undergo a change in water solubility while simultaneously also undergoing a conformational change. These combined changes, in conjunction with the optimization of copolymer compositions, were envisioned to yield invertible vesicles under biologically relevant conditions.

Our design of thiol reactive amphiphilic block copolypeptides incorporated water-soluble, conformationally disordered poly(L-methionine sulfoxide), $\mathbf{M^O}$, segments connected to water-insoluble, extended conformation poly(dehydroalanine), $\mathbf{A^{DH}}$, segments, i.e., $\mathbf{M^O_xA^{DH}_y}$ (**Figure 3.1**).

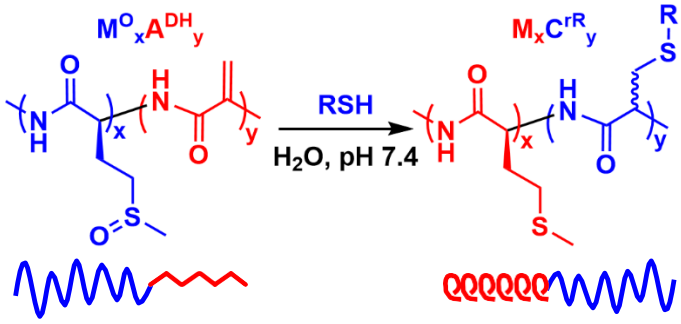

Figure 3.1. Proposed reversal of block copolypeptide amphiphilicity by reaction of $\mathbf{M^O_xA^{DH}_y}$ with thiols (endgroups not shown). Blue = hydrophilic; red = hydrophobic

Due to their amphiphilicity, $\mathbf{M^O_xA^{DH}_y}$ were expected to self-assemble in aqueous media. We have previously reported that $\mathbf{M^O}$ is highly biocompatible and can be used as a hydrophilic segment for the preparation of vesicle and hydrogel block copolypeptide assemblies.[20,21] We have also shown that $\mathbf{M^O}$ segments can react with thiols or enzymes under conditions that mimic a cytosolic environment to form hydrophobic, α-helical poly(L-methionine), **M**, segments and that this reaction can lead to vesicle disruption.[26]

Additionally, our group recently reported the preparation of hydrophobic $\mathbf{A^{DH}}$ and showed that the dehydroalanine residues can react readily with thiols to give disordered poly(S-alkyl-*rac*-cysteine)s, $\mathbf{C^{rR}}$.[30] If a hydrophilic thiol is used, the resulting $\mathbf{C^{rR}}$ can be water-soluble.[30] Individually, both of these polypeptide modifications are known to go to completion in aqueous media at pH 7.4.[26,30] The combination of $\mathbf{M^O}$ and $\mathbf{A^{DH}}$ segments in, $\mathbf{M^O_xA^{DH}_y}$ block copolypeptides was expected to result in both segments being able to react with thiols under biologically relevant conditions.

Further, the complete reaction of, $\mathbf{M^O_xA^{DH}_y}$ with a hydrophilic thiol should result in a reversal of amphiphilicity, where hydrophilic $\mathbf{M^O}$ is converted to hydrophobic M while hydrophobic $\mathbf{A^{DH}}$ is converted to hydrophilic $\mathbf{C^{rR}}$ (**Figure 3.1**). While the design rules for aqueous self-assembly of amphiphilic block copolypeptides containing α-helical or βsheet hydrophobic segments are well understood, the self-assembly of $\mathbf{A^{DH}}$ containing block copolymers has not been previously studied.[18,19] Here, an important goal was to determine how the unique chain conformation of $\mathbf{A^{DH}}$ influences structure formation in, $\mathbf{M^O_xA^{DH}_y}$ assemblies.[30] We then planned to use this knowledge to design copolypeptide compositions that can form vesicles in water.

An additional challenge of this project was the synthesis of $\mathbf{M^{O}_{x}A^{DH}_{y}}$, which requires the use of two different post-polymerization modification reactions that can interfere with each other. Here, we describe the successful preparation of $\mathbf{M^{O}_{x}A^{DH}_{y}}$ block copolypeptides, their self-assembly into vesicles in aqueous media, and how the vesicle assemblies respond to the addition of thiols under biologically relevant conditions. This work breaks new ground in the development of biologically relevant stimuli-responsive copolymer assemblies by utilizing a combination of naturally occurring thiol-reactive amino acid functionalities. The results also provide insights into understanding and controlling stimulus-responsive switching of assemblies as mimics of protein assemblies.

3.3 Results and Discussion

Our initial strategy to prepare, $\mathbf{M^{O}_{x}A^{DH}_{y}}$ copolypeptides relied on the stepwise addition of monomers L-methionine N-carboxyanhydride (Met NCA) and S-(*tert*-butylcarboxymethyl)-L-cysteine (tBuCM-Cys) NCA to $Co(PMe_3)_4$ initiator, which gave poly(L-methionine)-*b*-poly(S-(*tert*-butylcarboxymethyl)-L-cysteine), $\mathbf{M_xC^{BCM}_y}$, diblock copolypeptide precursors of desired compositions and chain lengths.[31] (**Figure 3.2**) *tert*-Butyl protecting groups were subsequently removed from this precursor, and then all thioether groups were oxidized to give samples of poly(L-methionine sulfoxide)-*b*-poly(S-(carboxymethyl)-L-cysteine sulfoxide), $\mathbf{M^{O}_{x}C^{CMO}_{y}}$.

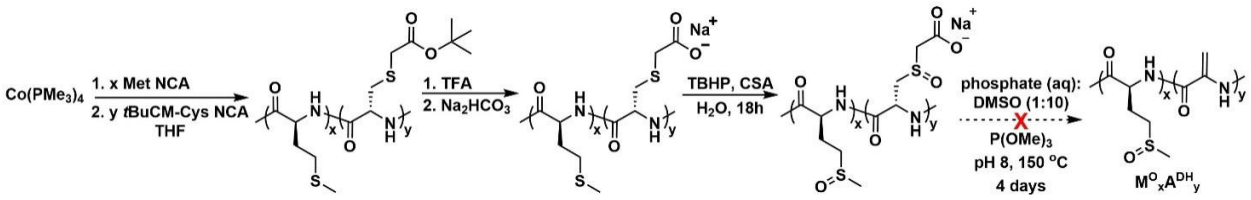

Figure 3.2. Attempted synthesis of $\mathbf{M^{O}_{x}A^{DH}_{y}}$ diblock copolypeptides via sequential addition of NCAs using $Co(PMe_3)_4$ initiator, followed by oxidation and elimination.

These copolymers were then subjected to a variety of conditions to convert S-(carboxymethyl)-L-cysteine sulfoxide residues to dehydroalanine residues via thermal or base-catalyzed elimination in order to obtain, $\mathbf{M^{O}_{x}A^{DH}_{y}}$ copolypeptides (**Figure 3.2**). While there is precedent for the conversion of isolated alkyl cysteine sulfoxide residues into dehydroalanine residues using sulfenic acid trapping reagents, we were unable to obtain the desired, $\mathbf{M^{O}_{x}A^{DH}_{y}}$ copolypeptides via this route.[30]

As an alternative, we have shown that the alkylation of thioether groups in poly(S-(carboxymethyl)-L-cysteine), $\mathbf{C^{CM}}$, is highly efficient in promoting the elimination and formation of A^{DH}.[30] However, alkylation of a $\mathbf{M_{x}C^{CM}_{y}}$ precursor would also alkylate the **M** segment and consequently prohibit its subsequent oxidation to $\mathbf{M^{O}}$.[33] While nucleophilic dealkylation of methionine sulfonium salts is possible, the reagents, usually thiols, would also react with A^{DH} residues.[30,34] To circumvent these interfering reactions, we developed a new synthetic route to, $\mathbf{M^{O}_{x}A^{DH}_{y}}$ copolypeptides that separates the oxidation and alkylation reactions so that they occur only within the desired segments (**Figure 3.3**).

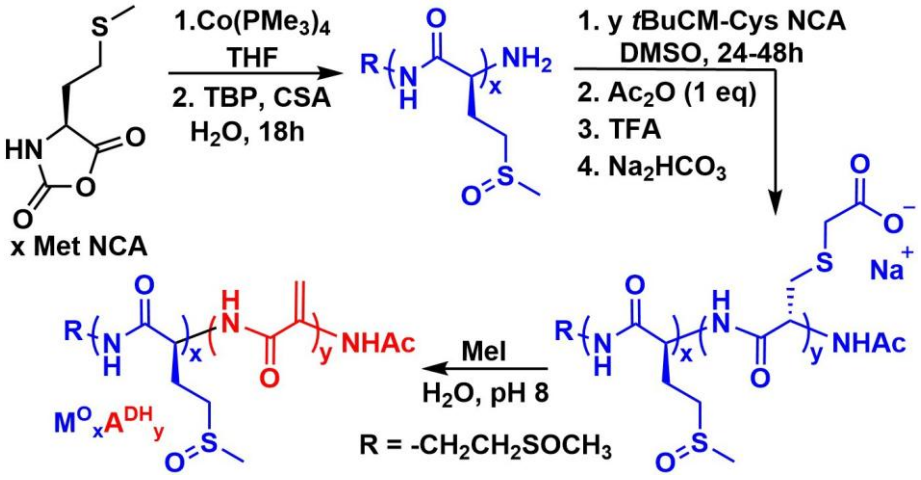

Figure 3.3. Synthesis of amphiphilic $\mathbf{M^{O}_{x}A^{DH}_{y}}$. Blue = hydrophilic; red = hydrophobic.

First, Met NCA was added to the $Co(PMe_3)_4$ initiator to give M chains of desired length, which were then converted to $\mathbf{M^O}$ via oxidation. The $\mathbf{M^O}$ chains, each containing a primary amine group on the N-terminus, were then used as macroinitiators for polymerization of tBuCM-Cys NCA in DMSO. The amino termini of the resulting block copolymers were end-capped using acetic anhydride, followed by removal of *tert*-butyl protecting groups and then neutralization to give $\mathbf{M_xC^{CM}_y}$ copolypeptides.[30] The thioether groups in $\mathbf{M_xC^{CM}_y}$ were then alkylated using methyl iodide, which resulted in facile elimination of the thioether byproduct to give $\mathbf{M^O_xA^{DH}_y}$ copolypeptides in high purity and overall good yields (**Table 3.1**).[30]

Table 3.1. Isolated yields of purified block copolypeptide intermediates and final products.

Sample	% Yield $\mathbf{M^O_xC^{BCM}_y}$	% Yield $\mathbf{M^O_xC^{CM}_y}$	% Yield $\mathbf{M^O_xA^{DH}_y}$
$\mathbf{M^O_{35}A^{DH}_{30}}$	86	68	**74**
$\mathbf{M^O_{60}A^{DH}_{30}}$	71	74	**52**
$\mathbf{M^O_{60}A^{DH}_{40}}$	92	73	**78**
$\mathbf{M^O_{60}A^{DH}_{60}}$	70	78	**85**
$\mathbf{M^O_{60}A^{DH}_{100}}$	**78**	**75**	**84**

Compositions and chain lengths of $\mathbf{M^O_xA^{DH}_y}$ copolypeptides were determined using ^{1}H NMR and GPC analysis (**Table 3.2, Table 3.3** and **Figure 3.4**). Since amphiphilic $\mathbf{M^O_xA^{DH}_y}$ samples were not fully soluble in common GPC solvents, these copolypeptides were converted to poly(S-methyl-L-methionine sulfonium chloride)-*b*-poly(dehydroalanine), $\mathbf{M^M_xA^{DH}_y}$, derivatives for GPC analysis in HFIP. All $\mathbf{M^M_xA^{DH}_y}$

samples, as well as $\mathbf{M^{M}}$ precursors, gave monomodal peaks and reasonable dispersity values (**Table 3.2**, **Table 3.3** and **Figure 3.4**).

Table 3.2. Properties of $\mathbf{M^{O}_{x}A^{DH}_{y}}$ block copolypeptides

Sample	Composition[a]	$Đ$ [b]	Diameter (nm)[c]	PDI[d]
$\mathbf{M^{O}_{35}A^{DH}_{30}}$	$\mathbf{M^{O}_{35}A^{DH}_{30}}$	1.15	251	.354
$\mathbf{M^{O}_{60}A^{DH}_{30}}$	$\mathbf{M^{O}_{60}A^{DH}_{32}}$	1.41	305	.142
$\mathbf{M^{O}_{60}A^{DH}_{40}}$	$\mathbf{M^{O}_{60}A^{DH}_{42}}$	1.25	644	.358
$\mathbf{M^{O}_{60}A^{DH}_{60}}$	$\mathbf{M^{O}_{60}A^{DH}_{63}}$	1.33	567	.302
$\mathbf{M^{O}_{60}A^{DH}_{100}}$	$\mathbf{M^{O}_{60}A^{DH}_{99}}$	1.32	275	.221

[a]Copolypeptide compositions determined by ^{1}H NMR. [b]Dispersity ($Đ$ = M_W/M_n) of copolypeptides. [c]Average hydrodynamic diameter of copolypeptide assemblies determined by DLS measurements on 1% (w/v). [d]Polydispersity (PDI) of copolypeptide assemblies determined by DLS

Table 3.3. Molecular weight and dispersity data from GPC analysis of polypeptide derivatives.

Sample	M_n[a]	M_w[a]	$Đ$[b]
$\mathbf{M^M_{35}}$	870	1070	1.23
$\mathbf{M^M_{35}A^{DH}_{30}}$	1840	2210	1.19
$\mathbf{M^M_{60}}$	3030	4490	1.48
$\mathbf{M^M_{60}A^{DH}_{30}}$	3860	5430	1.41
$\mathbf{M^M_{60}A^{DH}_{40}}$	4440	5530	1.25
$\mathbf{M^M_{60}A^{DH}_{60}}$	4690	6220	1.32
$\mathbf{M^M_{60}A^{DH}_{100}}$	5390	6930	1.32

$\mathbf{M^M_x}$ and $\mathbf{M^M_xA^{DH}_y}$ were prepared from the corresponding $\mathbf{M^O_x}$ and $\mathbf{M^O_xA^{DH}_y}$ samples. $\mathbf{M^M_x}$ and $\mathbf{M^M_xA^{DH}_y}$ derivatives were found to have improved solubility in HFIP compared to the corresponding $\mathbf{M^O_x}$ and $\mathbf{M^O_xA^{DH}_y}$ samples, which allowed for GPC analysis. [a] M_n and M_w values were calculated relative to polyethylene glycol standards. [b] Dispersity ($Đ$) = M_w/M_n.

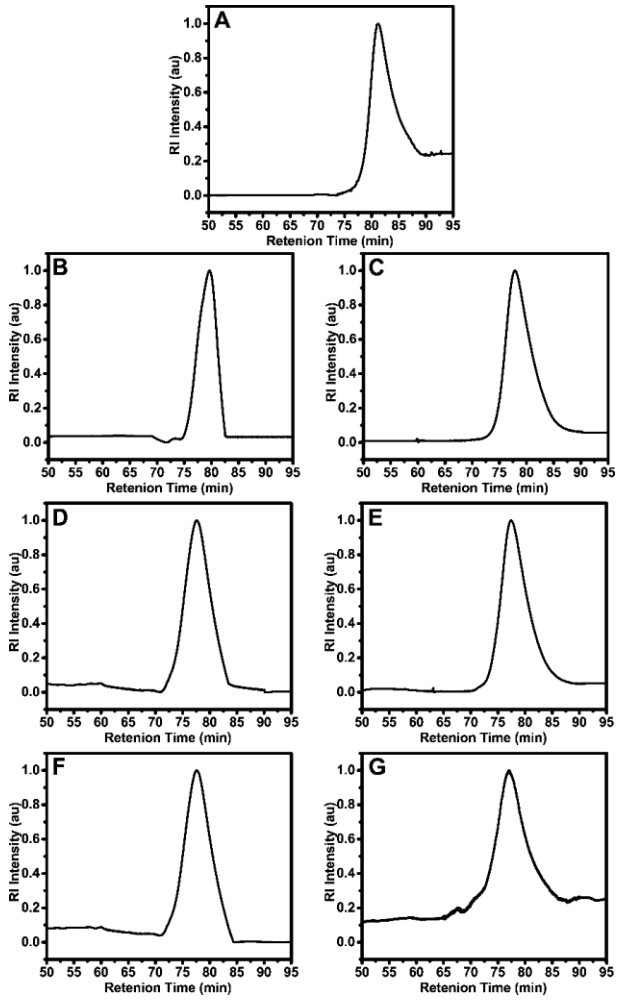

Figure 3.4. GPC chromatograms of polypeptide derivatives. (A) $\mathbf{M^{M}_{35}}$, (B) $\mathbf{M^{M}_{35}A^{DH}_{30}}$, (C) $\mathbf{M^{M}_{60}}$, (D) $\mathbf{M^{M}_{60}A^{DH}_{30}}$, (E) $\mathbf{M^{M}_{60}A^{DH}_{40}}$, (F) $\mathbf{M^{M}_{60}A^{DH}_{60}}$. (G) $\mathbf{M^{M}_{60}A^{DH}_{100}}$. All samples were dissolved at 15 mg/mL in HFIP for analysis.

Absolute chain lengths from end-group analysis by ^{1}H NMR were used for sample labeling, since molecular weights from GPC were relative to PEG standards. In order to evaluate how segment length affects aqueous self-assembled structures, $\mathbf{M^{O}_{x}A^{DH}_{y}}$ samples were prepared with a range of compositions. Initially, a series of samples were prepared with a constant $\mathbf{M^{O}_{x}}$ segment where x = 60 and $\mathbf{A^{DH}_{y}}$ segments where y = 30, 40, 60, and 100 (**Table 3.2**). $\mathbf{M^{O}_{60}}$ was chosen since we had previously determined that

this length was optimal for vesicle formation in amphiphilic copolypeptides containing α-helical hydrophobic segments, e.g., $\mathbf{M^{O}_{60}(L/F)_{20}}$, **L/F** = poly(L-leucine-*stat*-L-phenylalanine).[26]

The $\mathbf{A^{DH}_{y}}$ segment lengths were chosen to be greater than 20 residues due to the lower hydrophobicity of dehydroalanine compared to that of amino acids such as leucine and phenylalanine. A broad range of $\mathbf{A^{DH}_{y}}$ lengths was studied since it was uncertain how the unique chain conformation of $\mathbf{A^{DH}}$ would influence self-assembly.[30] Assemblies of $\mathbf{M^{O}_{60}A^{DH}_{y}}$ in water were prepared by nanoprecipitation, where copolypeptides were first dispersed in DMSO using mild bath sonication, followed by dropwise addition of an equal volume of deionized (DI) water. With vortexing, an additional volume of DI water was added, followed by exhaustive dialysis against DI water to give 1.0% (w/v) $\mathbf{M^{O}_{60}A^{DH}_{y}}$ suspensions.

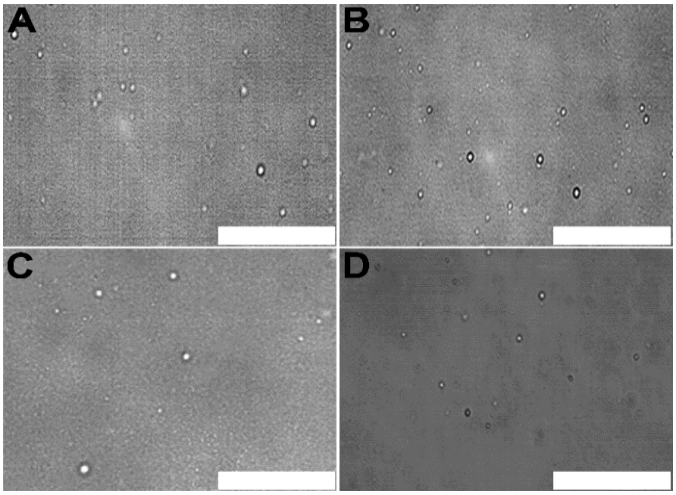

Figure 3.5. DIC images of vesicular assemblies in 1 wt% suspensions of different $\mathbf{M^{O}_{x}A^{DH}_{y}}$ copolypeptides in DI water. (A) $\mathbf{M^{O}_{60}A^{DH}_{30}}$, (B) $\mathbf{M^{O}_{60}A^{DH}_{40}}$, (C) $\mathbf{M^{O}_{60}A^{DH}_{60}}$, (D) $\mathbf{M^{O}_{60}A^{DH}_{100}}$. Scale bars = 10 μm

Examination of the suspensions using differential interference contrast (DIC) optical microscopy revealed the presence of round assemblies with submicrometer diameters for all $\mathbf{M^{O}_{60}A^{DH}_{y}}$ compositions (**Figure 3.5**). To determine whether the assemblies were vesicles or solid particles, the $\mathbf{M^{O}_{60}A^{DH}_{60}}$ assemblies were further examined using laser scanning confocal microscopy (LSCM). Hydrophilic and hydrophobic fluorescent probes were used to distinguish between assembled copolypeptide and encapsulated aqueous media. Specifically, a suspension of $\mathbf{M^{O}_{60}A^{DH}_{60}}$ was prepared using water containing hydrophilic Texas Red-labeled dextran (TR dextran, MW = 3000 Da), where all nonencapsulated TR dextran was subsequently removed from the suspension via dialysis.

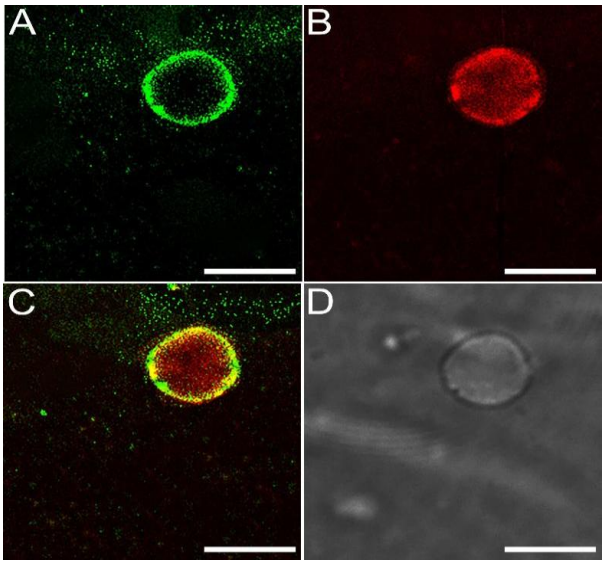

Figure 3.6. LSCM and DIC images of a 1 wt% $\mathbf{M^{O}_{60}A^{DH}_{60}}$ suspension in DI water. Vesicles were prepared in the presence of Texas Red dextran, and hydrophobic domains were labeled by incorporation of $DiOC_{18}$ probe. (A) $DiOC_{18}$ channel. (B) Texas Red channel. (C) Overlay of A and B. (D) DIC Image. z direction slice = 0.10 μm. Scale bars = 800 nm.

The copolypeptide assemblies were then labeled by the addition of a small volume of the hydrophobic $DiOC_{18}$ probe in DMSO.[25] After incubation for 3 h, the suspension was dialyzed to remove DMSO and excess $DiOC_{18}$. Imaging of these dual labeled suspensions revealed that the $\mathbf{M^{O}_{60}A^{DH}_{60}}$ assemblies are unilamellar water-filled vesicles as evidenced by the observation of $DiOC_{18}$-labeled polypeptide membranes that encapsulate TR dextran solution (**Figure 3.6**). The vesicular assemblies of $\mathbf{M^{O}_{60}A^{DH}_{60}}$ were found to be stable in size in 1× PBS buffer at 4 °C for 30 days via dynamic light scattering (DLS) analysis (**Figure 3.7**).

The formation of unilamellar $\mathbf{M^{O}_{60}A^{DH}_{60}}$ vesicle assemblies was consistent with the properties of other block copolypeptide vesicles, which are also all unilamellar.[24-26] This result may be due to the general stiffness of polypeptide membranes due to H-bonding interactions, as compared to more flexible copolymers.[18,19] What was unusual with the $\mathbf{M^{O}_{60}A^{DH}_{y}}$ suspensions was that all of the compositions prepared (y = 30 to 100) were found to form vesicle assemblies of similar size (**Figure 3.6**). In prior studies on the self-assembly of amphiphilic block copolypeptides containing α-helical hydrophobic segments, only a narrow range of hydrophobic segment lengths (*ca*. 20 to 30 residues) were found to form vesicles.[24−26] In these studies, shorter hydrophobic segments *(ca*. 10 residues) were found to give spherical micelles, and longer segments (>40 residues) gave sheets or disordered aggregates.[24,25] In addition, amphiphilic block copolypeptides

containing disordered racemic hydrophobic segments formed only spherical or irregular micelles regardless of composition.[22,23]

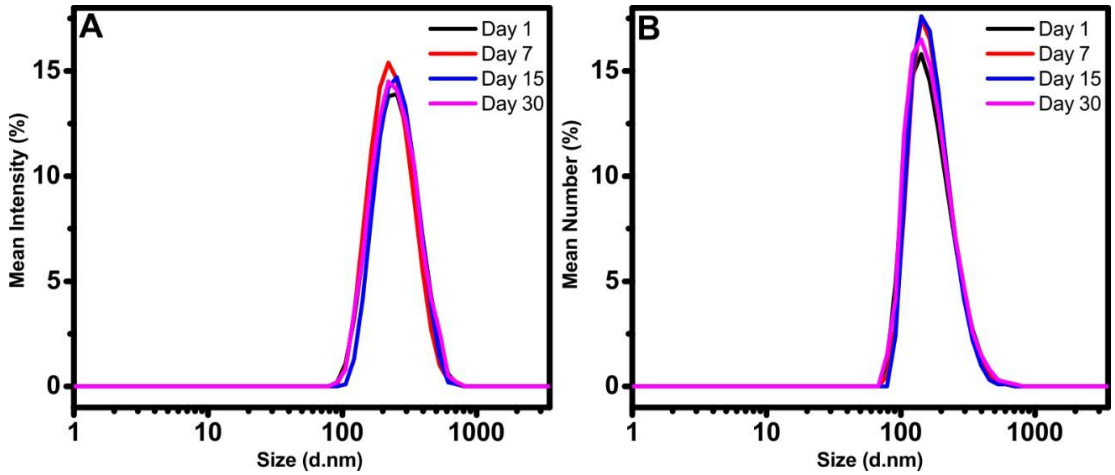

Figure 3.7. Stability of $\mathbf{M^{O}_{60}A^{DH}_{60}}$ vesicle assemblies in 1x PBS at 4 ºC for 30 days as quantified by DLS analysis. (A) Intensity and (B) number size distributions.

The hydrophobic $\mathbf{A^{DH}}$ segments in $\mathbf{M^{O}_{60}A^{DH}_{y}}$ appear to possess a degree of rigidity that favors low curvature membrane formation, but also more flexibility compared to α-helical polypeptide segments since they do not assemble into flat sheets at greater lengths.[30] Overall, $\mathbf{M^{O}_{x}A^{DH}_{y}}$ assemblies appear to be more tolerant of compositional adjustment compared to other vesicle-forming block copolypeptides. We sought to take advantage of this characteristic in the design of $\mathbf{M^{O}_{x}A^{DH}_{y}}$ vesicles capable of stimulus-driven inversion. For successful vesicle inversion, it is desirable that both copolymer segments are similar in length so that a similar vesicle favoring hydrophilic/hydrophobic balance is obtained in either state. Also, since inversion of $\mathbf{M^{O}_{x}A^{DH}_{y}}$ would give $\mathbf{M_{x}C^{rR}_{y}}$ (**Figure 3.2**), the resulting α-helical hydrophobic **M** segments would need to be reasonably short (*ca*. < 40 residues) to favor vesicle formation.[24,25]

Consequently, we chose a composition of $\mathbf{M^{O}_{35}A^{DH}_{30}}$ for the development of thiol-responsive invertible vesicles. $\mathbf{M^{O}_{35}A^{DH}_{30}}$ was synthesized, and a 1.0% (w/v) suspension in DI water was prepared, as described above (**Table 3.1**, **Table 3.2** and **Figure 3.4**). Similar to the $\mathbf{M^{O}_{60}A^{DH}_{y}}$ samples, $\mathbf{M^{O}_{35}A^{DH}_{30}}$ was found to assemble into round assemblies with submicrometer diameters as determined using DIC microscopy and DLS analysis (**Figure 3.8**).

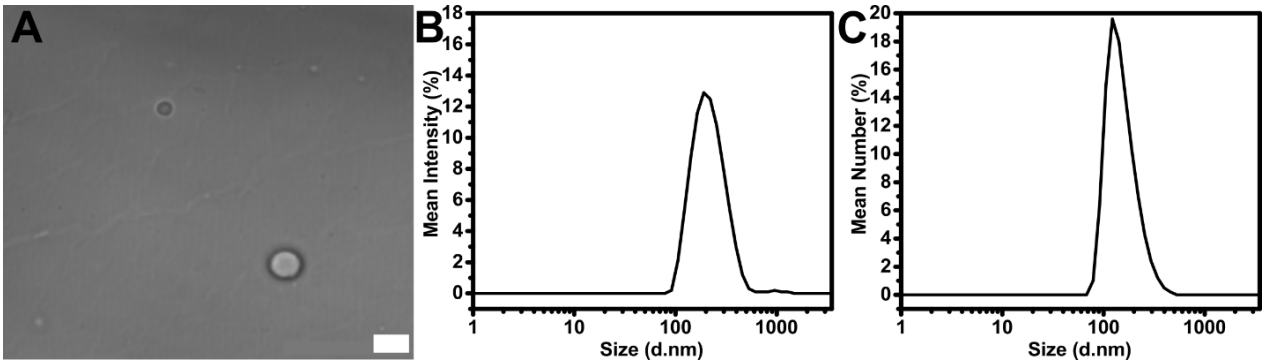

Figure 3.8. DIC optical microscopy and DLS data for a 1 wt% $\mathbf{M^{O}_{35}A^{DH}_{30}}$ suspension in DI water. (A) DIC image, scale bar = 800 nm. (B) Intensity and (C) number size distributions from DLS analysis.

Dual labeling of an aqueous $\mathbf{M^{O}_{35}A^{DH}_{30}}$ suspension using TR dextran and $DiOC_{18}$ as described above allowed for more detailed characterization of the assemblies. Imaging of the dual-labeled suspension confirmed that $\mathbf{M^{O}_{35}A^{DH}_{30}}$ also forms unilamellar water-filled vesicles as evidenced by the observation of single $DiOC_{18}$-labeled polypeptide membranes surrounding encapsulated TR dextran solution (**Figure 3.9** and **Figure 3.10**).

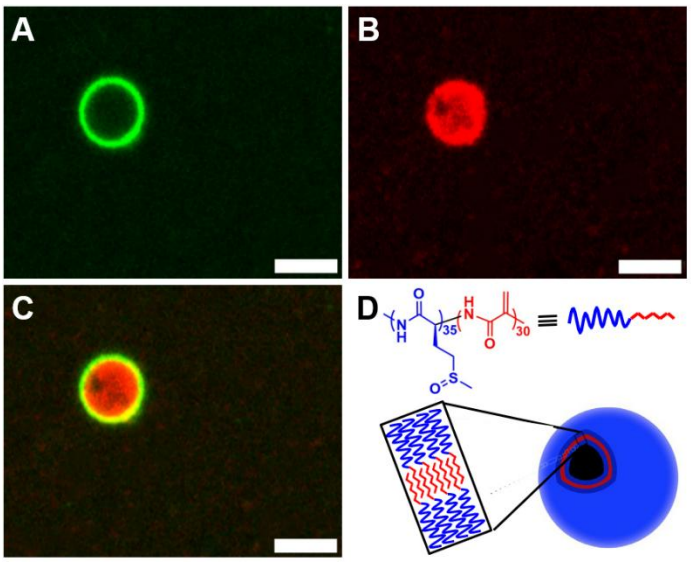

Figure 3.9. LSCM images of a $\mathbf{M^{O}_{35}A^{DH}_{30}}$ vesicle in water. Vesicles were prepared in the presence of TR dextran, and hydrophobic domains were labeled by incorporation of $DiOC_{18}$ probe. (A) $DiOC_{18}$ channel. (B) TR dextran channel. (C) Overlay of A and B. (D) Schematic showing amphiphilic nature of $\mathbf{M^{O}_{35}A^{DH}_{30}}$ chains (endgroups not shown), and their proposed assembly into unilamellar vesicles in water. z direction slice = 0.10 μm. Scale bars = 800 nm. Blue = hydrophilic; red = hydrophobic

$\mathbf{M^{O}_{35}A^{DH}_{30}}$vesicles were found to be stable over time (*vide infra*) and were thus considered suitable for studies on amphiphilic inversion using thiol stimuli. We first attempted to invert $\mathbf{M^{O}_{35}A^{DH}_{30}}$ vesicles under conditions mimicking the reducing environment of the cell cytosol. Thiol-containing glutathione (GSH) is present intracellularly at concentrations ranging from 0.1 to 15 mM and has been often used as a trigger to release cargos from therapeutic carriers within cells.[4–6,35] A 1.0% (w/v) suspension of $\mathbf{M^{O}_{35}A^{DH}_{30}}$ vesicles with encapsulated TR dextran cargo was incubated with 10 mM GSH in aqueous 150 mM NaCl at pH 7.4 and 37 °C. We expected that GSH would react with both segments in the copolypeptides to reverse amphiphilicity by conversion of $\mathbf{M^{O}_{35}A^{DH}_{30}}$ to

poly(Lmethionine)$_{35}$-*b*-poly(S-(glutathione)-*rac*-cysteine, Na+ salt)$_{30}$, **M$_{35}$C$^{rGT}_{30}$** (**Figure 3.11**). Aliquots of the reaction mixture were taken at different time points and dialyzed to remove nonencapsulated TR dextran, and the fluorescence intensity of remaining encapsulated TR dextran was recorded. After 13 days, all encapsulated TR dextran was released from **M$^{O}_{35}$A$^{DH}_{30}$** vesicles in the presence of GSH (**Figure 3.12).**

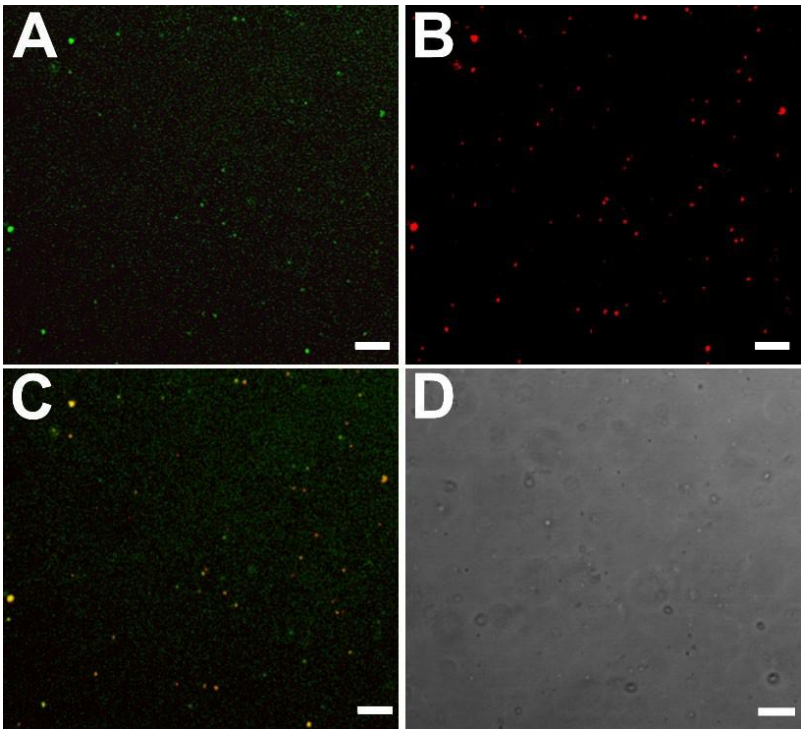

Figure 3.10. Low magnification LSCM and DIC images of a 1 wt% **M$^{O}_{35}$A$^{DH}_{30}$** suspension in DI water. Vesicles were prepared in the presence of Texas Red dextran, and hydrophobic domains were labeled by incorporation of DiOC$_{18}$ probe. (A) DiOC$_{18}$ channel. (B) Texas Red channel. (C) Overlay of A and B. (D) DIC Image. Scale bars = 5 μm.

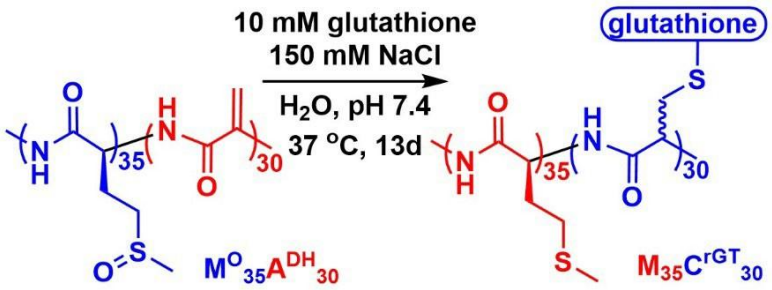

Figure 3.11. Reaction of $\mathbf{M^{O}_{35}A^{DH}_{30}}$ with glutathione

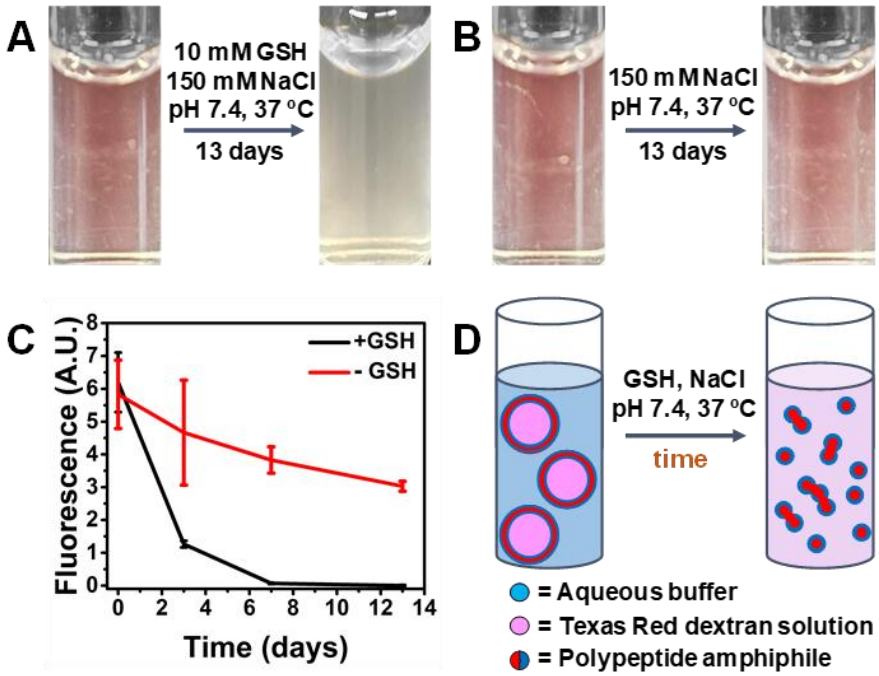

Figure 3.12. Release of TR dextran cargo from $\mathbf{M^{O}_{35}A^{DH}_{30}}$ vesicles in the presence of glutathione (GSH) under intracellular mimetic conditions. Images of 1.0 % (w/v) suspensions of $\mathbf{M^{O}_{35}A^{DH}_{30}}$ vesicles containing encapsulated TR dextran initially and after 13 days (A) with and (B) without addition of glutathione. All images of vials were taken after removal of non-encapsulated TR dextran by dialysis. (C) Graph showing retention of TR dextran in vesicles quantified by measuring fluorescence intensity of dialyzed vesicle suspensions over time A.U. = arbitrary units). (D) Schematic showing release of TR dextran cargo upon disruption of $\mathbf{M^{O}_{35}A^{DH}_{30}}$ vesicles after reaction with glutathione.

In a control study without GSH, greater than 60% of TR dextran remained encapsulated in the vesicles over the same time period (**Figure 3.12**). These results show that $\mathbf{M^{O}_{35}A^{DH}_{30}}$ vesicles possess the ability to release aqueous cargo in response to GSH, which may be useful for therapeutic delivery applications. ^{1}H NMR analysis of copolypeptide isolated from the GSH reaction after 13 days also showed complete modification of A^{DH} residues with glutathione and 90% reduction of $\mathbf{M^{O}}$ residues to **M** residues, confirming the effective reversal of block copolypeptide amphiphilicity.

However, an examination of the $\mathbf{M_{35}C^{rGT}_{30}}$ suspension after reaction with GSH using DIC microscopy revealed only the presence of irregular aggregates (**Figure 3.13**). No inverted vesicles were formed, possibly due to the limited solubility of $\mathbf{C^{rGT}}$ chains in water. To improve the likelihood of vesicle inversion, we studied the reaction of $\mathbf{M^{O}_{35}A^{DH}_{30}}$ with a more hydrophilic thiol, thioglycolic acid (TGA), which is known to give water-soluble poly(S-carboxymethyl-*rac*-cysteine), $\mathbf{C^{rMC}}$, upon reaction with $\mathbf{A^{DH}}$ chains.[30] A 1.0% (w/v) suspension of $\mathbf{M^{O}_{35}A^{DH}_{30}}$ vesicles with encapsulated TR dextran cargo was incubated with excess TGA in DI water at pH 8.0 and 20 °C.

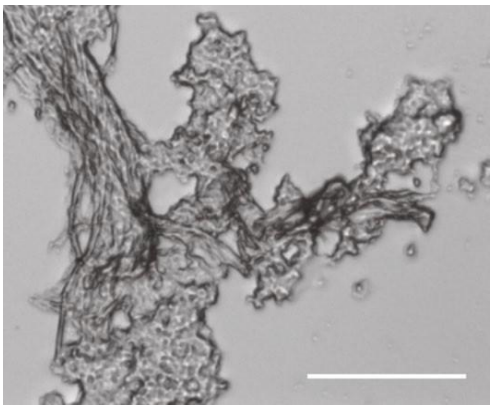

Figure 3.13. Representative DIC microscopy image of $\mathbf{M_{35}C^{rGT}_{30}}$ precipitate formed after reaction of $\mathbf{M^{O}_{35}A^{DH}_{30}}$ with glutathione. Scale bar = 5 μm.

We expected that TGA would reverse amphiphilicity by conversion of $\mathbf{M^{O}_{35}A^{DH}_{30}}$ to poly(L-methionine)$_{35}$-*b*-poly(S-(carboxymethyl)-*rac*-cysteine, Na^+ salt)$_{30}$ and $\mathbf{M_{35}C^{rMC}_{30}}$ (**Figure 3.14**). After 48 h, copolypeptide isolated from an aliquot of the suspension was found to have been completely converted from $\mathbf{M^{O}_{35}A^{DH}_{30}}$ to $\mathbf{M_{35}C^{rMC}_{30}}$ by ^{1}H NMR. After dialysis of this suspension, it was analyzed using DIC microscopy and DLS, which showed the presence of round assemblies with submicrometer diameters (**Figure 3.15**). Further analysis of the suspension after $DiOC_{18}$ labeling using LSCM confirmed the formation of inverted unilamellar vesicles containing encapsulated TR dextran (**Figure 3.16** and **Figure 3.17**).

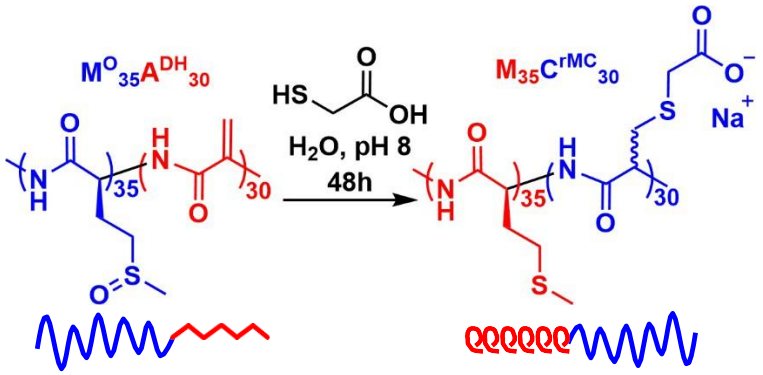

Figure 3.14. Reversal of amphiphilicity by conversion of $\mathbf{M^{O}_{35}A^{DH}_{30}}$ into $\mathbf{M_{35}C^{rCM}_{30}}$ (endgroups not shown). Blue = hydrophilic; red = hydrophobic.

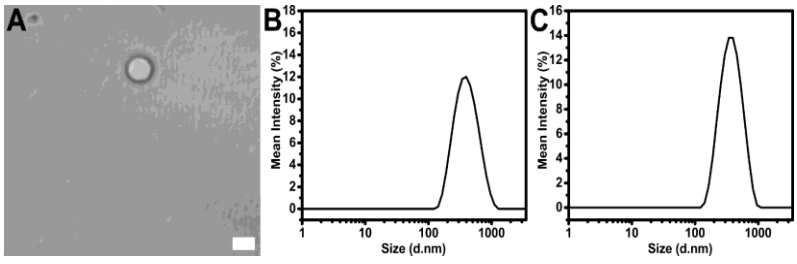

Figure 3.15. DIC microscopy and DLS data for $\mathbf{M_{35}C^{rCM}_{30}}$ vesicles formed *in situ* after the reaction of Texas Red dextran containing $\mathbf{M^{O}_{35}A^{DH}_{30}}$ vesicles with thioglycolic acid. (A) DIC image, scale bar = 700 nm. (B) Intensity and (C) number size distributions from DLS analysis. Diameter = 364 nm; PDI = 0.366.

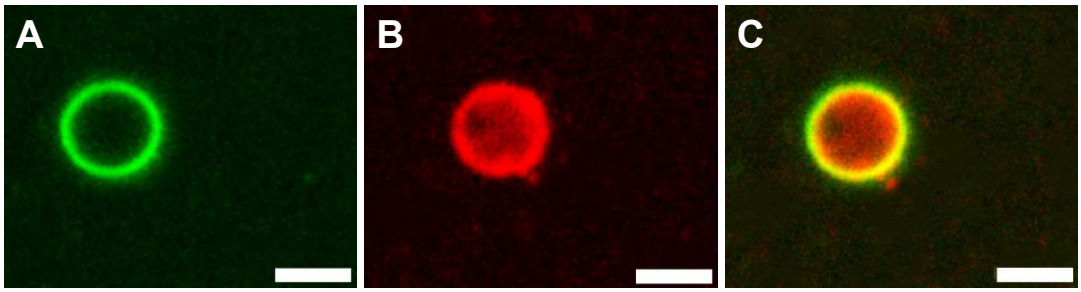

Figure 3.16. LSCM images of a $\mathbf{M_{35}C^{rCM}_{30}}$ vesicle in water. Vesicles formed *in situ* after the reaction of TR dextran containing $\mathbf{M^{O}_{35}A^{DH}_{30}}$ vesicles with thioglycolic acid. Hydrophobic domains were labeled by incorporation of $DiOC_{18}$ probe before imaging. (A) $DiOC_{18}$ channel. (B) TR dextran channel. (C) Overlay of A and B. z direction slice = 0.10 μm. Scale bars = 700 nm.

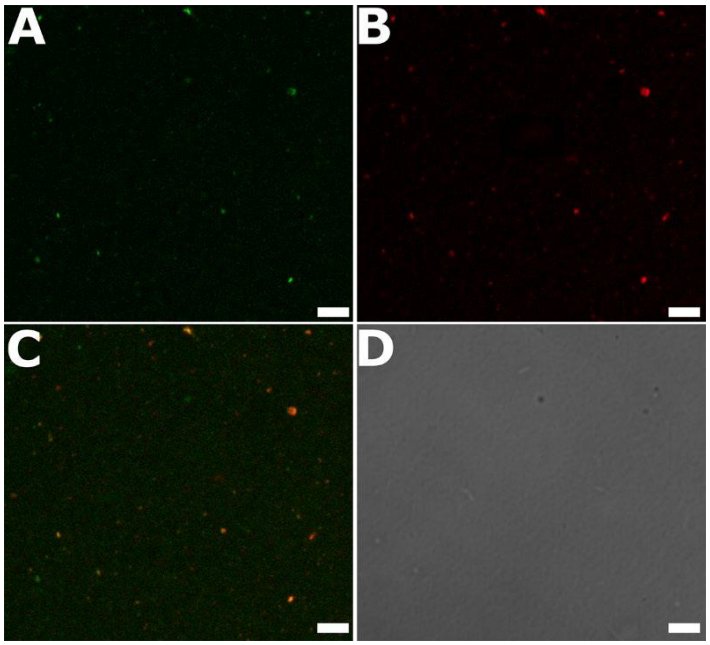

Figure 3.17. Low magnification LSCM and DIC images of $\mathbf{M_{35}C^{rCM}_{30}}$ vesicles formed *in situ* after the reaction of Texas Red dextran containing $\mathbf{M^{O}_{35}A^{DH}_{30}}$ vesicles with thioglycolic acid. Hydrophobic domains were labeled by incorporation of $DiOC_{18}$ probe before imaging. (A) $DiOC_{18}$ channel. (B) Texas Red channel. (C) Overlay of A and B. (D) DIC Image. Scale bars = 5 μm.

The amount of encapsulated TR dextran was quantified using fluorescence measurements and was found to be *ca*. 13% of the amount originally present in the $\mathbf{M^{O}_{35}A^{DH}_{30}}$ vesicles. Remarkably, the inverted $\mathbf{M_{35}C^{rMC}_{30}}$ vesicles were able to form *in situ* during the course of amphiphile reversal, as TGA reacted with both copolypeptide side chains. It appears that some TR dextran aqueous cargo was also retained or encapsulated during vesicle inversion. To independently verify that $\mathbf{M_{35}C^{rMC}_{30}}$ forms stable vesicles, we prepared and isolated a sample of $\mathbf{M_{35}C^{rMC}_{30}}$ and used the nanoprecipitation protocol described above to prepare a 1.0% (w/v) $\mathbf{M_{35}C^{rMC}_{30}}$ suspension in DI water, which was found to give vesicles similar to those formed *in situ* (**Figure 3.18**).

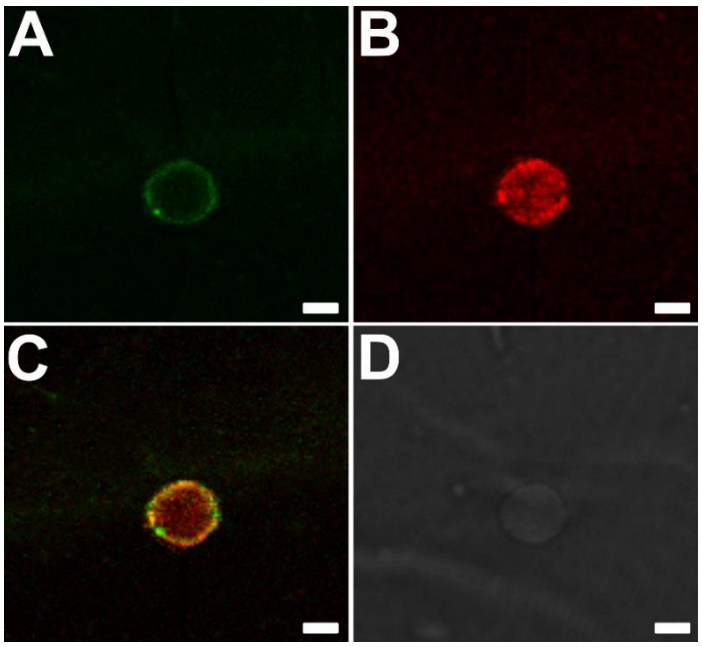

Figure 3.18. LSCM and DIC images of a 1 wt% $\mathbf{M_{35}C^{rCM}_{30}}$ suspension in DI water prepared from purified copolypeptide by nanoprecipitation. Vesicles were prepared in the presence of Texas Red dextran, and hydrophobic domains were labeled by incorporation of $DiOC_{18}$ probe. (A) $DiOC_{18}$ channel. (B) Texas Red channel. (C) Overlay of A and B. (D) DIC Image. z direction slice = 0.10 μm. Scale bars = 350 nm.

3.4 Conclusions

A route was developed for the preparation of amphiphilic $\mathbf{M^{O}_{x}A^{DH}_{y}}$ diblock copolypeptides, which were found to self-assemble into submicrometer-diameter unilamellar vesicles in aqueous media. The formation of vesicles was observed over an unprecedented range of copolypeptide compositions due to the unique properties of $\mathbf{A^{DH}}$ hydrophobic segments, which possess chain conformations that differ greatly from those of αhelical or racemic polypeptides.[30] This expanded compositional freedom is advantageous for the design of nanoscale copolypeptide vesicles with adjustable properties. $\mathbf{M^{O}_{x}A^{DH}_{y}}$ vesicles were used to study the reversal of copolypeptide amphiphilicity in response to the addition of thiol stimuli. $\mathbf{M^{O}_{35}A^{DH}_{30}}$ vesicles were incubated with GSH under conditions mimicking an intracellular environment, where both segments of the vesicles were able to fully react with GSH, resulting in vesicle disruption and the complete release of aqueous cargo.

Further, successful triggered inversion of block copolypeptide vesicles in aqueous media under biologically relevant conditions was achieved using $\mathbf{M^{O}_{35}A^{DH}_{30}}$ vesicles and TGA as a hydrophilic thiol trigger. In these reactions, the different functional groups in each copolypeptide segment were able to react efficiently with a single thiol trigger to reverse the copolypeptide amphiphilicity. This ability to convert stable biomimetic vesicles to stable inverted biomimetic vesicles using a mild biologically relevant stimulus is unprecedented. Since $\mathbf{M^{O}}$ has been found to be biocompatible and degradable in vivo, these materials have potential for applications in the controlled release of hydrophilic therapeutics and triggered encapsulation of biological media. [20,21,25,26]

3.5 Materials and Instrumentation

Methods and Materials were as described in Chapter 2 with the following additions: L-methionine NCA, poly(L-methionine) (**M**), poly(L-methionine sulfoxide) (**M^{O}**), poly(S-methyl-L-methionine sulfonium chloride) (**M^{M}**) were prepared according to literature procedures.[29,36,38]

S-(*tert*-Butyl carboxymethyl)-L-cysteine. This compound was prepared according to the protocol described in Chapter 2.[37]

S-(*tert*-Butyl carboxymethyl)-L-cysteine N-carboxyanhydride (*t*BuCM-Cys NCA).[4] This monomer was prepared according to the protocol described in Chapter 2.[37]

General procedure for determination of M chain lengths using end-group analysis after reaction with mPEG-NCO.[36] This procedure was performed following the protocol described in Chapter 2.

General procedure for polymerization of *t*BuCM-Cys NCA using a N-terminal amine containing M^{O} macroinitiator to give poly(L-methionine sulfoxide)-*b*-poly(S-(*tert*-butylcarboxymethyl)-L-cysteine), M$^{O}_{x}$C$^{BCM}_{y}$. Under nitrogen at room temperature, **M^{O}** was dissolved in DMSO at 25 mg/mL in a scintillation vial. Under constant stirring, the desired equivalents of solid *t*BuCM-Cys NCA were added to the reaction vessel, which was then sealed. Completion of polymerization was determined by FTIR (*ca.* 24-48 h). Acetic anhydride (1 eq per polypeptide chain) was then added to acetylate polypeptide N-terminal amine groups, and the reaction was allowed to proceed for 1 hr at room temperature. The resulting solution was transferred to 2 kDa dialysis tubing and dialyzed against DI H_2O (48 h, 4 dialyzate changes). The sample was then freeze dried to yield

the product as a white fluffy solid. No detectable reaction was found to occur between acetic anhydride and methionine sulfoxide side chain residues (i.e. Pummerer rearrangement), as determined by ^{1}H NMR.

General procedure for the preparation of poly(L-methionine sulfoxide)-*b*-poly(S-(carboxymethyl)-L-cysteine, Na$^+$ salt), $\mathbf{M^O_xC^{CM}_y}$.[30] Adapted from the protocol described in Chapter 2, $\mathbf{M^O_xC^{BCM}_y}$ was dissolved at 25 mg/mL in TFA and let stand for 5 hours. The sample was then diluted to 10 mg/mL with 50 mM sodium bicarbonate in DI H_2O and transferred to 2 kDa dialysis tubing. The sample was dialyzed against 50 mM sodium bicarbonate (24 hr, 2 dialyzate changes) and DI H_2O (24 hr, 2 dialyzate changes), and then freeze dried to yield the product as a white fluffy solid.

General procedure for the preparation of poly(L-methionine sulfoxide)-*b*-poly(dehydroalanine), $\mathbf{M^O_xA^{DH}_y}$.[30] Adapted from the protocol described in Chapter 2, $\mathbf{M^O_xC^{CM}_y}$ was dissolved at 20 mg/mL in pH 8 phosphate buffer and then methyl iodide (25 eq per $\mathbf{C^{CM}}$ residue) was added. The reaction was wrapped in foil and stirred for 3 days at 37 °C. The reaction was then transferred to 2 kDa dialysis tubing and dialyzed against DI H_2O (48 hr, 4 dialyzate changes), and then freeze dried to yield the product as a white fluffy powder.

General Procedure for the Preparation of $\mathbf{M^M_xA^{DH}_y}$ from $\mathbf{M^O_xA^{DH}_y}$ for GPC Analysis. $\mathbf{M^O_xA^{DH}_y}$ was suspended in DI H_2O at 10 mg/mL. Under constant stirring, a thioglycolic acid solution (thioglycolic acid: 1.92 mL, 150 eq per repeat unit, DI H_2O: 5 mL), pH adjusted to 8 with 12M NaOH, was added. The vial was sealed and allowed to stir for 48h at room temperature. The sample was then transferred to 2 kDa dialysis tubing and

dialyzed against 50 mM sodium bicarbonate in DI H_2O (48h, 4 dialyzate changes) and then DI H_2O (24h, 2 dialyzate changes). The contents of the dialysis bag were then added to a 20 mL scintillation vial, the pH was adjusted to pH 8 with saturated sodium bicarbonate, and iodomethane (20 eq per each residue) was added, and the reaction vessel was sealed and heated at 37 °C for 3 days. The sample was then transferred to 2 kDa dialysis tubing and dialyzed against 150 mM NaCl (48h, 4 dialyzate changes), DI H_2O (48h, 4 dialyzate changes) and then freeze dried to yield the product as a white fluffy powder.

Example procedure for attempted formation of $\mathbf{M^{O}_{x}A^{DH}_{y}}$ from $\mathbf{M_{x}C^{BCM}_{y}}$ via oxidation and elimination. L-Methionine NCA and *t*buCM-Cys NCA were sequentially polymerized using $(PMe_3)_4Co$ initiator according to published procedures to produce poly(L-methionine)-*b*-poly(S-(*tert*-butylcarboxymethyl)-L-cysteine) (**$\mathbf{M_{x}C^{BCM}_{y}}$**).[5] **$\mathbf{M_{x}C^{BCM}_{y}}$** was dissolved at 25 mg/mL in TFA and let stand for 5 hours. The sample was then diluted to 10 mg/mL with 50 mM sodium bicarbonate in DI H_2O and transferred to 2 kDa dialysis tubing. The sample was dialyzed against 50 mM sodium bicarbonate (24 hr, 2 dialyzate changes) and DI H_2O (24 hr, 2 dialyzate changes), and then freeze dried to yield poly(L-methionine)-*b*-poly(S-(carboxymethyl)-L-cysteine, Na^+ salt) (**$\mathbf{M_{x}C^{CM}_{y}}$**) as a white fluffy solid. **$\mathbf{M_{x}C^{CM}_{y}}$** was then oxidized according to published protocols to yield poly(L-methionine sulfoxide)-*b*-(S-(carboxymethyl)-L-cysteine sulfoxide, Na^+ salt) (**$\mathbf{M^{O}_{x}C^{CMO}_{y}}$**).[3] **$\mathbf{M^{O}_{x}C^{CMO}_{y}}$** was then dissolved in 9:1 DMSO/ water and the pH was adjusted to 8 with 1M NaOH. Trimethylphosphite (1 eq per **$\mathbf{C^{CMO}}$** residue) was then added as a sulfenic acid trapping reagent, and the reaction vessel was sealed and heated to 150 ºC for 4 days.[32] No elimination of **$\mathbf{C^{CMO}}$** to give **$\mathbf{A^{DH}}$** residues was found to occur.

Preparation of $M^{O}_{x}A^{DH}_{y}$ Vesicles in Water. Solid $M^{O}_{x}A^{DH}_{y}$ powder was dispersed in DMSO to give a 4 % (w/v) suspension, which was then placed in a bath sonicator for 10 minutes until the copolypeptide was evenly dispersed and no large particulates could be observed. An equal volume of DI H_2O was added dropwise, followed by vortexing the sample for 1 minute and then placing the sample in a bath sonicator for 5 minutes. Under constant vortexing, an additional equal volume of DI H_2O was slowly added to give a final sample concentration of 1% (w/v). The sample was then transferred to 2 kDa dialysis tubing and dialyzed against DI H_2O (24h, 4 dialyzate changes). The resulting suspension was used directly for subsequent studies.

Encapsulation of Texas Red Dextran Within $M^{O}_{x}A^{DH}_{y}$ Assemblies in Water.[25] A 1% (w/v) suspension of $M^{O}_{x}A^{DH}_{y}$ vesicles was prepared as described above except that a solution of Texas Red labeled dextran in DI H_2O (Molecular Probes, MW = 3000, 0.125 mg/mL) was used for dilution in place of pure DI H_2O. After dialysis of the vesicle suspension against DI H_2O using 2 kDa dialysis bags to remove DMSO, the suspensions were transferred to larger pore size 15 kDa dialysis bags and dialyzed against DI H_2O for 18 hours in order to remove all non-encapsulated Texas Red dextran. The resulting suspension was used directly for subsequent studies.

***In situ* Preparation of Inverted poly(L-methionine)$_{35}$-*b*-poly(S-(carboxymethyl)-*rac*-cysteine, Na^+ salt)$_{30}$, $M_{35}C^{rCM}_{30}$ Vesicles.**[37] Adapted from published protocols, a thioglycolic acid solution (thioglycolic acid: 1.92 mL, 150 eq per each residue and 2 mL DI H_2O), pH adjusted to 8 using 12M NaOH, was added to 2 mL of a 1% (w/v) suspension of $M^{O}_{35}A^{DH}_{30}$ vesicles loaded with Texas Red dextran. The suspension was stirred and allowed to react for 48 hours. Spectral data (^{1}H NMR) of an aliquot of polypeptide isolated

from the reaction showed complete conversion of $\mathbf{M^{O}_{35}A^{DH}_{30}}$ to $\mathbf{M_{35}C^{rCM}_{30}}$. An aliquot of the suspension was imaged to reveal vesicles with encapsulated Texas Red dextran. The amount of encapsulated Texas Red dextran was quantified using fluorescence measurements and was found to be *ca*. 13% of the amount originally present in the $\mathbf{M^{O}_{35}A^{DH}_{30}}$ vesicles (fluorescence intensity of $\mathbf{M^{O}_{35}A^{DH}_{30}}$ vesicles = 6.33×10^7 A.U.; fluorescence intensity of $\mathbf{M_{35}C^{rCM}_{30}}$ vesicles = 8.3×10^6 A.U.).

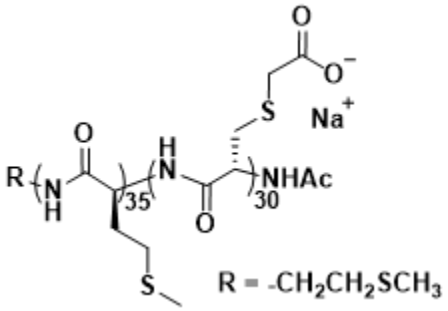

Bulk Preparation of Inverted Amphiphilic $\mathbf{M_{35}C^{rCM}_{30}}$. Solid $\mathbf{M^{O}_{35}A^{DH}_{30}}$ (20 mg) was suspended in DI H_2O at 10 mg/mL in a scintillation vial. Under constant stirring, a thioglycolic acid solution (thioglycolic acid: 1.92 mL, 150 eq per each residue and 5 mL DI H_2O), pH adjusted to 8 using 12M NaOH, was added. The vial was sealed and allowed to stir for 48h at room temperature. The suspension was then transferred to 2 kDa MWCO dialysis tubing and dialyzed against 50 mM sodium bicarbonate (24h, 2 dialyzate changes) followed by DI H_2O (24h, 2 dialyzate changes). The resulting suspension was then freeze dried to give $\mathbf{M_{35}C^{rCM}_{30}}$ as a white fluffy powder (22 mg, 76% yield).

^{1}H NMR (400 MHz, dTFA, 25 °C): δ 5.26 – 5.11 (d, 55H), δ 3.93 – 3.77 (d, 58H), δ 3.49 – 3.26 (d, 45H), δ 2.95 (s, 75H), δ 2.43 (s, 175H).

***In situ* Glutathione Triggered $M^{O}_{35}A^{DH}_{30}$ Vesicle Disruption Under Intracellular Mimetic Conditions.** Glutathione was dissolved in 1.50 M NaCl at 30 mg/mL and the pH was adjusted to 7.4 with 4M NaOH. 100 µL of the glutathione solution was added to 1 mL of a 1 wt% (w/v) suspension of $\mathbf{M^{O}_{35}A^{DH}_{30}}$ vesicles that were loaded with Texas Red dextran (prepared as above). The suspension was stirred at 37 °C for 13 days. The amount of Texas Red dextran remaining in vesicles over time was quantified by fluorescence measurements. After 13 days, and dialysis of the suspension against DI H_2O (48 h, 4 dialyzate changes), no Texas Red fluorescence was detected indicating complete release. ^{1}H NMR analysis of polypeptide isolated after 13 days showed complete functionalization of $\mathbf{A^{DH}}$ residues with glutathione, and 90% reduction of $\mathbf{M^{O}}$ residues to **M** residues (see Spectral Data). An identical experiment, except without glutathione, was also conducted as a control experiment to monitor passive Texas Red dextran leakage from the vesicles.

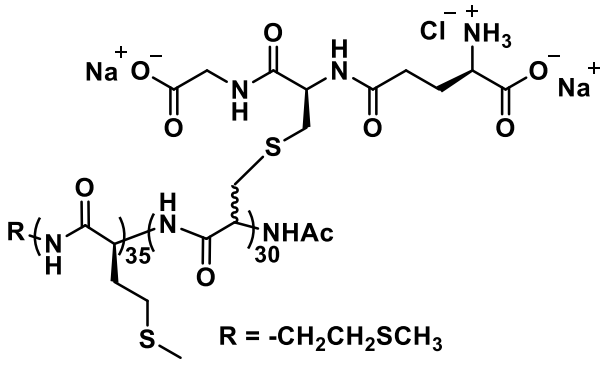

Bulk Reaction of $M^{O}_{35}A^{DH}_{30}$ with Glutathione to Give poly(L-methionine)$_{35}$-*b*-poly(S-(glutathione)-*rac*-cysteine, Na^+ salt)$_{30}$, $M_{35}C^{rGT}_{30}$. Glutathione was dissolved in 1.50 M NaCl at 30 mg/mL and the pH was adjusted to 8 with 4M NaOH. 100 µL of glutathione solution (see above) was added to a 1 mL solution of 10 mg/mL $\mathbf{M^{O}_{35}A^{DH}_{30}}$. The

suspension was stirred at 37 °C for 13 days. The resulting suspension was then transferred to 2 kDa dialysis tubing and dialyzed against 3 mM HCl (24h, 2 dialyzate changes), 50mM $NaHCO_3$ **(**24h, 2 dialyzate changes), and DI H_2O (48 h, 4 dialyzate changes). The suspension was then freeze dried to give $\mathbf{M_{35}C^{rGT}_{30}}$ as a white fluffy powder (14.7 mg, 67.1% yield)

^1H NMR (400 MHz, D_2O + Na_2CO_3, 25 °C): δ 4.70 (s, 30H), δ 3.76 (m, 120H), δ 2.95 (m, 60H), δ 2.54 (m, 60H), δ 2.18 (m, 60H). Solubility in D_2O was improved by addition of Na_2CO_3. Since resonances for $\mathbf{M^O}$ residues were absent in the product, the missing integrations observed for L-methionine peaks residues were likely due to aggregation and poor solubility of hydrophobic **M** segments in D_2O.

Quantification of Texas Red Dextran Release from Vesicles. To quantify the release of Texas Red dextran from vesicles, aliquots were removed from vesicle suspensions at different time points (0, 3, 7, and 13 days), and then transferred to 15 kDa dialysis tubing and dialyzed against DI H_2O (48 h, 4 dialyzate changes) to remove any released Texas Red dextran. Fluorescence measurements of dialyzed samples were performed in triplicate.

Preparation of $DiOC_{18}$ Labeled Vesicles for Laser Scanning Confocal Microscopy (LSCM). A suspension of $\mathbf{M_{35}C^{rCM}_{30}}$, $\mathbf{M^O_{60}A^{DH}_{60}}$ or $\mathbf{M^O_{35}A^{DH}_{30}}$ vesicles loaded with Texas Red dextran (1 mL) was mixed with a solution of hydrophobic $DiOC_{18}$ fluorescent probe (Molecular Probes, 30 μL of a 1 mg/mL solution in DMSO). The suspension was allowed to stand for 3 h to allow vesicles to absorb the probe and was then transferred to 15 kDa

dialysis tubing and dialyzed against DI H_2O (2 dialysate changes, 24 hr). The dialyzed suspension was used for subsequent LSCM images.

Stability of $M^{O}_{60}A^{DH}_{60}$ Assemblies under Physiological Mimetic Conditions. A suspension of $\mathbf{M^{O}_{60}A^{DH}_{60}}$ vesicles was prepared as described above. The suspension was diluted with 2x PBS buffer to give a vesicle suspension at 0.5% (w/v) in 1x PBS. The hydrodynamic diameter of the vesicle assemblies was measured 4 times over the course of 30 days using DLS. A minimal change in vesicle diameter was observed during this time span.

Dynamic Light Scattering (DLS). Hydrodynamic diameters of vesicles were determined using dynamic light scattering. Measurements were performed on 1 mL of a 1 wt% aqueous copolypeptide suspension using a Zetasizer Nano ZSP (Malvern Instruments) at ambient temperature. Photons were collected at a 173° scattering angle, and the scattering intensity data were processed using instrumental software to determine hydrodynamic diameters of assemblies. Measurements were performed in triplicate.

Differential Interference Contrast (DIC) Microscopy. Suspensions of copolypeptide vesicles (1 % w/v) were visualized on glass slides with a spacer between the slide and the coverslip (SecureSeal imaging spacer from Grace Bio-Labs), allowing the self-assembled structures to be minimally disturbed during focusing. Images were collected on an Olympus IX83 inverted microscope equipped with a 100× oil objective, a 2× multiplier lens, and Zero Drift Correction autofocus system.

Laser Scanning Confocal Microscopy (LSCM). Laser scanning confocal microscopy of 1 % (w/v) vesicle suspensions (prepared as described above) were performed on a

Zeiss LSM 880 Confocal Microscope with Aryscan equipped with 488 nm and 538 nm Ar laser lines (30 mW) for probe excitation. Imaging of an xy plane with an optical z slice of 0.10 μm was used to verify that the assemblies were water filled, unilamellar vesicles.

Characterization Data

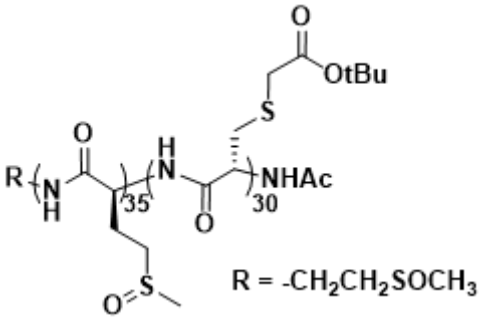

$M^{O}_{35}C^{BCM}_{30}$ (68 mg, 86% yield). Prepared using 35 mg of **M^{O}_{35}** and 30 eq of tBuCM-Cys NCA using the General Procedure provided above. ^{1}H NMR (400 MHz, dTFA, 25 °C): δ 4.91-4.83 (br m, 72H), δ 3.44 – 3.17 (br m, 250H), δ 2.95 (s, 95H), δ 2.59-2.44 (d, 70H), δ 1.60 (s, 314H).

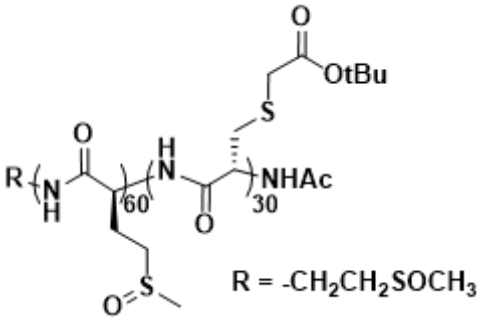

$M^{O}_{60}C^{BCM}_{30}$ (37 mg, 71% yield). Prepared using 30 mg of **M^{O}_{60}** and 30 eq of tBuCM-Cys NCA using the General Procedure provided above. ^{1}H NMR (400 MHz, dTFA, 25 °C): δ 5.01 (br m, 89H), δ 3.53 – 3.23 (br m, 295H), δ 2.97 (s, 180H), δ 2.68-2.47 (d, 124H), δ 1.65 (s, 285H).

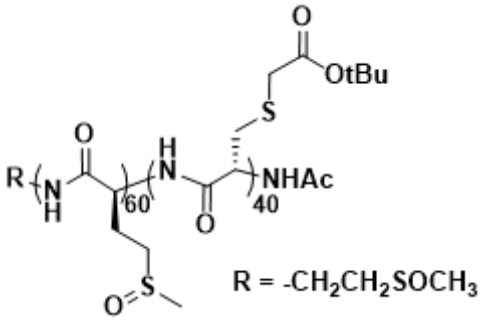

$M^{O}_{60}C^{BCM}_{40}$ (54 mg, 92% yield). Prepared using 30 mg of **M^{O}_{60}** and 40 eq of tBuCM-Cys NCA using the General Procedure provided above. ^{1}H NMR (400 MHz, dTFA, 25 °C): δ 4.98 (br m, 102H), δ 3.53 – 3.23 (br m, 299H), δ 2.97 (s, 180H), δ 2.68-2.47 (d, 122H), δ 1.65 (s, 386H).

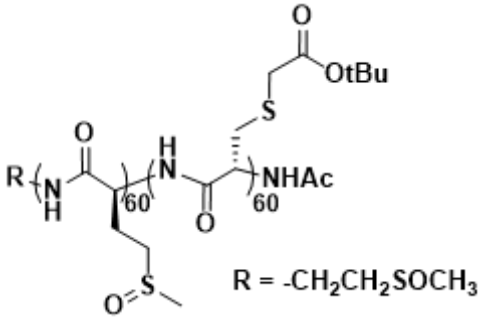

$M^{O}_{60}C^{BCM}_{60}$ (35 mg, 70% yield). Prepared using 20 mg of **M^{O}_{60}** and 60 eq of tBuCM-Cys NCA using the General Procedure provided above. ^{1}H NMR (400 MHz, dTFA, 25 °C): δ 4.98 (br m, 110H), δ 3.53 – 3.23 (br m, 360H), δ 2.97 (s, 145H), δ 2.68-2.47 (d, 120H), δ 1.65 (s, 568H).

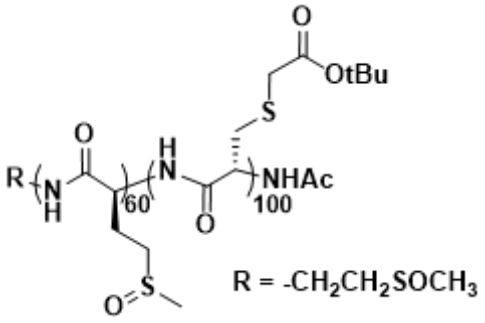

$M^{O}_{60}C^{BCM}_{100}$ (75 mg, 78% yield). Prepared using 30 mg of **M^{O}_{60}** and 100 eq of tBuCM-Cys NCA using the General Procedure provided above. ^{1}H NMR (400 MHz, dTFA, 25 °C): δ 4.98 (br m, 175H), δ 3.63 – 3.30 (br m, 605H), δ 2.97 (s, 176H), δ 2.68-2.47 (d, 120H), δ 1.65 (s, 893H).

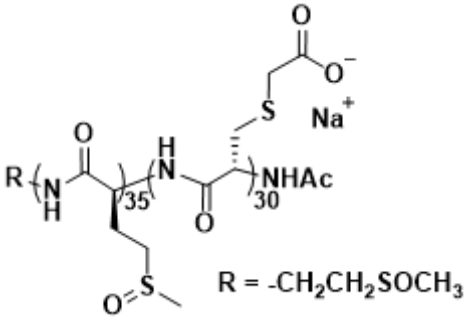

$M^{O}_{35}C^{CM}_{30}$ (42 mg, 68% yield). Prepared using the General Procedure provided above. ^{1}H NMR (400 MHz, D_2O, 25 °C): δ 4.51 (br s, 30H), δ 4.41 (br s, 35H), δ 3.19 (s, 60H), δ 2.91 (br m, 130H), δ 2.63 (s, 105H), δ 2.16 (br d, 70H).

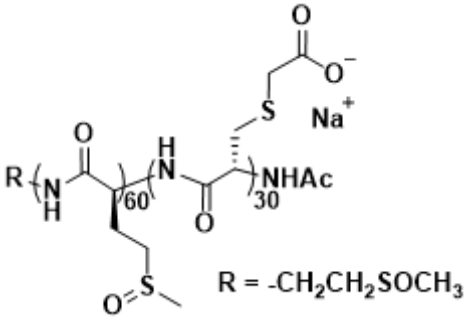

$M^{O}_{60}C^{CM}_{30}$ (25 mg, 74% yield). Prepared using the General Procedure provided above. ^{1}H NMR (400 MHz, D_2O, 25 °C): δ 4.51 (br s, 30H), δ 4.41 (br s, 60H), δ 3.19 (s, 60H), δ 2.91 (br m, 180H), δ 2.63 (s, 180H), δ 2.16 (br d, 120H).

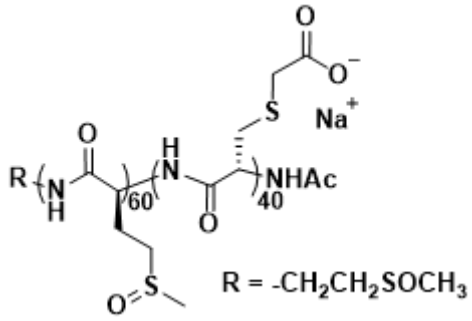

$M^{O}_{60}C^{CM}_{40}$ (36 mg, 73% yield). Prepared using the General Procedure provided above. ^{1}H NMR (400 MHz, D_2O, 25 °C): δ 4.51 (br s, 40H), δ 4.41 (br s, 60H), δ 3.19 (s, 80H), δ 2.91 (br m, 200H), δ 2.63 (s, 180H), δ 2.16 (br d, 120H).

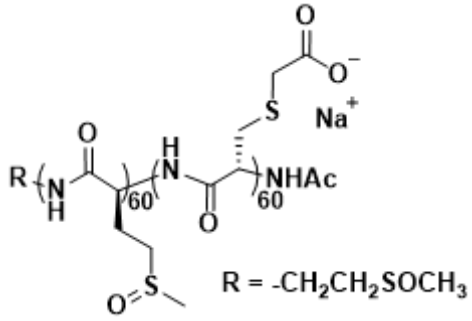

$M^{O}_{60}C^{CM}_{60}$ (25 mg, 78% yield). Prepared using the General Procedure provided above. ^{1}H NMR (400 MHz, D_2O, 25 °C): δ 4.51 (br s, 60H), δ 4.41 (br s, 60H), δ 3.19 (s, 120H), δ 2.91 (br m, 240H), δ 2.63 (s, 180H), δ 2.16 (br d, 120H).

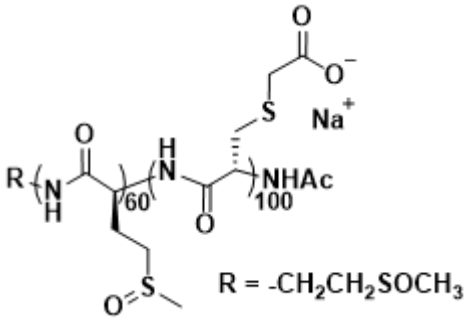

$M^{O}_{60}C^{CM}_{100}$ (50 mg, 75% yield). Prepared using the General Procedure provided above. ^{1}H NMR (400 MHz, D_2O, 25 °C): δ 4.51 (br s, 100H), δ 4.41 (br s, 60H), δ 3.19 (s, 200H), δ 2.91 (br m, 300H), δ 2.63 (s, 200H), δ 2.16 (br d, 120H).

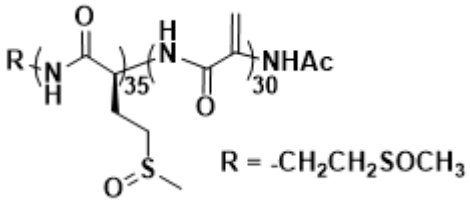

$M^{O}_{35}A^{DH}_{30}$ (21 mg, 74% yield). Prepared using the General Procedure provided above. ^{1}H NMR (400 MHz, d_6-DMSO, 25 °C): δ 9.5 (br s, 3H), δ 8.32 (s, 13H), δ 5.80 (d, 60H), δ 4.33 (s, 35H), δ 2.72 (s, 70H), δ 2.51 (s, 105H), δ 2.51 (d, 70H). Since resonances for S-(carboxymethyl)-L-cysteine residues were absent in the product, the low integrations observed for alkene peaks of dehydroalanine residues were likely due to aggregation of hydrophobic **A^{DH}** segments in D_2O/DMSO.[30]

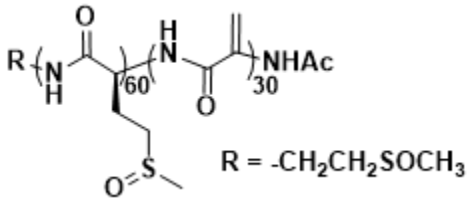

$M^{O}_{60}A^{DH}_{30}$ (10 mg, 52% yield). Prepared using the General Procedure provided above. ^{1}H NMR (400 MHz, d_6-DMSO, 25 °C): δ 8.32 (s, 60H), δ 4.33 (s, 60H), δ 2.72 (s, 120H), δ 2.51 (s, 180H), δ 2.51 (d, 120H). Since resonances for S-(carboxymethyl)-L-cysteine residues were absent in the product, the low integrations observed for alkene peaks of dehydroalanine residues were likely due to aggregation of hydrophobic **A^{DH}** segments in D_2O/DMSO.[30]

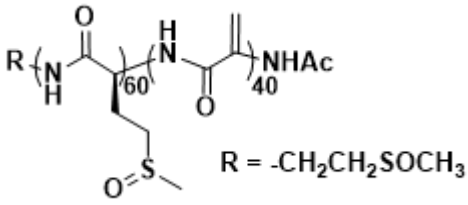

$M^{O}_{60}A^{DH}_{40}$ (20 mg, 78% yield). Prepared using the General Procedure provided above. ^{1}H NMR (400 MHz, d_6-DMSO, 25 °C): δ 8.32 (s, 60H), δ 4.33 (s, 60H), δ 2.72 (s, 120H), δ 2.51 (s, 180H), δ 2.51 (d, 120H). Since resonances for S-(carboxymethyl)-L-cysteine residues were absent in the product, the low integrations observed for alkene peaks of dehydroalanine residues were likely due to aggregation of hydrophobic **A^{DH}** segments in D_2O/DMSO.[30]

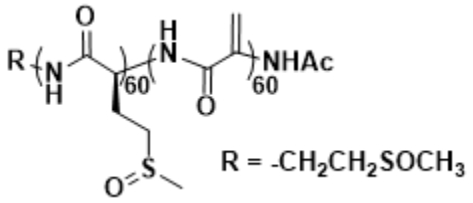

$M^{O}_{60}A^{DH}_{60}$ (14 mg, 85% yield). Prepared using the General Procedure provided above. ^{1}H NMR (400 MHz, d_6-DMSO, 25 °C): δ 9.5 (br s, 25H), δ 8.32 (s, 60H), δ 5.80 (d, 42H), δ 4.33 (s, 60H), δ 2.72 (s, 120H), δ 2.51 (s, 180H), δ 2.51 (d, 120H). Since resonances for S-(carboxymethyl)-L-cysteine residues were absent in the product, the low integrations observed for alkene peaks of dehydroalanine residues were likely due to aggregation of hydrophobic **A^{DH}** segments in D_2O/DMSO.[30]

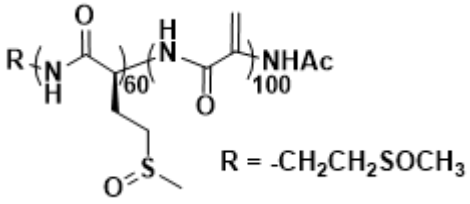

$M^{O}_{60}A^{DH}_{100}$ (25 mg, 84% yield). Prepared using the General Procedure provided above. ^{1}H NMR (400 MHz, d_6-DMSO, 25 °C): δ 9.5 (br s, 53H), δ 8.32 (s, 35H), δ 5.80 (d, 120H), δ 4.33 (s, 35H), δ 2.72 (s, 70H), δ 2.51 (s, 105H), δ 2.51 (d, 70H). Since resonances for S-(carboxymethyl)-L-cysteine residues were absent in the product, the low integrations observed for alkene peaks of dehydroalanine residues were likely due to aggregation of hydrophobic **A^{DH}** segments in D_2O/DMSO.[30]

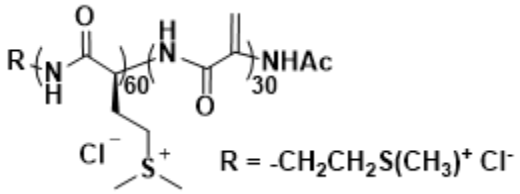

$M^{M}_{60}A^{DH}_{30}$ (7 mg, 58% yield). Prepared using the General Procedure provided above. ^{1}H NMR (400 MHz, D_2O, 25 °C): δ 3.77 (s, 120H), δ 3.32 (s, 360H), δ 2.69 (d, 120H). Since resonances for S-(carboxymethyl)-L-cysteine residues were absent in the product, the low integrations observed for alkene peaks of dehydroalanine residues were likely due to aggregation of hydrophobic **A^{DH}** segments in D_2O/DMSO.[30]

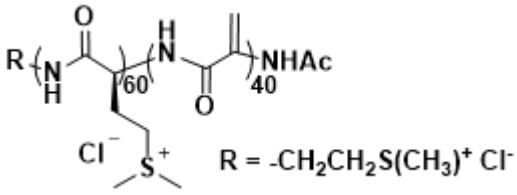

$M^{M}_{60}A^{DH}_{40}$ (10 mg, 81% yield). Prepared using the General Procedure provided above. ^{1}H NMR (400 MHz, D_2O, 25 °C): δ 4.55 (s, 60H), δ 3.46 (m, 120H), δ 2.99 (s, 360H), δ 2.34 (d, 120H). Since resonances for S-(carboxymethyl)-L-cysteine residues were absent in the product, the low integrations observed for alkene peaks of dehydroalanine residues were likely due to aggregation of hydrophobic **A^{DH}** segments in D_2O/DMSO.[30]

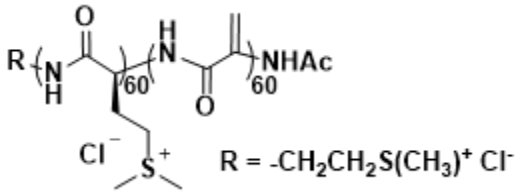

$M^{M}_{60}A^{DH}_{60}$ (8 mg, 65% yield). Prepared using the General Procedure provided above. ^{1}H NMR (400 MHz, D_2O, 25 °C): δ 5.26 (s, 60H), δ 4.33 (s, 60H), δ 4.23 (s, 120H), δ 3.82 (s, 360H), δ 3.17 (d, 120H). Since resonances for S-(carboxymethyl)-L-cysteine residues were absent in the product, the low integrations observed for alkene peaks of dehydroalanine residues were likely due to aggregation of hydrophobic **A^{DH}** segments in D_2O/DMSO.[30]

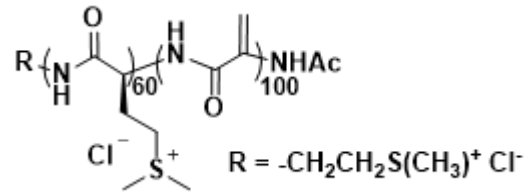

$M^{M}_{60}A^{DH}_{100}$ (11 mg, 89.4% yield). Prepared using the General Procedure provided above. ^{1}H NMR (400 MHz, D_2O, 25 °C): δ 5.80 (d, 29H), δ 4.33 (s, 60H), δ 2.72 (s, 120H), δ 2.51 (s, 180H), δ 2.51 (d, 120H). Since resonances for S-(carboxymethyl)-L-cysteine residues were absent in the product, the low integrations observed for alkene peaks of dehydroalanine residues were likely due to aggregation of hydrophobic **A^{DH}** segments in D_2O/DMSO.[30]

3.6 Spectral Data

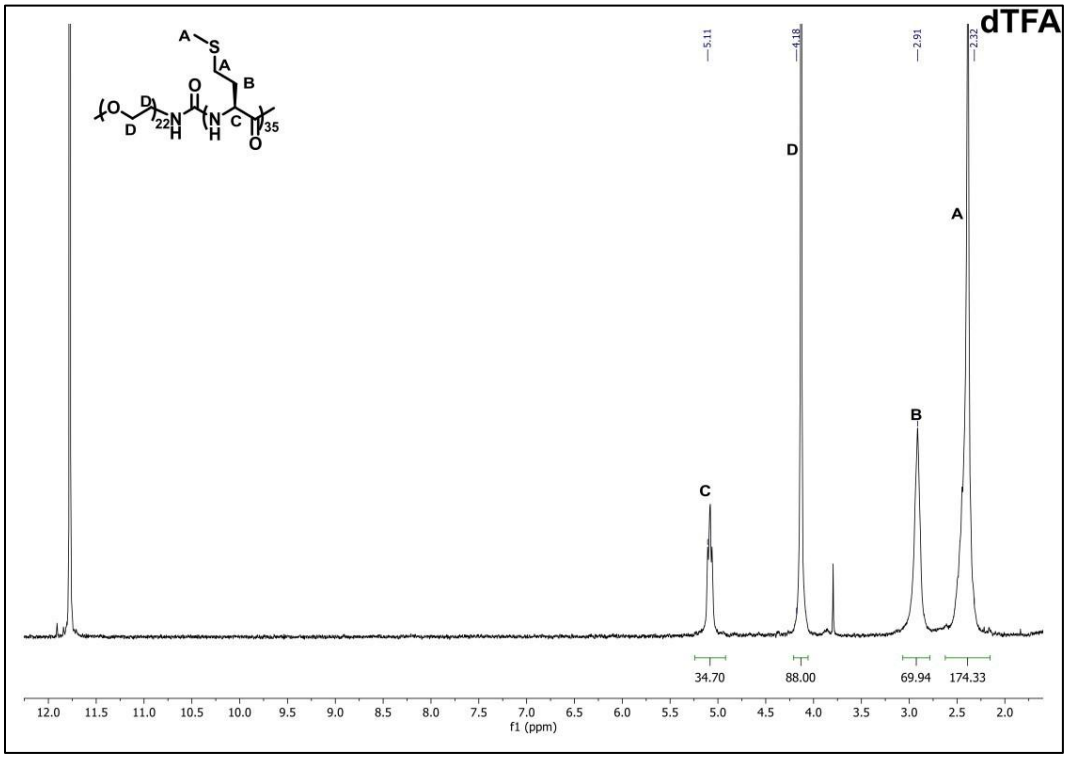

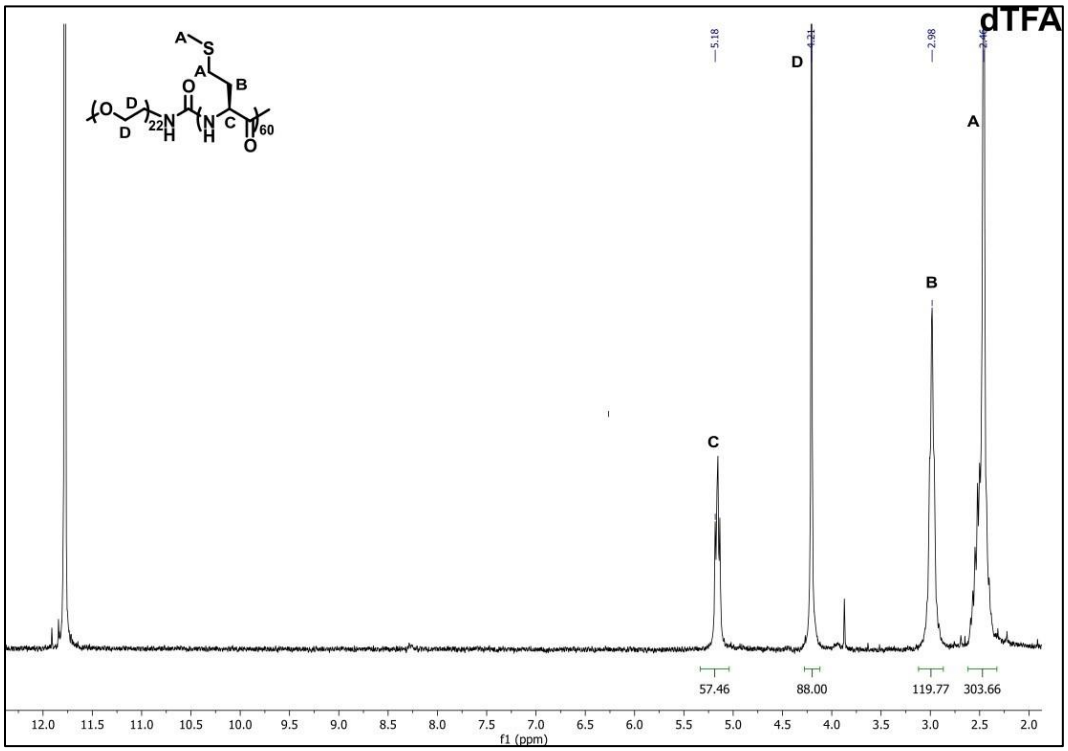

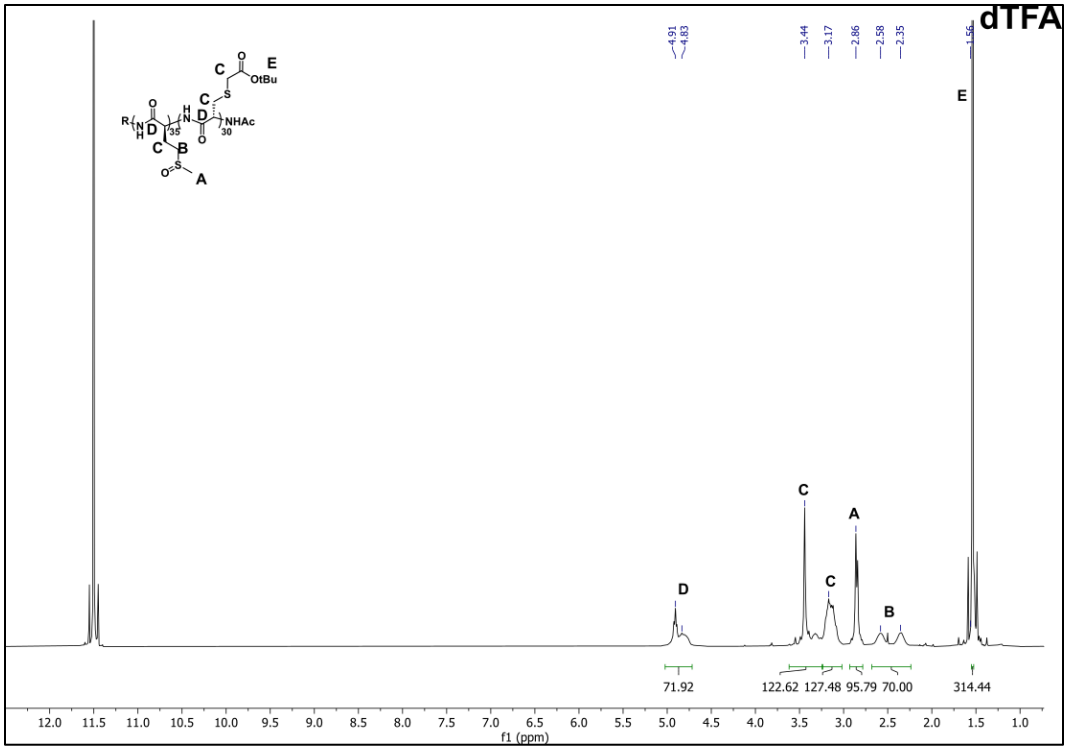
dTFA
4.91
4.83
3.44
3.17
2.86
2.58
2.35
1.56
E
C
A
C
D
B
71.92
122.62
127.48
95.79
70.00
314.44
f1 (ppm)

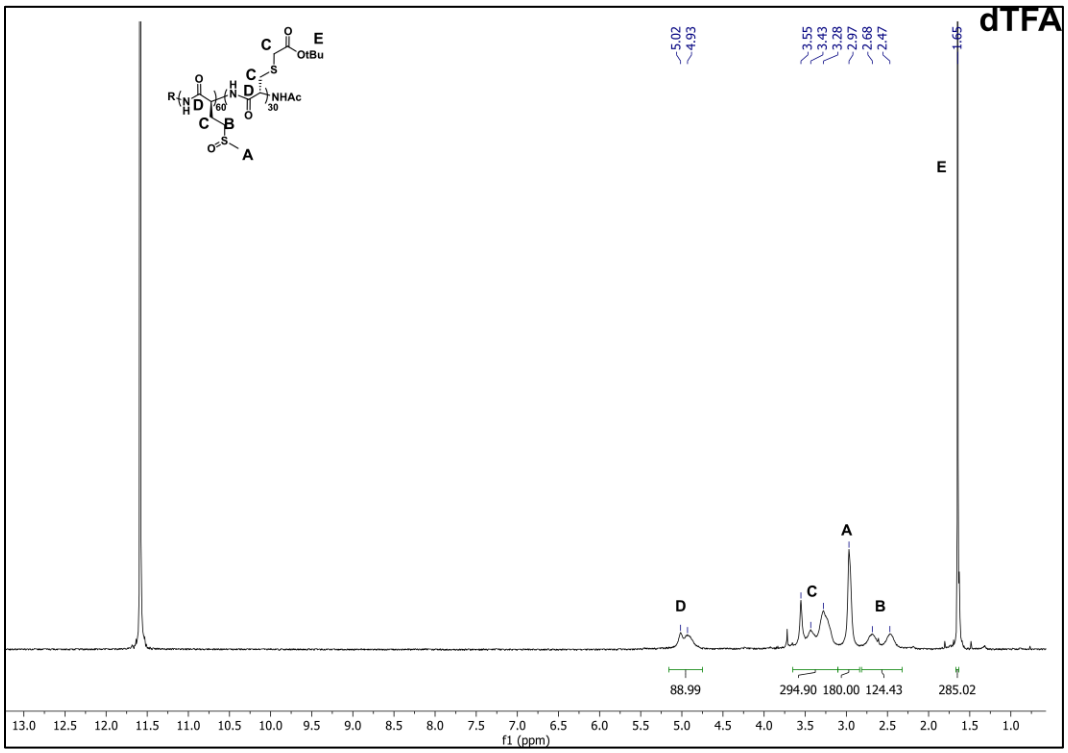
dTFA
5.02
4.93
3.55
3.43
3.28
2.97
2.68
2.47
1.65
E
A
C
D
B
88.99
294.90
180.00
124.43
285.02
f1 (ppm)

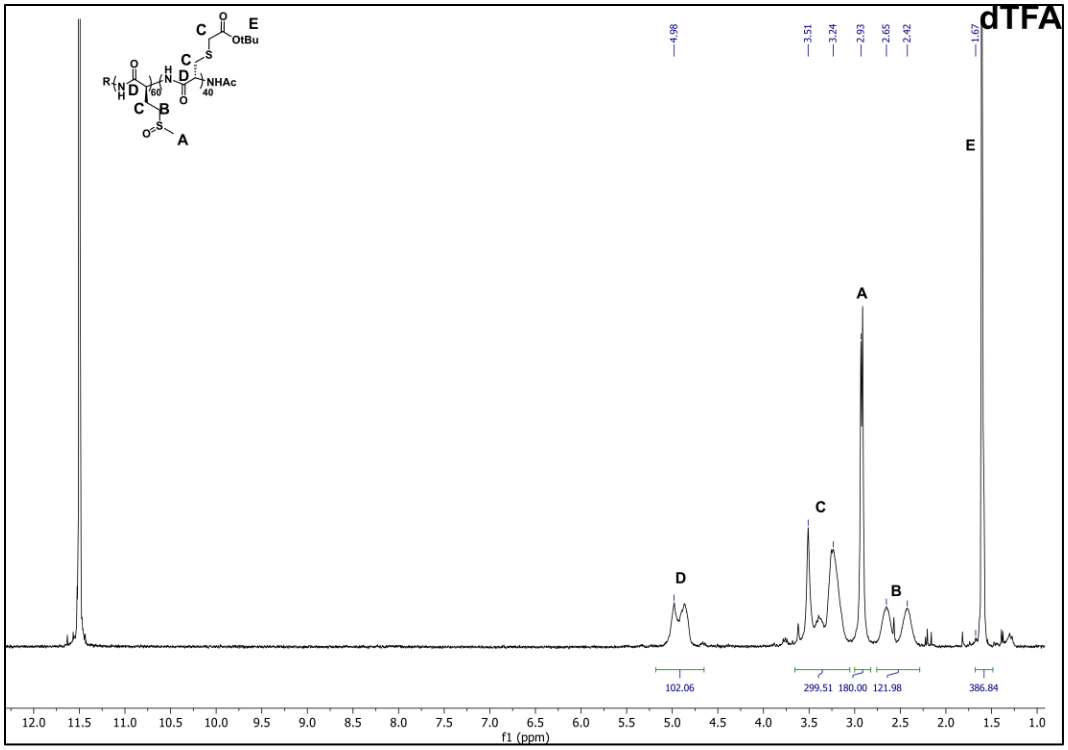
dTFA
4.98
3.51
3.24
2.93
2.65
2.42
1.67
A
B
C
D
E
102.06
299.51
180.00
121.98
386.84
f1 (ppm)

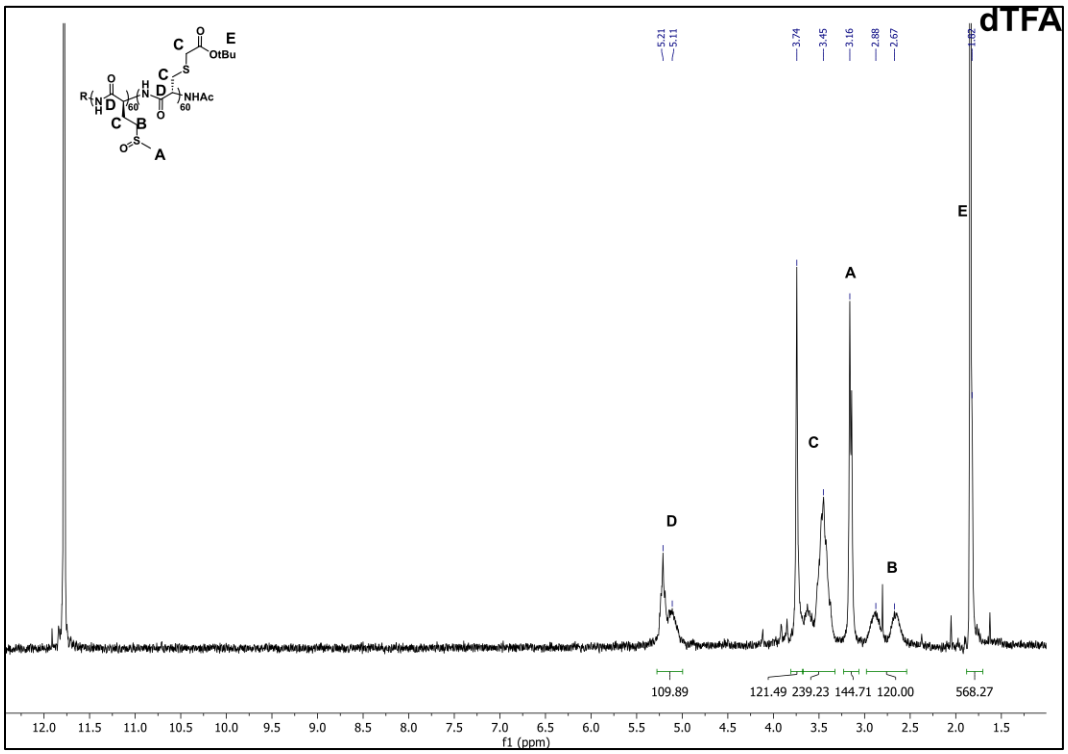
dTFA
5.21
5.11
3.74
3.45
3.16
2.88
2.67
1.02
A
B
C
D
E
109.89
121.49
239.23
144.71
120.00
568.27
f1 (ppm)

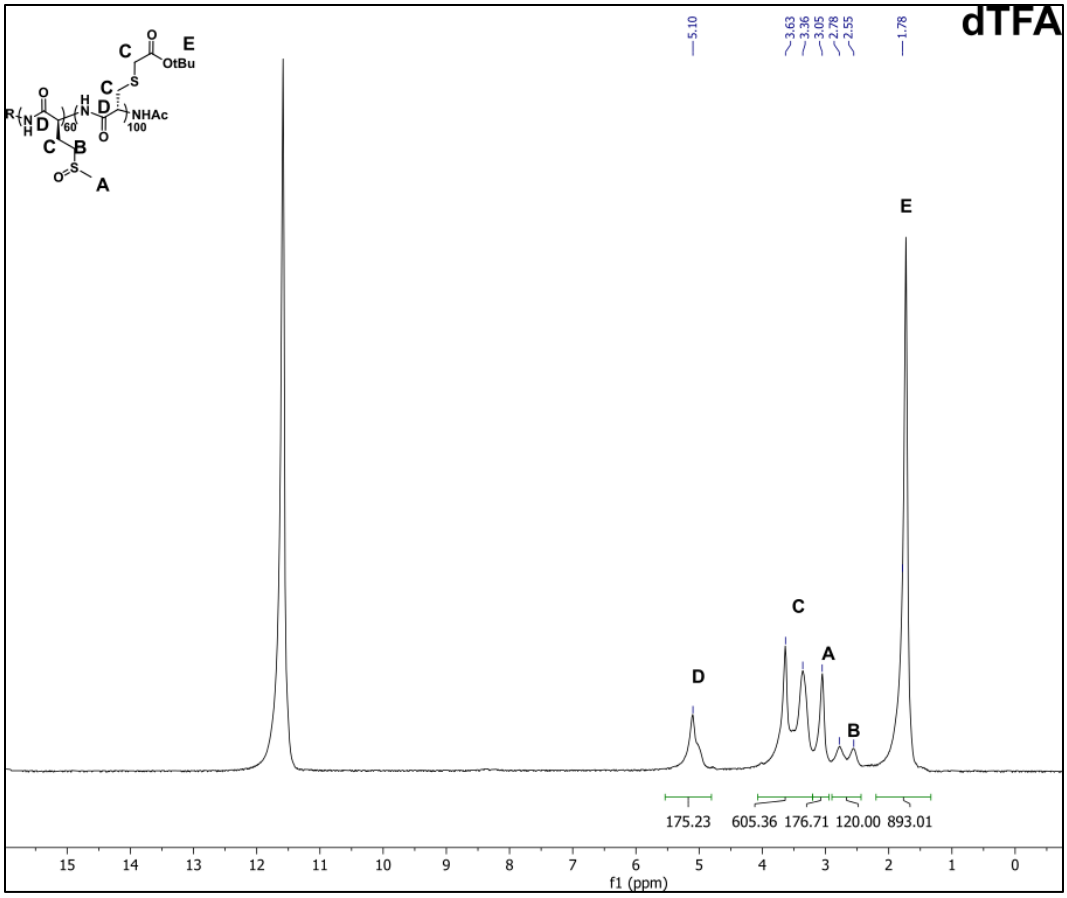
dTFA
5.10
3.63
3.36
3.05
2.78
2.55
1.78
E
C
A
D
B
175.23
605.36
176.71
120.00
893.01
f1 (ppm)

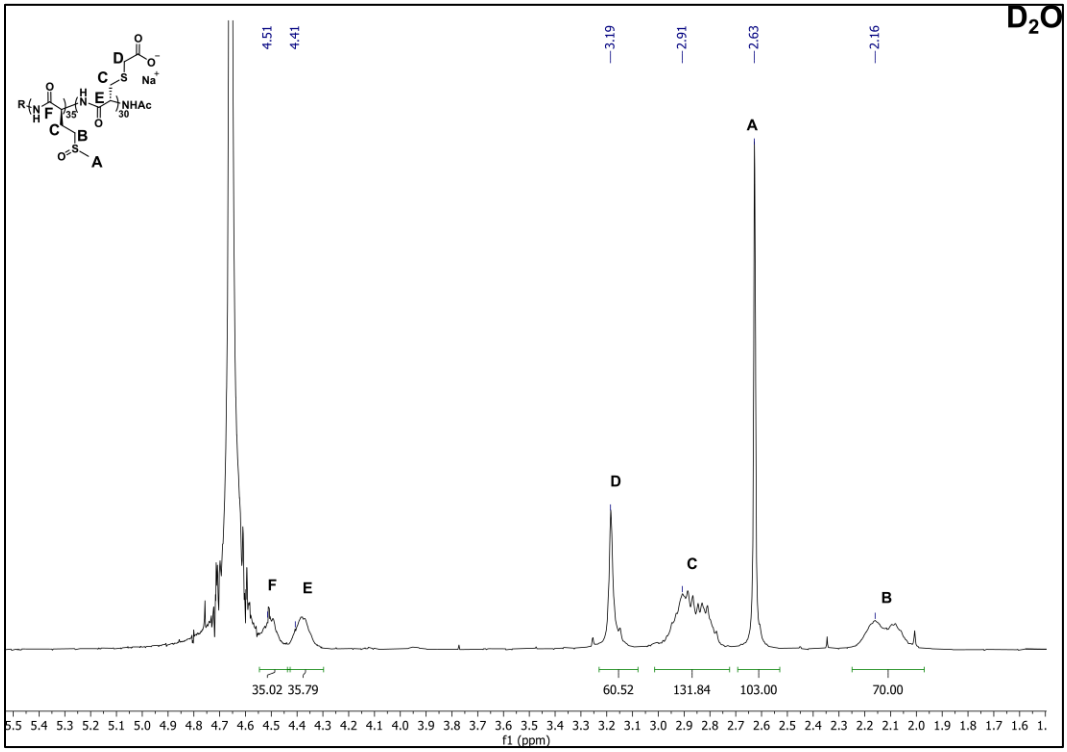
D2O
4.51
4.41
3.19
2.91
2.63
2.16
A
D
C
F
E
B
35.02
35.79
60.52
131.84
103.00
70.00
f1 (ppm)

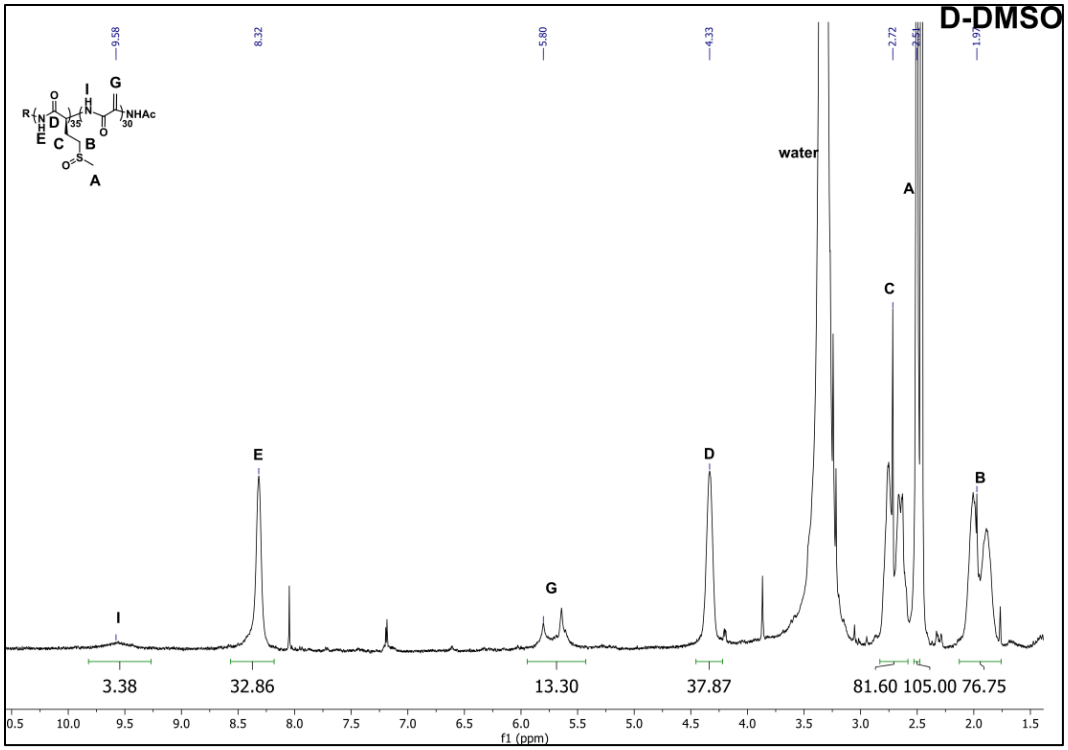
D-DMSO
9.58
8.32
5.80
4.33
2.72
2.51
1.98
water
A
C
E
D
B
G
I
3.38
32.86
13.30
37.87
81.60
105.00
76.75
f1 (ppm)

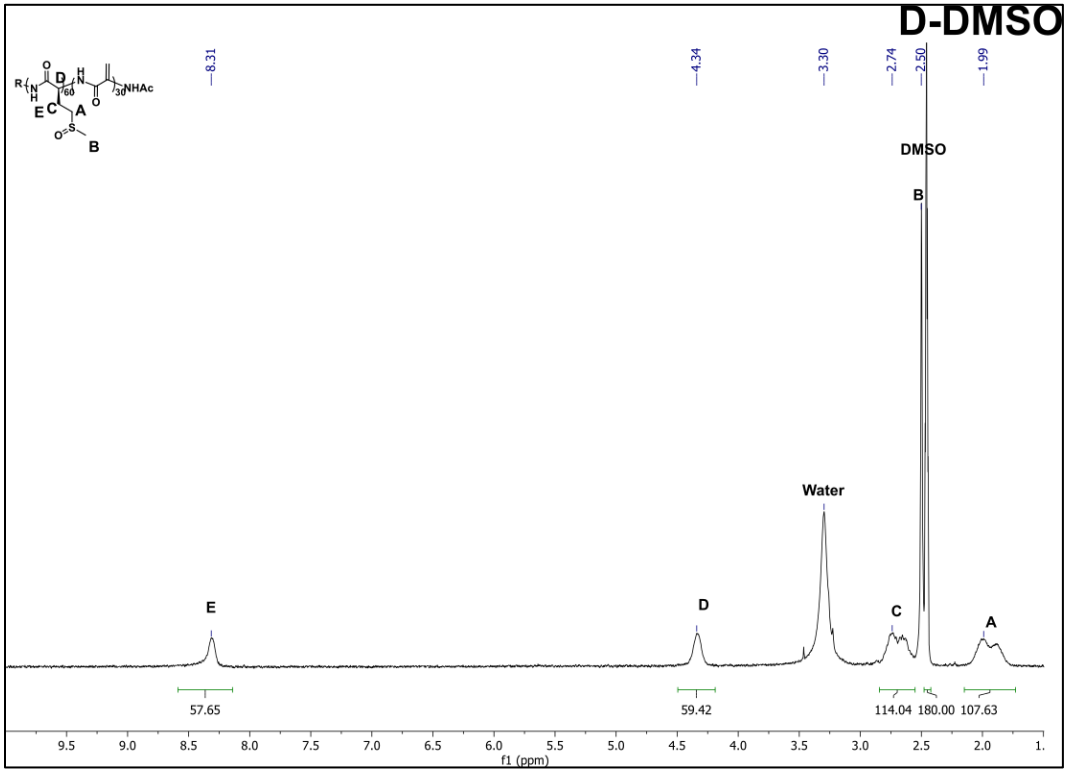
D-DMSO
8.31
4.34
3.30
2.74
2.50
1.99
DMSO
B
Water
E
D
C
A
57.65
59.42
114.04
180.00
107.63
f1 (ppm)

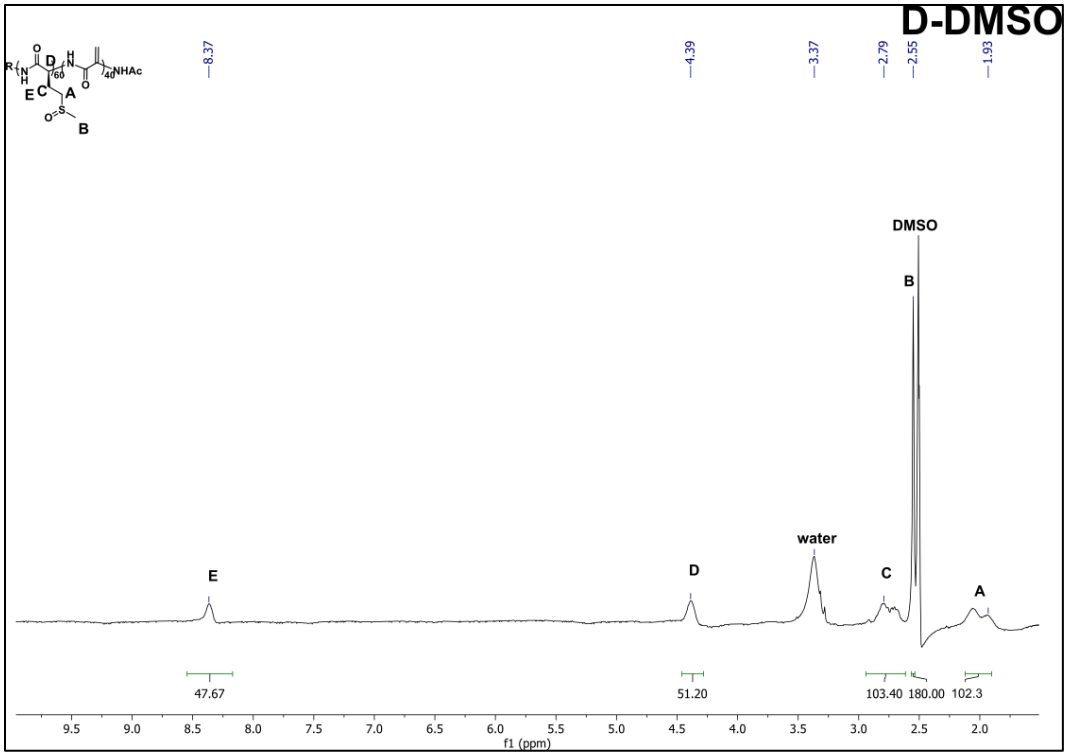
D-DMSO
8.37
4.39
3.37
2.79
2.55
1.93
DMSO
B
water
E
D
C
A
47.67
51.20
103.40
180.00
102.3
f1 (ppm)

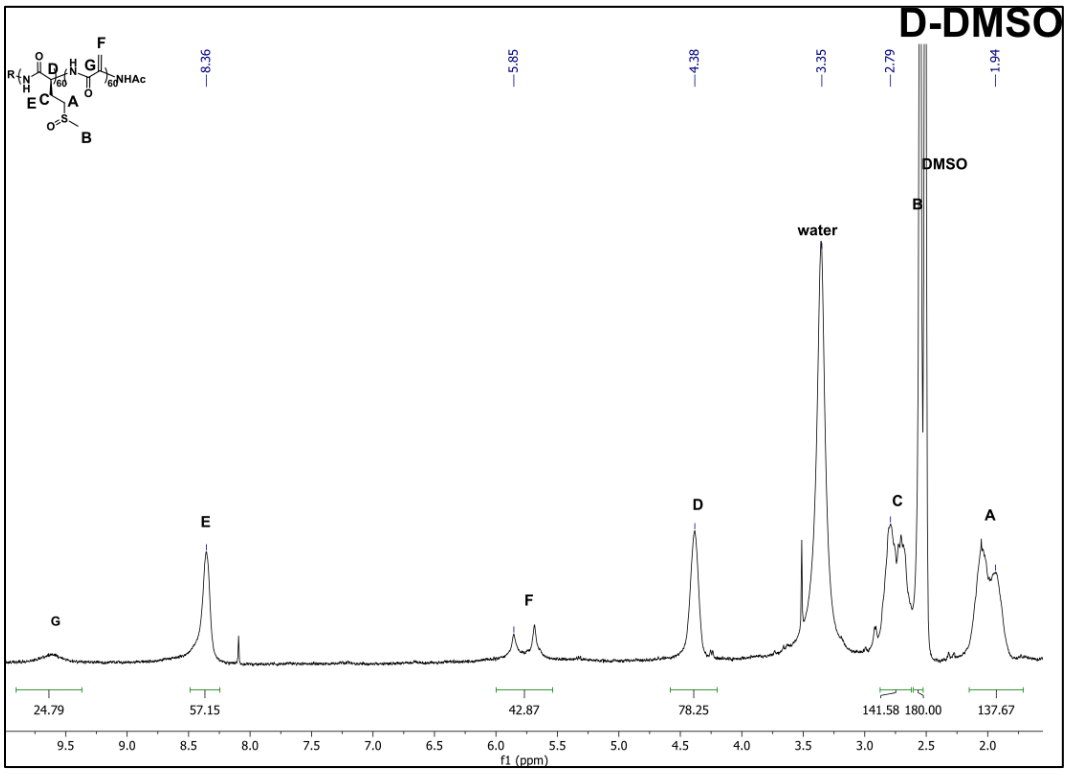
D-DMSO
8.36
5.85
4.38
3.35
2.79
1.94
DMSO
B
water
E
D
C
A
G
F
24.79
57.15
42.87
78.25
141.58
180.00
137.67
f1 (ppm)

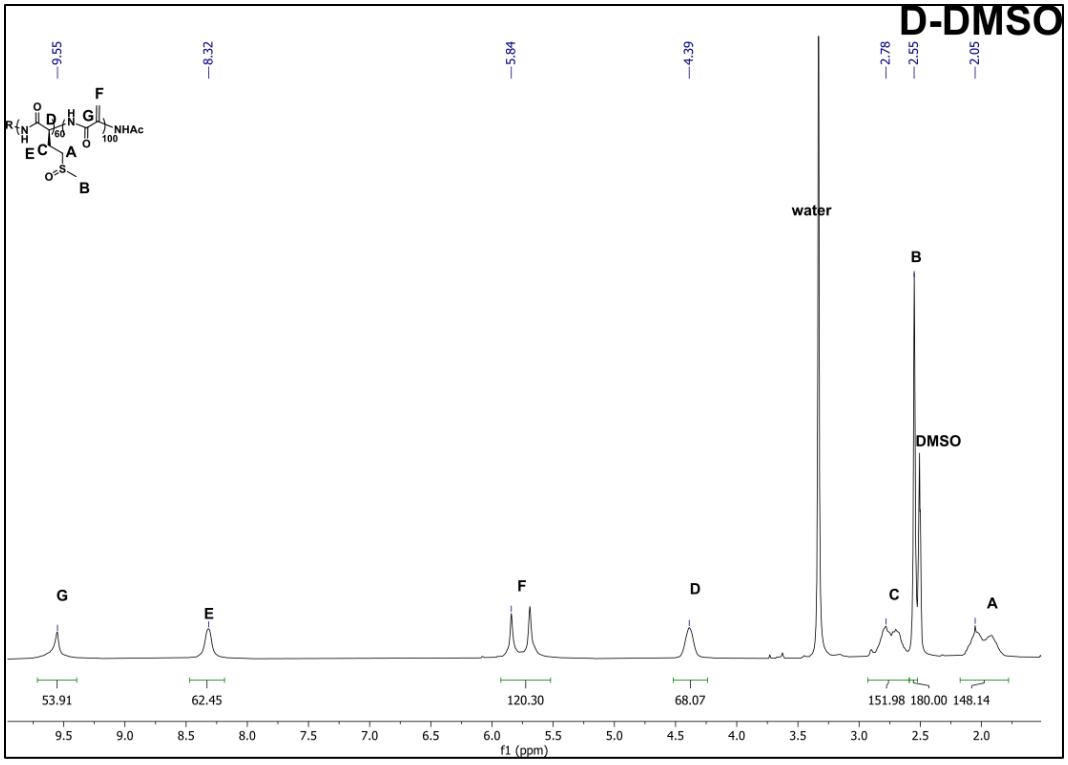
D-DMSO
9.55
8.32
5.84
4.39
2.78
2.55
2.05
water
B
DMSO
G
E
F
D
C
A
53.91
62.45
120.30
68.07
151.98
180.00
148.14
f1 (ppm)

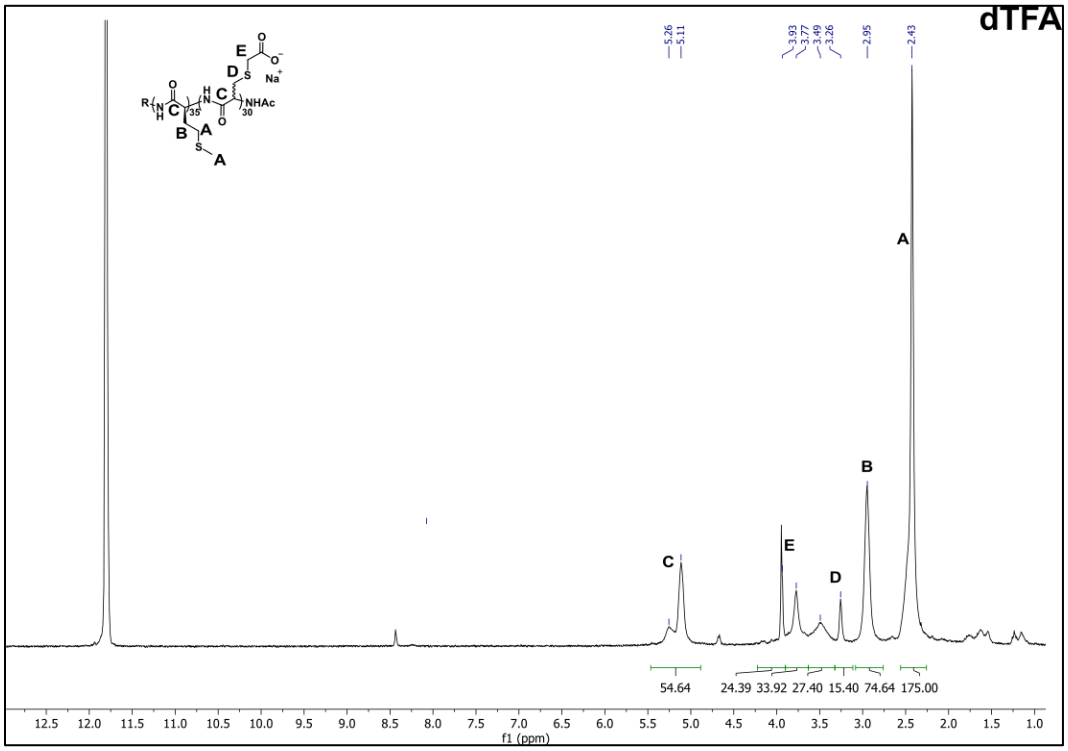
dTFA
5.26
5.11
3.93
3.77
3.49
3.26
2.95
2.43
A
B
C
E
D
54.64
24.39
33.92
27.40
15.40
74.64
175.00
f1 (ppm)

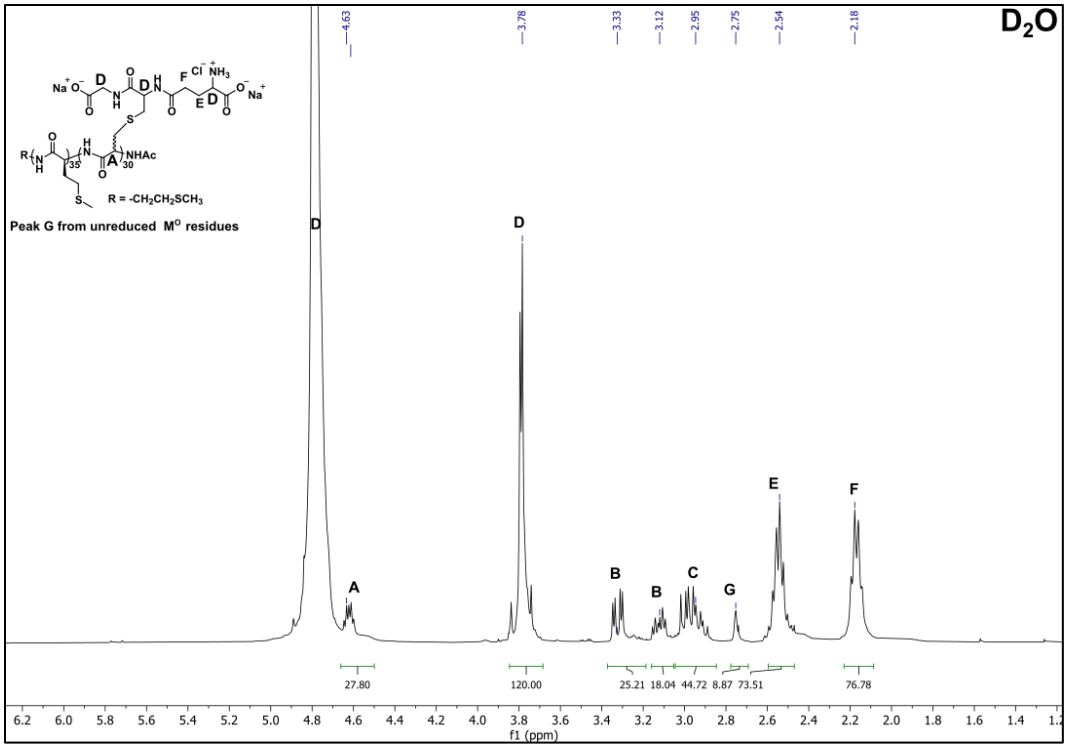
D2O
4.63
3.78
3.33
3.12
2.95
2.75
2.54
2.18
R = -CH2CH2SCH3
Peak G from unreduced MO residues
D
D
A
B
B
C
G
E
F
27.80
120.00
25.21 18.04 44.72 8.87 73.51
76.78
f1 (ppm)

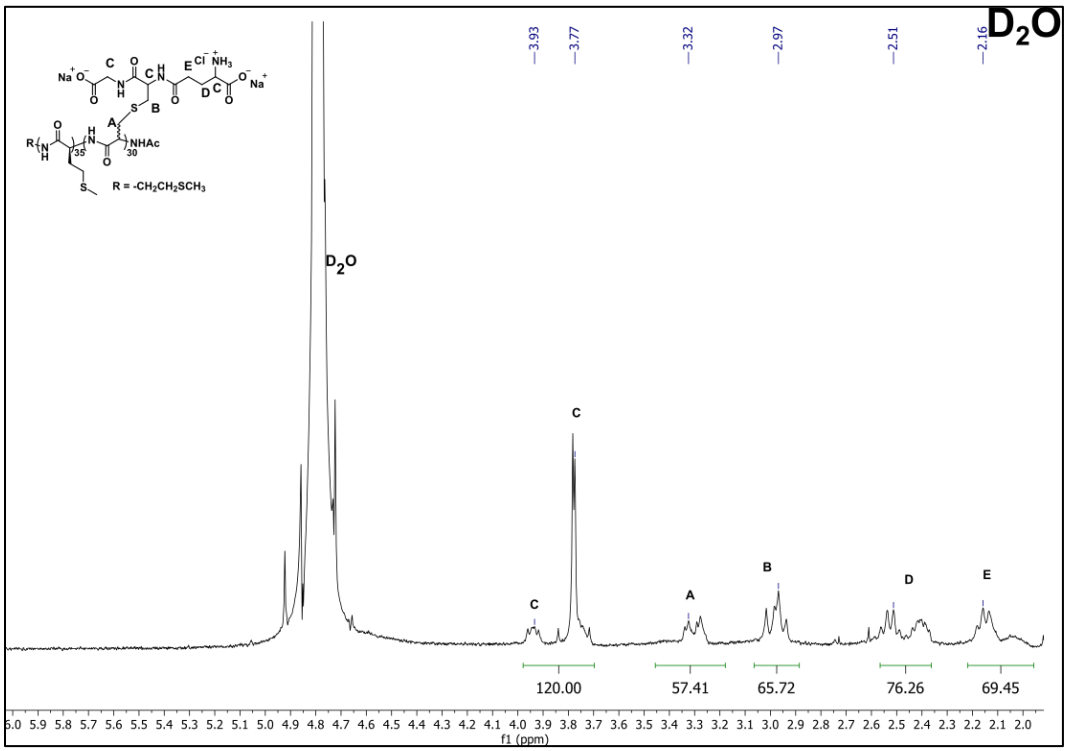
D2O
3.93
3.77
3.32
2.97
2.51
2.16
R = -CH2CH2SCH3
D2O
C
C
A
B
D
E
120.00
57.41
65.72
76.26
69.45
f1 (ppm)

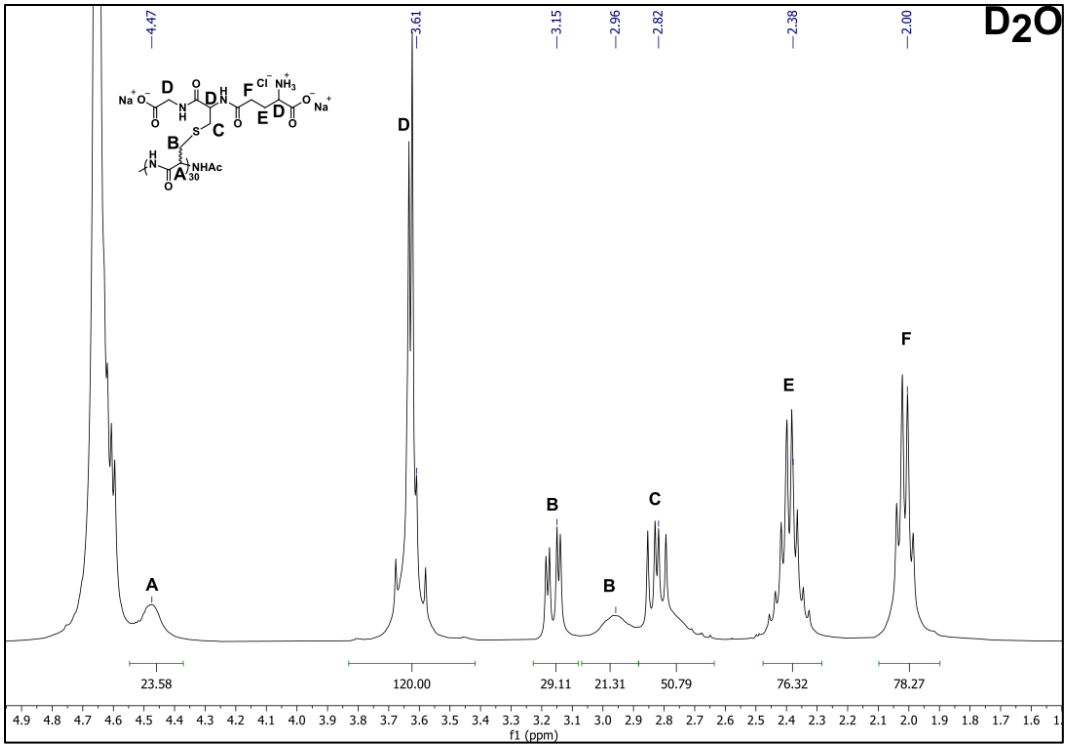
D2O
4.47
3.61
3.15
2.96
2.82
2.38
2.00
A
B
C
D
E
F
23.58
120.00
29.11
21.31
50.79
76.32
78.27
f1 (ppm)

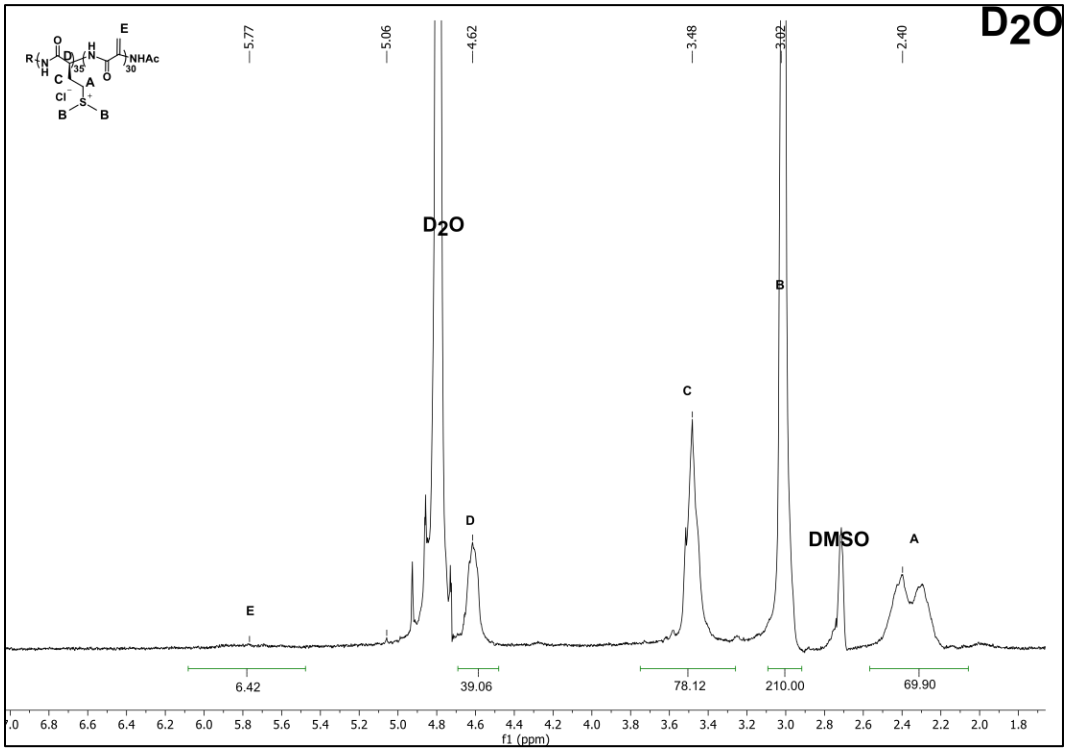
D2O
5.77
5.06
4.62
3.48
3.02
2.40
D2O
DMSO
A
B
C
D
E
6.42
39.06
78.12
210.00
69.90
f1 (ppm)

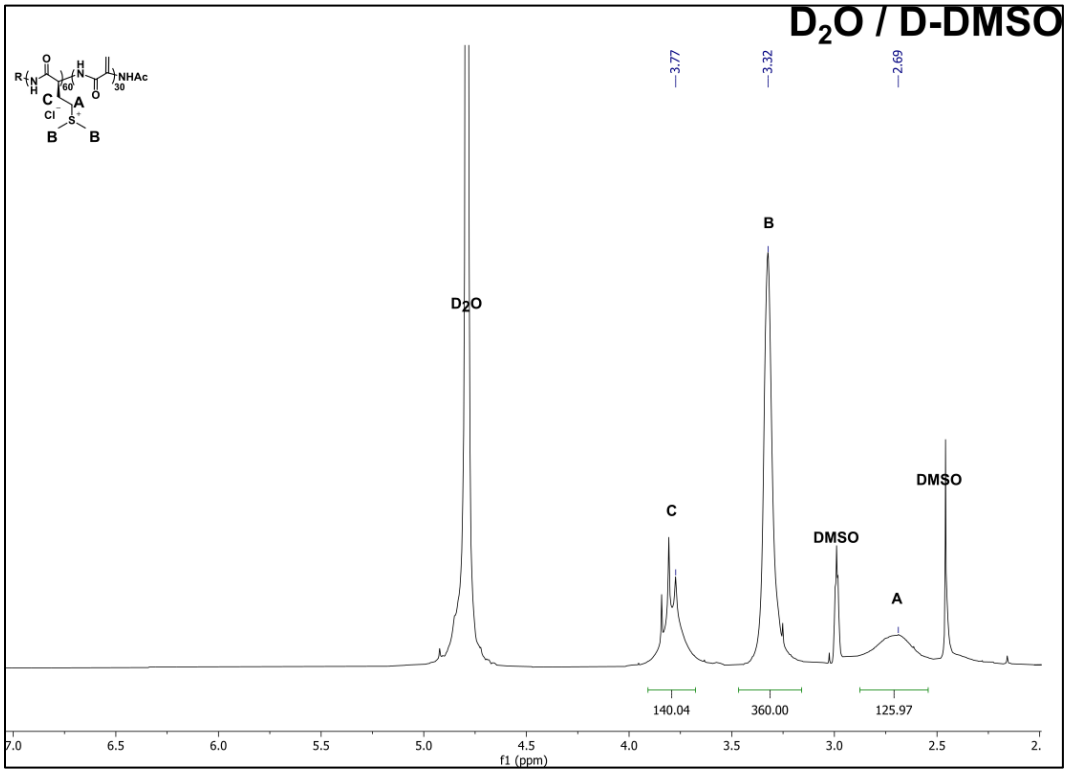
D2O / D-DMSO
3.77
3.32
2.69
D2O
B
C
DMSO
DMSO
A
140.04
360.00
125.97
f1 (ppm)

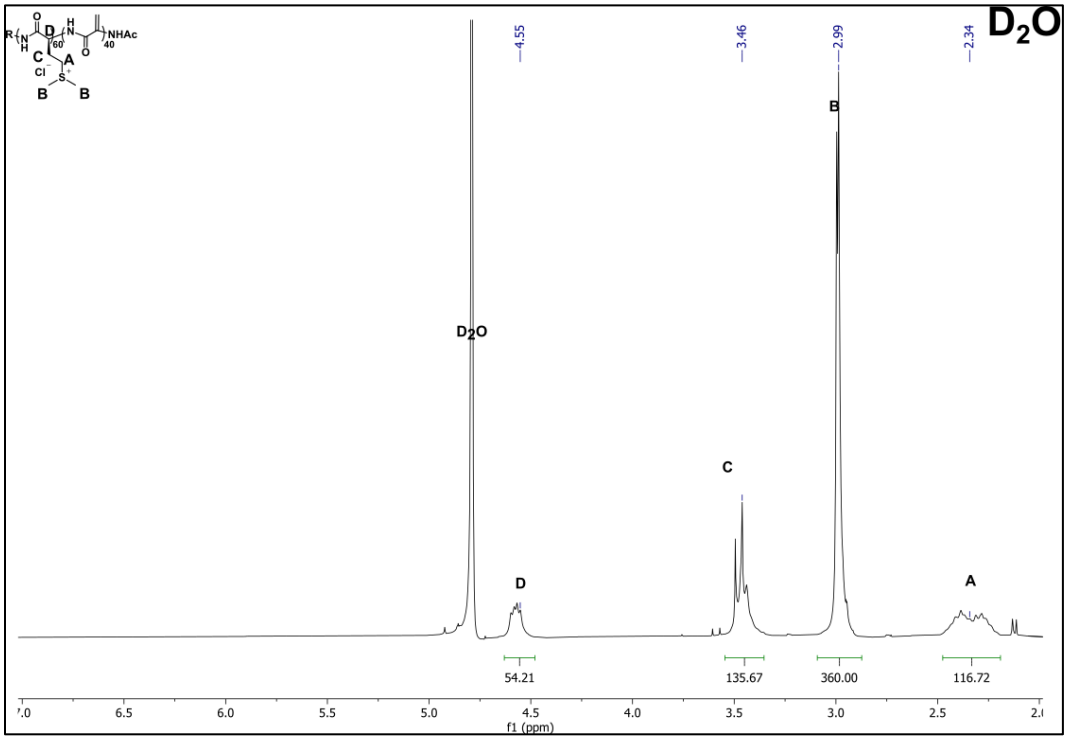
D2O
4.55
3.46
2.99
2.34
D2O
B
C
D
A
54.21
135.67
360.00
116.72
f1 (ppm)

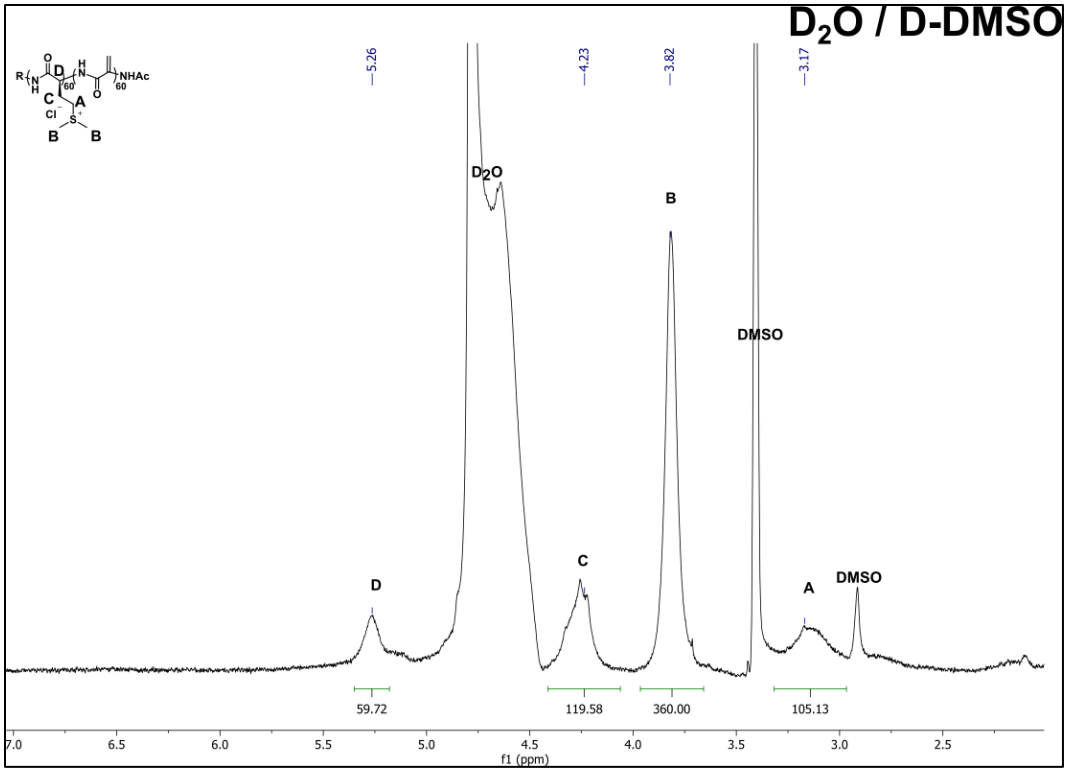
D2O / D-DMSO
5.26
4.23
3.82
3.17
D2O
B
DMSO
C
D
A
DMSO
59.72
119.58
360.00
105.13
f1 (ppm)

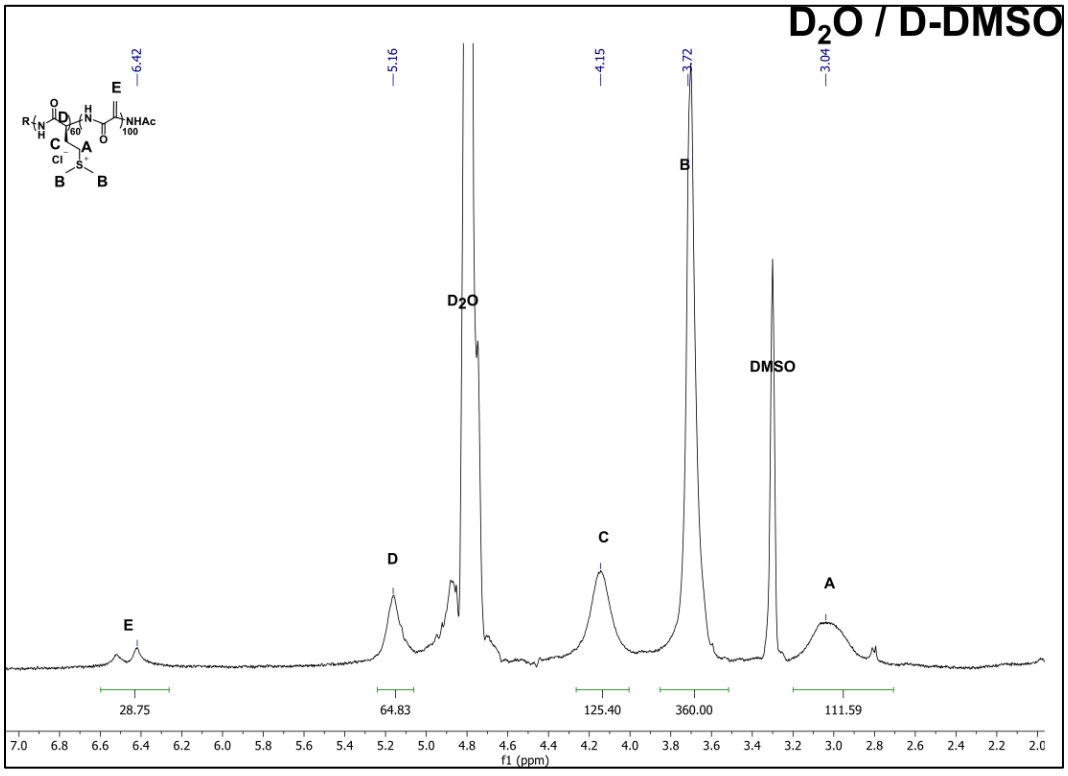
D2O / D-DMSO
6.42
5.16
4.15
3.72
3.04
E
B
D2O
DMSO
C
D
A
E
28.75
64.83
125.40
360.00
111.59
f1 (ppm)

3.7 References

1) Zelzer, M.; Todd, S. J.; Hirst, A. R.; McDonalde, T. O.; Ulijn, R. V. Enzyme responsive materials: design strategies and future developments. Biomater. Sci. 2013, 1, 11−39.

2) Hu, X.; Zhang, Y.; Xie, Z.; Jing, X.; Bellotti, A.; Gu, Z. Stimuli-responsive polymersomes for biomedical applications. Biomacromolecules 2017, 18, 649−673.

3) Song, Y.; Ding, Y.; Dong, C.-M. Stimuli-responsive polypeptide nanoassemblies: Recent progress and applications in cancer nanomedicine. WIREs Nanomed Nanobiotechnol. 2022, 14, No. e1742.

4) Li, F.; Qin, Y.; Lee, J.; Liao, H.; Wang, N.; Davis, T. P.; Qiao, R.; Ling, D. Stimuli-responsive nano-assemblies for remotely controlled drug delivery. J. Control Release 2020, 322, 566−592.

5) Wang, X.; Song, Z.; Wei, S.; Ji, G.; Zheng, X.; Fu, Z.; Cheng, J. Polypeptide-based drug delivery systems for programmed release. Biomaterials 2021, 275, 120913.

6) Zhang, P.; Li, M.; Xiao, C.; Chen, X. Stimuli-responsive polypeptides for controlled drug delivery. Chem. Commun. 2021, 57, 9489−9503.

7) Li, M.-H.; Keller, P. Stimuli-responsive polymer vesicles. Soft Matter 2009, 5, 927−937.

8) Grubbs, R. B.; Sun, Z. Shape-changing polymer assemblies. Chem. Soc. Rev. 2013, 42, 7436−7445.

9) Lu, C.; Urban, M. W. Stimuli-responsive polymer nano-science: Shape anisotropy, responsiveness, applications. Prog. Polym. Sci. 2018, 78, 24−46.

10) Bütün, V.; Billingham, N. C.; Armes, S. P. Unusual aggregation behavior of a novel Tertiary amine methacrylate-based diblock copolymer: formation of micelles and reverse micelles in aqueous solution. J. Am. Chem. Soc. 1998, 120, 11818−11819.

11) Arotçaréna, M.; Heise, B.; Ishaya, S.; Laschewsky, A. Switching the inside and the outside of aggregates of water-soluble block copolymers with double thermoresponsivity. J. Am. Chem. Soc. 2002, 124, 3787−3793.

12) Liu, F.; Eisenberg, A. Preparation and pH triggered inversion of vesicles from poly(acrylic acid)-block-polystyrene-block-poly(4-vinyl pyridine). J. Am. Chem. Soc. 2003, 125, 15059−15064.

13) Napoli, A.; Valentini, M.; Tirelli, N.; Müller, M.; Hubbell, J. A. Oxidation-responsive polymeric vesicles. Nat. Mater. 2004, 3, 183− 189.

14) Rodriguez-Hernández, J.; Lecommandoux, S. Reversible insideout micellization of pH-responsive and water-soluble vesicles based on polypeptide diblock copolymers. J. Am. Chem. Soc. 2005, 127, 2026−2027.

15) Jin, Q.; Liu, G.; Ji, J. Micelles and reverse micelles with a photo and thermo double-responsive block copolymer. J. Polym. Sci., Part A: Polym. Chem. 2010, 48, 2855−2861.

16) Yan, Q.; Zhao, Y. Polymeric microtubules that breathe: CO2- driven polymer controlled-self-assembly and shape transformation. Angew. Chem., Int. Ed. 2013, 52, 9948−9951.

17) Moughton, A. O.; O'Reilly, R. K. Thermally induced micelle to vesicle morphology transition for a charged chain end diblock copolymer. Chem. Commun. 2010, 46, 1091−1093.

18) Deming, T. J. Synthesis and self-assembly of well-defined block copolypeptides via controlled NCA polymerization. Adv. Polym. Sci. 2013, 262, 1−37.

19) Deming, T. J. Preparation and development of block copolypeptide vesicles and hydrogels for biological and medical applications. WIREs Nanomed. Nanobiotechnol. 2014, 6, 283−297.

20) Pitha, J.; Szente, L.; Greenberg, J. Poly-L-methionine sulfoxide: a biologically inert analogue of dimethyl sulfoxide with solubilizing potency. J. Pharm. Sci. 1983, 72, 665−668.

21) O'Shea, T. M.; Wollenberg, A. L.; Kim, J. H.; Ao, Y.; Deming, T. J.; Sofroniew, M. V. Foreign body responses in central nervous system mimic natural wound responses and alter biomaterial functions. Nat. Commun. 2020, 11, 6203.

22) Hanson, J. A.; Chang, C. B.; Graves, S. M.; Li, Z.; Mason, T. G.; Deming, T. J. Nanoscale double emulsions stabilized by single component block copolypeptides. Nature 2008, 455, 85−89.

23) Hanson, J. A.; Li, Z.; Deming, T. J. Nonionic block copolypeptide micelles containing a hydrophobic racemic-leucine core. Macromolecules 2010, 43, 6268−6269.

24) Bellomo, E.; Wyrsta, M. D.; Pakstis, L.; Pochan, D. J.; Deming, T. J. Stimuli responsive polypeptide vesicles via conformation specific assembly. Nat. Mater. 2004, 3, 244−248.

25) Holowka, E. P.; Pochan, D. J.; Deming, T. J. Charged polypeptide vesicles with controllable diameter. J. Am. Chem. Soc. 2005, 127, 12423−12428.

26) Rodriguez, A. R.; Kramer, J. R.; Deming, T. J. Enzyme-triggered cargo release from methionine sulfoxide containing copolypeptide vesicles. Biomacromolecules 2013, 14, 3610−3614.

27) Nowak, A. P.; Breedveld, V.; Pakstis, L.; Ozbas, B.; Pine, D. J.; Pochan, D.; Deming, T. J. Rapidly recovering hydrogel scaffolds from self-assembling diblock copolypeptide amphiphiles. Nature 2002, 417, 424−428.

28) Sun, Y.; Wollenberg, A. L.; O'Shea, T. M.; Cui, Y.; Zhou, Z. H.; Sofroniew, M. V.; Deming, T. J. Conformation directed formation of self-healing diblock copolypeptide hydrogels via polyion complexation. J. Am. Chem. Soc. 2017, 139, 15114−15121.

29) Wollenberg, A. L.; O'Shea, T. M.; Kim, J. H.; Czechanski, A.; Reinholdt, L. G.; Sofroniew, M. V.; Deming, T. J. Injectable polypeptide hydrogels via methionine modification for neural stem cell delivery. Biomaterials 2018, 178, 527−545.

30) Benavides, I.; Raftery, E. D.; Bell, A. G.; Evans, D.; Scott, W. A.; Houk, K. N.; Deming, T. J. Poly(dehydroalanine): synthesis, properties and functional diversification of a fluorescent polypeptide. J. Am. Chem. Soc. 2022, 144, 4214−4223.

31) Deming, T. J. Cobalt and iron initiators for the controlled polymerization of α-amino acid-N-carboxyanhydrides. Macromolecules 1999, 32, 4500−4502.

32) Rich, D. H.; Tam, J. P. Synthesis of dehydroamino acids and peptides by dehydrosulfenylation. Rate enhancement using sulfenic acid trapping agents. J. Org. Chem. 1977, 42, 3815−3820.

33) Deming, T. J. Sulfur switches for responsive peptide materials. Acc. Chem. Res. 2024, 57, 661−669.

34) Kramer, J. R.; Deming, T. J. Reversible chemoselective tagging and functionalization of methionine containing peptides. Chem. Commun. 2013, 49, 5144−5146.

35) Deponte, M. Glutathione catalysis and the reaction mechanisms of glutathione-dependent enzymes. Biochim. Biophys. Acta 2013, 1830, 3217−3266

36) Kramer, J. R.; Deming, T. J. General Method for Purification of α-Amino Acid-N-Carboxyanhydrides Using Flash Chromatography. Biomacromolecules 2010, 11, 3668–3672.

37) Morrison, C. A.; Chan, E. P.; Lee, T.; Deming, T. J. Switchable Coacervate Formation via Amino Acid Functionalization of Poly(Dehydroalanine). Biomacromolecules 2024, 25, 25542562.

38) Rodriguez, A. R.; Choe, U.-J.; Kamei, D. T.; Deming, T. J. Use of Methionine Alkylation to Prepare Cationic and Zwitterionic Block Copolypeptide Vesicles. Isr. J. Chem. 2016, 56, 607613.

Chapter 4: Shape Transformation of Poly(L-methionine sulfoxide)-*b*-poly(dehydroalanine) Vesicles

Adapted from: Morrison, C. A. and Deming, T. J. Shape Transformation of Poly(L-methionine sulfoxide)-*b*-poly(dehydroalanine) Vesicles. *ACS Macro Lett*. In press.

4.1 Abstract

The controlled transformation of polymeric vesicles into stable non-spherical morphologies is of interest as a means to mimic cells, create nano-reactors and improve their potential for therapeutic delivery applications. We have found that the poly(dehydroalanine) segments in poly(L-methionine sulfoxide)$_x$-*b*-poly(dehydroalanine)$_y$, $\mathbf{M^O_xA^{DH}_y}$ copolypeptides form membranes that provide plasticity and selective permeability in DMSO/water mixtures, which allows predictable control of vesicle shape by variation of dialysis conditions. The findings of this study expand vesicle shape transformation methods to biodegradable block copolypeptide vesicles, which are amenable to development for applications in therapeutic delivery.

4.2 Introduction

Controlled shape transformation of lipid membranes are well documented, and significant advances in the ability to mimic these biologically relevant transformations in synthetic polymer membranes have been made in recent years.[1-5] Using a variety of external stimuli, including osmotic stress, change in pH, chemical crosslinking, and light, a wide range of polymer vesicle deformations have been achieved.[3-5] The preparation of polymeric vesicles with stable non-spherical morphologies has been explored as a means to improve their properties in biological applications such as therapeutic delivery, as well as develop artificial cells and nano-reactors.[6-8] A current limitation in this field is that most polymers used for these studies are abiotic, and many are non-degradable.[3-5] For biological uses, it would be beneficial for such vesicles to utilize natural components.

Here, we report the controlled shape transformation of amino acid based poly(L-methionine sulfoxide)$_x$-*b*-poly(dehydroalanine)$_y$, $\mathbf{M^O_xA^{DH}_y}$, vesicles. The previously reported degradability and biomimetic stimuli-responsive properties of these vesicles are expected to provide advantages in advancing shape controlled vesicles for biological uses.[9-13]

A widely used method to deform spherical polymer vesicles is the use of a solvent switch (e.g. less polar to more polar), which is often followed by aqueous dialysis.[4] A difference in composition of solvents inside and outside the vesicle membrane leads to an osmotic pressure. As long as the vesicle membrane has plasticity and remains permeable, the spherical vesicles can deflate by transport of organic solvent through the membrane and out of the vesicle interior.[3-5] Addition of an osmolyte, e.g. a salt or monosaccharide, to the solvent outside of the membrane has a similar effect (**Figure 4.1**).[14,15] Once the hydrophobic membrane becomes impermeable, e.g. due to dilution of organic solvent in aqueous dialyzate, deflation ceases and the resulting vesicle morphology becomes stable.

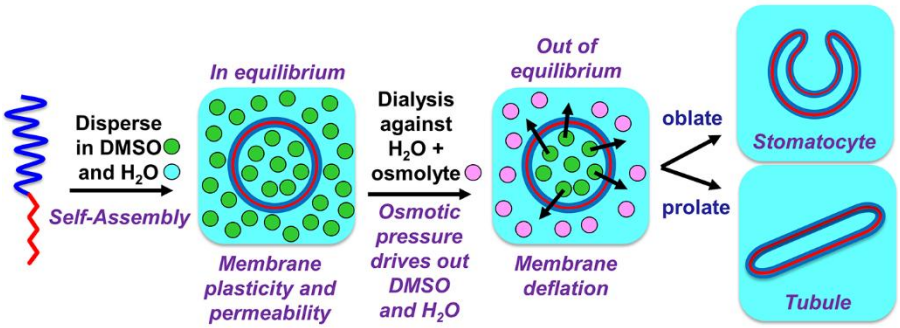

Figure 4.1: Overview of assembly of amphiphilic block copolymers into vesicles in water and their shape transformation using osmotic pressure.

Deflation of spherical vesicles can proceed via two different paths. The oblate pathway leads to flattening into discs that can curve into stomatocytes. Alternatively, the

prolate pathway leads to elongation into tubular vesicles, i.e. tubules (**Figure 4.1**).[3-5] The path taken depends on inherent properties of the vesicle membrane (e.g. inherent curvature due to block copolymer composition).[3-5]

4.3 Results and Discussion

Block copolypeptide vesicles and hydrogels can be degraded by enzymes *in vitro* or *in vivo*, and also can be engineered to react with biologically relevant molecules.[9-13,16] We recently reported a series of $\mathbf{M^{O}_{x}A^{DH}_{y}}$ (x = 30 or 60; y = 30 to 100) amphiphilic block copolypeptides, where hydrophilic $\mathbf{M^{O}}$ segments are degradable with stealth properties and both segments were found to react with thiols under physiological conditions leading to inversion of amphiphilicity (**Figure 4.2**).[13]

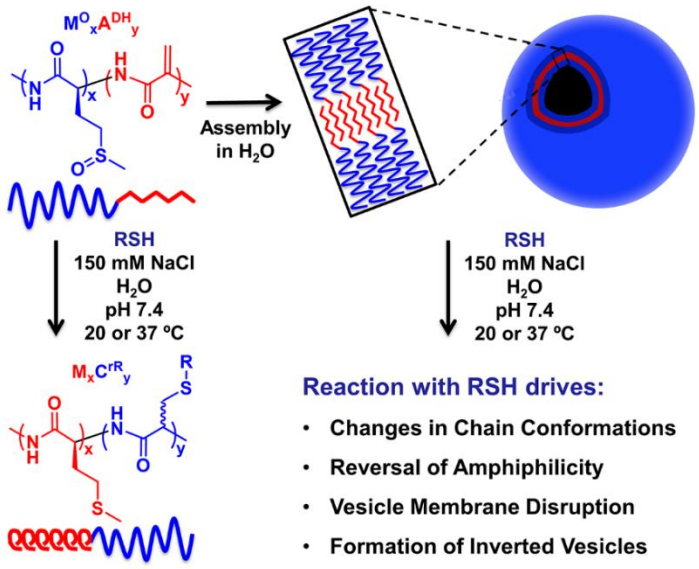

Figure 4.2. Structure of $\mathbf{M^{O}_{x}A^{DH}_{y}}$ copolypeptides, their self-assembly into spherical vesicles, and their reactivity with thiols.[13]

All $\mathbf{M^{O}_{x}A^{DH}_{y}}$ compositions studied were found to assemble into sub-micron spherical vesicles in aqueous media after nanoprecipitation using DMSO and water (**Figure 4.2**).[13] Here, we prepared a sample with a shorter hydrophobic $\mathbf{A^{DH}}$ segment,

$\mathbf{M^{O}_{60}A^{DH}_{20}}$ (**Figure 4.3**), which behaved quite differently in aqueous media. Spherical vesicles of $\mathbf{M^{O}_{60}A^{DH}_{20}}$ were occasionally observed after nanoprecipitation, yet in most preparations we instead observed formation of tubules (**Figure 4.4**).

These tubules were quite uniform, on average 4.4 μm long and 1.5 μm wide (**Table 4.1**), and were confirmed to be unilamellar tubules by nanoprecipitation in water containing hydrophilic Texas Red labeled dextran (TR dextran, MW = 3000 Da), followed by labeling of hydrophobic domains by addition of $DiOC_{18}$ probe in DMSO.[13] After dialysis to remove DMSO, unencapsulated TR dextran and excess $DiOC_{18}$, imaging of the dual labeled tubules revealed $DiOC_{18}$ labeled polypeptide membranes that encapsulate TR dextran solution (**Figure 4.4**).

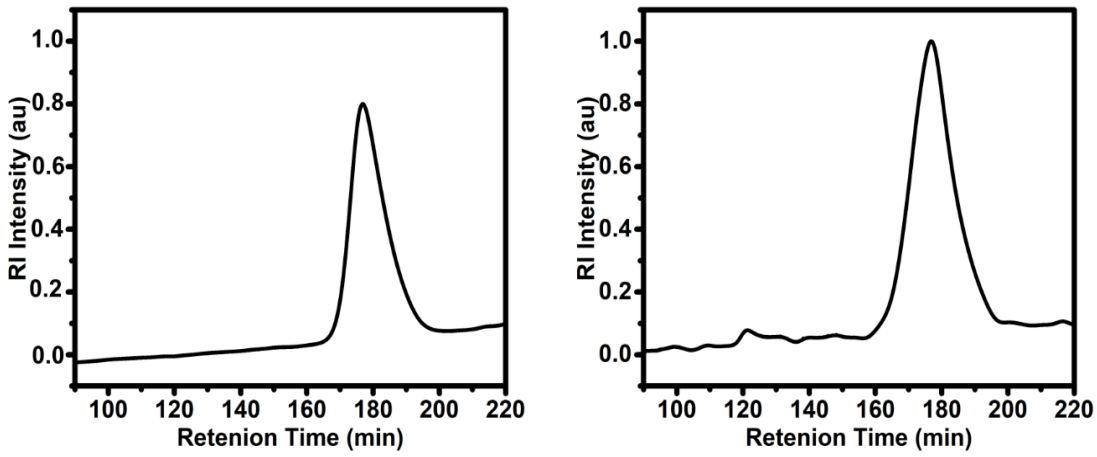

Figure 4.3. GPC Traces for $\mathbf{M^{M}_{60}}$ (Đ = 1.43, M_n = 2690 Da, M_w = 3860 Da) and $\mathbf{M^{M}_{60}A^{DH}_{20}}$ (Đ = 1.45, M_n = 3520 Da, M_w = 5120 Da).

To determine if formation of tubule shaped vesicles with $\mathbf{M^{O}_{60}A^{DH}_{20}}$ was due to copolypeptide composition or the nanoprecipitation process (a solvent switch), we examined vesicle formation in greater detail. Our default methodology for nanoprecipitation of $\mathbf{M^{O}_{x}A^{DH}_{y}}$ samples was dispersion of solid copolypeptide in a small

volume of DMSO, followed by addition of an equal volume of deionized (DI) water and dispersion using an ultrasonic bath. An equal volume of DI water was then added to this mixture while vortexting, giving a 1 wt% suspension of copolypeptide in a 1:3 DMSO:water mixture. This suspension (2 mL) was then dialyzed against DI water (3 L) with 4 dialyzate changes over 24 hours to give the final vesicle suspension.

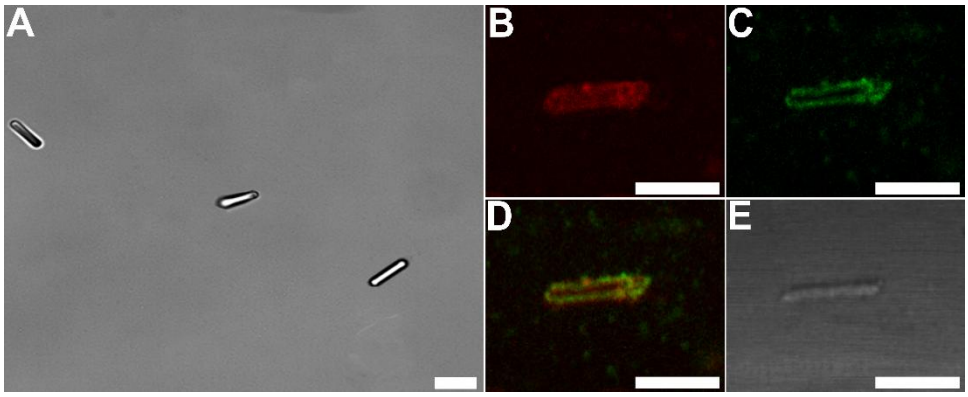

Figure 4.4. DIC and LSCM images of a 1 wt% aqueous suspension of $\mathbf{M^{O}_{60}A^{DH}_{20}}$ prepared via dialysis against DI water. (A) DIC image of unlabeled tubules. Labeled tubules for LSCM imaging were prepared in a solution of Texas Red dextran, and hydrophobic domains were labeled by incorporation of $DiOC_{18}$ probe. (B) Texas Red channel. (C) $DiOC_{18}$ channel. (D) Overlay of B and C. (E) Brightfield image. z direction slice = 0.10 μm. Scale bars = 5 μm.

Since hydrophobic $\mathbf{A^{DH}}$ has good solubility in DMSO, we expected that DMSO was able to plasticize and permeabilize the vesicle membranes at the beginning of the dialysis process.[12] In the presence of excess aqueous dialysate, DMSO should be driven out of the membranes by osmotic pressure, leading to vesicle deflation (**Figure 4.1**).[3-5] As the DMSO inside the membranes was depleted, the membranes would eventually lose permeability, resulting in stable tubules, instead of stomatocytes, but it likely relates to

packing of polypeptide segments in the membranes where $\mathbf{A^{DH}}$ segments may adopt extended conformations.[3-5,12]

Table 4.1 Dimensions of tubules for different preparations obtained using the measurement tool in ImageJ.. Each value is the average of 5 tubule measurements. Standard deviations are given in parentheses.

Tubule Dimensions	$\mathbf{M^{O}_{60}A^{DH}_{20}}$ - D-glucose	$\mathbf{M^{O}_{60}A^{DH}_{20}}$ + D-glucose	$\mathbf{M^{O}_{60}A^{DH}_{60}}$ + D-glucose
length (μm)	4.4 (0.3)	4.8 (0.9)	5.4 (1.1)
width (μm)	1.5 (0.2)	1.4 (0.2)	1.0 (0.1)

Under the conditions described above, tubule formation was only observed with the $\mathbf{M^{O}_{60}A^{DH}_{20}}$ composition, which had the smallest fraction of hydrophobic $\mathbf{A^{DH}}$ in our full series of samples.[13] Compared to compositions containing longer $\mathbf{A^{DH}}$ segments, the $\mathbf{M^{O}_{60}A^{DH}_{20}}$ sample was expected to give vesicles with the thinnest hydrophobic membranes, which should allow the fastest transport of DMSO through the membranes. Consequently, we expected that membranes containing longer $\mathbf{A^{DH}}$ segments would have slower DMSO transport under these conditions resulting in reduced vesicle deflation before loss of membrane permeability and retention of spherical shape, as we had observed.[13]

To test these hypotheses, we first attempted to enhance the deflation of $\mathbf{M^{O}_{60}A^{DH}_{20}}$ vesicles by dialysis against water containing, an osmolyte, 150 mM D-glucose. This osmolyte, which is not expected to be able to cross membranes itself, should create additional osmotic pressure during dialysis to drive water out of the vesicles (**Figure 4.5a**).[14,15] When $\mathbf{M^{O}_{60}A^{DH}_{20}}$ vesicles were prepared as above, except for the addition of 150 mM D-glucose to the dialysate, uniform tubules were consistently formed and no

spherical vesicles were observed. We also noted that $\mathbf{M^{O}_{60}A^{DH}_{20}}$ tubules formed under these conditions were found to be on average marginally longer (4.8 μm) and narrower (1.4 μm) compared to those obtained in the absence of 150 mM D-glucose (**Table 4.1**), consistent with greater vesicle deflation under increased osmotic pressure.

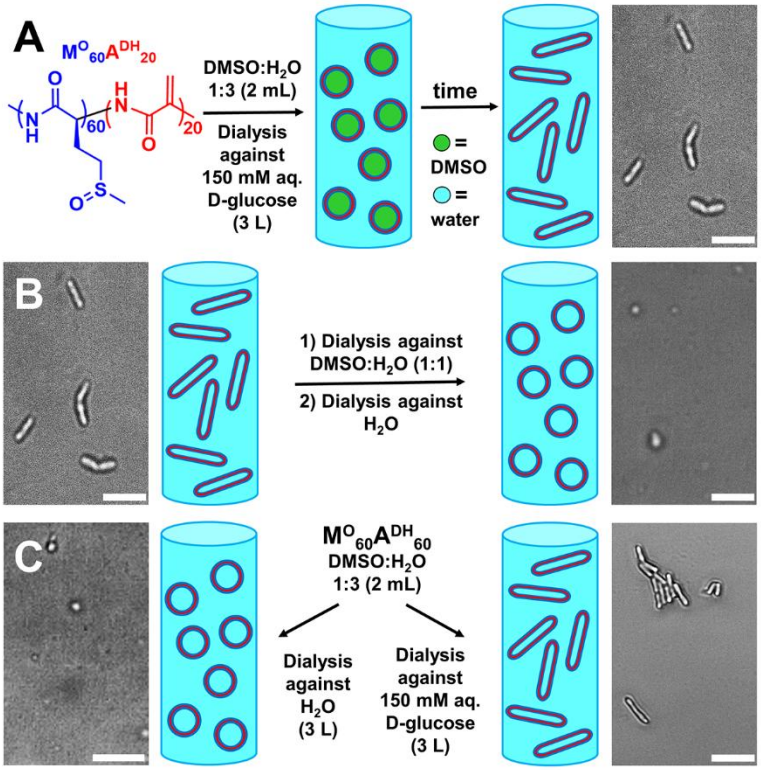

Figure 4.5: Control of $\mathbf{M^{O}_{60}A^{DH}_{y}}$ vesicle shape by variation of dialysis conditions. A) Dialysis of $\mathbf{M^{O}_{60}A^{DH}_{20}}$ against 150 mM D-glucose yields tubules. B) Dialysis of a suspension of $\mathbf{M^{O}_{60}A^{DH}_{20}}$ tubules against 1:1 DMSO:water yields spheres. C) Dialysis of $\mathbf{M^{O}_{60}A^{DH}_{60}}$ against DI water yields spherical vesicles, while dialysis of $\mathbf{M^{O}_{60}A^{DH}_{60}}$ against 150 mM D-glucose yields tubules. Samples were concentrated by mild centrifugation before imaging. Scale bars = 10 μm.

To confirm that osmotic pressure was responsible for formation of $\mathbf{M^{O}_{60}A^{DH}_{20}}$ tubules, we performed an additional study where the osmotic flow of DMSO out of vesicle membranes was reversed by addition of DMSO to the dialysate. $\mathbf{M^{O}_{60}A^{DH}_{20}}$ tubules were

prepared by dialysis against 150 mM D-glucose as described above, and then were dialyzed again against 1:1 DMSO:water, followed by dialysis against DI water. Imaging of the sample revealed that only spherical vesicles were present (**Figure 4.5b**). By introducing membrane permeability by addition of DMSO and creating osmotic pressure to drive DMSO into the tubules, the membranes were able to inflate into spheres (average diameter = *ca*. 1.9 μm), which were then quenched in the presence of excess DI water. The formation of spherical $\mathbf{M^{O}_{60}A^{DH}_{20}}$ vesicles from tubules confirmed that tubule formation is driven solely by deflation during vesicle formation and not by the specific $\mathbf{M^{O}_{60}A^{DH}_{20}}$ copolymer composition.

This result raised the possibility of whether or not other $\mathbf{M^{O}_{60}A^{DH}_{y}}$ compositions could also form tubules under appropriate conditions. To test this hypothesis, we varied the dialysis conditions for preparation of $\mathbf{M^{O}_{60}A^{DH}_{60}}$ assemblies. Consistent with prior observations, use of our default dialysis conditions described above gave only spherical vesicles (average diameter = *ca*. 0.57 μm, **Figure 4.5c**).[13] However, similar to $\mathbf{M^{O}_{60}A^{DH}_{20}}$, nanoprecipitation of $\mathbf{M^{O}_{60}A^{DH}_{60}}$ followed by dialysis against water containing 150 mM D-glucose yielded only elongated tubules that were on average marginally longer and narrower than $\mathbf{M^{O}_{60}A^{DH}_{20}}$ tubules (5.4 μm long; 1.0 μm wide) (**Figure 4.5c**, see **Table 4.1**). Although the thicker membranes of $\mathbf{M^{O}_{60}A^{DH}_{60}}$ are expected to have slower transport of DMSO and water relative to $\mathbf{M^{O}_{60}A^{DH}_{20}}$, the increased osmotic pressure due to addition of osmolyte was found to overcome this and allow vesicle deflation before loss of membrane permeability. Thus, by controlled variation of dialysis conditions, a range of $\mathbf{M^{O}_{60}A^{DH}_{y}}$ copolypeptide compositions can be assembled into either spheres or tubules, both of which are stable in aqueous media. It is worth noting that the significantly greater

size of $\mathbf{M^{O}_{60}A^{DH}_{60}}$ tubules compared to spherical vesicles suggests that vesicle fusion may occur during the formation of tubules.

4.5 Conclusions

Overall, the $\mathbf{A^{DH}}$ segments in $\mathbf{M^{O}_{60}A^{DH}_{y}}$ copolypeptides were found to form membranes capable of plasticity and selective permeability in DMSO/water mixtures, which allows predictable control of vesicle shape by variation of dialysis conditions. On the contrary, other previously reported block copolypeptide vesicles mainly utilize rigid, α-helical hydrophobic segments that restrict membrane permeability and consequently hinder the ability to change their shape.[17,18] The findings of this study expand vesicle shape transformation methods to biodegradable polypeptide vesicles, which are amenable to development for applications in therapeutic delivery. In particular, $\mathbf{M^{O}_{x}A^{DH}_{y}}$ vesicles have been previously shown to react with thiols under biologically relevant conditions, which may be useful for release of entrapped cargoes in an intracellular environment.[13]

4.5 Materials and Instrumentation

Methods and Materials were as described in Chapter 3 with the following additions.

S-(*tert*-Butyl carboxymethyl)-L-cysteine.[13] This compound was prepared according to the protocol described in Chapter 2.

S-(*tert*-Butyl carboxymethyl)-L-cysteine N-carboxyanhydride (*t*BuCM-Cys NCA).[13] This monomer was prepared according to the protocol described in Chapter 2.

General procedure for determination of M chain lengths using end-group analysis after reaction with mPEG-NCO.[12] This procedure was performed following the protocol described in Chapter 2.

Procedure for polymerization of *t*BuCM-Cys NCA via the N-terminal amine of a M^O macroinitiator to give poly(L-methionine sulfoxide)-*b*-poly(S-(*tert*-butylcarboxymethyl)-L-cysteine), $M^O_{60}C^{BCM}_{20}$.[13] This procedure was performed following the protocol described in Chapter 3

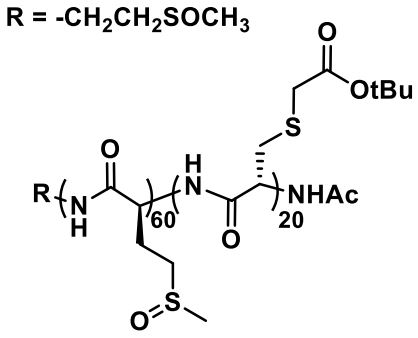

$M^O_{60}C^{BCM}_{20}$ (30 mg, 81% yield). Prepared using 25 mg of **M^O_{60}** and 20 eq of **tBuCM-Cys NCA** using the procedure provided above. ^{1}H NMR (400 MHz, d-TFA, 25 ºC): δ 4.99 (br m, 73H), δ 3.53 – 3.23 (br m, 212H), δ 2.95 (s, 150H), δ 2.59-2.44 (d, 120H), δ 1.60 (s, 151H).

Procedure for the preparation of poly(L-methionine sulfoxide)-*b*-poly(S-(carboxymethyl)-L-cysteine, Na^+ salt), $M^O_{60}C^{CM}_{20}$.[13] This procedure was performed following the protocol described in Chapter 3

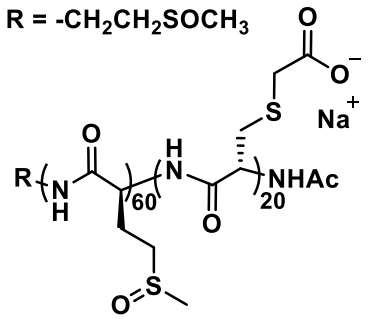

$M^{O}_{60}C^{CM}_{20}$ (20 mg, 72% yield). Prepared using the procedure provided above. ^{1}H NMR (400 MHz, D_2O, 25 ºC): δ 4.51 (br s, 20H), δ 4.41 (br s, 60H), δ 3.19 (s, 40H), δ 2.91 (br m, 160H), δ 2.63 (s, 180H), δ 2.16 (br d, 120H).

Procedure for the preparation of poly(L-methionine sulfoxide)-*b*-poly(dehydroalanine), $M^{O}_{60}A^{DH}_{20}$.[13] This procedure was performed following the protocol described in Chapter 3

R = -$CH_2CH_2SOCH_3$

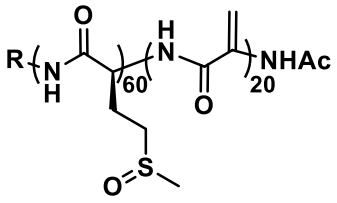

$M^{O}_{60}A^{DH}_{20}$ (12 mg, 74% yield). Prepared using the procedure provided above. ^{1}H NMR (400 MHz, d_6-DMSO, 25 ºC): δ 9.5 (br s, 20H), δ 8.32 (s, 60H), δ 5.80 (d, 40H), δ 4.33 (s, 60H), δ 2.72 (s, 120H), δ 2.51 (s, 180H), δ 2.51 (d, 12H). Since resonances for S-(carboxymethyl)-L-cysteine residues were absent in the product, the low integrations observed for alkene peaks of dehydroalanine residues were likely due to aggregation of hydrophobic **A^{DH}** segments in D_2O/DMSO.[12]

Procedure for the preparation of $M^{M}_{60}A^{DH}_{20}$ from $M^{O}_{60}A^{DH}_{20}$ for GPC analysis. This procedure was performed following the protocol described in Chapter 3.

R = -$CH_2CH_2S(CH_3)^{+}$ Cl^{-}

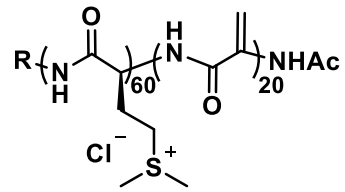

$M^{M}_{60}A^{DH}_{20}$ (10 mg, 81% yield). Prepared using the procedure provided above. ^{1}H NMR (400 MHz, D_2O, 25 ºC): δ 4.55 (s, 60H), δ 3.47 (s, 120H), δ 2.99 (s, 360H), δ 2.37 (d, 120H). Since resonances for S-(carboxymethyl)-L-cysteine residues were absent in the product, the low integrations observed for alkene peaks of dehydroalanine residues were likely due to aggregation of hydrophobic **A^{DH}** segments in D_2O/DMSO.[5]

Preparation of $M^{O}_{60}A^{DH}_{20}$ tubules via dialysis in water. 20 mg of solid **$M^{O}_{60}A^{DH}_{20}$** powder was dispersed in DMSO to give a 4 % (w/v) suspension, which was then placed in a bath sonicator for 10 minutes until the copolypeptide was evenly dispersed and no large particulates could be observed. An equal volume of DI H_2O was added dropwise, followed by vortexing the sample for 1 minute and then placing the sample in a bath sonicator for 5 minutes. Under constant vortexing, an additional equal volume of DI H_2O was slowly added to give a final sample concentration of 1% (w/v). The sample was then transferred to 2 kDa MWCO dialysis tubing and dialyzed against DI H_2O (3 L, 1,500x volume compared to initial sample volume, 24h, 4 dialyzate changes). The resulting suspension was used directly for subsequent analysis.

Preparation of $M^{O}_{60}A^{DH}_{20}$ spherical vesicles via dialysis in 1:1 DMSO:water. **$M^{O}_{60}A^{DH}_{20}$** tubules were first prepared as described above via dialysis in 150 mM glucose. The sample was then dialyzed against 1:1 v/v DMSO:water (3 L, 1,500x volume compared to sample volume, 48h) followed by DI H_2O (3 L, 1,500x volume compared to initial sample volume, 24h, 2 dialyzate changes). The resulting suspension was used directly for subsequent analysis.

Preparation of $M^{O}_{60}A^{DH}_{20}$ tubules via dialysis in 150 mM glucose. $M^{O}_{60}A^{DH}_{20}$ tubules were prepared as described above via dialysis in water with the following changes. The sample was dialyzed against 150 mM glucose (3L, 1,500x volume compared to initial sample volume, 48h, 4 dialyzate changes). The resulting suspension was used directly for subsequent analysis.

Preparation of $M^{O}_{60}A^{DH}_{60}$ tubules via dialysis in 150 mM glucose. $M^{O}_{60}A^{DH}_{60}$ tubules were prepared the same as $M^{O}_{60}A^{DH}_{20}$ vesicles via dialysis in water with the following changes. The sample was dialyzed against 150 mM glucose (3 L, 1,500x volume compared to initial sample volume, 48h, 4 dialyzate changes). The resulting suspension was used directly for subsequent analysis.

Encapsulation of Texas Red dextran within $M^{O}_{60}A^{DH}_{20}$ assemblies in water.[2] A 1% (w/v) suspension of $M^{O}_{60}A^{DH}_{20}$ tubules was prepared as described above via dialysis against water except that a solution of Texas Red labeled dextran in DI H_2O (Molecular Probes, MW = 3000, 0.125 mg/mL) was used for both dilution steps in place of pure DI H_2O. After dialysis of the tubule suspension against DI H_2O using 2 kDa MWCO dialysis tubing to remove DMSO, the suspensions were transferred to larger pore size 15 kDa MWCO dialysis tubing and dialyzed against DI H_2O for 18 hours in order to remove all non-encapsulated Texas Red dextran. The resulting suspension was used directly for subsequent analysis.

Preparation of $DiOC_{18}$ labeled tubules for laser scanning confocal microscopy (LSCM). A suspension of $M^{O}_{60}A^{DH}_{20}$ tubules loaded with Texas Red dextran (1 mL) was mixed with a solution of hydrophobic $DiOC_{18}$ fluorescent probe (Molecular Probes, 30 µL

of a 1 mg/mL solution in DMSO). The suspension was allowed to stand for 3 h to allow vesicles to absorb the probe and was then transferred to 15 kDa dialysis tubing and dialyzed against DI H_2O (2 dialysate changes, 24 h). The dialyzed suspension was used for subsequent LSCM images.

Differential Interference Contrast (DIC) microscopy. This procedure was performed following the protocol described in Chapter 3

Laser scanning confocal microscopy (LSCM). This procedure was performed following the protocol described in Chapter 3

4.6 Spectral Data

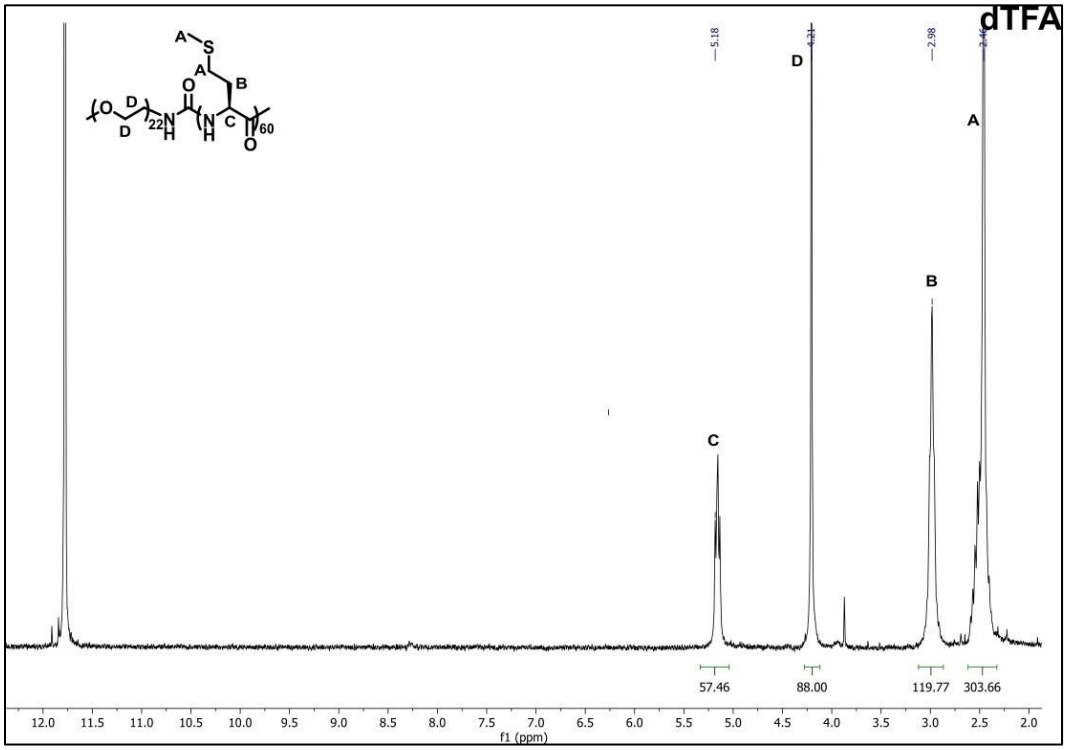

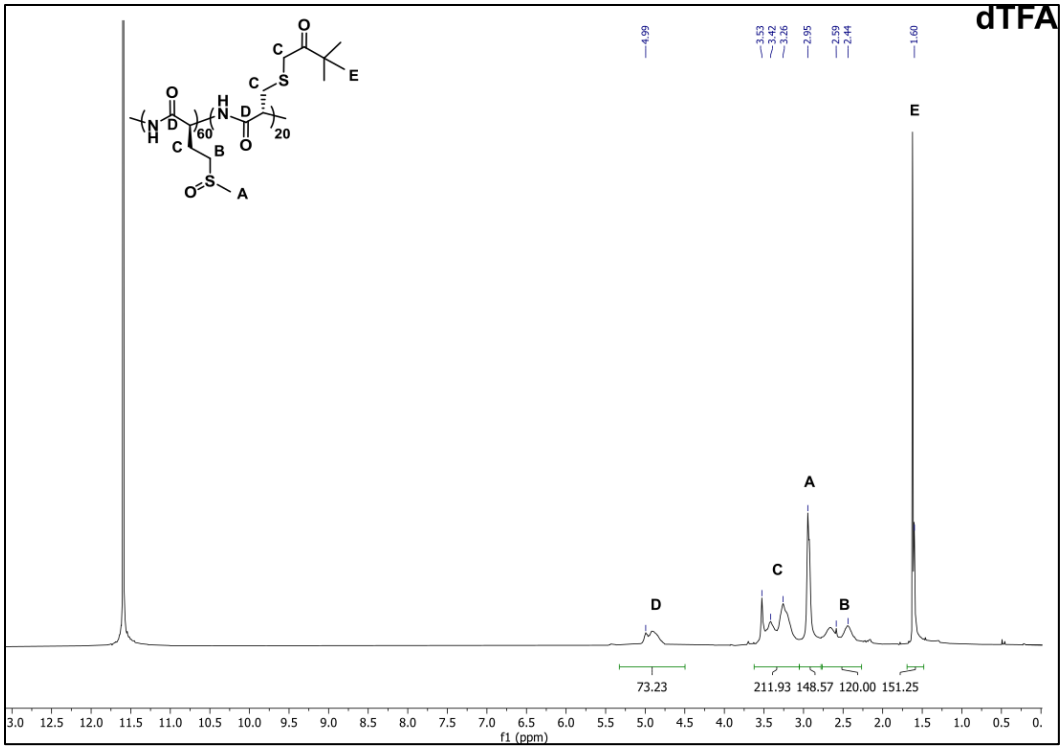
dTFA
4.99
3.53
3.42
3.26
2.95
2.59
2.44
1.60
E
A
C
D
B
73.23
211.93 148.57 120.00 151.25
f1 (ppm)

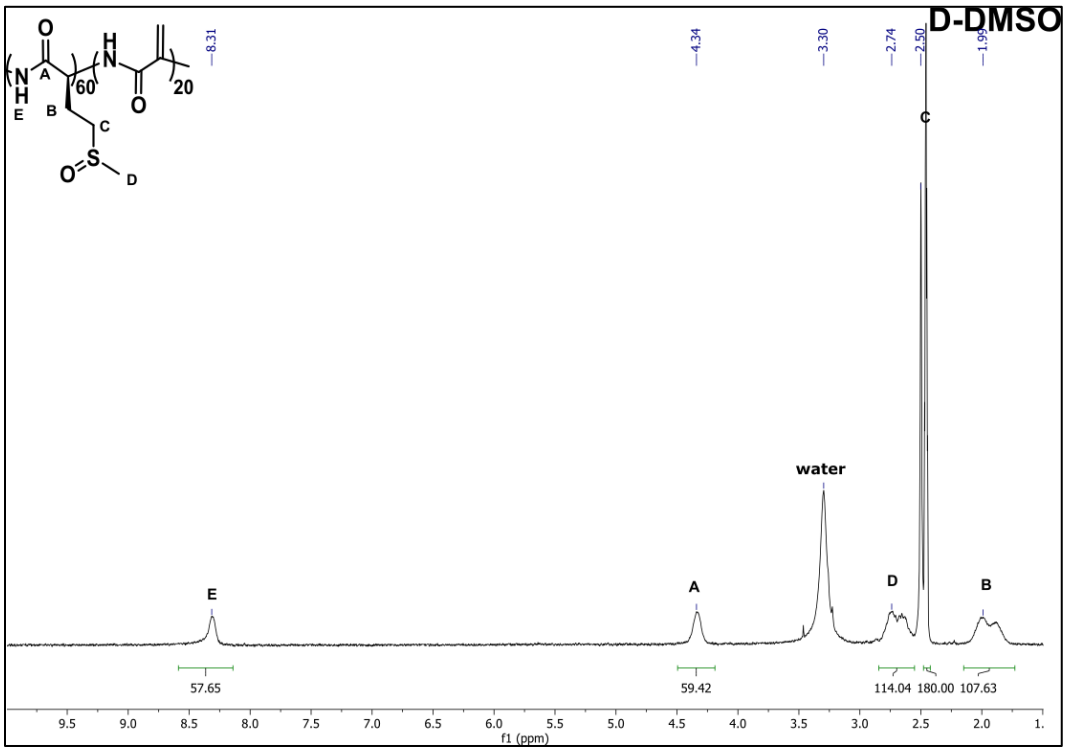
D-DMSO
8.31
4.34
3.30
2.74
2.50
1.99
C
water
E
A
D
B
57.65
59.42
114.04 180.00 107.63
f1 (ppm)

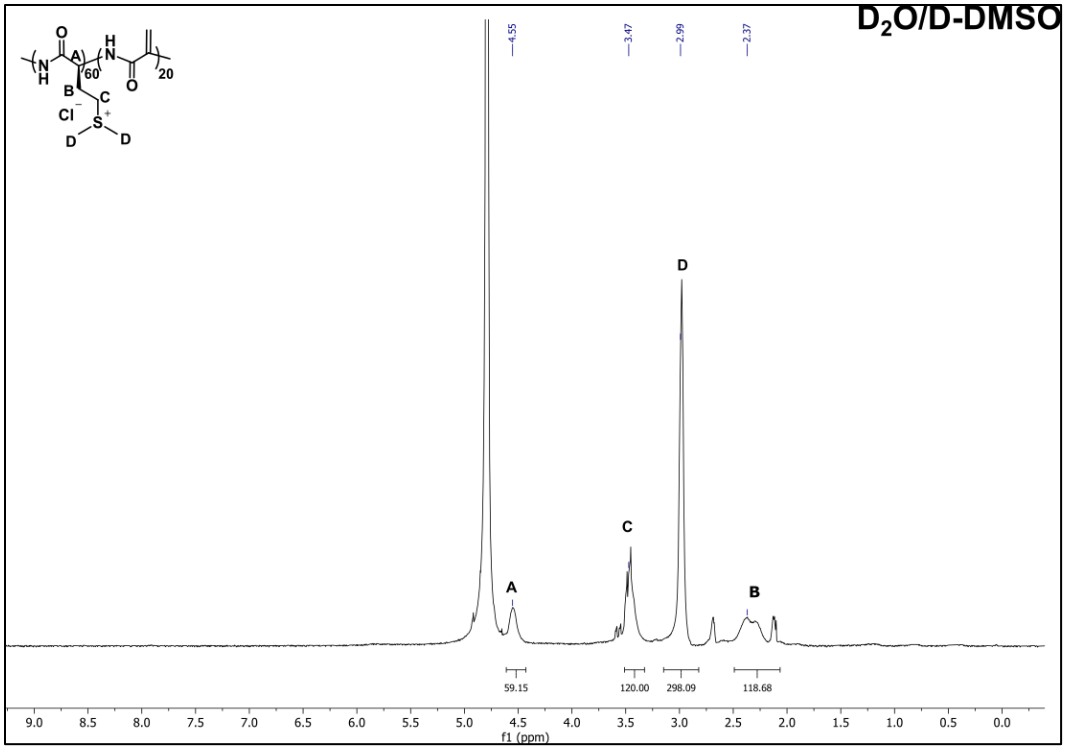

4.7 References

1) Seifert, U. Morphology and dynamics of vesicles. *Curr. Opin. Colloid Interface Sci.* **1996**, *1*, 350-357.

2) Svetina, S.; Žekš, B. Shape behavior of lipid vesicles as the basis of some cellular processes. *Anat. Rec.* **2002**, *268*, 215-225.

3) Wong, C. K.; Stenzel, M. H.; Thordarson, P. Non-spherical polymersomes: formation and characterization. *Chem. Soc. Rev.* **2019**, *48*, 4019-4035.

4) Zhang, X.; van Hest, J. C. M.; Men, Y. Review of shape transformation pathways of polymersomes: Implications for nanomotor, biomedicine, and artificial cell mimics. *ACS Appl. Nano Mater.* **2024**, *7*, 14865-14888.

5) Li, W.; Zhang, S.; Sun, M.; Kleuskens, S.; Wilson, D. A. Shape transformation of polymer vesicles. *Acc. Mater. Res.* **2024**, *5*, 453-466.

6) Geng, Y.; Dalhaimer, P.; Cai, S.; Tsai, R.; Tewari, M.; Minko, T.; Discher, D. E. Shape effects of filaments versus spherical particles in flow and drug delivery. *Nat. Nanotechnol.* **2007**, *2*, 249−255.

7) Wauters, A. C.; Scheerstra, J. F.; Vermeijlen, I. G.; Hammink, R.; Schluck, M.; Woythe, L.; Wu, H.; Albertazzi, L.; Figdor, C. G.; Tel, J.; Abdelmohsen, L. K. E. A.; van Hest, J. C. M. Artificial antigen-presenting cell topology dictates T cell activation. *ACS Nano* **2022**, *16*, 15072−15085.

8) Shao, J.; Cao, S.; Che, H.; De Martino, M. T.; Wu, H.; Abdelmohsen, L. K. E. A.; Van Hest, J. C. M. Twin-engine janus supramolecular nanomotors with counterbalanced motion. *J. Am. Chem. Soc.* **2022**, *144*, 11246−11252.

9) Rodriguez, A. R.; Kramer, J. R.; Deming, T. J. Enzyme-triggered cargo release from methionine sulfoxide containing copolypeptide vesicles. *Biomacromolecules* **2013**, *14*, 3610-3614.

10) Wollenberg, A. L.; O'Shea, T. M.; Kim, J. H.; Czechanski, A.; Reinholdt, L. G.; Sofroniew, M. V.; Deming, T. J. Injectable polypeptide hydrogels via methionine modification for neural stem cell delivery. *Biomaterials* **2018**, *178*, 527-545.

11) O'Shea, T. M.; Wollenberg, A. L.; Kim, J. H.; Ao, Y.; Deming, T. J.; Sofroniew, M. V. Foreign body responses in central nervous system mimic natural wound responses and alter biomaterial functions. *Nat. Commun.* **2020**, *11*, 6203.

12) Benavides, I.; Raftery, E. D.; Bell, A. G.; Evans, D.; Scott, W. A.; Houk, K. N.; Deming, T. J. Poly(dehydroalanine): synthesis, properties and functional diversification of a fluorescent polypeptide. *J. Amer. Chem. Soc.* **2022**, *144*, 4214-4223.

13) Morrison, C. A.; Chan, E. P.; Deming, T. J. Triggered inversion of dual responsive diblock copolypeptide vesicles. *J. Amer. Chem. Soc.* **2025**, *147*, 7617-7623.

14) Discher, B. M.; Won, Y.-Y.; Ege, D. S.; Lee, J. C.-M.; Bates, F. S.; Discher, D. E.; Hammer, D. A. Polymersomes: tough vesicles made from diblock copolymers. *Science* **1999**, *284*, 1143–1146.

15) Abdelmohsen, L. K. E. A.; Williams, D. S.; Pille, J.; Ozel, S. G.; Rikken, R. S. M.; Wilson, D. A.; Van Hest, J. C. M. Formation of well-defined, functional nanotubes via osmotically induced shape transformation of biodegradable polymersomes. *J. Am. Chem. Soc.* **2016**, *138*, 9353−9356.

16) Deming, T. J. Sulfur switches for responsive peptide materials. *Acc. Chem. Res*. **2024**, *57*, 661-669.

17) Bellomo, E.; Wyrsta, M. D.; Pakstis, L.; Pochan, D. J.; Deming, T. J. Stimuli responsive polypeptide vesicles via conformation specific assembly. *Nat. Mater.* **2004**, *3*, 244-248.

18) Holowka, E. P.; Pochan, D. J.; Deming, T. J. Charged polypeptide vesicles with controllable diameter. *J. Am. Chem. Soc.* **2005**, *127*, 12423 - 12428.

Chapter 5: Facile Preparation of Mucin Mimetic Glycosylated Poly(*rac*-cysteines) from Poly(dehydroalanine)

5.1 Abstract

Mucins have a diverse impact in maintaining health and in the progression of diseases. Currently, mucin and mucin mimetic therapeutics and their applications are limited by the synthetic challenges in replicating the structures and sugar presentation found in native mucins, and by their degradation via endogenous proteases. In this study, we report the synthesis of racemic mucin analogues bearing native glycans via the functionalization of poly(dehydroalanine) with un-protected thiol modified monosaccharides. Functionalization of poly(dehydroalanine) resulted in the formation of glycosylated poly(*rac*-cysteine)s containing mucin mimetic structures due to correct sugar attachment, high efficiency conjugation and long chain lengths (i.e. > 100 residues). Although these polypeptides utilize *S*-linked glycosylation and have a racemic backbone, they maintain many of the properties found in optically pure, synthetic *O*-glycosylated polypeptides. Here, we describe a facile method for the straightforward synthesis of *S*-linked, racemic glycopolypeptides for development of synthetic mucin mimetics.

5.2 Introduction

There is a need for reproducible preparation of sufficient quantities of mucin mimetics for use in diagnostics, therapeutics and other biomedical applications. Mucins are heavily glycosylated proteins that are a major component in the formation of mucus. Mucins have become increasingly recognized for their applications in drug delivery, anticancer vaccines, as hydrogels that mimic mucus, in biosensor development for cancer diagnoses, and as natural lubricants.[1–6] Glycosylated residues in mucins or mucin mimetic polypeptides typically contain only *O*-glycosylated L-serine or L-threonine amino

acids.[7–10] These *O*-linked glycosylated residues replicate the natural occurring glycosylation patterns found in glycoproteins and mucins, but there has also been recent interest in the use of *S*-glycosylation as well as D-amino acids in mucin mimetics.[10,11] These changes in glycosidic linkage and amino acid chirality have meaningful impacts on the synthetic mucins. Substitution of *O*-glycosylation with *S*-glycosylation helps prevent enzymatic deglycosylation, and racemic or D-amino acid polypeptides resist enzymatic degradation from endogenous proteases and have low immunogenicity due to their non-native chirality.[10,12,13,14,15] Furthermore, mucin mimetics containing *S*-glycosylation and/or D-amino acids have been shown to possess binding affinity similar to that of native mucins with the added benefit of enhanced lifetime in biological fluids.[10,12,16,17]

A formidable obstacle in the fabrication of mucin mimetics has been replication of the structure found in native mucins.[9] For example, many synthetic mucin mimetics have a nondegradable polymer backbone, while native mucins have a degradable polypeptide backbone.[1,9,18] However, there has been much recent progress in the synthesis of mucin mimetics using glycosylated polypeptides with native *O*-Ser and *O*-Thr, as well as non-native *S*-Cys linkages.[7,10] These glycosylated polypeptides have been found to possess extended chain conformations that can mimic natural mucins and maintain good affinity to biological targets.[7] Their degradability in the presence of endogenous enzymes can also be altered by the use of *S*-glycosylation and/or D-amino acids.[10] The Deming and Kramer laboratories have previously reported the synthesis of serine, threonine, and cysteine based glycopolypeptides through the polymerization of glycosylated N-carboxyanhydrides (NCAs).[7–10] However, this method involves tedious multistep syntheses of glycosylated amino acid precursors, and challenging purification of

glycosylated NCA monomers.[7–10] Incorporation of large or complex saccharides in these NCAs can further result in costly and time consuming steps that require a high level of synthetic expertise.[1,9] Without proper purification, impurities in the NCAs can limit the maximum polypeptide molecular weight that can be obtained.[19] Furthermore, due to the extensive synthesis and purification steps, most of these polypeptides have been limited to those containing mono or disaccharides and their overall low yields can limit large-scale production.[1,7,9] Once prepared and well purified, glycosylated NCAs have been shown to polymerize well, but the resulting polypeptides still must be deprotected.[1,9] It is also inherently challenging to control the sequential distribution of different residues in statistical copolymers containing glycosylated residues due steric crowding of the protected saccharides or unequal comonomer reactivities, leading to blocky or tapered sequences.[9,10,20]

Post-polymerization modification (PPM) offers an alternative route for preparation of glycopolypeptides via conjugation of saccharides to reactive precursor polypeptides (**Scheme 5.1**). This strategy generally requires fewer steps, easier purification, and allows more facile preparation of high molecular weight polymers. Previously, glycopeptides have been prepared via PPM by reaction with unmodified saccharides as well as saccharides modified to contain reactive functional groups such as azides, alkynes, thiols, epoxides, alkyl halides or isothiocyanates.[9,21–24] PPM methods also offer the advantage of creating statistical copolymers by the addition of more than one reactive species to the polymer.[25,26] However, inefficient sugar conjugation due to steric crowding on the polypeptide backbone or low solubility of the precursor polymer can prevent PPM

methods from achieving complete glycosylation, leading to the need for high efficiency conjugation reactions.[9]

Here, we describe a new approach for preparation of mucin mimetics via PPM. We have found that non-protected thiosugars can be directly conjugated to readily prepared poly(dehydroalanine), $\mathbf{A^{DH}}$, precursors in aqueous media to give fully glycosylated polypeptides. The sugars are connected through mucin mimetic, stable *S*-Cys linkages. This approach to mucin mimetic polypeptides offers potential advantages for more efficient and larger scale preparation of mucin mimetic polymers.

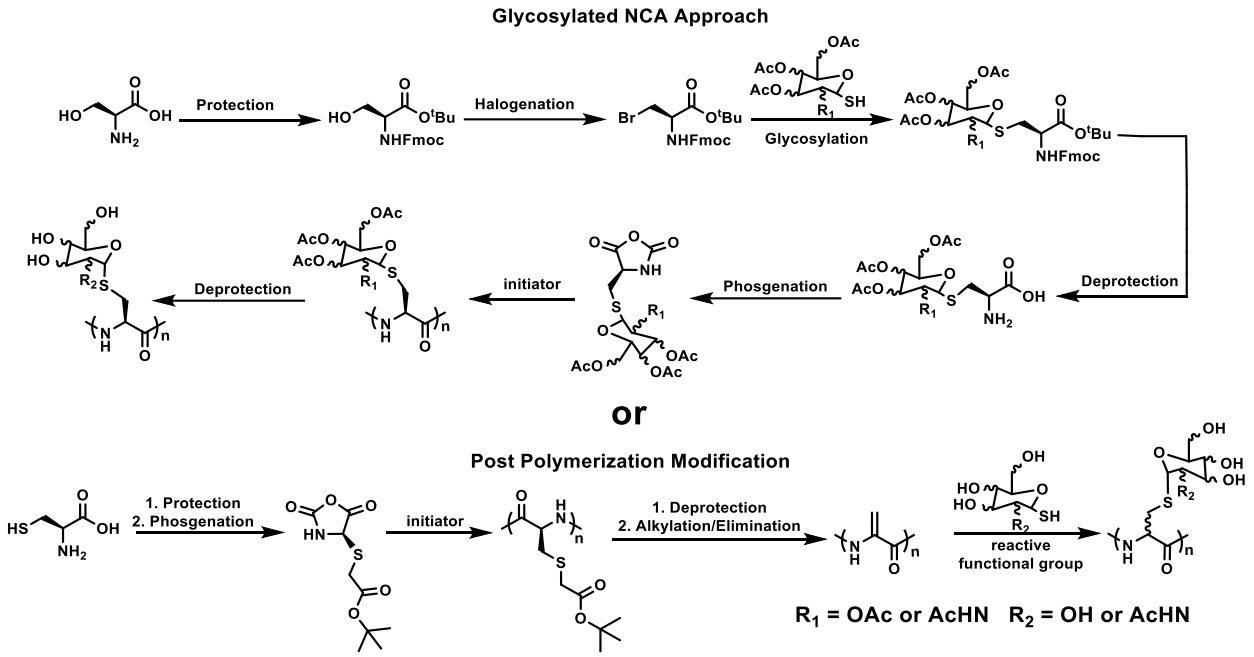

Scheme 5.1 Comparison of glycosylated NCA approach (adapted from Kohout et al., 2023) and post polymerization modification of $\mathbf{A^{DH}}$ to produce *S*-glycosylated polypeptides.[10]

$\mathbf{A^{DH}}$ is a readily prepared polypeptide that contains reactive electrophilic sidechains.[27] $\mathbf{A^{DH}}$ is synthesized in 3 steps in high yield (polymerization, deprotection,

and alkylation; overall yield: 82%) from S-(*tert*-butyl-carboxymethyl)-L-cysteine N-carboxyanhydride (tBuCM-Cys NCA) monomer, which itself is readily prepared and purified (**Scheme 5.2**).[27] Living polymerization of the tBuCM-Cys NCA allows for control of $\mathbf{A^{DH}}$ chain length (20 to >180 residues) as well as its incorporation into statistical and block copolymers.[27,28] Relevant to this study, we previously reported the reaction of the block copolymer poly(L-glutamate Na^+ salt)$_{88}$-*block*-poly(dehydroalanine)$_{85}$, ($\mathbf{E_{88}A^{DH}_{85}}$) with β-D-glucopyranoside sodium salt (βGlcSH) where >99% of dehydroalanine residues were glycosylated and the product was obtained in 95% isolated yield.[27]

Although the addition of βGlcSH to $\mathbf{A^{DH}}$ residues likely resulted in racemic glucosylated cysteine residues in the chains, recent studies have shown that incorporation of glycosylated D-amino acids into mucin mimetics doesn't necessarily reduce their affinity for biological targets.[10,12,15–17,27,29] Further, the incorporation of D-residues can provide enhanced stability against enzymatic degradation, which may be valuable for certain applications.[10,15–17] Here, we report the first synthesis of high molecular weight mucin mimetic polypeptides derived from $\mathbf{A^{DH}}$.

5.3 Results and Discussion

As a proof of concept that $\mathbf{A^{DH}}$ can be a useful precursor for the synthesis of mucin mimetic polypeptides, we sought to prepare fully glycosylated polypeptides with degrees of polymerization (DP) > 100.[7,10] We prepared the precursor poly(S-(*tert*-butylcarboxymethyl)-L-cysteine)$_{150}$ ($\mathbf{C^{BCM}_{150}}$) and converted this to $\mathbf{A^{DH}_{150}}$ using established methods (**Table 5.1**), and then sought to separately glycosylate $\mathbf{A^{DH}_{150}}$ with βGlcSH and 2-acetamido-2-deoxy-1-thio-α-D-galactopyranose (αGalNAcSH) as model

saccharides (**Scheme 5.2**). βGlcSH was chosen since it's readily available, and αGalNAcSH was chosen due to its ubiquitous presence as the glycan attached to the protein backbone in native mucins.[30] Using previously optimized methods, the sugars were reacted with $\mathbf{A^{DH}_{150}}$ (5 eq sugar per $\mathbf{A^{DH}}$ residue) in aqueous DMSO (**Scheme 5.2**), and the products, poly(S-(β-D-glucopyranosyl)-*rac*-cysteine)$_{150}$, **βGlc-*rac*-C$_{150}$**, and poly(S-(2-acetamido-2-deoxy-1-thio-α-D-galactopyranosyl)-*rac*-cysteine)$_{150}$, **αGalNAc-*rac*-C$_{150}$**, were isolated by dialysis and lyophilization (**Table 5.2**).[27,29]

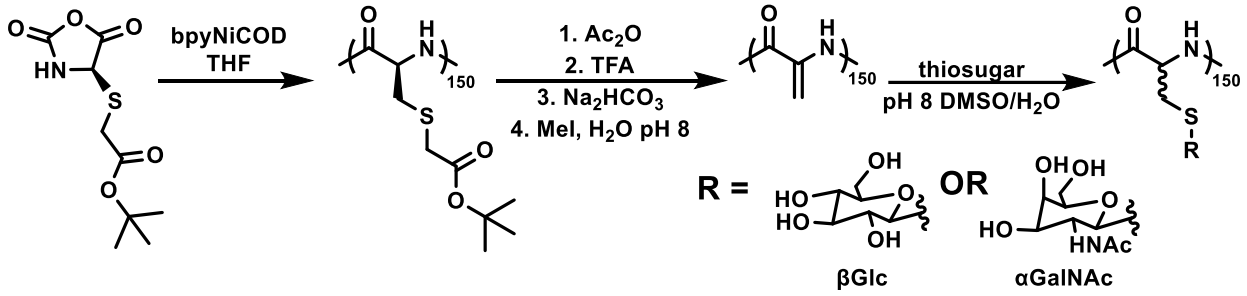

Scheme 5.2. Synthesis of **βGlc-*rac*-C$_{150}$** and **αGalNAc-*rac*-C$_{150}$** via post polymerization modification of $\mathbf{A^{DH}_{150}}$ with βGlcSH and αGalNAcSH.

Both **βGlc-*rac*-C$_{150}$** and **αGalNAc-*rac*-C$_{150}$** were to found to be >99% glycosylated by ^{1}H NMR, similar to other functional polypeptides prepared by reaction of $\mathbf{A^{DH}}$ with thiols.[27,29] From prior studies, we know that neither conversion of $\mathbf{C^{BCM}}$ to $\mathbf{A^{DH}}$ nor the subsequent modification of $\mathbf{A^{DH}}$ with thiols results in chain cleavage.[27,29] Hence the functionalized glycopolypeptides were expected to possess the same degree of polymerization and dispersity as the $\mathbf{C^{BCM}_{150}}$ precursor (**Figure 5.1**).

Table 5.1. Characterization data for $\mathbf{C^{BCM}_{150}}$. *a* = Yield of isolated, purified polypeptide. *b* = DP (number average degree of polymerization) and M_n (number average molar mass, g/mol) determined from end group analysis using ^{1}H NMR. *c* = M_n, M_w (weight average molar mass, g/mol) and $Đ$ (dispersity = M_w/M_n) of $\mathbf{C^{BCM}_{150}}$ were determined by GPC relative to polyethylene glycol (PEG) standards in hexafluoroisopropanol (HFIP) containing 0.5 wt% potassium trifluoroacetate salts (KTFA).

Sample	Yield (%)[a]	DP[b]	M_n[b] (NMR)	M_n[c]	M_w[c]	$Đ$[c]
$\mathbf{C^{BCM}_{150}}$	89	151	32,700	9,320	12,970	1.39

Table 5.2. *a* = Overall yields of isolated, purified polypeptides from reaction of different thiols (5 eq per dehydroalanine residue) with $\mathbf{A^{DH}_{150}}$. *b* = M_n (g/mol) calculated using DP determined for $\mathbf{C^{BCM}}$ precursor by end-group analysis. For all samples, the degree of polypeptide functionalization was found to be >99% by ^{1}H NMR.

Polypeptide	Thiol	Yield (%)[a]	M_n[b]
βGlc-*rac*-C$_{150}$	βGlcSH	62	29,400
αGalNAc-*rac*-C$_{150}$	αGalNAcSH	67	35,580
***rac*-C$^{HE}_{150}$**	$HOCH_2CH_2SH$	99	22,350

The extended conformation of mucins, often described as being similar to a poly(L-proline) II (PPII) helix, is thought to be important for their physical properties and biological activity.[7,8,10,11] The formation of an extended chain conformation is hypothesized to be due to steric interactions between the sugars since they are close to the polypeptide backbone, as well as potentially due to H-bonding interactions between the GalNAc amides and the polypeptide backbone. [7,8,10,11]

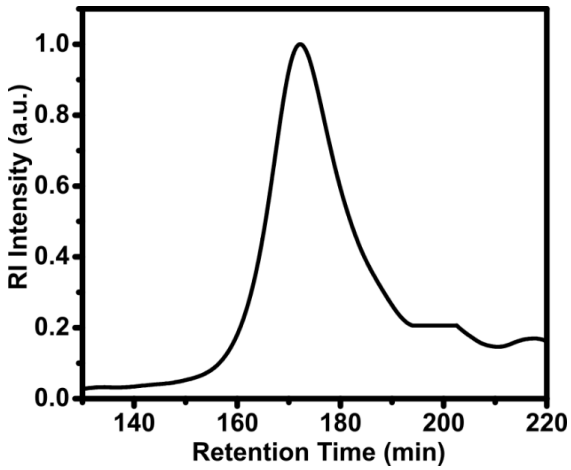

Figure 5.1. GPC chromatogram of polypeptide precursor $\mathbf{C^{BCM}_{150}}$. Sample was dissolved at 15 mg/mL in HFIP for analysis.

It has been shown that the optically pure mucin mimetic poly(O-(2-acetamido-2-deoxy-1-thio-α-D-galactopyranosyl)-L-serine)$_{300}$ **(αGalNAcSer$_{300}$)**, prepared from a glycosylated NCA precursor, adopts an extended PPII conformation.[7] This finding was supported by physical characterization of **αGalNAcSer$_{300}$** using Fourier transform infrared spectroscopy (FTIR), circular dichroism (CD) spectroscopy, and atomic force microscopy (AFM).[7,10] Here, we used these same methods in order to see if **βGlc-*rac*-C$_{150}$** and **αGalNAc-*rac*-C$_{150}$** prepared using our methodology possess similar extended conformations. Although the polypeptide backbone in our samples likely contains both D- and L- residues, we wanted to determine if steric interactions between sugars might be sufficient to drive the chains into extended conformations.

We initially evaluated our samples using FTIR (**Figure 5.2**) to evaluate their conformations. While most poly(S-alkyl-L-cysteines) or other thioether containing racemic polymers, such as poly(*rac*-allylglycine), typically form insoluble β-sheet structures, our **βGlc-*rac*-C$_{150}$** and **αGalNAc-*rac*-C$_{150}$** polypeptides were water soluble, similar to other

poly(S-alkyl-*rac*-cys) polymers derived from $\mathbf{A^{DH}}$.[31] However, **βGlc-*rac*-C$_{150}$** and **αGalNAc-*rac*-C$_{150}$** were found to have amide II bands that border on the range typically observed for β-sheet conformations.[27,31] Amide II bands in a similar range (1536 cm^{-1}) were also observed for samples of poly(S-(2-acetamido-2-deoxy-1-thio-α-D-galactopyranosyl)-L-cysteine) reported earlier, which were described as possessing "soluble β-sheets".[10] Hence, from solid-state FTIR analysis, **βGlc-*rac*-C$_{150}$** and **αGalNAc-*rac*-C$_{150}$** appear to possess similar conformations to a previously reported optically pure analog.

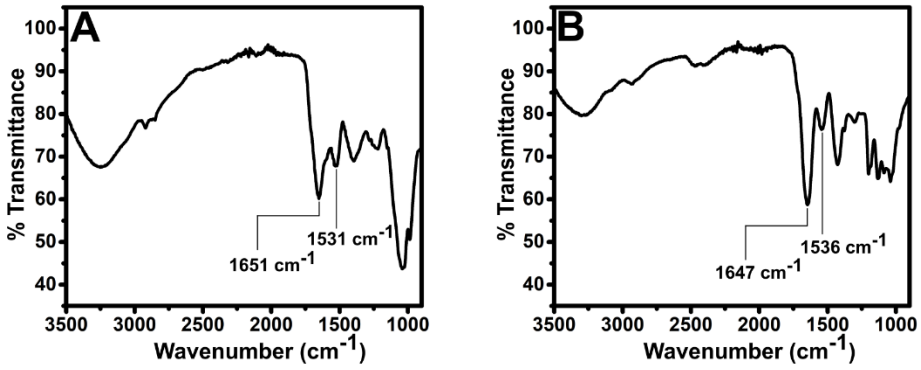

Figure 5.2. Solid state FTIR of A) **βGlc-*rac*-C$_{150}$** and B) **αGalNAc-*rac*-C$_{150}$**.

Next, we used circular dichroism spectroscopy to further explore the conformation of our samples. Due to the racemic polypeptide backbones, we had low expectations of detecting any form of secondary structure.[27] Our previously reported, non-glycosylated poly(S-alkyl-*rac*-cys) samples lacked any CD signal even when conjugated with thiols containing optically active groups.[27,29] Here, we observed CD spectra that differed from our previous poly(S-alkyl-*rac*-cys) polypeptides for both samples in DI H_2O at pH 7 and concentrations of 0.1 mg/mL at 25 °C (**Figure 5.2**).[7,8,10,11,25] The spectra of both samples differed greatly from the CD spectra observed for α-helical or β-sheet

conformations.[7,8,10,11,25] The spectra of **βGlc-*rac*-C$_{150}$** and **αGalNAc-*rac*-C$_{150}$** were similar to the CD spectrum of previously reported poly(S-(2-acetamido-2-deoxy-1-thio-α-D-galactopyranosyl)-L-cysteine).[7,8,10,11,25] In this sample, the CD spectrum is dominated by a large positive band at *ca*. 190 nm, and lacks the small positive band at *ca*. 219 nm that has been correlated in glycosylated poly(serine)s with the adoption of a polyproline II conformation.[7,10,32] From these data, it appears that **βGlc-*rac*-C$_{150}$** and **αGalNAc-*rac*-C$_{150}$** possess conformations that are similar to optically pure poly(S-(2-acetamido-2-deoxy-1-thio-α-D-galactopyranosyl)-L-cysteine).

As a control, we also performed CD spectroscopy on poly(S-(2-hydroxyethyl)-*rac*-cysteine)$_{150}$ (***rac*-C$^{HE}_{150}$**), which is not expected to adopt an extended chain conformation. As opposed to **βGlc-*rac*-C$_{150}$** and **αGalNAc-*rac*-C$_{150}$,** the CD spectrum of the ***rac*-C$^{HE}_{150}$** control gave only a flat, featureless spectrum consistent with a conformationally disordered, racemic polypeptide (**Figure 5.3**). The large positive bands present in the CD spectra for **βGlc-*rac*-C$_{150}$** and **αGalNAc-*rac*-C$_{150}$** appear to indicate some form of ordered conformation. We next acquired CD spectra of βGlcSH, αGalNAcSH, and GalNAcOH to determine if the bands seen in CD of the polymers are just due to signal from sugar molecules. βGlcSH and αGalNAcSH gave no CD signals, while GalNAcOH showed a positive band below 205 nm similar to our samples (**Figure 5.4**). The intensity differences between the monosaccharides, **βGlc-*rac*-C$_{150}$,** and **αGalNAc-*rac*-C$_{150}$** may be due to the asymmetric additions of sugars across **A$^{DH}_{150}$** or the chiral orientation of the sugars along the polypeptide backbone causing the formation of ordered, extended conformations.[7,8,10]

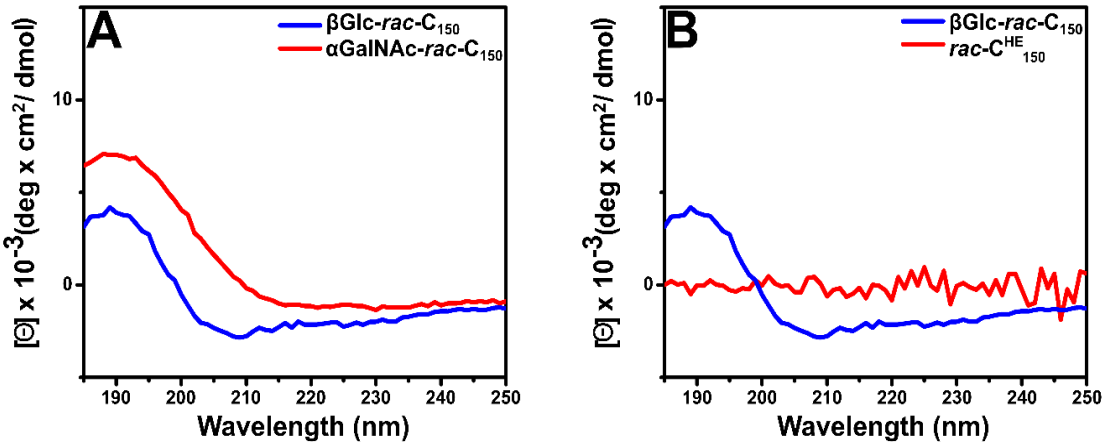

Figure 5.3: Overlay CD spectra of (A) **βGlc-*rac*-C$_{150}$** and **αGalNAc-*rac*-C$_{150}$** and (B) **βGlc-*rac*-C$_{150}$** and ***rac*-C$^{HE}_{150}$** obtained in DI H_2O at pH 7 and concentrations of 0.1 mg/mL at 25 °C.

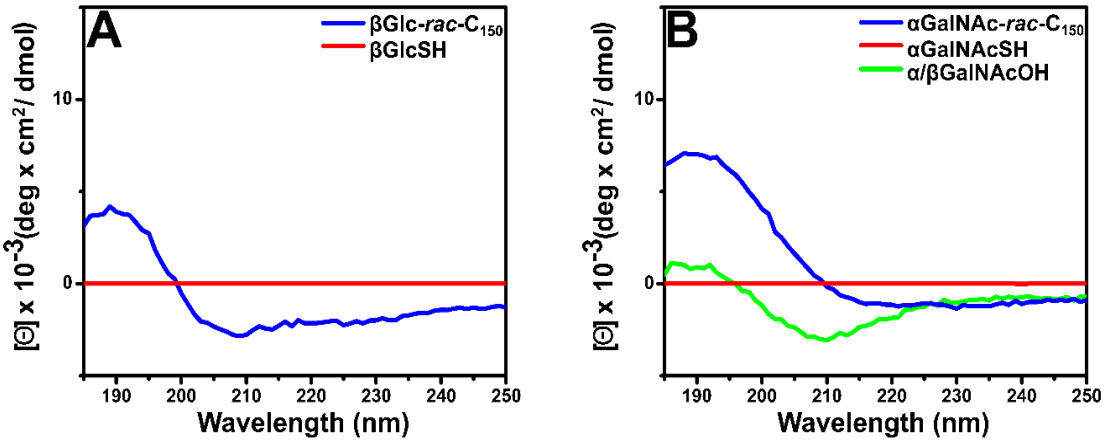

Figure 5.4. Overlay CD spectra of (A) **βGlc-*rac*-C$_{150}$** and βGlcSH and (B) **αGalNAc-*rac*-C$_{150}$,** αGalNAcSH and GalNAcOH obtained in DI H_2O at pH 7 and concentrations of 0.1 mg/mL at 25 °C.

To confirm if the CD spectra of our glycopolypeptides indicate some form of extended conformations in these samples, we examined individual chains of **βGlc-*rac*-C$_{150}$** using atomic force microscopy (AFM).[7] We performed AFM imaging similarly to a previously described protocol for imaging single glycopolypeptide chains.[7] We deposited

a 10 nM concentration solution of **βGlc-*rac*-C$_{150}$** onto freshly cleaved mica, blotted off excess solution, dried the sample, and imaged under air.[7] **βGlc-*rac*-C$_{150}$** was found to possess an extended rod-like chain conformation similar to those seen in optically pure glycopolypeptides and mucins extracted from natural sources (**Figure 5.5**).[7,33] Following the same preparation protocol, we collected AFM images of non-ionic ***rac*-C$^{HE}_{150}$** as a control, which was found to deposit as coil-like blobs. Based on these observations, the steric interactions imposed by adjacent saccharides at every residue in the polypeptide backbone appear to direct the polypeptide into adopting an extended rod-like conformation.[7]

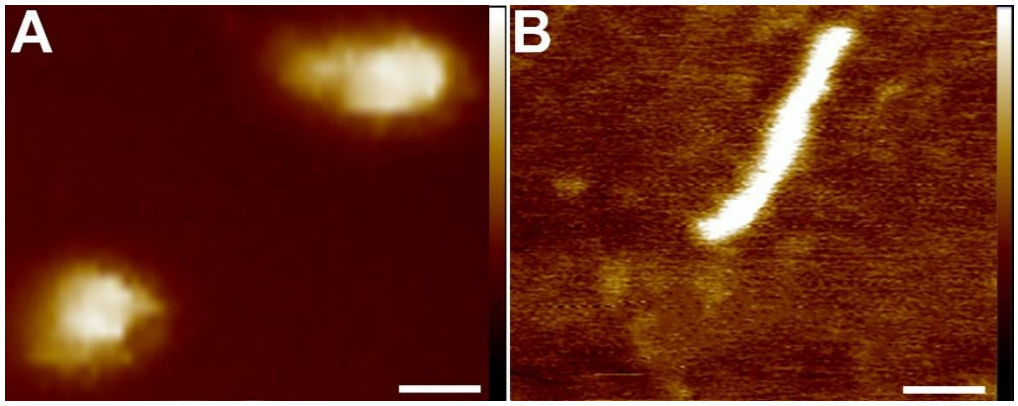

Figure 5.5: AFM images of A) ***rac*-C$^{HE}_{150}$** and B) **βGlc-*rac*-C$_{150}$**. Scale bars = 25 nm. Height bars: 0 to 41 nm for ***rac*-C$^{HE}_{150}$**, 0 to 1.6 nm for **βGlc-*rac*-C$_{150}$**. Dimensions of **βGlc-*rac*-C$_{150}$**: height = ~1.5 nm, width = ~8 nm, and length = ~70 nm.

5.4 Conclusions

A new method for synthesis of *S*-glycosylated poly(*rac*-cysteine) polypeptides has been described. The water soluble samples **βGlc-*rac*-C$_{150}$** and **αGalNAc-*rac*-C$_{150}$** were found to possess structural and conformation properties similar to other previously described optically pure mucin mimetic polypeptides.[7,10,34] Other thiosugars are

commercially available or have been prepared, and may be amenable for preparation of a variety of *S*-glycosylated poly(*rac*-cysteine) polypeptides using our methodology.[35,36] The formation of both D- and L- residues in this methodology may provide resistance to enzymatic degradation that is potentially useful for biomedical applications.[10,12,16,17] The combination of the straightforward post polymerization modification and high yields of saccharide conjugation makes this methodology attractive for preparation of glycoprotein mimics.

5.5 Materials and Instrumentation

Methods and Materials were as described in Chapter 2 with the following additions: 1-thio-β-D-glucopyranoside sodium salt (βGlcSH, Combi-Blocks) was used as received. poly(S-(*tert*-butylcarboxymethyl)-L-cysteine)$_{150}$, $\mathbf{C^{BCM}_{150}}$, poly(S-carboxymethyl-L-cysteine)$_{150}$, sodium salt, $\mathbf{C^{CM}_{150}}$, and poly(dehydroalanine), $\mathbf{A^{DH}_{150}}$, were all prepared according to the protocols described in Chapter 2. Poly(S-(2-hydroxyethyl)-*rac*-cysteine)$_{150}$, ***rac*-$\mathbf{C^{HE}_{150}}$**, was prepared from $\mathbf{A^{DH}_{150}}$ according to published procedures and spectral data were in agreement with literature.[27]

S-(*tert*-Butyl carboxymethyl)-L-cysteine.[28] This compound was prepared according to the protocol described in Chapter 2.

S-(*tert*-Butyl carboxymethyl)-L-cysteine N-carboxyanhydride (*t*BuCM-Cys NCA).[28] This monomer was prepared according to the protocol described in Chapter 2.

2-Acetamido-2-deoxy-1,3,4,6-tetra-O-acetyl-β-D-galactopyranose

This procedure was adapted from a published protocol.[10] D-Galactosamine HCl (3.0 g, 14.0 mmol) was suspended in Ac_2O (16 mL) and pyridine (30 mL). DMAP (0.20 g) was added and the reaction was allowed to stir at ambient temperature overnight. The reaction was poured into two 50 mL falcon tubes each containing 30 mL of 4 °C. DI H_2O and the precipitates that formed were collected via centrifugation. The combined precipitates were washed 3 additional times with 50 mL DI H_2O and then dried overnight at room temperature. The product was isolated as a white powder (4.50 g, 83%). Spectral data were in agreement with the literature.[35]

2-Acetamido-2-deoxy-1-thio-α-D-galactopyranose, αGalNAcSH This compound was prepared from 2-acetamido-2-deoxy-1,3,4,6-tetra-O-acetyl-β-D-galactopyranose using a published protocol. Spectral data were in agreement with the literature.[35]

General procedure for determination of M chain lengths using end-group analysis after reaction with mPEG-NCO. This procedure was performed following the protocol described in Chapter 2.

Functionalization of A^{DH}_{150} with 1-thio-β-D-glucopyranoside sodium salt. A^{DH}_{150} powder (20 mg) was dissolved in 4 mL of DMSO. To the solution was added 150 mg of 1-thio-β-D-glucopyranoside sodium salt (5 eq per $\mathbf{A^{DH}}$ sidechain) dissolved in 3 mL of pH 8 sodium phosphate buffer. The turbid suspension was stirred for 24 hours at room temperature where it became clear overnight. The solution was then transferred to a 2 kDa MWCO dialysis bag and dialyzed against 50 mM $NaHCO_3$ (24 h, 2 dialyzate

changes) and then DI H_2O (24 h, 2 dialyzate changes). The solution was then freeze dried to yield **βGlc-*rac*-C$_{150}$** as a fluffy white powder (51 mg, 62%).

^{1}H NMR (400 MHz, D_2O, 25 °C) δ 4.63 (bm, 450 H), 3.96 (t, 148 H), 3.77 (bs, 166 H), 3.63 - 2.95 (bm, 827 H).

Functionalization of A$^{DH}_{150}$ with 2-acetamido-2-deoxy-1-thio-α-D-galactopyranose. **A$^{DH}_{150}$** powder (15 mg) was dissolved in 3 mL of DMSO. To the solution was added 230 mg of 2-acetamido-2-deoxy-1-thio-α-D-galactopyranose (5 eq per **A^{DH}** sidechain) dissolved in 4.6 mL of pH 8 sodium phosphate buffer. The turbid suspension was stirred for 24 hours at room temperature where it became clear overnight. The solution was then transferred to a 2 kDa MWCO dialysis bag and dialyzed against 50 mM $NaHCO_3$ (24 h, 2 dialyzate changes) and then DI H_2O (24 h, 2 dialyzate changes). The solution was then freeze dried to yield **αGalNAc-*rac*-C$_{150}$** as a fluffy white powder (41 mg, 67%).

^{1}H NMR (400 MHz, D_2O, 25 °C) δ 5.89 (s, 104 H), 4.68 (102 H), 4.48 (bs, 262 H), 4.14 (bs, 250 H), 3.92 (bs, 481 H), 3.49 (bs, 237 H), 2.28 (s, 450 H)

Circular Dichroism Spectroscopy Polypeptide samples were analyzed at a concentration of 0.1 mg/mL in DI H_2O adjusted to pH 7.0 with 0.1 M NaOH. The data were reported in units of molar ellipticity [θ] (deg·cm^2·dmol^{-1}), which was calculated using [θ] = (θ × 100 × MW)/(*c* × *l*), where θ is the measured ellipticity (millidegrees), MW is the average residue molecular mass (g/mol), *c* is the polypeptide concentration (mg/mL), and *l* is the cuvette path length (cm).

Atomic Force Microscopy Solutions of polypeptides in Milli-Q water (10 μL) at 100-200 nM concentration were deposited on freshly cleaved bare mica for 1 minute, rinsed with

Milli-Q water, then gently dried under a stream of N_2 perpendicular to the mica surface before imaging.

5.6 Spectral Data

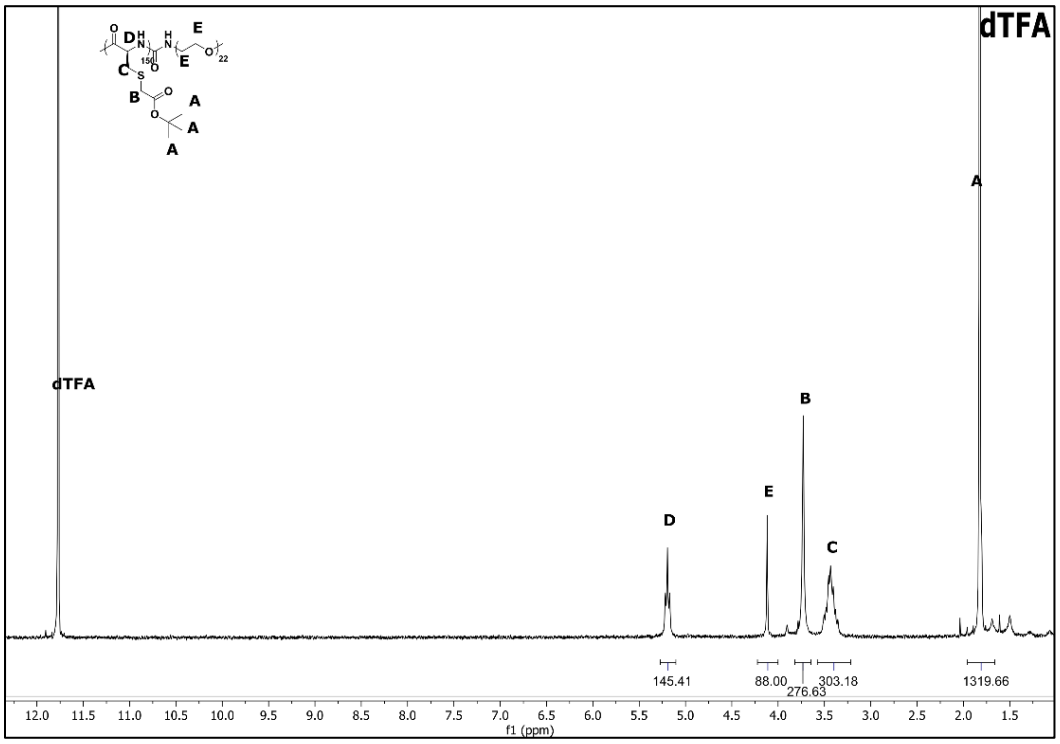

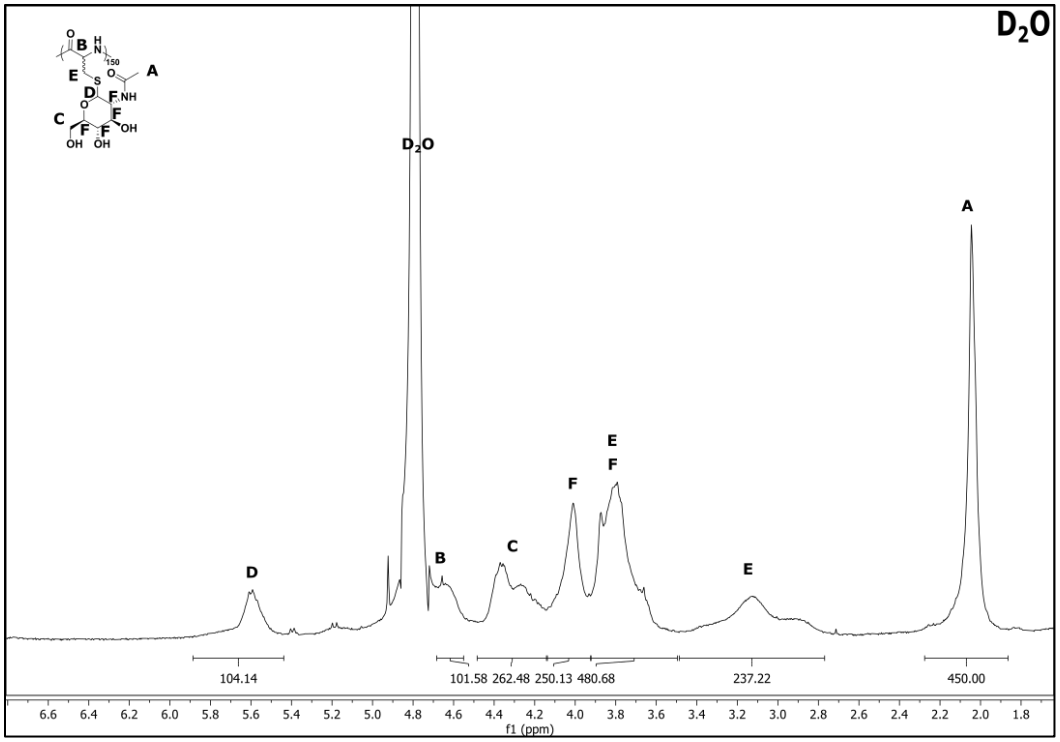
D2O
D2O
A
E
F
C
B
D
104.14
101.58
262.48
250.13
480.68
237.22
450.00
f1 (ppm)

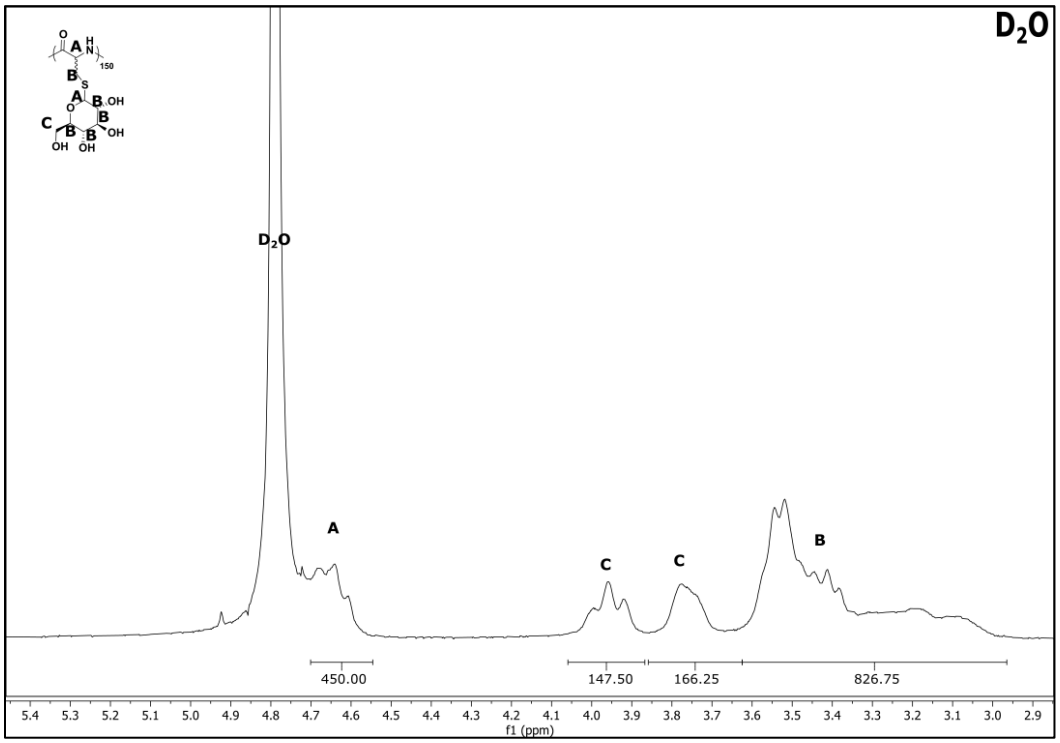
D2O
D2O
A
C
C
B
450.00
147.50
166.25
826.75
f1 (ppm)

5.7 References

1) Kohout, V. R.; Wardzala, C. L.; Kramer, J. R. Synthesis and Biomedical Applications of Mucin Mimic Materials. *Adv. Drug Deliv. Rev.* **2022**, *191*, 114540.

2) Bej, R.; Haag, R. Mucus-Inspired Dynamic Hydrogels: Synthesis and Future Perspectives. *J. Am. Chem. Soc.* **2022**, *144* (44), 20137–20152.

3) Petrou, G.; Crouzier, T. Mucins as Multifunctional Building Blocks of Biomaterials. **2018**.

4) Yousefi, M.; Dehghani, S.; Nosrati, R.; Zare, H.; Evazalipour, M.; Mosafer, J.; Tehrani, B. S.; Pasdar, A.; Mokhtarzadeh, A.; Ramezani, M. Aptasensors as a New Sensing Technology Developed for the Detection of MUC1 Mucin: A Review. *Biosens. Bioelectron.* **2019**, *130*, 1–19.

5) Kufe, D. W. Mucins in Cancer: Function, Prognosis and Therapy. *Nat. Rev. Cancer* **2009**, *9* (12), 874–885.

6) Grondin, J. A.; Kwon, Y. H.; Far, P. M.; Haq, S.; Khan, W. I. Mucins in Intestinal Mucosal Defense and Inflammation: Learning From Clinical and Experimental Studies. *Front. Immunol.* **2020**, *11*, 2054.

7) Kramer, J. R.; Onoa, B.; Bustamante, C.; Bertozzi, C. R. Chemically Tunable Mucin Chimeras Assembled on Living Cells. *Proc. Natl. Acad. Sci.* **2015**, *112* (41), 12574–12579.

8) Deleray, A. C.; Kramer, J. R. Biomimetic Glycosylated Polythreonines by N-Carboxyanhydride Polymerization. *Biomacromolecules* **2022**, *23* (3), 1453–1461.

9) Kramer, J. R.; Deming, T. J. Recent Advances in Glycopolypeptide Synthesis. *Polym. Chem.* **2013**, *5* (3), 671–682.

10) Kohout, V. R.; Wardzala, C. L.; Kramer, J. R. Mirror Image Mucins and Thio Mucins with Tunable Biodegradation. *J. Am. Chem. Soc.* **2023**, *145* (30), 16573–16583.

11) Clauss, Z. S.; Kramer, J. R. Design, Synthesis and Biological Applications of Glycopolypeptides. *Adv. Drug Deliv. Rev.* **2021**, *169*, 152–167.

12) Qiao, M.; Zhang, L.; Jiao, R.; Zhang, S.; Li, B.; Zhang, X. Chemical and Enzymatic Synthesis of *S*-Linked Sugars and Glycoconjugates. *Tetrahedron* **2021**, *81*, 131920.

13) Stepper, J.; Shastri, S.; Loo, T. S.; Preston, J. C.; Novak, P.; Man, P.; Moore, C. H.; Havlíček, V.; Patchett, M. L.; Norris, G. E. Cysteine *S*-Glycosylation, a New Post-Translational Modification Found in Glycopeptide Bacteriocins. *FEBS Lett.* **2011**, *585* (4), 645–650.

14) Shi, S.; Wang, J.; Wang, T.; Ren, H.; Zhou, Y.; Li, G.; He, C.; Chen, X. Influence of Residual Chirality on the Conformation and Enzymatic Degradation of Glycopolypeptide Based Biomaterials. *Sci. China Technol. Sci.* **2021**, *64* (3), 641–650.

15) Feng, Z.; Xu, B. Inspiration from the Mirror: D-Amino Acid Containing Peptides in Biomedical Approaches. *Biomol. Concepts* **2016**, *7* (3), 179–187.

16) Li, X.; Du, X.; Li, J.; Gao, Y.; Pan, Y.; Shi, J.; Zhou, N.; Xu, B. Introducing D-Amino Acid or Simple Glycoside into Small Peptides to Enable Supramolecular

Hydrogelators to Resist Proteolysis. *Langmuir ACS J. Surf. Colloids* **2012**, *28* (37), 13512–13517.

17) Wang, S.-S.; Gao, X.; Solar, V. D.; Yu, X.; Antonopoulos, A.; Friedman, A. E.; Matich, E. K.; Atilla-Gokcumen, G. E.; Nasirikenari, M.; Lau, J. T.; Dell, A.; Haslam, S. M.; Laine, R. A.; Matta, K. L.; Neelamegham, S. Thioglycosides Are Efficient Metabolic Decoys of Glycosylation That Reduce Selectin Dependent Leukocyte Adhesion. *Cell Chem. Biol.* **2018**, *25* (12), 1519-1532.e5.

18) Navarro, L. A.; French, D. L.; Zauscher, S. Advances in Mucin Mimic Synthesis and Applications in Surface Science. *Curr. Opin. Colloid Interface Sci.* **2018**, *38*, 122–134.

19) Kramer, J. R.; Deming, T. J. General Method for Purification of α-Amino Acid-N-Carboxyanhydrides Using Flash Chromatography. *Biomacromolecules* **2010**, *11* (12), 3668–3672..

20) Badreldin, M.; Salas-Ambrosio, P.; Bourasseau, S.; Lecommandoux, S.; Harrisson, S.; Bonduelle, C. Toward Synthetic Intrinsically Disordered Polypeptides (IDPs): Controlled Incorporation of Glycine in the Ring-Opening Polymerization of N-Carboxyanhydrides. *Biomacromolecules* **2024**, *25* (5), 3033–3043.

21) Wollenberg, A. L.; Perlin, P.; Deming, T. J. Versatile N-Methylaminooxy-Functionalized Polypeptides for Preparation of Neoglycoconjugates. *Biomacromolecules* **2019**, *20* (4), 1756–1764.

22) Kramer, J. R.; Schmidt, N. W.; Mayle, K. M.; Kamei, D. T.; Wong, G. C. L.; Deming, T. J. Reinventing Cell Penetrating Peptides Using Glycosylated Methionine Sulfonium Ion Sequences. *ACS Cent. Sci.* **2015**, *1* (2), 83–88.

23) Gharakhanian, E. G.; Deming, T. J. Chemoselective Synthesis of Functional Homocysteine Residues in Polypeptides and Peptides. *Chem. Commun.* **2016**, *52* (30), 5336–5339.

24) Kramer, J. R.; Deming, T. J. Reversible Chemoselective Tagging and Functionalization of Methionine Containing Peptides. *Chem. Commun.* **2013**, *49* (45), 5144–5146.

25) Gharakhanian, E. G.; Deming, T. J. Role of Side-Chain Molecular Features in Tuning Lower Critical Solution Temperatures (LCSTs) of Oligoethylene Glycol Modified Polypeptides. *J. Phys. Chem. B* **2016**, *120* (26), 6096–6101.

26) Zhou, H.; Wu, G.; Zhang, Z.; Zhu, Z.; Zhao, T.; Zhou, Q.; Chen, H.; Zhao, Z.; Dai, Y.; Jing, X.; Ji, W.; Yan, X.; Yang, L.; Gao, Y.; Wang, H.; Lu, H. Data-Driven Design of Random Heteropolypeptides as Synthetic Polyclonal Antibodies. *J. Am. Chem. Soc.* **2025**, *147* (24), 21077–21088.

27) Benavides, I.; Raftery, E. D.; Bell, A. G.; Evans, D.; Scott, W. A.; Houk, K. N.; Deming, T. J. Poly(Dehydroalanine): Synthesis, Properties, and Functional Diversification of a Fluorescent Polypeptide. *J. Am. Chem. Soc.* **2022**, *144* (9), 4214–4223.

28) Morrison, C. A.; Chan, E. P.; Deming, T. J. Triggered Inversion of Dual Responsive Diblock Copolypeptide Vesicles. *J. Am. Chem. Soc.* **2025**, *147* (9), 7617–7623.

29) Morrison, C. A.; Chan, E. P.; Lee, T.; Deming, T. J. Switchable Coacervate Formation via Amino Acid Functionalization of Poly(Dehydroalanine). *Biomacromolecules* **2024**.

30) Brockhausen, I.; Schachter, H.; Stanley, P. O-GalNAc Glycans. In *Essentials of Glycobiology. 2nd edition*; Cold Spring Harbor Laboratory Press, 2009.

31) Perlin, P.; Gharakhanian, E. G.; Deming, T. J. Homoallylglycine Residues Are Superior Precursors to Orthogonally Modified Thioether Containing Polypeptides. *Chem. Commun.* **2018**, *54* (48), 6196–6199.

32) Zhou, M. N.; Delaveris, C. S.; Kramer, J. R.; Kenkel, J. A.; Engleman, E. G.; Bertozzi, C. R. N-Carboxyanhydride Polymerization of Glycopolypeptides That Activate Antigen-Presenting Cells through Dectin-1 and Dectin-2. *Angew. Chem. Int. Ed.* **2018**, *57* (12), 3137–3142.

33) McMaster, T. J.; Berry, M.; Corfield, A. P.; Miles, M. J. Atomic Force Microscopy of the Submolecular Architecture of Hydrated Ocular Mucins. *Biophys. J.* **1999**, *77* (1), 533–541.

34) Kramer, J. R.; Deming, T. J. Glycopolypeptides with a Redox-Triggered Helix-to-Coil Transition. *J. Am. Chem. Soc.* **2012**, *134* (9), 4112–4115.

35) Knapp, S.; Myers, D. S. Synthesis of α-GalNAc Thioconjugates from an α-GalNAc Mercaptan. *J. Org. Chem.* **2002**, *67* (9), 2995–2999.

36) Elhalabi, J.; Rice, K. G. Thiosugar Nucleotide Analogues: Synthesis of Uridine 5′-(2,3,6-Tri-O-Acetyl-4-S-Acetyl-4-Thio-α-d-Galactopyranosyl Diphosphate). *Carbohydr. Res.* **2001**, *335* (3), 159–165.